SISSA
Scuola Internazionale Superiore di Studi Avanzati

Neuroscience Area

PhD course in Neurobiology

Immediate changes in CNS networks triggered by a physical trauma to the spinal cord

Candidate:

Atiyeh Mohammadshirazi

Advisor:

Prof Giuliano Taccola

Academic Year 2023-2024

ACKNOWLEDGEMENTS

I would like to express my deepest gratitude to my supervisor, Prof. Giuliano Taccola, whose guidance, expertise, and support have been crucial throughout my research journey. Working under his mentorship has been an insightful journey, and I have learned far more than just science.

I also wish to extend my appreciation to Prof. Nistri, Dr. Falcone, Dr. Mazzone and all my collaborators and lab mates, whose contributions and insights have enriched this work. Their efforts have made this research possible, and I am deeply thankful for their partnership.

And finally, to my closest friend and husband, Dr. Sina Shafiezadeh, for his unwavering love, patience, and understanding. His steadfast support during my challenging moments and his joy in celebrating my successes have been a constant source of strength. This achievement would not have been possible without him.

ABSTRACT

Spinal cord injury (SCI) results in irreversible functional impairments due to intricate molecular and cellular processes, leading to neuronal damage. Despite its significance, the immediate consequences of SCI, including the transient disappearance of reflex responses below the injury site, termed as spinal shock, have been underexplored due to the lack of consistent preclinical models.

In the first part of this PhD thesis project, an in vitro preparation of the isolated central nervous system (CNS) from neonatal rats was characterized. This preparation exhibited stable respiratory rhythms, evoked motor responses, fictive locomotor (FL) activities, and functional ascending and descending pathways. The in vitro CNS showed the crucial role of suprapontine centers in the modulation of spontaneous respiratory rhythms, electrically evoked reflexes, and spinal network activity.

The second part of the project adopts a novel custom-made micro impactor to deliver a calibrated impact to the ventral surface of the thoracic spinal cord. Ventral root (VR) recordings continuously monitored baseline spontaneous activities and electrically-induced reflex responses before and after injury. Following the impact, an immediate transient depolarization occurred, coinciding with a rapid drop in tissue oxygen levels and significant cell death at the injury site, alongside complete disconnection of longitudinal tracts. Reflex responses were temporarily abolished, mimicking the progression of the spinal shock, while the coordination among motor pools during FL was affected. Perfusion with low chloride-modified Krebs medium amplified the depolarization, suggesting that chloride ions are implicated in the peak of the injury potential. Furthermore, remote changes in cortical glial cells were observed shortly after spinal injury.

Eventually, various pharmacological agents were tested to mitigate injury-induced depolarization. Notably, only Transient Receptor Potential Vanilloid 4 (TRPV4) antagonism successfully reduced the depolarization amplitude, indicating for the first time that mechanoreceptors sustain the immediate depolarization after a spinal trauma. The reappearance of VR reflexes was accelerated through the blockade of TRPV4 channels, gap junctions, and GABAergic transmission, although with distinct timing and yield.

In conclusion, this study provides a novel experimental platform for investigating the immediate events following traumatic SCI, revealing the pivotal roles of chloride imbalance and mechanoreceptors in the cascade of pathological events that characterize acute SCI pathophysiology.

PUBLICATIONS ARISING FROM THE THESIS

1. Mazzone G. L., **Mohammadshirazi A.**, Aquino J. B., Nistri A., Taccola G.; GABAergic mechanisms can redress the tilted balance between excitation and inhibition in damaged spinal networks; Molecular neurobiology; 07 Apr 2021; doi: 10.1007/s12035-021-02370-5
2. **Mohammadshirazi A.**, Apicella R., Zylberberg B. A., Mazzone G. L., Taccola G.; Suprapontine structures modulate brainstem and spinal networks; Cellular and molecular neurobiology; 02 Feb 2023; doi: 10.1007/s10571-023-01321-z
3. **Mohammadshirazi A.**, Mazzone G. L., Zylberberg B. A., Mio L., Pistorio G., Falcone C., Taccola G.; Focal traumatic injury to the spinal cord causes an immediate and massive spreading depolarization sustained by chloride ions, with transient network dysfunction and remote cortical glia changes; Cellular and Molecular Neurobiology, submitted on 27 Aug 2024, Under review (preprint doi: 10.1101/2024.07.15.603535)
4. **Mohammadshirazi A.**, Taccola G.; An electrophysiological study about the pharmacological manipulation of the immediate consequences of a spinal trauma reveals a crucial role for TRPV4 antagonism, to be submitted (preprint doi: 10.1101/2024.10.03.616499)
5. **Mohammadshirazi A.**, Ermolaeva M. E., Taccola G.; In vitro models provide unique insights on the early consequences of a spinal cord injury, manuscript in preparation

CONTENTS

INTRODUCTION

1. An overview on traumatic SCIs

Spinal cord injury (SCI) is a neurological condition characterized by a damage to the spinal cord caused by traumatic events such as falls, vehicle accidents, and violence, or non-traumatic factors such as tumors, degenerative diseases, vascular conditions, infections, toxins, or birth defects (Ahuja et al., 2017; WHO, 2024). According to the World Health Organization (WHO) in 2024 , the majority of SCI cases result from trauma, and globally over 15 million people live with SCI, with a higher prevalence in men (WHO, 2024).

SCI involves a complex pathological process with both immediate and delayed tissue damage (Bennett et al., 2024). The initial traumatic damage named primary injury, produces immediate mechanical disruption, dislocation of the vertebral column and hemorrhage, hens sudden cell death and axonal disruption at the region of the spinal cord within the first two hours post injury (Fig. I A; Siddiqui et al., 2015; Ahuja et al., 2017; Bennett et al., 2024). After minutes to hours , the primary injury triggers a cascade of events named secondary injury, that worsen and amplifies the damage of spinal tissue through the increase of extracellular glutamate leading to excitotoxicity and cellular death, inflammation, oxidative stress, edema, and apoptosis (Ahuja et al., 2017; Alizadeh et al., 2019). Following the acute phase, these processes evolve over time, and a subacute phase characterized by ongoing inflammation and glial scar formation at the site of impact occurs. The cascade of cell death mechanisms activated during the acute (2 - 48 h post-injury; Siddiqui et al., 2015) and subacute (48 h - 14 days post-injury; Siddiqui et al., 2015) phases of SCI inflict more severe damage than the primary trauma. This evidence forms the foundation for developing early neuroprotective interventions (Ahuja et al., 2017). Finally, the onset of the chronic phase leads to plastic rearrangements that can rarely lead to spontaneous recoveries and, more often, to lifelong neurological impairments (Silva et al., 2014).

An SCI demonstrates that the mature central nervous system (CNS) cannot regenerate nor repair itself after traumatic insults in mammals (Varadarajan et al., 2022). In addition to cell death, the limited regenerative capacity of post-mitotic mature neurons (Kole et al., 2013), inflammatory responses, and glial scar formation further impede recovery (Fry, 2001; Varadarajan et al., 2022) and vanish any spontaneous regeneration attempts that take place right after a neural lesion even in adult stage (Bradbury and Burnside, 2019). Moreover, inhibitory factors such as Chondroitin sulfate proteoglycan, myelin-associated inhibitors, and semaphorin 3A make the microenvironment of the injury non-permissive to axonal regrowth (Bradbury et al., 2002; Huebner and Strittmatter, 2009; Yang et al., 2020a). Due to the mature human spinal cord's inability to self-repair, an SCI often causes a permanent loss of sensory and motor control over the body parts innervated by spinal neurons located below the level of injury. Eventually, an SCI results in a long-life debilitating condition characterized by motor

paralysis and a variegated spectrum of functional deficits and complications. Depending on the level and severity of the lesion, after an SCI, individuals may experience quadriplegia or tetraplegia, where all four limbs are affected, or paraplegia, which involves paralysis of the lower limbs while upper body function remains intact (Rupp et al., 2021). To date, there is no cure against paralysis, and current rehabilitation focuses mainly on strengthening the able part of the body to compensate for the loss of volitional motor control over the paralyzed limbs.

Support in daily tasks mainly occurs through classical mobility aids, such as a wheelchair and crutches, and using newly introduced technologies, such as exoskeletons (Benabid et al., 2019) and advanced brain machine interfaces (Yang et al., 2020a). Robotic devices mainly aim to help movements and increase neural plasticity through repetitive and functional movements. Brain machine interfaces (BMI), either surgically implanted or non-invasive transcranial types, record the brain signals and decode them to drive an assistant device known as BMI-controlled neuroprosthetics for motor functions (Mekki et al., 2018; Yang et al., 2020b). In another version the processed information from the sensorimotor cortex is relayed into the electrical stimulator targeting distinct sites of the dorsal surface of the lumbosacral spinal cord (Lorach et al., 2023).

Exoskeletons aid in supporting the body and move the joints through motorized actuators with different levels of assistance (Nepomuceno et al., 2024). They help to reduce spasticity, neuropathic pain, and improve the cardiovascular system by providing a moderate-intensity exercise (Mekki et al., 2018). However, the benefits of exoskeletons in volitional motor recoveries are highly related to the severity and level of the injury, but still, controversial results do not suggest the same pattern of mobility improvements (Nepomuceno et al., 2024).

Another approach to modulating neural circuits in clinics is using electrical spinal cord stimulation (ESS; Inanici et al., 2018). ESS can be delivered either epidurally or transcutaneously. Epidural stimulation involves the surgical implantation of electrodes directly onto the dura mater, providing direct and consistent activation of spinal circuits (Taccola et al., 2020; Choi et al., 2021). In contrast, transcutaneous stimulation is a non-invasive approach through electrodes on the skin of the back over the spine (Rahman et al., 2022). These methods are reported to improve sensorimotor function and autonomic functions by changing the cortical, subcortical, and spinal transmission and, eventually neuronal network dynamics (Rahman et al., 2022).

Despite these advancements reported in a minority of individuals with SCI, all the mentioned strategies struggle to be introduced in clinics due to their lack of efficacy. This highlights the pressing need for more comprehensive and universally effective therapeutic approaches.

2. Immediate effects of an SCI: the spinal shock

One of the main missing tiles for the overall understanding of an SCI is the identification of the immediate events that take place during a physical impact to the spinal cord. In particular, it is still unknown how the primary mechanical insult to the spinal tissue contributes to trigger the subsequent cascade of pathological events known as secondary damage, which eventually extends tissue damage and hinders the chances of achieving a functional recovery (Carlson et al., 1998).

Indeed, after injury, a temporary loss or depression of all or most spinal reflex activity takes place below the lesion. This phenomenon, first described by Hall in 1841 (Hall, 1841), is called spinal shock, and the underlying mechanisms are not fully clarified (Fig. I B; Ditunno et al., 2004). Spinal shock is particularly profound in higher primates, especially humans (Guttmann, 1970; Atkinson and Atkinson, 1996; Smith and Jeffery, 2005). Studies demonstrated that full recovery of tibial H-reflex after SCI takes 3-4 weeks in rats, 4-6 weeks in cats, and 12-16 weeks in humans (Ditunno et al., 2004). A spinal shock clinically persists for days or weeks, depending on which reflex is being tested for reappearance (Fig. II). However, when duration is defined based on the initial recovery of any reflex, then the spinal shock lasts no longer than 20-60 min, usually with the gradual recovery of delayed plantar response pursued by cutaneous, deep tendon, and bladder reflexes (Simpson et al., 1996; Ditunno et al., 2004). The reflexes remain suppressed for a longer time as they are originated from motor pools closer to the injury site (Guttmann, 1970; Atkinson and Atkinson, 1996). Thus, a positive correlation between the distance of sacral dermatomes from the injury and the likelihood of retaining the reflexes has been observed. For instance, individuals with high-level cervical SCIs are more likely to retain sacral reflexes, such as the bulbocavernosus and anal wink reflexes (Atkinson and Atkinson, 1996; Ko et al., 1999).

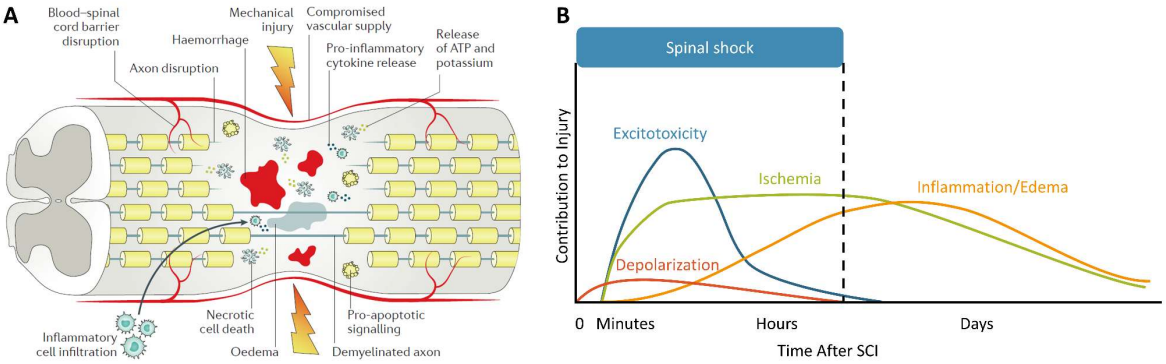

Fig. I. The progression of an acute SCI

A. The primary mechanical injury produces cell death and axonal disruption and leads to a secondary damage characterized a cascade of events in the acute phase, including hemorrhage, ischemia, inflammation, and the release of cytotoxic products (from Ahuja et al., 2017).

B. The timeline of key events following an SCI encompassing the depolarization (injury potential), excitotoxicity, ischemia, and edema. Among the numerous contributes to the acute SCI, the immediate

and transient depolarization, remains the least explored also in terms of its long-term consequences (modified from Schwab et al., 2006).

	0–1 day	*1–3 days*	*1–4 weeks*	*1–12 months*
DPR	+++	+++	+/0	+/0
BC reflex	+/0	++	++	++
AW reflex	+/0	++	++	++
CM reflex	+/0	++	++	++
Babinski sign	0	+	++	++
Flexor withdrawal reflex	0	+/0	++	+++
DTRs	0	+/0	++	+++
Tibial H-reflex	0	++	+	+++
Extensor spasm	0	0	0	+++
Interlimb reflexes	0	0	0	+++
Reflex neurogenic bladder	0	0	0	+++
Autonomic hyper-reflexia	0	0	0	+++

Fig. II. Recovery of reflexes following an SCI in human
The reappearance of reflexes after SCI varies among individuals and depends on which reflex is being tested. The delayed plantar reflex (DPR) is usually the first to reappear, followed by the polysynaptic reflexes such as bulbocavernosus (BC), cremasteric (CM), abdominal wall reflex (AW),Babinski sign, and deep tendon reflex (DTR) (from Ditunno et al., 2004).

The termination of spinal shock occurs more rapidly in cases of incomplete lesions and usually does not follow the same pattern of recovery in individuals with incomplete versus complete SCI (Ko et al., 1999; Ko, 2018). Since spinal shock is a transient phenomenon and is considered an inevitable process, no specific treatment is recommended beyond the standard supportive measures already undertaken for spinal cord injury, such as hemodynamic and respiratory stabilization and surgical decompression (Fehlings and Perrin, 2005; Ziu et al., 2024). Nevertheless, the consequences triggered by spinal shock are unknown and may be permanent.

The lack of reflex activity has been mainly attributed both to the sudden disappearance of the predominantly facilitatory tonic influence exerted by descending supraspinal tracts (Sherrington, 1897; Mccouch et al., 1966), and to an increased presynaptic inhibition (Ashby et al., 1974; Calancie et al., 1993). In addition, depression of synaptic activities also depends on the hyperpolarization of spinal neurons due to an increased outflux of potassium from the damaged site that also blocks the axon conduction in white matter tracts (Barnes et al., 1962; Eidelberg et al., 1975; Nacimiento and Noth, 1999). Neurons are unable to generate action potentials when sustained depolarization exceeds the action potential threshold, causing inactivation of the membrane ionic channels responsible for action potential generation. This results in hypo-excitability due to depolarization, leading to a state of “electrical silence” (Dreier, 2011). In addition to these mechanisms, membrane shunting can further contribute to the suppression of neural activity. This shunting inhibition dampens neuronal excitability, reinforcing the overall suppression of synaptic transmission and contributing to the state of electrical silence following injury (Gao and Ziskind-Conhaim, 1995; Mazzone et al., 2021).

Experimentally, the dynamics of a spinal shock parallel those of the early depolarization of the entire spinal cord following a trauma, also known as injury potential (Fig. III), which spreads rostrally and caudally from the site of impact. This early depolarization is sustained by a transient extracellular ionic disbalance (Goodman et al., 1985; Wang et al., 2015) and is analogous to the cortical spreading depression (SD), which exhibits a marked, enduring reduction in the intrinsic electrical activity of neurons, eventually spreading from the original source out in all directions with reported velocity of 2-5 mm/min in human and involving increasingly distant parts of the cerebral cortex (Leao, 1944, 1947; Lauritzen et al., 2011). SD is defined as an electrochemical wave mediated by extracellular high concentrations of potassium (Grafstein, 1956) and glutamate (Harreveld, 1959), which activate ligand-gated and voltage-gated channels of adjacent neurons, astrocytes, microglia, and vascular smooth cells (Wendt et al., 2016; Lindquist, 2023). SD is characterized by an imbalance of homeostasis, neuronal swelling, and distortion of dendritic spines (Dreier, 2011). During SD, there is an initial rise in the concentration of potassium (K^+), followed by a decrease in chloride (Cl^-), calcium (Ca^{2+}), and Sodium (Na^+) concentrations (Kraig and Nicholson, 1978; Somjen, 2001). These ionic shifts disrupt the electrochemical gradients essential for normal neuronal function and contribute to the pathological process observed during cortical SD.

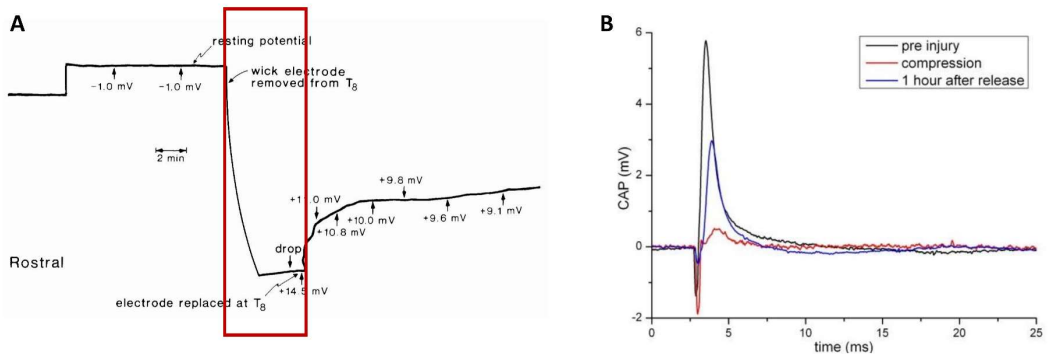

Fig. III. Injury Potentials and Reflex Recovery Following SCI
A. Following traumatic SCI, an injury potential appears, though it has not been fully recorded. The electrophysiological recording shown was obtained from the surface of the 8th thoracic spinal segment in a rat. The rectangle highlights a 4-minute gap in the recording (modified from Goodman et al., 1985).
B. Superimposed recordings of compound action potentials (CAPs) demonstrate the reduction and subsequent recovery of reflex responses after an ex vivo spinal cord compression and mimicking the effects of spinal shock (from Wang et al., 2015).

A cortical SD is triggered, among other causes such as migraine, aneurysm and stroke, by traumatic brain injuries (Hermann et al., 1999; Lauritzen et al., 2011; Dreier, 2011). Experimentally, SD can be induced by various methods such as hypotonicity, low extracellular Cl^- concentrations, application of

KCl, and a pinprick injury (Streit et al., 1995; Gorji et al., 2004). These experimental conditions mimic the disturbances in ionic balance and mechanical stress that can occur in vivo, providing insight into the mechanisms underlying SD.

In both amphibians and rodents, a compressive injury to the cord is followed both by SD-like waves characterized by a velocity of propagation of around 2-15 mm/min, and by a rapid and reversible increase in extracellular concentrations of K^+ ions (Lauritzen, 1994; Streit et al., 1995; Gorji et al., 2004; Windmüller et al., 2005; Lauritzen et al., 2011). Interestingly, electrically evoked potentials were transiently abolished during spinal SD waves, eventually returning to baseline values only after about twenty minutes. This phenomenon suggests that spinal SD might determine areflexia after spinal shock (Gorji et al., 2004). The same study also described how the SD evoked by an injury to the brain cortex reduced the excitability of neurons located in cervical spinal segments, indicating that SD-like waves induced by an injury maintain a form of conduction among cortical and spinal structures (Gorji et al., 2004).

3. Acute consequences of an SCI on remote districts of the CNS

The occurrence of any neuronal changes in the brain after SCI remains a subject of debate, with conclusions spanning from the absence of cellular loss (Crawley et al., 2004) to extensive retrograde neurodegeneration (Feringa and Vahlsing, 1985; Hains et al., 2003). While cortical reorganization can facilitate functional recovery, it also holds the potential for maladaptive outcomes such as phantom sensations and neuropathic pain. Detailed studies on spinal cord contusion in mice have described SCIs as complex events affecting the entire CNS, seldom leading to cognitive changes and depressive-like behaviors, often associated with reactive microglia and chronic neuronal loss in the hippocampus and cerebral cortex (Wu et al., 2014). By 14 days post-SCI, microglial activation significantly increases, as their morphology shifts from a resting to an activated state in both the hippocampus and cerebral cortex, accompanied by significant changes in cell-cycle-related gene expression (Wu et al., 2014). The same evidence has been displayed in the in vitro chemical model of neonatal SCI where digesting microglia was acutely expressed at the site of injury (Taccola et al., 2010). Moreover, as early as two hours after thoracic injury in rats, the cytoplasmic calcium-binding protein S100b rises in both serum and cerebrospinal fluid (CSF), peaking at six hours post-injury (Cao et al., 2008). S100b is released by mainly astrocytes to support neurite outgrowth and offer protection against oxidative stress (Nasser et al., 2015). S100b levels correlate with the severity of the injury (Cao et al., 2008), as confirmed by a chemical in vitro model of SCI study (Mazzone and Nistri, 2014). Furthermore, S100b has been considered as an early biomarker for excitotoxic damage following an SCI (Mazzone and Nistri, 2014).

Functional reorganization of motor cortex is also occurring after an SCI and is influenced by several factors. The extent of reorganization can vary widely, from negligible changes to significant cortical

remapping (Moxon et al., 2014). This variability is critically dependent on the species, the age at which the injury occurs, the duration since the injury, and the behavioral activities and therapeutic interventions post-injury (Moxon et al., 2014).

SCI can induce reorganization of the cerebral cortex and thalamus through both anterograde and retrograde mechanisms (Nardone et al., 2013). Studies have shown a neuronal death of the cerebral cortex in acute phase following a thoracic transection in rats. Axotomized pyramidal cells in the primary motor cortex undergo apoptosis as a direct result of being severed from the corticospinal tract, with approximately 40% of these cells exhibiting signs of apoptosis one week after injury. Notably, the number of axotomized cells showing signs of apoptosis decreases over time, with fewer cells displaying apoptotic markers at 2-4 weeks post-injury (Hains et al., 2003). Furthermore, following thoracic SCI, axotomized corticospinal axons originating from the hindlimb sensorimotor cortex sprout in the cervical spinal cord and rewire to establish a new forelimb corticospinal projection from the rostral region of the previously hindlimb cortex (Ghosh et al., 2010).

Furthermore, studies showed following a thoracic SCI, sensory deafferentation leads to alternations in the plasticity of the cortex (Endo et al., 2007). As early as three days post-injury, cortical representation in response to spared forelimb stimulation enlarges and invades adjacent sensory-deprived hindlimb territory in the primary somatosensory cortex (Endo et al., 2007). Gene regulation in sensory-deprived areas also changes, with the Nogo receptor, a regulator that restricts experience-dependent plasticity, being downregulated, and brain-derived neurotrophic factor (BDNF), a key signaling molecule in synaptic plasticity, being upregulated within the first day following SCI (Endo et al., 2007). Additionally, increased expression of cell-cycle-related genes and proteins is detected chronically in the hippocampus and cerebral cortex (Wu et al., 2014).

In terms of more acute effects, within 10-30 minutes from mid-thoracic transection of the spinal cord, cortical spontaneous activity becomes more silent, and forepaw-evoked responses from the primary somatosensory cortex enlarge in amplitude (Aguilar et al., 2010). In the hemisection model, increased cortical forepaw responses become significant within 30 minutes in the contralateral cortex and after 2.5 hours in the ipsilateral cortex, whereas cortical spontaneous activity reduced significantly in both hemispheres by 2.5 hours post-hemisection (Yagüe et al., 2014). The observed increase in forepaw responses may be attributed to the unmasking of pre-existing excitatory connections, facilitated by the removal of cortical inhibition (Jacobs and Donoghue, 1991; Nardone et al., 2013). A reduction in GABA (gamma-aminobutyric acid) that inhibits excitatory horizontal connections in the cerebral cortex leads to higher excitations in the cerebral cortex (Raineteau and Schwab, 2001).

Investigating the complex interactions between anatomical changes due to SCI and sensorimotor cortex reorganization is essential for identifying early and non-invasive biomarkers in the brain. Such

biomarkers would measure the extent of SCI's impact on structural integrity, would improve prognostic assessments, and refine clinical trials (Nardone et al., 2013). Studies suggest chronic inflammatory changes (Wu et al., 2014); however, it remains unknown whether immediate pathological signals are transiently triggered in the brain right after an impact to the spinal cord. The presence of such acute pathological signs could provide novel markers to have a better characterization of the severity of a lesion and predict potential recoveries.

4. Spontaneous recoveries from SCI

Although intrinsic recovery potential after an SCI is poor, some scattered and unpredictable spontaneous neurologic recoveries have been reported with more prevalency in cases of tetraplegia compared to paraplegia, and incomplete compared to complete injury (Kirshblum et al., 2004, 2021). The majority of changes in the American Spinal Injury Association (ASIA; Rupp et al., 2021) Impairment Scale and motor recovery occur within the initial 6–9 months post-injury, with the most rapid improvements observed in the first three months (Burns and Ditunno, 2001; Kirshblum et al., 2021) therefore studies of treatments yield the best results when administered promptly after an injury (Fawcett et al., 2007). A cohort clinical study investigated the relationship between time to rehabilitation and outcomes in traumatic SCIs, showing that earlier rehabilitation improves functional status at discharge (Herzer et al., 2016).

The prognosis for neurological recovery is highly variable and is primarily determined by the initial severity of the injury (Ahuja et al., 2017). In less severe injuries, a substantial spontaneous regain of functions plateaued at 4-6 months after injury (Burns and Ditunno, 2001; Geisler et al., 2001), and less substantial recovery occurs within five years (Kirshblum et al., 2004). More senior age is associated with lessened neurological and functional recovery following spinal cord injury. Moreover, there is insufficient evidence to suggest that gender significantly impacts neurological recovery (Kirshblum et al., 2021).

Endogenous mechanisms enable some levels of partial regeneration of an injured spinal cord. In cases of incomplete SCI, initial functional recovery typically occurs within the first days to weeks post-injury, primarily due to the reversal of metabolic changes at the lesion site (Raineteau and Schwab, 2001; Lynskey, 2008). Following the initial demyelination around the lesion site, spontaneous partial remyelination can occur through the invasion of Schwann cells or the activation of oligodendrocyte progenitors. Reorganization in incomplete SCI potentially occurs through synaptic plasticity in pre-existing circuits and anatomical plasticity, involving the growth of new axonal branches and dendrites as compensatory collateral sprouting (Raineteau and Schwab, 2001; Ahuja et al., 2017).

The most spontaneous functional recovery occurs within the zone of partial preservation, which can often lead to a slight functional recovery (Fawcett et al., 2007). Studies in mice suggest that in models

with damage to the dorsal corticospinal tract (CST), which comprises 96% of CST axons, the intact dorsolateral CST (3%) and ventral CST (1%) are crucial for spontaneous functional motor recovery (Hilton et al., 2016; Rasmussen and Carlsen, 2016).

The underlying processes driving spontaneous functional recovery remain largely elusive. Specifically, the relative contributions of axonal regeneration and compensatory mechanisms employed by intact neurons to this recovery process are not fully understood (Rasmussen and Carlsen, 2016). Thus, spontaneous recoveries still challenge our understanding of the pathophysiological mechanisms of an SCI and of the residual potential of the cord to repair spinal circuits. Understanding the mechanisms behind spontaneous recovery from SCI could provide critical insights into new therapeutic strategies. By identifying the endogenous processes that promote partial regeneration future treatments may be designed to enhance the endogenous recovery potential.

5. Traumatic injuries to the immature spinal tissue

Pediatric spinal injuries, accounting for 1-10 % of all SCIs (Carreon et al., 2004), occur with higher rates at cervical segments compared to adults due to cephalo-cervical disproportion (Hagan et al., 2022). However, children demonstrate significantly higher rates of spontaneous functional recovery than adults (Eleraky et al., 2000; Wang et al., 2004). The pediatric spinal cord's greater elasticity contributes to distinct injury patterns and enhanced neurological recovery (Eleraky et al., 2000). In particular, cervical injuries in children, especially those that are incomplete, tend to have more positive prognoses compared to similar injuries in adults (Dickman et al., 1989; Eleraky et al., 2000). Furthermore, children who survive the initial hospitalization after an SCI show a higher long-term survival rate compared to other age groups (Dickman et al., 1989).

Comparative studies on traumatic injuries indicate that plasticity and regeneration capacity of developing mammalian spinal tissue are significantly higher than adults (Wang et al., 2004; Stewart et al., 2022). Neonatal mammals exhibit a superior capacity for repair, particularly in the sprouting of growing neurites, compared to adults (Woodward et al., 1993). Moreover, five weeks after spinal transection in two-week-old rats, most tracts, including rubrospinal, vestibulospinal, and reticulospinal, demonstrated axonal regeneration (Wakabayashi et al., 2001). Similarly, in one-day-old cats, the hemisection of the spinal cord showed that corticospinal projections reroute around the lesion, sparing motor function, a phenomenon not observed in adults (Bregman and Goldberger, 1982). Indeed, in neonatal SCIs, where the suprasegmental structures and inhibitory descending pathways are not yet fully developed, reflexes recover more rapidly (Guttmann, 1970; Kunkel-Bagden et al., 1992)

Moreover, aging alters the acute pathophysiology of SCI by enhancing inflammatory responses and altering subcellular microenvironments. It is also associated with reduced trophic factor and cytokine

secretion, impaired axon growth, and diminished recruitment of macrophages at the lesion site (Stewart et al., 2022). Both experimental and clinical studies confirm that younger individuals exhibit greater neuronal plasticity, including the ability to reroute neural pathways and promote axonal sprouting, leading to improved neurological outcomes following SCI (Wang et al., 2004). However, further investigation is needed to elucidate the pathophysiological mechanisms underlying neonatal SCIs, with the goal of understanding the mechanisms at the base of the enhanced recovery in children and potentially extending these benefits to all individuals with SCI.

6. Current models of SCI: strengths and weaknesses

Obstacles to the comprehension of a spinal shock and the related early transient changes in the entire CNS reside in some technical challenges that arise from the preclinical models currently available. There is no unique experimental model of SCI in a specific animal that comprehensively addresses all scientific inquiries since the models tend to the standardization, but clinical lesions are extremely variegated in terms of type, level, site, and severity (Ahuja et al., 2017). Thus, adopting a variety of experimental approaches is essential to address diverse research questions, ranging from understanding the mechanisms of SCI to exploring potential regenerative outcomes and enhancing functional recovery. The choice of the level of the spinal cord, type of injury, and species is pivotal in advancing research (Sharif-Alhoseini et al., 2017; Fouad et al., 2020). Numerous SCI models have been introduced encompassing contusion, compression, complete and incomplete transactions, dislocation, distraction, ischemic models, chemical and electric models (Cheriyan et al., 2014; Sharif-Alhoseini et al., 2017). The experimental models include studies performed on in vitro tissues for investigating basic mechanisms, as well as experiments on fully anesthetized in vivo animals for more translational purposes. The most commonly used preclinical SCI models are contusion, which effectively replicates the neuropathology of human injuries, and trans- hemisection, which is ideal for studying anatomical regeneration (Sharif-Alhoseini et al., 2017). Rodent SCI models are widely used because they are affordable and resemble human pathology, particularly in the development of large cystic cavities at the injury site (Kjell and Olson, 2016; Sharif-Alhoseini et al., 2017). Additionally, the progression of an SCI is faster in rodents, thus four weeks after the injury is enough to reach chronic phase that require several months in larger mammalians. Albeit the cyst is absent in mice models; however, genetically modified mouse allows to manipulate clusters of specific cells to identify the distinct role of certain neuronal populations in the pathophysiology of SCI (Ma et al., 2001; Kjell and Olson, 2016). Despite the significant advantages offered by in vivo SCI models, they present technical limitations when it comes to capturing the immediate events following a traumatic injury. For example, the earliest electrophysiological recording of injury potential has been conducted only four minutes after the injury, leaving instants following a physical trauma unexplored (Goodman et al., 1985). Indeed, any

interference generated by standard experimental impactors masks electrophysiological recordings. Moreover, due to ethical concerns, the animal must be completely anesthetized before the injury in all in vivo models, which is not a real replicate of the unpredictable trauma in human. Studies have indicated that certain anesthetics possess neuroprotective properties. These effects are thought to arise from their ability to modulate various cellular and molecular pathways involved in secondary injury mechanisms following the initial trauma (Ishikawa et al., 2014). Isoflurane and barbiturates, in particular, have demonstrated the ability to mitigate cell death induced by excitotoxicity and ischemia, offering significant neuroprotection (Park et al., 2005; Ishikawa et al., 2014). Isoflurane, for example, induces delayed preconditioning against spinal cord ischemic injury through the release of free radicals, as observed in rabbit models (Sang et al., 2006). Propofol another anesthetic, has been found to offer neuroprotection by reducing motoneuron loss against kainite-induced excitotoxicity in the spinal cord (Kaur et al., 2016). Similarly, ketamine, acting as a noncompetitive NMDA (N-methyl-D-aspartate) receptor antagonist, has shown strong protective effects against spinal cord ischemia/reperfusion injury and has been effective in preserving antioxidant activity within spinal cord tissues (Yu et al., 2008). These findings suggest that the use of in vitro models of SCI can eliminate the confounding effects of anesthetics in animal experiments, ensuring more accurate assessments of SCI interventions.

Monitoring the long-term recovery after chronic SCI in in vitro models is unfeasible; however, their reproducibility makes them excellent tools for investigating post-traumatic events in both acute and secondary injury (Patar et al., 2019). Various techniques such as spinal cord strips, isolated spinal cord preparations, organoids, and organotypic slice culture (OSC) in rodents are widely employed to emulate compression (Fehlings and Nashmi, 1995; Shi and Blight, 1996; Kouhzaei et al., 2013; Wang et al., 2015; Ramirez et al., 2021), weight drop (Krassioukov et al., 2002; Pandamooz et al., 2019), transection (Weightman et al., 2014), and chemical injury (Takeda et al., 1993; Taccola et al., 2008, 2010) models. The adoption of neonatal preparations in vitro presents the opportunity to avoid any drug-induced anesthesia at the time of the injury, mitigating the risk of systemic cardiovascular instability and subsequent network depression or hypoxic neuronal damage induced by chemical anesthetics (Nout et al., 2012; Shabbir et al., 2015; Bajrektarevic and Nistri, 2016).

7. A novel in vitro model to mimic calibrated impacts to neonatal spinal cords

Since the introduction of the pioneering device by Allen (Allen, 1911), various modifications of the original weight drop impactor have been developed and standardized for use with adult rodents (Wrathall et al., 1985; Kwo et al., 1989; Basso et al., 1996). However, only a few studies have described SCI models using immature spinal tissues (Petruska et al., 2007; Ichiyama et al., 2011). To address technical artifacts and avoid the effects of anesthetics, the use of the isolated spinal cord from neonatal

rats has been proposed (Taccola et al., 2010; Mladinic et al., 2013). This approach allows for the examination of developing tissue under controlled conditions and offers potential insights into acute pediatric injuries (Carreon et al., 2004).

In our laboratory, a newly designed low-noise calibrated micro impactor provides precise traumatic injuries to the neonatal rodent spinal cord (Giuliano Taccola and John Fischetti, 2023). This device enables us to deliver different injury intensities and calibrations, facilitating the examination of early injury events. The device's low-noise design and stability at the impact site ensure continuous and stable DC recordings during and after the impact, without artifacts that could corrupt signal acquisition. Because the impactor is carefully shielded, it minimizes mechanical interference from conventional impactors' engines and pistons, which can otherwise affect electrophysiological recordings near the lesion site. It also enhances consistency in injury severity between animals by skipping variability from breathing and heartbeat.

To our knowledge, no other electrophysiological setups are available for recording spinal potentials in real-time. Existing attempts have recorded data only after a delay of over four minutes post-impact, following electrode replacement and repositioning, which undermines the reliability of pre-injury controls (Goodman et al., 1985). Using this setup, we can quantify the immediate events triggered by a physical insult to the spinal cord and continuously track their propagation both caudally to adjacent spinal segments and rostrally to brain structures. Additionally, we can evaluate any spontaneous functional recoveries within the neonatal spinal circuitry at least in the first 3 hours after trauma.

AIMS OF THE STUDY

The principal goal of this study is to investigate the immediate consequences of traumatic SCI, a topic that has not been extensively explored. By introducing a novel in vitro model of SCI, this research seeks to enhance our understanding of the early events following spinal cord trauma while continuously monitoring the preparation. The aim of the PhD project has been divided into three more targeted sub-aims:

Phase 1: Characterization of a novel in vitro preparation of the entire CNS isolated from neonatal rats.

- Probe the viability and functionality of the novel in vitro model of entire CNS from neonatal rats
- Examine the rhythmic spontaneous respiratory activity from upper cervical VRs and assess changes in respiratory patterns following the ablation of higher brain centers.
- Investigate conduction velocity of electrically induced responses though both ascending and descending white matter.
- Analyze motor-evoked responses elicited by electrical stimulation of various brain regions.
- Explore the role of supraspinal structures in modulating motor output.

Phase 2: Description of the early events occurring after a calibrated SCI in vitro using a customized micro-impactor.

- Validate the use of a novel impactor for simulating a contusive SCI in vitro and verify functional and histological disconnection of the cord after the traumatic damage.
- Probe the spontaneous respiratory rhythm before and after the injury.
- Monitor the dynamics of motor reflex responses around the time of injury.
- Examine the activity of spinal locomotor circuits and cord oxygenation before and after the injury.
- Examine the ionic disbalance associated with early events following the injury.
- Ascertain any immediate consequences in the brain after a spinal cord trauma.

Phase 3: Explore any pharmacological modulation of the early events following an SCI.

- Characterize the neurochemistry of the immediate phase of spinal cord injury.
- Explore the pharmacological modulation of the early events occurring after an SCI.
- Examine the dynamic of reflex recovery after spinal cord trauma in the presence of pharmacological agents.

Molecular Neurobiology (2021) 58:3769–3786
https://doi.org/10.1007/s12035-021-02370-5

GABAergic Mechanisms Can Redress the Tilted Balance between Excitation and Inhibition in Damaged Spinal Networks

Graciela Lujan Mazzone[1] · Atiyeh Mohammadshirazi[2] · Jorge Benjamin Aquino[1] · Andrea Nistri[2] · Giuliano Taccola[2]

Received: 8 November 2020 / Accepted: 22 March 2021 / Published online: 7 April 2021

Abstract
Correct operation of neuronal networks depends on the interplay between synaptic excitation and inhibition processes leading to a dynamic state termed balanced network. In the spinal cord, balanced network activity is fundamental for the expression of locomotor patterns necessary for rhythmic activation of limb extensor and flexor muscles. After spinal cord lesion, paralysis ensues often followed by spasticity. These conditions imply that, below the damaged site, the state of balanced networks has been disrupted and that restoration might be attempted by modulating the excitability of sublesional spinal neurons. Because of the widespread expression of inhibitory GABAergic neurons in the spinal cord, their role in the early and late phases of spinal cord injury deserves full attention. Thus, an early surge in extracellular GABA might be involved in the onset of spinal shock while a relative deficit of GABAergic mechanisms may be a contributor to spasticity. We discuss the role of GABA A receptors at synaptic and extrasynaptic level to modulate network excitability and to offer a pharmacological target for symptom control. In particular, it is proposed that activation of GABA A receptors with synthetic GABA agonists may downregulate motoneuron hyperexcitability (due to enhanced persistent ionic currents) and, therefore, diminish spasticity. This approach might constitute a complementary strategy to regulate network excitability after injury so that reconstruction of damaged spinal networks with new materials or cell transplants might proceed more successfully.

Keywords GABA · Spinal circuits · Spinal cord injury · Spinal shock · Neuroprotection · Spasticity

Synaptic Inhibition Is an Important Component of Spinal Locomotor Networks

In mammals, rhythmic motor tasks such as locomotion require balanced network activity based on the coordinated interaction between synaptic excitation and inhibition [1–3]. While inhibition typically dampens neuronal excitability, its overall impact traditionally depends on the reciprocal coupling to excitation in a "push-pull fashion," whereby inhibition declines as excitation rises and neuron excitability grows, and vice versa [4]. Studies of spinal networks have, however, indicated that, in certain circuits impinging upon motoneurons, synaptic inhibition remains operative even during excitation, suggesting that there are multiple sources of inhibitory inputs beyond the mutual interaction between excitatory and inhibitory local circuits [3]. These observations support the concept of recurrent connectivity [5] that should include a robust component of recurrent inhibition to prevent network instability and ensure multifunction flexibility [6]. In this framework, an important role is played by the neurotransmitter gamma-aminobutyric acid (GABA) that controls not only locomotor cycles but also network assembly during early development [7]. These properties are particularly expressed by a spinal circuit termed central pattern generator (CPG; [8, 9] that can produce rhythmic locomotor activity independent from sensory inputs). Such a process is readily replicated with a model system like the isolated rodent spinal cord which generates alternating rhythmic patterns termed fictive locomotion because of the absence of muscle targets [10]. While excitation is primarily mediated by glutamate and its pharmacological block arrests locomotion [11], blocking inhibition

✉ Giuliano Taccola
taccola@sissa.it

[1] Instituto de Medicina Traslacional (IIMT), CONICET-Universidad Austral, Av. Juan Domingo Perón 1500, B1629AHJ, Pilar, Argentina

[2] Neuroscience Department, International School for Advanced Studies (SISSA), Via Bonomea 265, 34136 Trieste, Italy

evoked by amino acid transmitters like GABA and glycine suppresses alternation of motor output by the CPG and replaces it with slow rhythmic motor discharges detected synchronously in ventral roots. This phenomenon is exemplified in Fig. 1 in which the fictive locomotor patterns elicited by co-applied *N*-methyl-D-aspartate (NMDA) and serotonin (5HT, see Fig. 1a) and recorded from ventral roots (VRs) are converted into slow synchronous discharges (Fig. 1b).

It should be noted that the GABA receptor antagonist bicuculline [13] is selectively blocking a distinct class of GABA receptors termed GABA A receptors (GABA ARs) known to mediate fast synaptic inhibition [14, 15] as well as to modulate neuronal excitability through extrasynaptic GABA receptors [16, 17]. The term "fast" inhibition, therefore, refers to the short time course underlining the loss of excitability mainly caused by hyperpolarization of the neuronal membrane (for less than 100 ms; [18]). Data in Fig. 1b also indicate that strychnine, a potent glycine receptor antagonist, contributes to block fast inhibition and suggests that, in addition to GABA, glycine is an important mediator of locomotor activity [19, 20].

Indeed, intrasegmental GABAergic and glycinergic interneurons with short axons have been found in ventral laminae where locomotor circuits are located [21]. On in vitro spinal networks, application of strychnine alone evokes irregular and asynchronous discharges while application of bicuculline per se produces a more structured repetitive activity [22, 23]. It may also be suggested that when one type of synaptic inhibition is blocked, the other one can at least in part expand its role because the circuitry is not arrested in a state of sustained excitation. It is noteworthy that the persistent rhythmic activity evoked by the convulsants strychnine and bicuculline is not associated with extensive neuronal or glial death [24, 25], indicating that spinal networks are far more resistant than brain networks to seizure-evoked neurodegeneration [26].

Principal Properties of GABAergic Mechanisms in the Spinal Cord

GABA is produced by decarboxylation of L-glutamate by glutamic acid decarboxylase (GAD), of which two isoforms

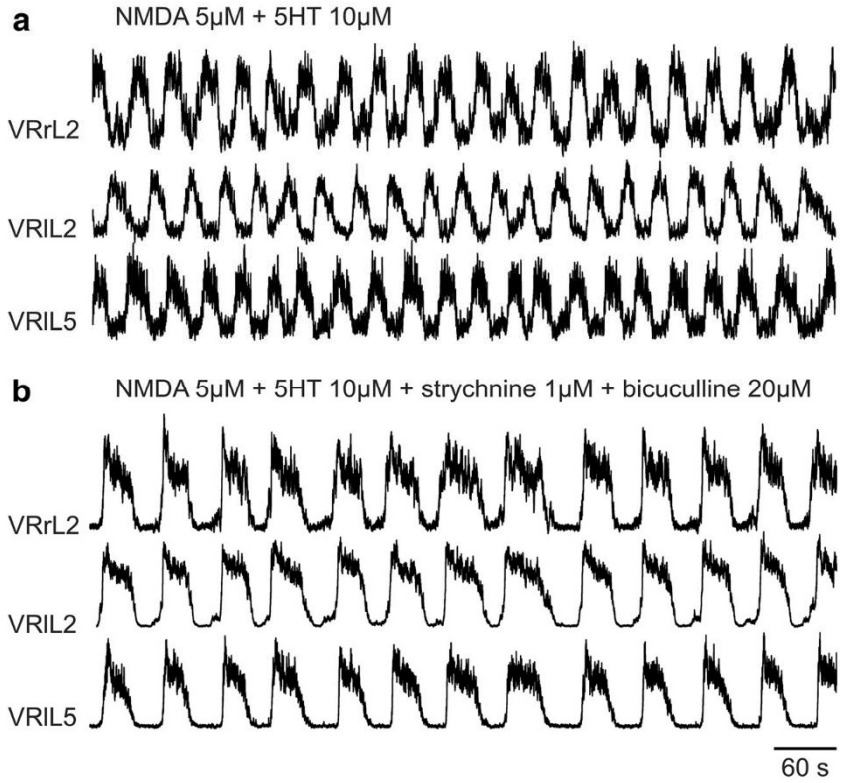

Fig. 1 During locomotor patterns, fast synaptic transmission is essential to allow the sequential activation of antagonistic motor pools innervating flexor and extensor hindlimb muscles. **a** A stable locomotor-like rhythm is induced in the spinal cord isolated from a neonatal rat by co-application of the glutamate agonist NMDA plus 5HT. The rhythm reflects the basic pattern of activation of lower limb muscles during real locomotion, which is composed of electrical discharges characteristically alternating between right (r) and left (l) ventral roots (VRs, exemplified in this figure at the second lumbar segment; L2) and between flexor (L2)- and extensor (L5)-related ventral roots on the same side of the cord (shown in this figure as the left L2 and L5). **b** On the same preparation, strychnine plus bicuculline are further applied to block glycinergic and GABAergic fast inhibitory transmission, respectively. Starting from 30 s after drug application, the double alternating pattern is replaced by a stable and slower rhythm that becomes synchronous among all ventral roots (unpublished traces, replicating results originally reported by Beato and Nistri, [12])

exist: the transiently activated GAD65, which synthesizes vesicular GABA to be released by exocytosis, and the constitutively active GAD67, responsible for cytosolic GABA released by paracrine diffusion [27, 28]. In the spinal cord, GAD67 immunostaining has been found in cell bodies and fibers, while GAD65 is mainly located at synaptic terminals [29]. In addition to GABA locally released by spinal neurons and glial cells, GABAergic descending projections from the ventromedial medulla of the brainstem reach ventral and dorsal horns [30–32]. The development of the spinal GABAergic system is guided by several descending projections and the perinatal interruption of these projections impairs the regulation of GABA synthesizing enzymes [33] and receptors in the spinal cord [34]. For instance, interruption of descending serotoninergic input disrupts maturation of spinal GABAergic systems [34].

GABA acts on multiple ionotropic receptors, namely the A subtype, which drives a fast synaptic inhibition and the C subtype, whose role in the spinal cord is however limited, even if functionally expressed in the postnatal mammalian spinal cord [35]. Moreover, GABA acts as mediator of presynaptic inhibition by activating the G protein–coupled B receptor involved in a slower neuromodulating action particularly at presynaptic level via inhibition of calcium conductances [15, 18].

In adult neurons, GABA A receptor–mediated inhibition is due to the permeation of Cl^- (and HCO_3^-) through an intrinsic channel that drives an influx of Cl^- into the postsynaptic cell (Fig. 2a) [36, 37]. Conversely, in the first postnatal days of life, the opening of GABA ARs coincides with the Cl^- electrochemical gradient (driving force) set at the less negative value and, thus, it drives Cl^- efflux across the neuronal membrane. This phenomenon decreases intracellular negative charges with consequent cell depolarization from resting potential. It should also be noted that the opening of Cl^- channels reduces membrane resistance and temporarily determines a conductance short-circuit (shunting), which limits further depolarization by incoming excitatory inputs. Thus, GABA-mediated depolarization exerts an inhibitory function in neonatal spinal neurons [37]. An action similar to GABA on neonatal neurons is displayed by afferent terminals throughout their maturation and adult stages, due to the high concentrations of intracellular Cl^- in Dorsal root ganglions (DRGs) [38].

It is important to emphasize that, in the neonatal spinal cord, the functional outcome of GABA-mediated activity may depend on the location of GABAergic synapses on postsynaptic neurons and their Cl^- equilibrium potential [39] because the shunting effect is briefer than the membrane depolarization that, if prolonged, may facilitate excitation [39].

Noteworthily, there is also a subpopulation of extrasynaptic GABA ARs with distinct subunit composition and high affinity to GABA [16, 17, 40], generating tonic modulation of

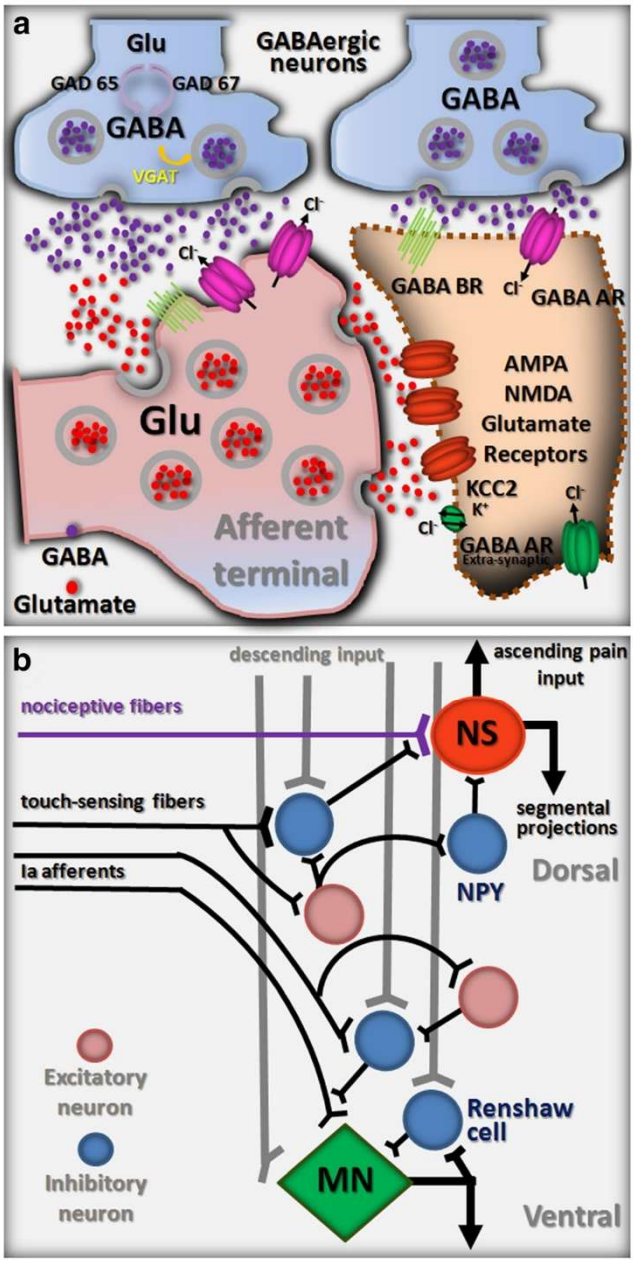

Fig. 2 GABA-mediated inhibition at the cellular and network levels. **a** Schematic representation of two prototypical GABAergic synapses mediating pre (left)- and post (right)-synaptic inhibition, respectively. The main cellular and molecular players relevant to a spinal cord injury are depicted as discussed in this review. **b** Simplified wiring diagram of the basic GABAergic circuits involved in presynaptic inhibition of afferent input. NS, nociceptive-specific projection neuron; MN, motoneuron

sensory transmission [41]. As exemplified in Fig. 3a, b, for the strong distribution of GABAergic GAD67 neurons in the dorsal horn, the corresponding expression of GABA ARs is intense in inner dorsal laminae (II, III), around the central canal (X), and the ventral horns (VII-IX), where GABA ARs are found at axo-axonic contacts and extra-synaptic sites [43, 44].

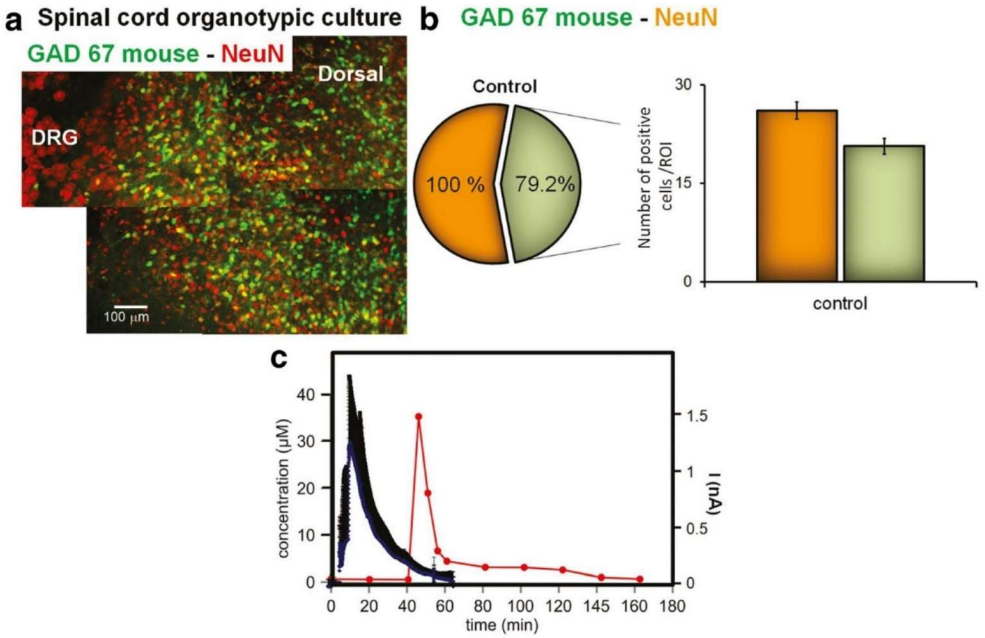

Fig. 3 Expression of GABAergic neurons in the spinal cord and real-time glutamate release from spinal cord following experimental spinal cord injury (SCI). **a** Typical neuronal staining with neuronal nuclear protein (NeuN; red) restricted to the spinal cord tissue region in a spinal cord slice of a GAD67-glial filament protein (GFP) expressing mouse (green). Example of 22 DIV slice with two regions of interest (ROIs), namely a dorsal and a ventral horn, and a dorsal root ganglion (DRG). **b** Histograms showing the number of GAD67-positive cells (light green columns) or NeuN-positive cells (orange columns) at 22DIV, in control slices. Inset with the circle chart showing the percentage of GAD67 from NeuN-positive cells (redrawn from Mazzone and Nistri, 2019). **c** Examples of the time-course of endogenous glutamate release detected by glutamate biosensor in cultures that were treated with 0.5 mM kainate (blue traces, mean ± SD, n=5 slices). Glutamate concentrations in microdialysis samples collected after spinal cord injury, filled circles (redrawn from [42])

Neuronal Chloride Homeostasis in the Spinal Cord is Regulated by Two Transporters

The synaptic action of GABA and glycine depends on the intracellular concentration of Cl^- that is primarily maintained by cation-chloride co-transporters [45]. Among the most important families of Cl^- transporters, the Na^+-K^+-$2Cl^-$ cotransporter 1 (NKCC1) and KCC2 reciprocally control the intracellular Cl^- concentration whose efflux causes, for instance, primary afferent-mediated depolarization with depression of excitatory inputs [46, 47]. Cl^- transport into the cell is mostly due to NKCC1 activity, whereas KCC2 extrudes Cl^- via a fast and concentration-dependent process generated by Na^+/K^+-ATPase [46, 47]. Previous studies have demonstrated that Cl^- transporter expression and Cl^- homeostasis are regulated by developmental changes that include gene transcription modification, posttranslational and trafficking alterations [47–49]. NKCC1 expression is widespread in neurons, glial, blood vessels, and other epithelial cells in the developing and mature central nervous system [50]. On the contrary, KCC2 is restricted to the somatodendritic membrane of mature central neurons and is almost absent in neuronal axons, peripheral neurons, and non-neuronal cells [51, 52]. Due to the broad NKCC1 distribution, NKCC1 null mice have been used to examine the transporter expression and its impact to induce abnormal GABA responses by DRG [53] and cortical neurons [54].

The strength of postsynaptic inhibition, related to Cl^- homeostasis, is hampered in several pathophysiological conditions [55] such as seizure, epilepsy, stroke, and ischemic injury [33, 56] and proprioception disorders [57]. Indeed, impaired excitation/inhibition balance due to changed NKCC1 or KCC2 expression was also related to chronic stress [58], brain or peripheral injury [47, 59], and locomotor activity after spinal cord injury [60, 61] or developmental changes [62–64].

In rodent models of spinal cord injury, the role of intracellular chloride concentration and the modulation of cation chloride co-transporter expression have been amply investigated [65, 66]. In particular, synaptic inhibition, KCC2 and NKCC1 expression, and functional recovery were reportedly improved by programmed exercise or bumetanide, a pharmacological antagonist of NKCC1, 28 days after spinal cord transection in rats [67]. Similarly, a reduction in tissue damage and edema was observed by using bumetanide in a spinal cord contusion model [68]. A recent study has shown that the application of anodal trans-spinal direct current stimulation plus bumetanide administration downregulated the expression of NKCC1 after spinal cord contusion with significant amelioration of spasticity and locomotor muscle tone [69]. This is strong evidence

that modulation of chloride homeostasis by NKCC1 pharmacological regulation during pathological conditions such as spinal cord injury can favor locomotor network improvement.

Presynaptic GABAergic Inhibition and Neuropathic Pain

Depolarizing axo-axonic synapses on primary afferent fibers filter incoming input from the periphery via membrane shunting and Na^+ channel inactivation [38]. This basic wiring scheme fulfills multiple functions in sensory-motor networks. Indeed, a first mechanism to gate pain signals is represented by touch-sensing fibers depolarizing nociceptive primary afferents, thus causing pre-synaptic inhibition of nociceptive input. Furthermore, presynaptic primary afferent depolarization also contributes to shaping motor reflexes and efficiently modulates rhythmic motor behaviors, such as stepping and scratching, in response to proprioceptive input about joint position. Descending commands targeted to local interneurons control the efficiency of presynaptic inhibition triggered by peripheral inputs (Fig. 2b). Although this key frame is complicated by additional neuronal elements that release several types of neurotransmitters and neuropeptides onto primary afferents, the role of GABAergic interneurons remains crucial.

Based on the expression of transcription factors, different subtypes of spinal interneuron with distinct settling positions, neurotransmitter expression, and profiles of connectivity have been identified [70], among which a few have an inhibitory phenotype [9]. In particular, an adenovirus vector including a neuropeptide Y promoter has been recently used to discover, in the superficial dorsal horn, a subset of inhibitory GABAergic interneurons (AAV-NpyP) with the ability to prevent the conversion of touch-sensing signals into pain-like behavioral responses [71]. This class of interneuron receives mono- or polysynaptic excitatory inputs from touch-sensing fibers and uses GABA for transmitting inhibitory signals to lamina I neurons that project to the brain, thus avoiding abnormal excitation following innocuous mechanical stimulations (Fig. 2b). Dysfunctions of GABAergic transmission at the level of dorsal microcircuits impair the mechanisms of presynaptic inhibition, resulting in neuropathic pain states [72]. Neuropathic pain is one of the most frequent complications in paraplegics, with an incidence of 53% [73], and is often treated with GABAergic drugs [74, 75].

Indeed, the severity of neuropathic pain states following an experimental SCI [76] and other neurologic disturbances [77] is correlated to a reduced GABAergic tone, as the loss of GABAergic inhibitory interneurons in the superficial dorsal horn is verified by the reduction in GAD65/67 immunostaining. Thus, interventions for restoring the impaired production of GABA and GADs in the dorsal horns also alleviate pain states [77].

NKCC1 is crucial for the accumulation of Cl^- in DRG neurons, leading to depolarizing GABA responses on primary afferents. Different studies demonstrated a transient upregulation of NKCC1 at DRG neurons after nerve injury indicating that Cl^- efflux contributes to presynaptic inhibition and neuropathic pain induction [78–80]. Consequently, transgenic knockout mice lacking NKCC1 show impairments of presynaptic inhibition and significant alterations in locomotor and pain behaviors [53, 81]. Recently, disruption of NKCC1/KCC2 balance and chloride gradient below the injury site were found after spinal cord cervical contusion demonstrating the contribution of Cl^- homeostasis for spasticity and chronic pain [82]. Indeed, in a rat model of neuropathic pain, the use of the extrusion enhancer CLP257, a KCC2-selective analog that lowers Cl^- intracellular concentration, can alleviate hypersensitivity [83]. Hyperalgesia and allodynia were improved by using bumetanide for 2 weeks following sciatic nerve lesion, demonstrating the role of cation chloride co-transporter expression to modulate nociceptive pathways [84]. These data demonstrate that neuronal GABA neurotransmission is dependent on precise regulation of the level of intracellular chloride, which is determined by the coordinated activities of cation chloride co-transporters and could open new perspectives to prevent or alleviate neuropathic pain and functional recovery after SCI.

Collectively, these data show notably similar features between SCI and neuropathic pain, as they may both originate from alterations of presynaptic GABAergic mechanisms, which in turn broaden the potential translation of novel approaches to redress the tilted balance between excitation and inhibition in either neurological conditions.

Glycine Is a Fast Inhibitory Transmitter in the Spinal Cord

In adult rats, GABAergic axon terminals represent only 20% of the inhibitory input converging onto lumbar motoneurons, while the remaining 80% are glycinergic [85].

Glycine is a fast inhibitory transmitter on spinal motoneurons [19, 86], and it might be co-released with GABA at certain synapses [87]. However, not all synaptic boutons on motoneurons have both inhibitory neurotransmitters, but rather a strong prevalence of glycine alone [88]. Postsynaptic GABA A and glycine receptors are often, albeit not necessarily, co-localized [89] and aggregated in clusters formed by the submembrane scaffolding protein gephyrin [90, 91].

The glycinergic system is relatively insensitive to spinal transection [92]. Indeed, both the density of glycine receptors on motoneurons and the kinetics of glycine-mediated currents remain unchanged [34]. In accordance with these observations, the concentration of glycine, as determined by HPLC on spinal cord homogenates (2–12 h

after spinal cord contusion), is preserved [93]. Only much later (3 weeks from transection), the expression of glycine receptors is temporarily decreased with subsequent recovery and re-emergence of physiological reflexes [94]. After complete spinal transection, the comparatively well-preserved glycinergic system at segmental level below the lesion may represent one significant component for neurorehabilitation protocols [92].

Since the main focus of the present review manuscript is the dysfunction of GABAergic mechanisms in damaged spinal networks, we refer the reader to previous work to examine the role of glycine after SCI [34, 92, 94–97].

Early Peak of GABA Immediately after SCI

Mechanical impact to the spinal cord massively increases the extracellular concentration of several neurotransmitters including GABA. Experimentally, a strong increase of GABA at the lesion site has been observed shortly after an SCI in vivo [42] following the very early rise in glutamate concentration (Fig. 3c). The increased extracellular concentration of GABA rapidly declines following SCI and later recovers to the pre-trauma levels [42, 93, 98]. The peak of GABA after SCI originates from not only the destruction of the membrane of GABAergic and glia cells but also the synaptic release at the site of injury [99] facilitated by spreading depolarization along the injured tissue [100]. The contribution of circulating GABA leaking through the impaired blood-spinal barrier is probably a minor one as GABA concentrations in the plasma [101, 102] are far below the ones found at the lesion site. Nevertheless, there might be enough GABA to activate highly sensitive extra-synaptic GABA receptors such as the ones incorporating the δ subunit [40]. An additional contribution to the peak in extracellular GABA immediately after SCI comes from the reversed function of membrane GABA transporters that depend on Na^+ concentrations. In both neurons and glia, physiological reuptake of GABA is coupled to Na^+ and Cl^- inflow into the cell [103]. The increased concentration of intracellular Na^+ (and Cl^-) caused by spreading depolarization following an acute injury reverts the transport systems to extrude GABA [104]. At the same time, downregulation of the vesicular GABA transporter caused by SCI [105] increases the amount of cytosolic GABA available for extrusion.

The peak of GABA corresponds to the onset of a transient depression of spinal reflexes below the level of injury named spinal shock [106] typically present after severe spinal contusions in rats [107], although rarely found after surgical transection of the cord [108]. We, therefore, propose a role for GABA in spinal shock alongside a similar role for glycine [96].

Fast Synaptic GABAergic Transmission Is Early Affected by Spinal Cord Injury

The excitation/inhibition balance ensures physiological motor responses executed by healthy spinal cords and may be directly altered by SCI. Future studies are required to clearly identify the components of the locomotor systems primarily altered after SCI and their impact on the excitation/inhibition balance. In broad terms, changes in excitation/inhibition balance might originate from an alteration in cellular mechanisms and/or disruption and rewiring of local networks. Hence, in response to spinal damage, GABAergic cells show particular vulnerability, as their number decreases [109]. One reason for their vulnerability might be their location because important members of the spinal GABAergic population are commissural interneurons, which cross the midline and project ventrally, thus offering a long section liable to injury [110]. Furthermore, the ventral region is vulnerable to SCI because of its dense vascularization prone to produce large hemorrhage and neuronal loss [111]. In addition, in the acute phase of SCI, complex neurodegenerative events develop to generate a secondary injury that amplifies and spreads damage to the neighboring tissue [112]. Our former studies have provided a comparative description of the different neuronal cell types with particular vulnerability to injury [25, 113, 114]. In the early phases of experimental SCI, significant reduction in GABAergic GAD65 expression occurs at the injury site [115].

One important contributor to secondary injury is the overactivation of glutamate receptors, leading to a massive influx of calcium ions into spinal cells and contributing to the release of free radicals from mitochondria, such as reactive oxygen and nitrogen species, in turn triggering intracellular toxic cascades (excitotoxicity; [25, 113, 116–118]).

The oxidative stress occurring during secondary damage is one important cause for the impairment in GABAergic neurotransmission, because reactive oxygen species increase synaptic release of GABA [119, 120] that desensitizes GABA ARs [121]. Reactive oxygen species also alter the function of GABA A receptor-gated Cl^- channels due to a reduced driving force for Cl^- because of failure of its transport [122]. In addition, free radicals alter the binding characteristics of GABA, possibly by affecting redox-sensitive receptor sites or via peroxidation of membrane lipids surrounding the receptor [122].

GABAergic descending inputs that control motoneuron excitability are also damaged by SCI contributing to functional motor deficits and other disabling consequences. In the majority of people with chronic SCI, paralyzed muscles are often accompanied by involuntary contractions (spasticity), increased resistance to passive stretch (muscle hypertonia), and exaggerated motor responses to light peripheral

stimulation (hyperreflexia; [123]). Indeed, despite the reduced excitability of axons at the periphery [124], a brief sensory stimulation (< 20 ms) evokes a prolonged depolarization (~ 1 s) of single motor units apparently without efficient synaptic inhibition. Conversely, the same light afferent stimulus applied to neurologically intact subjects generates a sustained depolarization interposed by an inhibitory phase [125]. The increased amplitude that characterizes motor responses after SCI and the lack of inhibitory contributions have been associated with multiple neuronal mechanisms at both cell and network levels. While the increased excitation should be, at least in part, attributed to the activation of Na^+ and Ca^{2+} persistent inward currents (PICs) in motoneurons [126–130], a pivotal role in reduced inhibition has been ascribed to depression in GABAergic transmission [92, 131]. Indeed, at presynaptic level, despite the increased size of GABAergic synapses, the lower number of vesicles in the active zone [132] determines less neurotransmitter available for release. At the same time, an SCI also produces aberrant hyper-connectivity among GABAergic interneurons, with the formation of new axo-axonic synapses [132] that, along with changes in Cl^- transporter isoforms, might contribute to the disinhibition reported after SCI [133].

Noteworthily, dysregulation of the balance between excitation and inhibition may also result from changes in other components of the spinal network after injury. For instance, aberrant sprouting of primary afferents or expansion of interneuronal receptive and projective fields after SCI may augment the excitatory drive to spinal networks [134]. On the other hand, inhibition is affected by the interruption of serotoninergic descending tracts, which modulate inhibitory interneurons, like Renshaw cells [135, 136]. Moreover, Renshaw cell recurrent circuitry might become disconnected from motoneurons [137] suppressing their excitatory drive to Renshaw cells, in turn reducing the GABAergic inhibitory feedback. Also, changes in long-term gene expression, such as upregulation and phosphorylation of several signaling proteins in spinal ventral horns, have been linked to early and long-term changes in spinal excitability, leading to spasticity states after spinal trauma [138].

Furthermore, circuit reorganization after spinal cord injury occurs also at the supraspinal level. The strength of brainstem reflexes is enhanced as a result of increased excitability and reduced GABA-mediated inhibition in the brainstem circuits that project to spinal interneurons [139].

Table 1 shows interventions aimed at normalizing the altered excitability after injury from multiple experimental settings. Pharmacological manipulations, transplants of different cell lineages, and activity-dependent protocols have been applied in the acute and chronic phases of SCI to exploit GABA-related mechanisms and rescue homeostasis between excitation and inhibition.

Despite the plethora of experimental approaches, restoring physiological spinal inhibition in the clinic remains a timely and demanding challenge that requires further studies. Indeed, potentiating the GABAergic system, when not carefully timed, might even hinder activity-based rehabilitation and electrical neuromodulation protocols for motor recovery, by depressing synaptic transmission [149] and reducing excitability of locomotor spinal circuits [150].

Pharmacological Neuroprotection by GABA Modulation after Experimental Lesion

Several GABAergic mechanisms targeted at restoring functional homeostasis and rescuing neuronal loss after injury have been explored with different experimental models (Table 1). For their part, reduced preparations from neonatal rodents suggest that a large rise in extracellular glutamate is responsible for the excitotoxicity arising early after SCI (Fig. 3c). In this model, excitotoxicity is produced by transient application of the powerful glutamate analog kainate [151]. While glutamate excitotoxicity can be attenuated with agents that decrease its release [152–156], a distinct approach is to boost inhibition to render spinal neurons less excitable. Thus, neuroprotection by general anesthetics like methoxyflurane and propofol indicates that this process effectively counteracts excitotoxicity [157–159] albeit through distinct molecular mechanisms. In fact, while methoxyflurane primarily acts by hyperpolarizing motoneurons via opening a voltage-independent K^+ channel [159], propofol enhances GABA ARs activity by binding to a discrete allosteric site [158]. The implication of these results is that neuronal inhibition, regardless of its effector mechanisms, is an important factor to contrast excitotoxicity. Nevertheless, using general anesthetics as a neuroprotective drug is complex and prompts the search for alternative approaches. In line with this strategy, more direct investigation into the effects of GABA receptor agonists and antagonists on experimental spinal damage has shown that modulation of extrasynaptic GABA ARs could prevent excitotoxic death of spinal organotypic cultures [143]. In particular, the allosteric GABA A modulator midazolam and the GABA agonist 4,5,6,7-tetrahydroisoxazolo [5,4-c] pyridin-3-ol (THIP; preferentially acting on extrasynaptic receptors) are powerfully effective [143]. In addition, the GABA AR antagonist bicuculline prevents the neuroprotective effect of propofol via GABA AR function, suggesting the importance of GABA receptor activity in modulating excitotoxicity [157]. Endogenous neurosteroids can also induce neuroprotection by upregulating GAD67 enzyme level [160] or GABA AR function [161]. Thus, even if transient changes in GABAergic synaptic transmission after SCI might not be immediately translated into neuroprotection, other GABAergic targets are available to perform this role.

Table 1 GABAergic mechanisms targeted to rescue altered inhibition

Intervention		Model	GABAergic mechanisms	Main outcome	Reference
Physical exercise	• Treadmill running	• Partial sciatic nerve (PSL) ligation in adult C57BL/6 J mice	• Restoration GABAergic interneuron numbers • Upregulation of GAD65/67 immunoreactivities	• Alleviates allodynia and heat hyperalgesia • Positive correlation between GABA levels and the thresholds of von Frey or plantar tests	Kami et al. (2016) [77]
Physical exercise & Pharmacology	• Cycling exercise • Bumetanide (NKCC1 antagonist) • DIOA([(dihydroindenyl)oxy]alkanoic acid; KCC2 antagonist)	• SCI complete transection in adult female Sprague Dawley rats	• Increase in KCC2 levels and decrease in NKCC1 expression levels • Blockage of NKCC1 impacts on reflex recovery • Apparent modulation of KCC2, but not NKCC1, by BDNF	• Exercise contributes to functional recovery by restoring chloride homeostasis	Côté et al. (2014) [67]
Pharmacology	• CLP290 (KCC2 agonist) • Bumetanide (NKCC1 inhibitor) • 8-OH-DPAT (5HT1A/7 agonist) • Quipazine (5HT2A/C agonist) • CP101606 (NMDA receptor antagonist) • Baclofen • L838414 (GABA A-positive allosteric modulator)	• SCI bilateral hemisection in adult mice	• Increase in KCC2 function	• Restores inhibition in the injured spinal cord, leading to functional recovery	Chen et al. (2018) [140]
	• CLP257 • CLP290	• NG-108 cell line and HEK293-cl cells • Horizontal spinal dorsal horn slices obtained from animals with peripheral nerve injury (PNI) • PNI in adult male Sprague-Dawley rats	• CLP257 and CLP290 enhance Cl^- extrusion	• CLP257 has antinociceptive properties in PNI animals	Gagnon et al. (2013) [83]
	• Intrathecal administration of brain-derived neurotrophic factor (BDNF) and of BDNF sequestering agent, TrkB-IgG	• SCI transection in adult male Sprague-Dawley rats	• Increase in KCC2 expression post-SCI by BDNF	• BDNF plays an antinociceptive role	Huang et al. (2017) [141]
	• Activation of 5-HT2A receptors with TCB-2	• SCI hemisection in adult female Wistar rats • Peroneal and tibial nerve injury by ligation and transection • Injection of TCB-2 and intrathecal DIOA injection	• Increase in membrane KCC2 expression	• Restores motoneuronal inhibition, and reduces SCI-induced spasticity, mechanical and thermal hyperalgesia • Nerve injury-induced neuropathic pain was not attenuated by TCB-2	Sánchez-Brualla et al. (2018) [142]
	• Midazolam (allosteric GABAA modulator) • THIP (GABA agonist) • Bicuculline • Gabazine (antagonist of GABA ARs) • Strychnine • L-Alanine	• Mouse organotypic spinal slice cultures, excitotoxicity induced by kainate	• Increase in GABA receptor activity through pharmacological GABA agonism	• Decreases excitotoxic death in spinal networks in vitro	Mazzone and Nistri (2019) [143]
	• TGN-20 (AQP4 inhibitor) and bumetanide	• SCI contusion rats	• Upregulation of AQP4 mRNA and reduction of NKCC1 expression	• Reduces SCI edema and tissue destruction	Yan et al. (2018) [68]

Table 1 (continued)

Intervention		Model	GABAergic mechanisms	Main outcome	Reference
	• Anodal trans-spinal direct current stimulation and bumetanide	• SCI contusion in CD-1 mice	• Upregulation of NKCC1	• Reduces spasticity and increases muscle tone	Mekhael et al. (2019) [69]
Transplantation	• Transplantation of MGE-like cells derived from human embryonic stem cells (hESC-MGEs)	• SCI moderate contusion in B6.CB17- Prkdcscid/SzJ transgenic mouse	• Migration and differentiation into GABAergic neurons subtypes	• Transplanted cells functionally integrate into host's spinal cord • Attenuate mechanical allodynia of hind paws • Sustained motor recovery	Fandel et al. (2016) [144]
	• Transplantation of embryonic precursors of GABAergic neurons from medial ganglionic eminence (MGE)	• Peripheral nerve injury models of neuropathic pain in adult mouse	• Differentiation into GABAergic neurons	• Transplanted cells functionally integrate into host's dorsal horn circuits	Llewellyn-Smith et al. (2017) [145]
	• Transplantation of fetal neural stem cells (fNSC) extracted from the telencephalic vesicles (TV) and the ventral medulla (VM)	• SCI contusion in adult Wistar rats	• Differentiation into GABAergic neurons • Greater proportion of GABAergic cells from the TV group compared to the VM group	• Improves from thermal hyperalgesia • Ameliorates mechanical allodynia	Batista et al. (2019) [146]
	• Transplantation of differentiated human induced pluripotent stem cell-derived GABAergic (iGABAergic) neurons	• Peroneal and tibial nerve injury by ligation and transection in adult mice	• Differentiation into GABAergic neurons. • VGAT and GAD65/67 expression	• Transplanted cells functionally integrate into host's dorsal horn active inhibitory circuits • Reduces tactile allodynia	Manion et al. (2020) [147]
	• Transplantation of GABAergic neural progenitor cell and intensive locomotor training (ILT)	• SCI compression in adult male Sprague Dawley rats	• Upregulation of KCC2	• Reduces mechanical allodynia and thermal hyperalgesia • Reduces pro-inflammatory markers	Dugan et al. (2020) [148]
Genetic manipulation	• NKCC1 gene ablation in DRGs • Bumetanide	• NKCC1 knockout mice, deletion of exon 9 of the gene	• Absence of Cl- accumulation in DRGs • Absence of GABA depolarizing responses	• Alters nociception and motor coordination	Sung et al. (2000) [53]

Interestingly, cultured motoneurons show that the excitotoxic action of glutamate is limited by direct application of GABA agonists [162, 163].

The neuroprotective role of GABA as well as the activation of different GABA receptors following insults to the CNS [15] may represent potential targets to limit damage and develop innovative and selective therapeutical approaches.

However, side effects of current pharmacological therapy for other neurological disturbances, as epilepsy, suggest potential risks from potentiating GABAergic mechanisms [164]. Likewise, the use of the anticonvulsant baclofen determines muscle weakness and sedative effects [165], along with a baclofen-withdrawal syndrome, with a psychotic status when the drug is abruptly discontinued [166]. However, since GABA BRs are less prone to receptor desensitization, the abovementioned adverse effects are likely to be more pronounced than interventions targeted to GABA ARs.

Neurons and Astrocytes May Counteract Excitotoxicity via GABAergic Mechanisms

One key element to modulate synaptic transmission and neuronal network activity seems to be the presence of astrocytes and the type of neuron involved [167]. It is now widely accepted that astrocytes can modulate neuronal activity through the tripartite synapse [168]. Thus, cells immunoreactive to S100β (a cytoplasmic calcium-binding protein mainly expressed by glia), may take part in tissue protection and repair, as well as they are useful biomarkers for brain or spinal cord injury [169]. These cells are the most abundant astrocyte cell type in the ventral horn area and less abundant in the dorsal horn [170]. The differential distribution of glial cells within the spinal cord regions might be an important factor in considering the high vulnerability of neurons to excitotoxicity [25, 113, 114]. Accumulating evidence demonstrates the role of astrocytes in GABA synthesis and release, as well as in the activation of GABA receptors on neighboring neurons [60]. During synaptic transmission, GABA release triggers astrocytic release of calcium from the endoplasmic reticulum via the inositol 1, 4, 5-trisphosphate pathway [171]. As pointed out by Christensen and collaborators [172], in the dorsal horn of adult turtle, astrocytes coordinate calcium-mediated excitation and tonic inhibition by GABA ARs to induce phasic release of GABA. Finally, lampreys show spontaneous functional recovery and neuroprotection after complete SCI that depends on astrocytes properties related to GABA accumulation and neurotransmitter uptake [173].

Although promising for the design of novel interventions to rescue cellular loss after spinal damage, these results must be considered with caution and must be supported by compelling new studies to validate any translation to clinical use. Potential limitations can originate when interpreting results coming from different species, genders, age, phases of lesion, and injury protocols (Table 1). In fact, the distribution of GABA ARs and their binding properties might vary among different strains [174], while also circulating sex hormones affect the sensitivity of GABA ARs to the allosteric endogenous modulator allopregnanolone in females [175]. Moreover, mechanical properties of the spinal cord change with size, making it hard to compare the severity of experimental injuries among studies of animals at different developmental stages [176].

Prolonged Dysfunction of Fast GABAergic Transmission after SCI

After spinal cord transection, the number of GABA ARs increases in fast flexor motoneuronal pools and synaptic clustering augments as a consequence of subunit overexpression. This latter feature is reversed to control after step training and aids functional recovery [177]. Furthermore, long-term changes in protein and mRNA levels of GAD67 (but not GAD65) have been found after a chronic transection, possibly leading to increased GABA production in spinal neurons below the site of injury [29]. Interestingly, GAD67 is the predominant form in ventral horn neurons around motoneuronal pools [178] and the recovery of locomotor functions in SCI rats corresponds to a return of GAD67 toward baseline levels [179].

Enhancement in motoneuron excitability stems from their dysregulation of intracellular Cl^- caused by the spinal lesion itself [180]. In lumbar motoneurons, thoracic SCI reduces the expression of KCC2 which co-transports potassium and Cl^- outside the cell [181]. The switch of GABA A from inhibition to excitation contributes to the spasticity of hind limbs [182]. In fact, upregulation of KCC2 after transection restores some locomotor activity in the mouse [140].

The interaction between excitation and inhibition at chronic stages of SCI remains an incompletely understood process as much as the relative weight of GABA and glycine mediated transmission. In fact, although glycine receptor operation is also sensitive to intracellular Cl^- [183, 184], the kinetics of glycinergic currents are not affected after spinal transection [34] and the administration of glycine continues to produce inhibitory effects and limit spasticity after SCI [95]. Pharmacological block of both GABA A and glycine receptors prolongs spasms in chronically transected animals, confirming that a degree of fast inhibition remains efficacious even after lesion [95, 185]. In keeping with these observations, optogenetic activation of spinal inhibitory interneurons silences spasms evoked by electrical afferent stimulation [185]. Conversely, Edgerton and Roy [186] have proposed low doses of pharmacological blockers of Cl^--mediated inhibition for recovery of gait in injured animals. Antagonism of

inhibitory transmission has been claimed to facilitate locomotion by limiting excessive inhibition following SCI [97, 187, 188].

In sum, after SCI, the excitability of spinal networks at rest is changed at distinct nodes of the pre-motor neuronal circuitry by the appearance of complex contributions with a very fine balance among them. On the one hand, GABA-mediated depolarizing signals result from the reversed Cl^- gradient [182, 189]. On the other hand, supplementary GABA-mediated inhibitory input arises from upregulation of GABA synthesis [178], overexpression of GABA AR subunits [34, 177], and a greater activation of inhibitory interneurons [185]. Ultimately, whether synaptically released GABA can either inhibit or facilitate excitatory inputs depends on the time course of the event and its membrane topography on the post-synaptic neuron [39]. Hence, the longer lasting the effect of GABA is, the higher is the likelihood of inducing neuronal excitation.

Factors Regulating the Excitability of Motoneurons after SCI

First, chronic changes in motoneuronal excitability after human SCI depend on how close these cells are to the site of spinal injury. Namely, while perilesional motoneurons are hypo-excitable, those farther from the lesion epicenter show increased excitability [190]. In line with this finding, in subjects with incomplete SCI, corticospinal pathways evoke aberrantly high facilitation of motor output distant from the epicenter of the lesion. Conversely, no change is reported at the level of injury and nearby segments [191]. Animal experiments indicate that sustained depolarization of sacral motoneurons below the lesion [192] is accompanied by hypertonia, hyperreflexia, and clonus [193, 194]. Other studies have demonstrated aberrant membrane properties of lumbar motoneurons underlying hind limb spasticity after thoracic spinal lesions in rodents although direct evidence for the excitability of motoneurons close to the contusion site is still missing [181, 189]. While motoneuron properties (essential to support motoneuron firing) slowly recover to their preinjury state, their corresponding receptive fields remain broad so that sensory input to even a small area of the limb can trigger widespread excitation capable of generating whole-limb spasms [195]. Further studies are eagerly awaited to explore whether different states of excitability of motoneurons proximal and distal to an SCI are related to the early transient changes in extracellular GABA concentrations at the epicenter of injury. Potentially, these findings might bring novel pharmacological interventions to acutely modulate GABAergic transmission below the lesion [196] with the timely goal of preventing the onset of spasticity in addition to the widely-used administration of the GABA BR agonist baclofen [197]. In particular, an important issue is whether activation of spinal GABA ARs may be able to counteract the upregulation of the persistent sodium current of motoneurons typically observed after lesion [198]. This conductance is considered to be the target for neuromodulation, a phenomenon in which GABA is expected to play a role [199]. PICs which comprise sodium as well as calcium conductances [126–130, 200] contribute to the nonlinearity between the level of network excitation and motor output [201]. As spinal neurons possess strong plasticity during recovery after SCI [202], GABA AR currents display more powerful control over PIC activation than glycinergic currents, an effect attributable to their slower kinetics [196]. Additionally, extrasynaptic GABA ARs (with their high sensitivity to even low GABA concentrations) may represent a further mechanism to downplay neuronal excitability even when synaptic transmission has failed after SCI. Nevertheless, the functional outcome of modulation by GABA receptor activity may also depend on the shifting balance between hyperpolarizing and depolarizing action of GABA due to post lesional changes in chloride transmembrane gradient [140, 180–182, 189] and their timing as discussed earlier.

In conclusion, restoration of locomotor network activity after injury depends on the correct interplay between excitation and inhibition and recovery of the fine balance between synaptic and non-synaptic GABA AR activity. These goals are eminently suitable for pharmacological investigations.

We suggest that this is a complementary strategy to concur with the use of new materials and cell transplants to a successful repair or reconfiguration of damaged locomotor networks that need a suitable functional milieu to reestablish their correct operation.

Abbreviations 5HT, Serotonin; CPG, Central pattern generator; DRG, Dorsal root ganglion; GABA, Gamma-aminobutyric acid; GAD, Glutamic acid decarboxylase; GFP, Glial filament protein; L, Lumbar; MN, Motoneuron; NeuN, Neuronal nuclear protein; NMDA, *N*-methyl-D-aspartate; NS, Nociceptive-specific projection neuron; PICs, Persistent inward currents; ROIs, Regions of interest; SCI, Spinal cord injury; SD, standard deviation; THIP, 4,5,6,7-Tetrahydroisoxazolo [5,4-c] pyridin-3-ol; VGAT, vesicular GABA transporter; VRs, ventral roots

Acknowledgements The authors are grateful to Dr. Elisa Ius for her excellent assistance in preparing the manuscript.

Availability of Data and Material Not applicable

Author Contribution GLM and GT had the idea for the article; GLM, AM, AN, and GT performed the literature search and data analysis; GLM, AM, AN, and GT drafted the work; and GLM, AM, JBA, AN, and GT critically revised the work.

Funding Open access funding provided by Scuola Internazionale Superiore di Studi Avanzati - SISSA within the CRUI-CARE Agreement. This study was supported by an intramural SISSA grant, CONICET, and Regular Associate Scheme of the Abdus Salam International Centre for Theoretical Physics (ICTP).

Declarations

Consent to Participate Not applicable

Consent for Publication Not applicable

Conflict of interest The authors declare no competing interests.

References

1. Berg RW, Alaburda A, Hounsgaard J (2007) Balanced inhibition and excitation drive spike activity in spinal half-centers. Science 315:390–393. https://doi.org/10.1126/science.1134960
2. Cazalets JR, Borde M, Clarac F (1996) The synaptic drive from the spinal locomotor network to motoneurons in the newborn rat. J Neurosci 16:298–306
3. Petersen PC, Vestergaard M, Jensen KHR, Berg RW (2014) Premotor spinal network with balanced excitation and inhibition during motor patterns has high resilience to structural division. J Neurosci 34:2774–2784. https://doi.org/10.1523/JNEUROSCI.3349-13.2014
4. Johnson MD, Hyngstrom AS, Manuel M, Heckman CJ (2012) Push-pull control of motor output. J Neurosci 32:4592–4599. https://doi.org/10.1523/JNEUROSCI.4709-11.2012
5. Shu Y, Hasenstaub A, McCormick DA (2003) Turning on and off recurrent balanced cortical activity. Nature 423:288–293. https://doi.org/10.1038/nature01616
6. Berkowitz A, Hao Z-Z (2011) Partly shared spinal cord networks for locomotion and scratching. Integr Comp Biol 51:890–902. https://doi.org/10.1093/icb/icr041
7. Ziskind-Conhaim L (2013) Neuronal correlates of the dominant role of GABAergic transmission in the developing mouse locomotor circuitry. Ann N Y Acad Sci 1279:43–53. https://doi.org/10.1111/nyas.12064
8. Grillner S, Jessell TM (2009) Measured motion: searching for simplicity in spinal locomotor networks. Curr Opin Neurobiol 19:572–586. https://doi.org/10.1016/j.conb.2009.10.011
9. Kiehn O (2016) Decoding the organization of spinal circuits that control locomotion. Nat Rev Neurosci 17:224–238. https://doi.org/10.1038/nrn.2016.9
10. Kudo N, Yamada T (1987) N-methyl-D,L-aspartate-induced locomotor activity in a spinal cord-hindlimb muscles preparation of the newborn rat studied in vitro. Neurosci Lett 75:43–48. https://doi.org/10.1016/0304-3940(87)90072-3
11. Cazalets JR, Sqalli-Houssaini Y, Clarac F (1992) Activation of the central pattern generators for locomotion by serotonin and excitatory amino acids in neonatal rat. J Physiol 455:187–204
12. Beato M, Nistri A (1999) Interaction between disinhibited bursting and fictive locomotor patterns in the rat isolated spinal cord. J Neurophysiol 82:2029–2038
13. Curtis DR, Duggan AW, Felix D, Johnston GA (1970) GABA, bicuculline and central inhibition. Nature 226:1222–1224. https://doi.org/10.1038/2261222a0
14. Nistri A, Constanti A (1979) Pharmacological characterization of different types of GABA and glutamate receptors in vertebrates and invertebrates. Prog Neurobiol 13:117–235. https://doi.org/10.1016/0301-0082(79)90016-9
15. Sivilotti L, Nistri A (1991) GABA receptor mechanisms in the central nervous system. Prog Neurobiol 36:35–92. https://doi.org/10.1016/0301-0082(91)90036-Z
16. Baur R, Kaur KH, Sigel E (2009) Structure of alpha6 beta3 delta GABA(A) receptors and their lack of ethanol sensitivity. J Neurochem 111:1172–1181. https://doi.org/10.1111/j.1471-4159.2009.06387.x
17. Sigel E, Steinmann ME (2012) Structure, function, and modulation of GABA(A) receptors. J Biol Chem 287:40224–40231. https://doi.org/10.1074/jbc.R112.386664
18. Davis KL, Charney D, Coyle JT, Nemeroff C (2002) Neuropsychopharmacology - 5th Generation of Progress. Lippincott, Williams, & Wilkins, Philadelphia, Pennsylvania, pp 159–168
19. Curtis DR, Hösli L, Johnston GA (1967) Inhibition of spinal neurons by glycine. Nature 215:1502–1503. https://doi.org/10.1038/2151502a0
20. Davidoff RA, Shank RP, Graham LT et al (1967) Association of glycine with spinal interneurones. Nature 214:680–681
21. Liu TT, Bannatyne BA, Maxwell DJ (2010) Organization and neurochemical properties of intersegmental interneurons in the lumbar enlargement of the adult rat. Neuroscience 171:461–484. https://doi.org/10.1016/j.neuroscience.2010.09.012
22. Bonnot A, Morin D (1998) Hemisegmental localisation of rhythmic networks in the lumbosacral spinal cord of neonate mouse. Brain Res 793:136–148. https://doi.org/10.1016/s0006-8993(98)00153-x
23. Streit J (1993) Regular oscillations of synaptic activity in spinal networks in vitro. J Neurophysiol 70:871–878
24. Mladinic M, Nistri A, Taccola G (2013) Acute spinal cord injury in vitro: insight into basic mechanisms. In: Aldskogius H (ed) Animal Models of Spinal Cord Repair. Humana Press, Totowa, pp. 39–62
25. Taccola G, Margaryan G, Mladinic M, Nistri A (2008) Kainate and metabolic perturbation mimicking spinal injury differentially contribute to early damage of locomotor networks in the in vitro neonatal rat spinal cord. Neuroscience 155:538–555. https://doi.org/10.1016/j.neuroscience.2008.06.008
26. Ben-Ari Y (2001) Cell death and synaptic reorganizations produced by seizures. Epilepsia 42(Suppl 3):5–7. https://doi.org/10.1046/j.1528-1157.2001.042suppl.3005.x
27. Soghomonian JJ, Martin DL (1998) Two isoforms of glutamate decarboxylase: why? Trends Pharmacol Sci 19:500–505. https://doi.org/10.1016/s0165-6147(98)01270-x
28. Wei J, Wu J-Y (2008) Post-translational regulation of L-glutamic acid decarboxylase in the brain. Neurochem Res 33:1459–1465. https://doi.org/10.1007/s11064-008-9600-5
29. Tillakaratne NJ, Mouria M, Ziv NB et al (2000) Increased expression of glutamate decarboxylase (GAD(67)) in feline lumbar spinal cord after complete thoracic spinal cord transection. J Neurosci Res 60:219–230
30. Antal M, Petkó M, Polgár E et al (1996) Direct evidence of an extensive GABAergic innervation of the spinal dorsal horn by fibres descending from the rostral ventromedial medulla. Neuroscience 73:509–518. https://doi.org/10.1016/0306-4522(96)00063-2

31. Holstege JC (1991) Ultrastructural evidence for GABAergic brain stem projections to spinal motoneurons in the rat. J Neurosci 11: 159–167
32. Hossaini M, Goos JAC, Kohli SK, Holstege JC (2012) Distribution of glycine/GABA neurons in the ventromedial medulla with descending spinal projections and evidence for an ascending glycine/GABA projection. PLoS ONE 7:e35293. https://doi.org/10.1371/journal.pone.0035293
33. Russ JB, Verina T, Comer JD et al (2013) Corticospinal tract insult alters GABAergic circuitry in the mammalian spinal cord. Front Neural Circuits 7:150. https://doi.org/10.3389/fncir.2013.00150
34. Sadlaoud K, Tazerart S, Brocard C et al (2010) Differential plasticity of the GABAergic and glycinergic synaptic transmission to rat lumbar motoneurons after spinal cord injury. J Neurosci 30: 3358–3369. https://doi.org/10.1523/JNEUROSCI.6310-09.2010
35. Rozzo A, Armellin M, Franzot J et al (2002) Expression and dendritic mRNA localization of GABAC receptor rho1 and rho2 subunits in developing rat brain and spinal cord. Eur J Neurosci 15: 1747–1758. https://doi.org/10.1046/j.1460-9568.2002.02013.x
36. Kaila K (1994) Ionic basis of GABAA receptor channel function in the nervous system. Prog Neurobiol 42:489–537. https://doi.org/10.1016/0301-0082(94)90049-3
37. Marchetti C, Pagnotta S, Donato R, Nistri A (2002) Inhibition of spinal or hypoglossal motoneurons of the newborn rat by glycine or GABA. Eur J Neurosci 15:975–983. https://doi.org/10.1046/j.1460-9568.2002.01927.x
38. Guo D, Hu J (2014) Spinal presynaptic inhibition in pain control. Neuroscience 283:95–106. https://doi.org/10.1016/j.neuroscience.2014.09.032
39. Jean-Xavier C, Mentis GZ, O'Donovan MJ et al (2007) Dual personality of GABA/glycine-mediated depolarizations in immature spinal cord. Proc Nat Acad Sci U S A 104:11477–11482. https://doi.org/10.1073/pnas.0704832104
40. Benkherouf AY, Taina K-R, Meera P et al (2019) Extrasynaptic δ-GABAA receptors are high-affinity muscimol receptors. J Neurochem 149:41–53. https://doi.org/10.1111/jnc.14646
41. Lucas-Osma AM, Li Y, Lin S et al (2018) Extrasynaptic α5GABAA receptors on proprioceptive afferents produce a tonic depolarization that modulates sodium channel function in the rat spinal cord. J Neurophysiol 120:2953–2974. https://doi.org/10.1152/jn.00499.2018
42. McAdoo DJ, Robak G, Xu GY, Hughes MG (2000) Adenosine release upon spinal cord injury. Brain Res 854:152–157. https://doi.org/10.1016/s0006-8993(99)02333-1
43. Sur C, McKernan R, Triller A (1995) Subcellular localization of the GABAA receptor gamma 2 subunit in the rat spinal cord. Eur J Neurosci 7:1323–1332. https://doi.org/10.1111/j.1460-9568.1995.tb01123.x
44. Alvarez FJ, Taylor-Blake B, Fyffe RE et al (1996) Distribution of immunoreactivity for the beta 2 and beta 3 subunits of the GABAA receptor in the mammalian spinal cord. J Comp Neurol 365:392–412
45. Viemari J-C, Bos R, Boulenguez P et al (2011) Chapter 1–importance of chloride homeostasis in the operation of rhythmic motor networks. Prog Brain Res 188:3–14. https://doi.org/10.1016/B978-0-444-53825-3.00006-1
46. Nilius B, Droogmans G (2003) Amazing chloride channels: an overview. Acta Physiol Scand 177:119–147. https://doi.org/10.1046/j.1365-201X.2003.01060.x
47. Price TJ, Cervero F, Gold MS et al (2009) Chloride regulation in the pain pathway. Brain Res Rev 60:149–170. https://doi.org/10.1016/j.brainresrev.2008.12.015
48. Blaesse P, Airaksinen MS, Rivera C, Kaila K (2009) Cation-chloride cotransporters and neuronal function. Neuron 61:820–838. https://doi.org/10.1016/j.neuron.2009.03.003
49. Sun D, Murali SG (1999) Na^+-K^+-$2Cl^-$ cotransporter in immature cortical neurons: a role in intracellular Cl^- regulation. J Neurophysiol 81:1939–1948. https://doi.org/10.1152/jn.1999.81.4.1939
50. Virtanen MA, Uvarov P, Hübner CA, Kaila K (2020) NKCC1, an Elusive molecular target in brain development: making sense of the existing data. Cells 9:2607. https://doi.org/10.3390/cells9122607
51. Stein V, Hermans-Borgmeyer I, Jentsch TJ, Hübner CA (2004) Expression of the KCl cotransporter KCC2 parallels neuronal maturation and the emergence of low intracellular chloride. J Comp Neurol 468:57–64. https://doi.org/10.1002/cne.10983
52. Tillman L, Zhang J (2019) Crossing the chloride channel: the current and potential therapeutic value of the neuronal K^+-Cl^- cotransporter KCC2. Biomed Res Int 2019:8941046. https://doi.org/10.1155/2019/8941046
53. Sung K-W, Kirby M, McDonald MP et al (2000) Abnormal GABAA receptor-mediated currents in dorsal root ganglion neurons isolated from Na–K–2Cl cotransporter null mice. J Neurosci 20:7531–7538. https://doi.org/10.1523/JNEUROSCI.20-20-07531.2000
54. Khirug S, Yamada J, Afzalov R et al (2008) GABAergic depolarization of the axon initial segment in cortical principal neurons is caused by the Na-K-2Cl cotransporter NKCC1. J Neurosci 28: 4635–4639. https://doi.org/10.1523/JNEUROSCI.0908-08.2008
55. Delpire E, Mount DB (2002) Human and murine phenotypes associated with defects in cation-chloride cotransport. Annu Rev Physiol 64:803–843. https://doi.org/10.1146/annurev.physiol.64.081501.155847
56. Hampel P, Römermann K, Gailus B et al (2021) Effects of the NKCC1 inhibitors bumetanide, azosemide, and torasemide alone or in combination with phenobarbital on seizure threshold in epileptic and nonepileptic mice. Neuropharmacology 185:108449. https://doi.org/10.1016/j.neuropharm.2021.108449
57. Willis WD (1999) Dorsal root potentials and dorsal root reflexes: a double-edged sword. Exp Brain Res 124:395–421. https://doi.org/10.1007/s002210050637
58. Tsukahara T, Masuhara M, Iwai H et al (2015) Repeated stress-induced expression pattern alterations of the hippocampal chloride transporters KCC2 and NKCC1 associated with behavioral abnormalities in female mice. Biochem Biophys Res Commun 465: 145–151. https://doi.org/10.1016/j.bbrc.2015.07.153
59. Jaggi AS, Kaur A, Bali A, Singh N (2015) Expanding spectrum of sodium potassium chloride co-transporters in the pathophysiology of diseases. Curr Neuropharmacol 13:369–388. https://doi.org/10.2174/1570159x13666150205130359
60. Hsu Y-T, Chang Y-G, Chern Y (2018) Insights into GABAAergic system alteration in Huntington's disease. Open Biol 8:180165. https://doi.org/10.1098/rsob.180165
61. Lozovaya N, Ben-Ari Y, Hammond C (2018) Striatal dual cholinergic /GABAergic transmission in Parkinson disease: friends or foes? Cell Stress 2:147–149. https://doi.org/10.15698/cst2018.06.142
62. Allain A-E, Cazenave W, Delpy A et al (2016) Nonsynaptic glycine release is involved in the early KCC2 expression. Dev Neurobiol 76:764–779. https://doi.org/10.1002/dneu.22358
63. Bos R, Brocard F, Vinay L (2011) Primary afferent terminals acting as excitatory interneurons contribute to spontaneous motor activities in the immature spinal cord. J Neurosci 31:10184–10188. https://doi.org/10.1523/JNEUROSCI.0068-11.2011
64. Phan H-L, Pflieger J-F (2013) Immunolocalization of cation-chloride cotransporters in the developing and mature spinal cord of opossums, Monodelphis domestica. Front Neuroanat 7:12. https://doi.org/10.3389/fnana.2013.00012
65. Cramer SW, Baggott C, Cain J et al (2008) The role of cation-dependent chloride transporters in neuropathic pain following spinal cord injury. Mol Pain 4:36. https://doi.org/10.1186/1744-8069-4-36

66. Hasbargen T, Ahmed MM, Miranpuri G et al (2010) Role of NKCC1 and KCC2 in the development of chronic neuropathic pain following spinal cord injury. Ann N Y Acad Sci 1198:168–172. https://doi.org/10.1111/j.1749-6632.2010.05462.x
67. Côté M-P, Gandhi S, Zambrotta M, Houlé JD (2014) Exercise modulates chloride homeostasis after spinal cord injury. J Neurosci 34:8976–8987. https://doi.org/10.1523/JNEUROSCI.0678-14.2014
68. Yan X, Liu J, Wang X et al (2018) Pretreatment with AQP4 and NKCC1 inhibitors concurrently attenuated spinal cord edema and tissue damage after spinal cord injury in rats. Front Physiol 9:6. https://doi.org/10.3389/fphys.2018.00006
69. Mekhael W, Begum S, Samaddar S et al (2019) Repeated anodal trans-spinal direct current stimulation results in long-term reduction of spasticity in mice with spinal cord injury. J Physiol 597:2201–2223. https://doi.org/10.1113/JP276952
70. Tanabe Y, Jessell TM (1996) Diversity and pattern in the developing spinal cord. Science 274:1115–1123. https://doi.org/10.1126/science.274.5290.1115
71. Tashima R, Koga K, Yoshikawa Y et al (2021) A subset of spinal dorsal horn interneurons crucial for gating touch-evoked pain-like behavior. Proc Natl Acad Sci U S A 118:e2021220118. https://doi.org/10.1073/pnas.2021220118
72. Yin Y, Yi M-H, Kim DW (2018) Impaired autophagy of GABAergic interneurons in neuropathic pain. Pain Res Manag 2018:9185368. https://doi.org/10.1155/2018/9185368
73. Burke D, Fullen BM, Stokes D, Lennon O (2017) Neuropathic pain prevalence following spinal cord injury: a systematic review and meta-analysis. Eur J Pain 21:29–44. https://doi.org/10.1002/ejp.905
74. Kumru H, Benito-Penalva J, Kofler M, Vidal J (2018) Analgesic effect of intrathecal baclofen bolus on neuropathic pain in spinal cord injury patients. Brain Res Bull 140:205–211. https://doi.org/10.1016/j.brainresbull.2018.05.013
75. Zarepour L, Gharaylou Z, Hadjighassem M et al (2020) Preliminary study of analgesic effect of bumetanide on neuropathic pain in patients with spinal cord injury. J Clin Neurosci 81:477–484. https://doi.org/10.1016/j.jocn.2020.10.010
76. Meisner JG, Marsh AD, Marsh DR (2010) Loss of GABAergic interneurons in laminae I-III of the spinal cord dorsal horn contributes to reduced GABAergic tone and neuropathic pain after spinal cord injury. J Neurotrauma 27:729–737. https://doi.org/10.1089/neu.2009.1166
77. Kami K, Taguchi Ms S, Tajima F, Senba E (2016) Exercise modulates chloride homeostasis after spinal cord injury. Mol Pain 12. https://doi.org/10.1177/1744806916629059
78. Chen S-R, Zhu L, Chen H et al (2014) Increased spinal cord Na^+-K^+-$2Cl^-$ cotransporter-1 (NKCC1) activity contributes to impairment of synaptic inhibition in paclitaxel-induced neuropathic pain. J Biol Chem 289:31111–31120. https://doi.org/10.1074/jbc.M114.600320
79. Pieraut S, Lucas O, Sangari S et al (2011) An autocrine neuronal interleukin-6 loop mediates chloride accumulation and NKCC1 phosphorylation in axotomized sensory neurons. J Neurosci 31:13516–13526. https://doi.org/10.1523/JNEUROSCI.3382-11.2011
80. Wei B, Kumada T, Furukawa T et al (2013) Pre- and post-synaptic switches of GABA actions associated with Cl^- homeostatic changes are induced in the spinal nucleus of the trigeminal nerve in a rat model of trigeminal neuropathic pain. Neuroscience 228:334–348. https://doi.org/10.1016/j.neuroscience.2012.10.043
81. Laird JMA, García-Nicas E, Delpire EJ, Cervero F (2004) Presynaptic inhibition and spinal pain processing in mice: a possible role of the NKCC1 cation-chloride co-transporter in hyperalgesia. Neurosci Lett 361:200–203. https://doi.org/10.1016/j.neulet.2003.12.015
82. Allen LL, Seven YB, Baker TL, Mitchell GS (2019) Cervical spinal contusion alters Na^+-K^+-$2Cl^-$ and K^+-Cl^- cation-chloride cotransporter expression in phrenic motor neurons. Respir Physiol Neurobiol 261:15–23. https://doi.org/10.1016/j.resp.2018.12.009
83. Gagnon M, Bergeron MJ, Lavertu G et al (2013) Chloride extrusion enhancers as novel therapeutics for neurological diseases. Nat Med 19:1524–1528. https://doi.org/10.1038/nm.3356
84. Mòdol L, Cobianchi S, Navarro X (2014) Prevention of NKCC1 phosphorylation avoids downregulation of KCC2 in central sensory pathways and reduces neuropathic pain after peripheral nerve injury. Pain 155:1577–1590. https://doi.org/10.1016/j.pain.2014.05.004
85. Khalki L, Sadlaoud K, Lerond J et al (2018) Changes in innervation of lumbar motoneurons and organization of premotor network following training of transected adult rats. Exp Neurol 299:1–14. https://doi.org/10.1016/j.expneurol.2017.09.002
86. Werman R, Davidoff RA, Aprison MH (1967) Inhibition of motoneurones by iontophoresis of glycine. Nature 214:681–683. https://doi.org/10.1038/214681a0
87. Jonas P, Bischofberger J, Sandkühler J (1998) Corelease of two fast neurotransmitters at a central synapse. Science 281:419–424. https://doi.org/10.1126/science.281.5375.419
88. Shigenaga Y, Moritani M, Oh SJ et al (2005) The distribution of inhibitory and excitatory synapses on single, reconstructed jaw-opening motoneurons in the cat. Neuroscience 133:507–518. https://doi.org/10.1016/j.neuroscience.2005.02.022
89. Baer K, Waldvogel HJ, During MJ et al (2003) Association of gephyrin and glycine receptors in the human brainstem and spinal cord: an immunohistochemical analysis. Neuroscience 122:773–784. https://doi.org/10.1016/s0306-4522(03)00543-8
90. Pfeiffer F, Simler R, Grenningloh G, Betz H (1984) Monoclonal antibodies and peptide mapping reveal structural similarities between the subunits of the glycine receptor of rat spinal cord. Proc Natl Acad Sci U S A 81:7224–7227. https://doi.org/10.1073/pnas.81.22.7224
91. Triller A, Cluzeaud F, Pfeiffer F et al (1985) Distribution of glycine receptors at central synapses: an immunoelectron microscopy study. J Cell Biol 101:683–688. https://doi.org/10.1083/jcb.101.2.683
92. Bras H, Liabeuf S (2020) Differential effects of spinal cord transection on glycinergic and GABAergic synaptic signaling in sublesional lumbar motoneurons. J Chem Neuroanat 101847. https://doi.org/10.1016/j.jchemneu.2020.101847
93. Diaz-Ruiz A, Salgado-Ceballos H, Montes S et al (2007) Acute alterations of glutamate, glutamine, GABA, and other amino acids after spinal cord contusion in rats. Neurochem Res 32:57–63. https://doi.org/10.1007/s11064-006-9225-5
94. Sadlaoud K, Khalki L, Brocard F et al (2020) Alteration of glycinergic receptor expression in lumbar spinal motoneurons is involved in the mechanisms underlying spasticity after spinal cord injury. J Chem Neuroanat 106:101787. https://doi.org/10.1016/j.jchemneu.2020.101787
95. Simpson RK, Gondo M, Robertson CS, Goodman JC (1995) The influence of glycine and related compounds on spinal cord injury-induced spasticity. Neurochem Res 20:1203–1210. https://doi.org/10.1007/BF00995384
96. Simpson RK, Robertson CS, Goodman JC (1996) The role of glycine in spinal shock. J Spinal Cord Med 19:215–224. https://doi.org/10.1080/10790268.1996.11719437
97. de Leon RD, Tamaki H, Hodgson JA et al (1999) Hindlimb locomotor and postural training modulates glycinergic inhibition in the spinal cord of the adult spinal cat. J Neurophysiol 82:359–369. https://doi.org/10.1152/jn.1999.82.1.359
98. Panter SS, Yum SW, Faden AI (1990) Alteration in extracellular amino acids after traumatic spinal cord injury. Ann Neurol 27:96–99. https://doi.org/10.1002/ana.410270115
99. Demediuk P, Daly MP, Faden AI (1989) Effect of impact trauma on neurotransmitter and nonneurotransmitter amino acids in rat

spinal cord. J Neurochem 52:1529–1536. https://doi.org/10.1111/j.1471-4159.1989.tb09204.x
100. Gorji A, Zahn PK, Pogatzki EM, Speckmann E-J (2004) Spinal and cortical spreading depression enhance spinal cord activity. Neurobiol Dis 15:70–79. https://doi.org/10.1016/j.nbd.2003.09.014
101. Petty F, Sherman AD (1984) Plasma GABA levels in psychiatric illness. J Affect Disord 6:131–138. https://doi.org/10.1016/0165-0327(84)90018-1
102. Bhandage AK, Cunningham JL, Jin Z et al (2019) Depression, GABA, and age correlate with plasma levels of inflammatory markers. Int J Mol Sci 20. https://doi.org/10.3390/ijms20246172
103. Willford SL, Anderson CM, Spencer SR, Eskandari S (2015) Evidence for a revised ion/substrate coupling stoichiometry of GABA transporters. J Membr Biol 248:795–810. https://doi.org/10.1007/s00232-015-9797-6
104. Raiteri L, Stigliani S, Zedda L et al (2002) Multiple mechanisms of transmitter release evoked by "pathologically" elevated extracellular [K^+]: involvement of transporter reversal and mitochondrial calcium. J Neurochem 80:706–714. https://doi.org/10.1046/j.0022-3042.2001.00750.x
105. Song G, Cechvala C, Resnick DK et al (2001) GeneChip analysis after acute spinal cord injury in rat. J Neurochem 79:804–815. https://doi.org/10.1046/j.1471-4159.2001.00626.x
106. Ditunno JF, Little JW, Tessler A, Burns AS (2004) Spinal shock revisited: a four-phase model. Spinal Cord 42:383–395. https://doi.org/10.1038/sj.sc.3101603
107. Taccola G, Gad P, Culaclii S et al (2020) Acute neuromodulation restores spinally-induced motor responses after severe spinal cord injury. Exp Neurol 327:113246. https://doi.org/10.1016/j.expneurol.2020.113246
108. Coskun C, Avci B, Ocak N et al (2010) Effect of repeatedly given CDP-choline on cardiovascular and tissue injury in spinal shock conditions: investigation of the acute phase. J Pharm Pharmacol 62:497–506. https://doi.org/10.1211/jpp.62.04.0013
109. Rafati DS, Geissler K, Johnson K et al (2008) Nuclear factor-kappaB decoy amelioration of spinal cord injury-induced inflammation and behavior outcomes. J Neurosci Res 86:566–580. https://doi.org/10.1002/jnr.21508
110. Restrepo CE, Lundfald L, Szabó G et al (2009) Transmitter-phenotypes of commissural interneurons in the lumbar spinal cord of newborn mice. J Comp Neurol 517:177–192. https://doi.org/10.1002/cne.22144
111. Mautes AE, Weinzierl MR, Donovan F, Noble LJ (2000) Vascular events after spinal cord injury: contribution to secondary pathogenesis. PhysTher 80:673–687
112. Tator CH, Fehlings MG (1991) Review of the secondary injury theory of acute spinal cord trauma with emphasis on vascular mechanisms. J Neurosurg 75:15–26. https://doi.org/10.3171/jns.1991.75.1.0015
113. Taccola G, Mladinic M, Nistri A (2010) Dynamics of early locomotor network dysfunction following a focal lesion in an in vitro model of spinal injury. Eur J Neurosci 31:60–78. https://doi.org/10.1111/j.1460-9568.2009.07040.x
114. Mazzone GL, Margaryan G, Kuzhandaivel A et al (2010) Kainate-induced delayed onset of excitotoxicity with functional loss unrelated to the extent of neuronal damage in the in vitro spinal cord. Neuroscience 168:451–462. https://doi.org/10.1016/j.neuroscience.2010.03.055
115. Deumens R, Mazzone GL, Taccola G (2013) Early spread of hyperexcitability to caudal dorsal horn networks after a chemically-induced lesion of the rat spinal cord in vitro. Neuroscience 229:155–163. https://doi.org/10.1016/j.neuroscience.2012.10.036
116. Faden AI, Simon RP (1988) A potential role for excitotoxins in the pathophysiology of spinal cord injury. Ann Neurol 23:623–626. https://doi.org/10.1002/ana.410230618
117. Liu D, Xu GY, Pan E, McAdoo DJ (1999) Neurotoxicity of glutamate at the concentration released upon spinal cord injury. Neuroscience 93:1383–1389. https://doi.org/10.1016/s0306-4522(99)00278-x
118. Mailly F, Marin P, Israël M et al (1999) Increase in external glutamate and NMDA receptor activation contribute to H2O2-induced neuronal apoptosis. J Neurochem 73:1181–1188. https://doi.org/10.1046/j.1471-4159.1999.0731181.x
119. Saransaari P, Oja SS (1998) Release of endogenous glutamate, aspartate, GABA, and taurine from hippocampal slices from adult and developing mice under cell-damaging conditions. Neurochem Res 23:563–570. https://doi.org/10.1023/a:1022494921018
120. Rego AC, Santos MS, Oliveira CR (1996) Oxidative stress, hypoxia, and ischemia-like conditions increase the release of endogenous amino acids by distinct mechanisms in cultured retinal cells. J Neurochem 66:2506–2516. https://doi.org/10.1046/j.1471-4159.1996.66062506.x
121. Masiulis S, Desai R, Uchański T et al (2019) GABAA receptor signalling mechanisms revealed by structural pharmacology. Nature 565:454–459. https://doi.org/10.1038/s41586-018-0832-5
122. Sah R, Galeffi F, Ahrens R et al (2002) Modulation of the GABA(A)-gated chloride channel by reactive oxygen species. J Neurochem 80:383–391. https://doi.org/10.1046/j.0022-3042.2001.00706.x
123. Basmajian JV (1957) New views on muscular tone and relaxation. Can Med Assoc J 77:203–205
124. Lin CS-Y, Macefield VG, Elam M et al (2007) Axonal changes in spinal cord injured patients distal to the site of injury. Brain 130:985–994. https://doi.org/10.1093/brain/awl339
125. Norton JA, Bennett DJ, Knash ME et al (2008) Changes in sensory-evoked synaptic activation of motoneurons after spinal cord injury in man. Brain 131:1478–1491. https://doi.org/10.1093/brain/awn050
126. Schwindt P, Crill WE (1977) A persistent negative resistance in cat lumbar motoneurons. Brain Res 120:173–178. https://doi.org/10.1016/0006-8993(77)90510-8
127. Flatman JA, Schwindt PC, Crill WE, Stafstrom CE (1983) Multiple actions of N-methyl-D-aspartate on cat neocortical neurons in vitro. Brain Res 266:169–173. https://doi.org/10.1016/0006-8993(83)91323-9
128. Bennett DJ, Hultborn H, Fedirchuk B, Gorassini M (1998) Synaptic activation of plateaus in hindlimb motoneurons of decerebrate cats. J Neurophysiol 80:2023–2037. https://doi.org/10.1152/jn.1998.80.4.2023
129. Li Y, Gorassini MA, Bennett DJ (2004) Role of persistent sodium and calcium currents in motoneuron firing and spasticity in chronic spinal rats. J Neurophysiol 91:767–783. https://doi.org/10.1152/jn.00788.2003
130. Hamm TM, Turkin VV, Bandekar NK et al (2010) Persistent currents and discharge patterns in rat hindlimb motoneurons. J Neurophysiol 104:1566–1577. https://doi.org/10.1152/jn.00380.2010
131. Kakinohana O, Hefferan MP, Nakamura S et al (2006) Development of GABA-sensitive spasticity and rigidity in rats after transient spinal cord ischemia: a qualitative and quantitative electrophysiological and histopathological study. Neuroscience 141:1569–1583. https://doi.org/10.1016/j.neuroscience.2006.04.083
132. Tai Q, Palazzolo K, Mautes A et al (1997) Ultrastructural characteristics of glutamatergic and GABAergic terminals in cat lamina IX before and after spinal cord injury. J Spinal Cord Med 20:311–318. https://doi.org/10.1080/10790268.1997.11719481
133. Nacimiento W, Sappok T, Brook GA et al (1995) Structural changes of anterior horn neurons and their synaptic input caudal to a low thoracic spinal cord hemisection in the adult rat: a light

and electron microscopic study. Acta Neuropathol 90:552–564. https://doi.org/10.1007/BF00318567
134. Ondarza AB, Ye Z, Hulsebosch CE (2003) Direct evidence of primary afferent sprouting in distant segments following spinal cord injury in the rat: colocalization of GAP-43 and CGRP. Exp Neurol 184:373–380. https://doi.org/10.1016/j.expneurol.2003.07.002
135. Carr PA, Pearson JC, Fyffe RE (1999) Distribution of 5-hydroxytryptamine-immunoreactive boutons on immunohistochemically-identified Renshaw cells in cat and rat lumbar spinal cord. Brain Res 823:198–201. https://doi.org/10.1016/s0006-8993(98)01210-4
136. Jordan LM, McCrea DA (1976) Analysis of the effects of p-methoxy-phenylethylamine on spinal cord neurones. Br J Pharmacol 57:191–199. https://doi.org/10.1111/j.1476-5381.1976.tb07467.x
137. Wootz H, Fitzsimons-Kantamneni E, Larhammar M et al (2013) Alterations in the motor neuron-renshaw cell circuit in the Sod1(G93A) mouse model. J Comp Neurol 521:1449–1469. https://doi.org/10.1002/cne.23266
138. Kupcova Skalnikova H, Navarro R, Marsala S et al (2013) Signaling proteins in spinal parenchyma and dorsal root ganglion in rat with spinal injury-induced spasticity. J Proteome 91:41–57. https://doi.org/10.1016/j.jprot.2013.06.028
139. Kumru H, Vidal J, Kofler M et al (2010) Alterations in excitatory and inhibitory brainstem interneuronal circuits after severe spinal cord injury. J Neurotrauma 27:721–728. https://doi.org/10.1089/neu.2009.1089
140. Chen B, Li Y, Yu B et al (2018) Reactivation of dormant relay pathways in injured spinal cord by KCC2 manipulations. Cell 174:521–535.e13. https://doi.org/10.1016/j.cell.2018.06.005
141. Huang YJ, Lee KH, Grau JW (2017) Complete spinal cord injury (SCI) transforms how brain derived neurotrophic factor (BDNF) affects nociceptive sensitization. Exp Neurol 288:38–50. https://doi.org/10.1016/j.expneurol.2016.11.001
142. Sánchez-Brualla I, Boulenguez P, Brocard C et al (2018) Activation of 5-HT 2A receptors restores KCC2 function and reduces neuropathic pain after spinal cord injury. Neuroscience 387:48–57. https://doi.org/10.1016/j.neuroscience.2017.08.033
143. Mazzone GL, Nistri A (2019) Modulation of extrasynaptic GABAergic receptor activity influences glutamate release and neuronal survival following excitotoxic damage to mouse spinal cord neurons. Neurochem Int 128:175–185. https://doi.org/10.1016/j.neuint.2019.04.018
144. Fandel TM, Trivedi A, Nicholas CR et al (2016) Transplanted human stem cell-derived interneuron precursors mitigate mouse bladder dysfunction and central neuropathic pain after spinal cord injury. Cell Stem Cell 19:544–557. https://doi.org/10.1016/j.stem.2016.08.020
145. Llewellyn-Smith IJ, Basbaum AI, Bráz JM (2017) Long-term, dynamic synaptic reorganization after GABAergic precursor cell transplantation into adult mouse spinal cord. J Comp Neurol 526:480–495. https://doi.org/10.1002/cne.24346
146. Batista CM, Mariano ED, Dale CS et al (2019) Pain inhibition through transplantation of fetal neuronal progenitors into the injured spinal cord in rats. Neural Regen Res 14:2011–2019. https://doi.org/10.4103/1673-5374.259624
147. Manion J, Khuong T, Harney D et al (2020) Human induced pluripotent stem cell-derived GABAergic interneuron transplants attenuate neuropathic pain. Pain 161:379–387. https://doi.org/10.1097/j.pain.0000000000001733
148. Dugan EA, Jergova S, Sagen J (2020) Mutually beneficial effects of intensive exercise and GABAergic neural progenitor cell transplants in reducing neuropathic pain and spinal pathology in rats with spinal cord injury. Exp Neurol 327:113208. https://doi.org/10.1016/j.expneurol.2020.113208
149. Lev-Tov A, Pinco M (1992) In vitro studies of prolonged synaptic depression in the neonatal rat spinal cord. J Physiol 447:149–169. https://doi.org/10.1113/jphysiol.1992.sp018996
150. Dose F, Taccola G (2012) Coapplication of noisy patterned electrical stimuli and NMDA plus serotonin facilitates fictive locomotion in the rat spinal cord. J Neurophysiol 108:2977–2990. https://doi.org/10.1152/jn.00554.2012
151. Mazzone GL, Nistri A (2011) Electrochemical detection of endogenous glutamate release from rat spinal cord organotypic slices as a real-time method to monitor excitotoxicity. J Neurosci Methods 197:128–132. https://doi.org/10.1016/j.jneumeth.2011.01.033
152. McLamore ES, Mohanty S, Shi J et al (2010) A self-referencing glutamate biosensor for measuring real time neuronal glutamate flux. J Neurosci Methods 189:14–22. https://doi.org/10.1016/j.jneumeth.2010.03.001
153. Lau A, Tymianski M (2010) Glutamate receptors, neurotoxicity and neurodegeneration. Pflugers Arch 460:525–542
154. Mazzone GL, Nistri A (2011) Delayed neuroprotection by riluzole against excitotoxic damage evoked by kainate on rat organotypic spinal cord cultures. Neuroscience 190:318–327. https://doi.org/10.1016/j.neuroscience.2011.06.013
155. Mazzone GL, Nistri A (2011) Effect of the PARP-1 inhibitor PJ 34 on excitotoxic damage evoked by kainate on rat spinal cord organotypic slices. Cell Mol Neurobiol 31:469–478. https://doi.org/10.1007/s10571-010-9640-7
156. Sámano C, Nistri A (2019) Mechanism of neuroprotection against experimental spinal cord injury by riluzole or methylprednisolone. Neurochem Res 44:200–213. https://doi.org/10.1007/s11064-017-2459-6
157. Bajrektarevic D, Nistri A (2016) Delayed application of the anesthetic propofol contrasts the neurotoxic effects of kainate on rat organotypic spinal slice cultures. Neurotoxicology 54:1–10. https://doi.org/10.1016/j.neuro.2016.03.001
158. Kaur J, Flores Gutiérrez J, Nistri A (2016) Neuroprotective effect of propofol against excitotoxic injury to locomotor networks of the rat spinal cord in vitro. Eur J Neurosci 44:2418–2430. https://doi.org/10.1111/ejn.13353
159. Shabbir A, Bianchetti E, Nistri A (2015) The volatile anesthetic methoxyflurane protects motoneurons against excitotoxicity in an in vitro model of rat spinal cord injury. Neuroscience 285:269–280. https://doi.org/10.1016/j.neuroscience.2014.11.023
160. Cheng Q, Sun G-J, Liu S-B et al (2016) A novel translocator protein 18 kDa ligand, ZBD-2, exerts neuroprotective effects against acute spinal cord injury. Clin Exp Pharmacol Physiol 43:930–938. https://doi.org/10.1111/1440-1681.12606
161. Labombarda F, Ghoumari AM, Liere P et al (2013) Neuroprotection by steroids after neurotrauma in organotypic spinal cord cultures: a key role for progesterone receptors and steroidal modulators of GABA(A) receptors. Neuropharmacology 71:46–55. https://doi.org/10.1016/j.neuropharm.2013.03.010
162. Fontana G, Taccola G, Galante J et al (2001) AMPA-evoked acetylcholine release from cultured spinal cord motoneurons and its inhibition by GABA and glycine. Neuroscience 106:183–191. https://doi.org/10.1016/s0306-4522(01)00272-x
163. Cervetto C, Taccola G (2008) GABAA and strychnine-sensitive glycine receptors modulate N-methyl-D-aspartate-evoked acetylcholine release from rat spinal motoneurons: a possible role in neuroprotection. Neuroscience 154:1517–1524. https://doi.org/10.1016/j.neuroscience.2008.04.066

164. Rogvi-Hansen B, Gram L (1995) Adverse effects of established and new antiepileptic drugs: an attempted comparison. Pharmacol Ther 68:425–434. https://doi.org/10.1016/0163-7258(95)02014-4
165. Montané E, Vallano A, Laporte JR (2004) Oral antispastic drugs in nonprogressive neurologic diseases: a systematic review. Neurology 63:1357–1363. https://doi.org/10.1212/01.wnl.0000141863.52691.44
166. Leo RJ, Baer D (2005) Delirium associated with baclofen withdrawal: a review of common presentations and management strategies. Psychosomatics 46:503–507. https://doi.org/10.1176/appi.psy.46.6.503
167. Losi G, Gomez-Gonzalo M, Zonta M et al (2019) Cellular and molecular mechanisms of new onset seizure generation. Aging Clin Exp Res. https://doi.org/10.1007/s40520-019-01396-z
168. Araque A, Parpura V, Sanzgiri RP et al (1999) Tripartite synapses: glia, the unacknowledged partner. Trends Neurosci 22:208–215. https://doi.org/10.1016/S0166-2236(98)01349-6
169. Mazzone GL, Nistri A (2014) S100β as an early biomarker of excitotoxic damage in spinal cord organotypic cultures. J Neurochem 130:598–604. https://doi.org/10.1111/jnc.12748
170. Cifra A, Mazzone GL, Nani F et al (2012) Postnatal developmental profile of neurons and glia in motor nuclei of the brainstem and spinal cord, and its comparison with organotypic slice cultures. Dev Neurobiol 72:1140–1160. https://doi.org/10.1002/dneu.20991
171. Liu J, McDaid L, Araque A et al (2019) GABA regulation of burst firing in hippocampal astrocyte neural circuit: a biophysical model. Front Cell Neurosci 13:335. https://doi.org/10.3389/fncel.2019.00335
172. Christensen RK, Delgado-Lezama R, Russo RE et al (2018) Spinal dorsal horn astrocytes release GABA in response to synaptic activation. J Physiol Lond 596:4983–4994. https://doi.org/10.1113/JP276562
173. Fernández-López B, Valle-Maroto SM, Barreiro-Iglesias A, Rodicio MC (2014) Neuronal release and successful astrocyte uptake of aminoacidergic neurotransmitters after spinal cord injury in lampreys. Glia 62:1254–1269. https://doi.org/10.1002/glia.22678
174. Lei Y, Yaroslavsky I, Tejani-Butt SM (2009) Strain differences in the distribution of N-methyl-d-aspartate and gamma (gamma)-aminobutyric acid-A receptors in rat brain. Life Sci 85:794–799. https://doi.org/10.1016/j.lfs.2009.10.010
175. Dornellas APS, Macedo GC, McFarland MH et al (2020) Allopregnanolone decreases evoked dopamine release differently in rats by sex and estrous stage. Front Pharmacol 11:608887. https://doi.org/10.3389/fphar.2020.608887
176. Clarke EC, Cheng S, Bilston LE (2009) The mechanical properties of neonatal rat spinal cord in vitro, and comparisons with adult. J Biomech 42:1397–1402. https://doi.org/10.1016/j.jbiomech.2009.04.008
177. Khristy W, Ali NJ, Bravo AB et al (2009) Changes in GABA(A) receptor subunit gamma 2 in extensor and flexor motoneurons and astrocytes after spinal cord transection and motor training. Brain Res 1273:9–17. https://doi.org/10.1016/j.brainres.2009.03.060
178. Mackie M, Hughes DI, Maxwell DJ et al (2003) Distribution and colocalisation of glutamate decarboxylase isoforms in the rat spinal cord. Neuroscience 119:461–472. https://doi.org/10.1016/s0306-4522(03)00174-x
179. Tillakaratne NJK, de Leon RD, Hoang TX et al (2002) Use-dependent modulation of inhibitory capacity in the feline lumbar spinal cord. J Neurosci 22:3130–3143 20026278
180. Lu Y, Zheng J, Xiong L et al (2008) Spinal cord injury-induced attenuation of GABAergic inhibition in spinal dorsal horn circuits is associated with down-regulation of the chloride transporter KCC2 in rat. J Physiol Lond 586:5701–5715. https://doi.org/10.1113/jphysiol.2008.152348
181. Boulenguez P, Liabeuf S, Bos R et al (2010) Down-regulation of the potassium-chloride cotransporter KCC2 contributes to spasticity after spinal cord injury. Nat Med 16:302–307. https://doi.org/10.1038/nm.2107
182. Boulenguez P, Vinay L (2009) Strategies to restore motor functions after spinal cord injury. Curr Opin Neurobiol 19:587–600. https://doi.org/10.1016/j.conb.2009.10.005
183. Beato M (2008) The time course of transmitter at glycinergic synapses onto motoneurons. J Neurosci 28:7412–7425. https://doi.org/10.1523/JNEUROSCI.0581-08.2008
184. Pitt SJ, Sivilotti LG, Beato M (2008) High intracellular chloride slows the decay of glycinergic currents. J Neurosci 28:11454–11467. https://doi.org/10.1523/JNEUROSCI.3890-08.2008
185. Bellardita C, Caggiano V, Leiras R et al (2017) Spatiotemporal correlation of spinal network dynamics underlying spasms in chronic spinalized mice. Elife 6:e23011. https://doi.org/10.7554/eLife.23011
186. Edgerton VR, Roy RR (2010) Spasticity: a switch from inhibition to excitation. Nat Med 16:270–271. https://doi.org/10.1038/nm0310-270
187. Robinson GA, Goldberger ME (1986) The development and recovery of motor function in spinal cats. I. The infant lesion effect. Exp Brain Res 62:373–386. https://doi.org/10.1007/BF00238857
188. Edgerton VR, de Leon RD, Tillakaratne N et al (1997) Use-dependent plasticity in spinal stepping and standing. Adv Neurol 72:233–247
189. Brocard C, Plantier V, Boulenguez P et al (2016) Cleavage of Na(+) channels by calpain increases persistent Na(+) current and promotes spasticity after spinal cord injury. Nat Med 22:404–411. https://doi.org/10.1038/nm.4061
190. Thomas CK, Häger CK, Klein CS (2017) Increases in human motoneuron excitability after cervical spinal cord injury depend on the level of injury. J Neurophysiol 117:684–691. https://doi.org/10.1152/jn.00676.2016
191. Bunday KL, Oudega M, Perez MA (2013) Aberrant crossed corticospinal facilitation in muscles distant from a spinal cord injury. PLoS ONE 8:e76747. https://doi.org/10.1371/journal.pone.0076747
192. Li Y, Bennett DJ (2003) Persistent sodium and calcium currents cause plateau potentials in motoneurons of chronic spinal rats. J Neurophysiol 90:857–869. https://doi.org/10.1152/jn.00236.2003
193. Bennett DJ, Gorassini M, Fouad K et al (1999) Spasticity in rats with sacral spinal cord injury. J Neurotrauma 16:69–84. https://doi.org/10.1089/neu.1999.16.69
194. Bellardita C, Marcantoni M, Löw P, Kiehn O (2018) Sacral spinal cord transection and isolated sacral cord preparation to study chronic spinal cord injury in adult mice. Bio Protoc 8:e2784. https://doi.org/10.21769/BioProtoc.2784
195. Johnson MD, Kajtaz E, Cain CM, Heckman CJ (2013) Motoneuron intrinsic properties, but not their receptive fields, recover in chronic spinal injury. J Neurosci 33:18806–18813. https://doi.org/10.1523/JNEUROSCI.2609-13.2013
196. Venugopal S, Hamm TM, Crook SM, Jung R (2011) Modulation of inhibitory strength and kinetics facilitates regulation of persistent inward currents and motoneuron excitability following spinal cord injury. J Neurophysiol 106:2167–2179. https://doi.org/10.1152/jn.00359.2011
197. Davidoff RA (1978) Pharmacology of spasticity. Neurology 28:46–51. https://doi.org/10.1212/wnl.28.9_part_2.46

198. ElBasiouny SM, Schuster JE, Heckman CJ (2010) Persistent inward currents in spinal motoneurons: important for normal function but potentially harmful after spinal cord injury and in amyotrophic lateral sclerosis. Clin Neurophysiol 121:1669–1679. https://doi.org/10.1016/j.clinph.2009.12.041
199. Powers RK, Heckman CJ (2017) Synaptic control of the shape of the motoneuron pool input-output function. J Neurophysiol 117: 1171–1184. https://doi.org/10.1152/jn.00850.2016
200. Tazerart S, Viemari J-C, Darbon P et al (2007) Contribution of persistent sodium current to locomotor pattern generation in neonatal rats. J Neurophysiol 98:613–628. https://doi.org/10.1152/jn.00316.2007
201. Binder MD, Powers RK, Heckman CJ (2020) Nonlinear input-output functions of motoneurons. Physiology (Bethesda) 35:31–39. https://doi.org/10.1152/physiol.00026.2019
202. Johnson MD, Frigon A, Hurteau M-F et al (2017) Reflex wind-up in early chronic spinal injury: plasticity of motor outputs. J Neurophysiol 117:2065–2074. https://doi.org/10.1152/jn.00981.2016

Cellular and Molecular Neurobiology (2023) 43:2831–2856
https://doi.org/10.1007/s10571-023-01321-z

ORIGINAL RESEARCH

Suprapontine Structures Modulate Brainstem and Spinal Networks

Atiyeh Mohammadshirazi[1,2] · Rosamaria Apicella[1,2] · Benjamín A. Zylberberg[3] · Graciela L. Mazzone[3] · Giuliano Taccola[1,2]

Received: 25 November 2022 / Accepted: 19 January 2023 / Published online: 2 February 2023

Abstract

Several spinal motor output and essential rhythmic behaviors are controlled by supraspinal structures, although their contribution to neuronal networks for respiration and locomotion at birth still requires better characterization. As preparations of isolated brainstem and spinal networks only focus on local circuitry, we introduced the in vitro central nervous system (CNS) from neonatal rodents to simultaneously record a stable respiratory rhythm from both cervical and lumbar ventral roots (VRs). Electrical pulses supplied to multiple sites of brainstem evoked distinct VR responses with staggered onset in the rostrocaudal direction. Stimulation of ventrolateral medulla (VLM) resulted in higher events from homolateral VRs. Stimulating a lumbar dorsal root (DR) elicited responses even from cervical VRs, albeit small and delayed, confirming functional ascending pathways. Oximetric assessments detected optimal oxygen levels on brainstem and cortical surfaces, and histological analysis of internal brain structures indicated preserved neuron viability without astrogliosis. Serial ablations showed precollicular decerebration reducing respiratory burst duration and frequency and diminishing the area of lumbar DR and VR potentials elicited by DR stimulation, while pontobulbar transection increased the frequency and duration of respiratory bursts. Keeping legs attached allows for expressing a respiratory rhythm during hindlimb stimulation. Trains of pulses evoked episodes of fictive locomotion (FL) when delivered to VLM or to a DR, the latter with a slightly better FL than in isolated cords.
In summary, suprapontine centers regulate spontaneous respiratory rhythms, as well as electrically evoked reflexes and spinal network activity. The current approach contributes to clarifying modulatory brain influences on the brainstem and spinal microcircuits during development.

Graphical Abstract

Novel preparation of the entire isolated CNS from newborn rats unveils suprapontine modulation on brainstem and spinal networks. Preparation views (A) with and without legs attached (B). Successful fictive respiration occurs with fast dissection

✉ Giuliano Taccola
taccola@sissa.it

[1] Neuroscience Department, International School for Advanced Studies (SISSA), Via Bonomea 265, 34136 Trieste, Italy

[2] Applied Neurophysiology and Neuropharmacology Lab, Istituto di Medicina Fisica e Riabilitazione (IMFR), Via Gervasutta 48, Udine, UD, Italy

[3] Instituto de Investigaciones en Medicina Traslacional (IIMT)-CONICET - Universidad Austral, Av. Pte. Perón 1500, Pilar, Buenos Aires, Argentina

from P0-P2 rats (C). Decerebration speeds up respiratory rhythm (D) and reduces spinal reflexes derived from both ventral and dorsal lumbar roots (E).

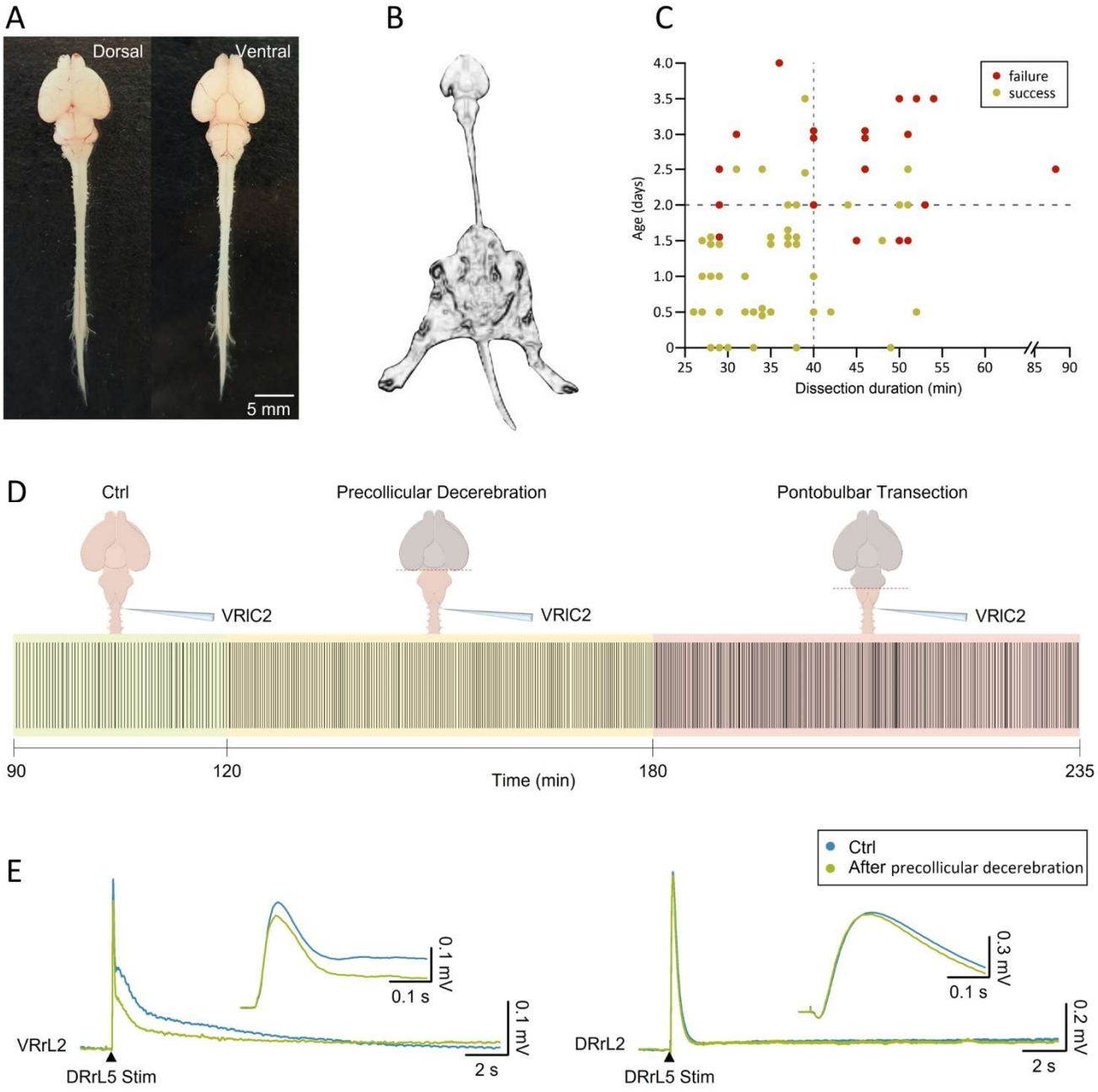

Keywords Motor-evoked potentials · Fictive respiration · Fictive locomotion · Decerebration · Leg attached · Isolated central nervous system · Tissue oxygenation

Abbreviations

ANOVA	Analysis of variance
AU	Arbitrary units
CCF	Cross-correlation function
C	Cervical
CNS	Central nervous system
DAPI	4', 6-Diamidino-2-phenylindole
DR	Dorsal root
DRDRP	Dorsal root dorsal root potential
DRVRP	Dorsal root ventral root potential

GFAP	Glial fibrillary acidic protein
l	Left
L	Lumbar
P	Postnatal
PBS	Phosphate-buffered saline
r	Right
Thr	Threshold
T	Thoracic
VR	Ventral root

Introduction

Locomotion is a complex motor behavior resulting from the continuous integration of multiple neuronal input. Descending commands from the brain trigger and modulate the intrinsic rhythmic activity of spinal circuits, which are further refined by continuous afferent sensory signals from the periphery. Disconnection from higher centers and the complete deafferentation from the body periphery make the neonatal rodents' spinal cord, isolated from the lower thoracic segments to the cauda equina, an optimal model to address both development and functional organization of the rhythmogenic lumbar networks (named central pattern generators, CPGs) responsible for generating the patterned activation of lower limb muscles during locomotion (Kiehn and Butt 2003). Indeed, the pharmacological modulation of locomotor CPGs (Cazalets et al. 1992; Blivis et al. 2007; Tazerart et al. 2008; Dose et al. 2014) and their recruitment by repetitive electrical stimulation of dorsal afferents (Marchetti et al. 2001; Etlin et al. 2010; Taccola 2011; Dose and Taccola 2016) have been successfully described using the isolated spinal cord from neonatal rodents. Furthermore, preparations of the isolated spinal cord with legs attached were introduced both for tracing real stepping and muscle recruitment during ongoing CPG activation (Kiehn and Kjaerulff 1996) and for eliciting afferent input aimed at spinal networks (Mandadi and Whelan 2009; Dingu et al. 2018).

Noteworthy, these reduced preparations focus on local spinal microcircuits. A more conservative approach also considers the presence of intact pons and brainstem (Suzue 1984) to explore the descending activation of lumbar circuits through repetitive electrical pulses applied to the ventrolateral medulla (VLM; Zaporozhets et al. 2004) and to investigate the functional coupling between locomotor spinal circuits and respiratory networks located in the brainstem (Giraudin et al. 2012). However, all these reduced preparations preclude the possibility to explore the modulatory role of suprapontine structures on spinal and brainstem circuits at birth, as well as the changes in these interactions during development.

Compelling evidence from in vivo animals shows suprapontine structures modulating respiration and locomotion already in newborns (Horn and Waldrop 1998). Still in newborns, it has been demonstrated that the caudal hypothalamus affects respiratory function (Lakke 1997; Dreshaj et al. 2003), and basal ganglia are pivotal for regulating postural muscle tone during rhythmic motor behavior of limbs (Van Hartesveldt and Lindquist 1978; Takakusaki et al. 2004). However, an in vitro preparation of the entire rodent CNS has never been introduced, as it is widely accepted that the postnatal rodent tissue likely suffers from hypoxia if the dissection lasts longer than the brief time required for isolating the sole spinal cord (Wilson et al. 2003). The pioneering work of John Nicholls tried to circumvent this limitation by introducing a more immature preparation using opossums at birth (Nicholls et al. 1990), corresponding to 14-day rat embryos, as they are less vulnerable to hypoxic conditions. The whole CNS isolated in vitro from opossum neonates allowed to acquire several important outcomes, such as compound action potentials evoked by stimulating the CNS, spinal reflexes, and the spontaneous rhythmical nerve activity related to respiration. Histological viability of the entire CNS isolated from newborn opossums was confirmed for up to four days in Krebs' fluid, and up to seven in enriched media under sterile conditions (Nicholls et al. 1990; Eugenín and Nicholls, 2000). However, due to its immaturity, the postnatal opossum preparation lacks the cerebellum, depriving the study of its potential contribution to modulating respiratory and motor functions (Lutherer et al. 1989).

The importance of exploring suprapontine influences on both brainstem and spinal networks in a more structured mammalian preparation of the entire CNS in vitro, made us wonder whether well-established faster procedures of tissue dissection on 0–2-day-old pups only, would allow isolation of the complete CNS, cerebellum included, from neonatal rats.

The functionality of the preparation was assessed by: the persistence of a spontaneous respiratory rhythm from cervical roots for at least 4 hours from anesthesia, the well-preserved oxygen levels in cortical and brainstem tissues for the entire length of experiments, the histological validation of neuronal viability after 4 hours in vitro, the presence of electrically evoked motor responses after brainstem and spinal cord stimulation, and the expression of episodes of locomotor-like oscillations elicited by trains of pulses delivered to dorsal afferents and VLM. All of the tested functional outcomes were subject to some modulatory influences from suprapontine centers.

In summary, the current study defined an in vitro preparation of the entire mammalian CNS for studying the cellular basis of rhythmical activity and their development in the first postnatal days. In addition, the novel experimental setting clarified the presence, from the first days of life, of

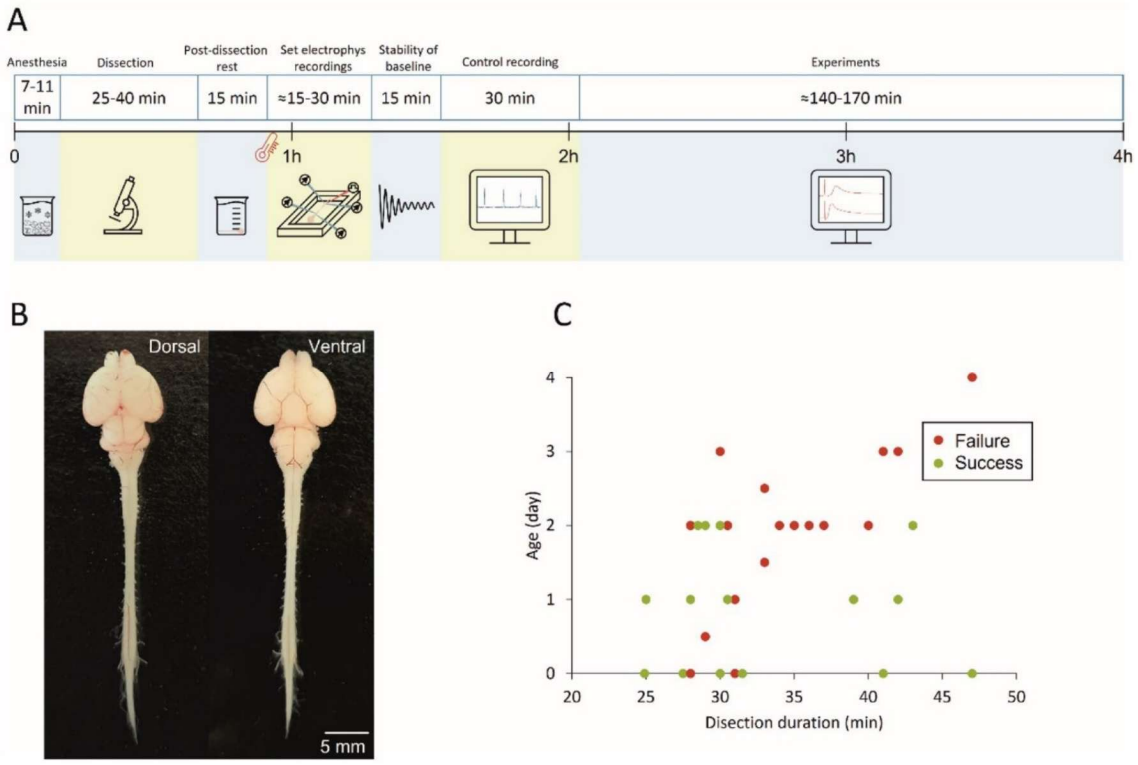

Fig. 1 Experimental design of the study. **A** A timeline describing the experimental procedures, from cryoanesthesia to dissection, post-dissection rest, setting of electrophysiological recordings, pause to stabilize the baseline, and, eventually, control and experimental recordings. Note that as soon as the preparation was placed in the recording chamber, bath temperature was progressively raised to 25–27 °C. **B** Photographs displaying dorsal and ventral views of the isolated entire CNS preparation from a P1 newborn. **C** Scatter plot describes the presence of a stable fictive respiration for each preparation, arranged by age and time of dissection ($n = 32$). Green dots correspond to successes (> 4 h of fictive respiration), while red dots represent failures (< 4 h of fictive respiration)

modulatory influences from suprapontine structures, which determine faster and broader respiratory bursts, while also marginally facilitating episodes of locomotor-like cycles elicited by afferent stimulation.

Methods

In Vitro Preparation of the Isolated Entire CNS

All procedures were approved by the International School for Advanced Studies (SISSA) ethics committee and are in accordance with the guidelines of the National Institutes of Health (NIH) and with the Italian Animal Welfare Act 24/3/2014 n. 26, implementing the European Union directive on animal experimentation (2010/63/EU). All efforts were made to minimize the number and suffering of animals. A total of 148 postnatal Wistar rats (P0–P4) of both sexes were used at random.

As graphically summarized by the timeline in Fig. 1A, 7–11 minutes of cryoanesthesia (Phifer and Terry 1986; Danneman and Mandrell 1997; Zimmer et al. 2020) anticipated surgical procedures at room temperature. After the disappearance of the tail pinch reflex, the forehead was ablated at the level of the orbital line, the skin removed from the animal's skull and back, and the chest and forelimbs ventrally detached. The preparation was then placed on a Sylgard-filled petri dish under a microscope and fully covered with oxygenated Krebs solution, which was frequently replaced. Krebs solution contained (in mM): 113 NaCl, 4.5 KCl, 1 $MgCl_2 7H_2O$, 2 $CaCl_2$, 1 NaH_2PO_4, 25 $NaHCO_3$, and 30 glucose, gassed with 95% O_2-5% CO_2, pH 7.4, 298 mOsm/kg. Afterward, craniotomy and ventral and dorsal laminectomies were performed to expose the entire CNS, which was then isolated from the olfactory bulbs down to the cauda equina by carefully transecting all cranial nerves, dorsal roots (DRs) and ventral roots (VRs; Nicholls et al. 1990). Figure 1B pictures the whole CNS preparation from a P1 newborn in dorsal and ventral views. On average, dissection

procedures lasted about 30 min. A post-dissection resting period of 15 min was systematically respected after surgical dissection (Fig. 1A).

For electrophysiological recordings, the preparation was then placed ventral side up in a recording chamber (Fig. 1A; chamber depth = 4000 µm) continuously perfused with Krebs solution (7 mL/min), while the bath temperature was progressively raised and maintained in the range of 25 to 27 °C by a single channel temperature controller (TC-324C Warner Instruments, USA). Once the baseline stabilized (15 min; Fig. 1A), 30 min of stable control (Fig. 1A) was acquired through extracellular recordings.

For the preparation of the entire CNS with legs attached, dorsal and ventral laminectomies were performed down to the lowest thoracic level (Th13), preserving the remaining lumbosacral vertebra and nerves attached to hindlimbs. DRs and VRs were kept as long as possible, removing only the dorsal root ganglia (DRG).

Plots in Figs. 1C and 9B report the age of the animal on the x-axis and the length of surgical dissection on the y-axis, identifying a bottom-left region (younger preparations undergoing fast surgical procedures) where preparations showed the highest percentage of successfully recorded respiratory rhythms for at least 4 h from the anesthesia performed at the beginning of tissue isolation. Based on the outcome of this set of preliminary experiments, P0-3 newborns were selected for the rest of the study.

Extracellular Recordings

DC-coupled recordings were acquired from VRs and DRs through tight-fitting suction electrodes connected to a differential amplifier (DP-304, Warner Instruments, Hamden, CT, USA; high-pass filter = 0.1 Hz, low-pass filter = 10 kHz, gain × 1000), then digitized (Digidata 1440, Molecular Devices Corporation, Downingtown, PA, USA; digital Bessel low-pass filter at 10 Hz; sampling rate = 50 kHz) and visualized real-time with the software Clampex 10.7 (Molecular Devices Corporation, Downingtown, PA, USA).

Electrical Stimulation

Single and repetitive rectangular electrical pulses (duration = 0.1 ms, frequency = 0.03 Hz) were delivered to caudal DRs (L4-S1) through a programmable stimulator (STG4002, Multichannel System, Reutlingen, Germany) using bipolar glass suction electrodes with two close silver wires spaced by 300–500 µm. The intensity of stimulation (6–800 µA) is expressed as times to threshold, where the latter is the lowest intensity supplied to a DR to elicit an appreciable depolarizing potential from the homolateral VR. As for input–output experiments, to elicit motor potentials in response to DR stimulation (DRVRPs), 30 single pulses (duration = 0.1 ms) at intensities of 1, 1.5, 2, 3, 5 × Thr were delivered at a frequency of 0.03 Hz.

Punctiform stimulation of multiple sites of the brain was conducted with a custom-made bipolar concentric electrode composed of an internal 250-µm-width stainless steel electrode (UE KK1, FHC, Bowdoinham, USA) and a helical silver wire wrapped around the tip of a glass pipette (700-µm-diameter tip). Multisite stimulation of the brainstem consists in a train of 30 rectangular pulses at 0.03 Hz (duration = 1 ms; intensity = 2 × Thr, 1800–5000 µA). In experiments involving brainstem stimulation, threshold was defined as the lowest intensity applied to the VLM to obtain an appreciable depolarizing response from lower lumbar VRs. In each experiment, 10 distinct stimulating spots (named A–J) were consistently found on each side of the brainstem based on the anatomy of visible ventral arteries. Two stimulating sites are positioned on the median basal artery (namely A on the most rostral pons, and G at the intersection of basilar and anterior inferior cerebellar arteries). B is positioned about 0.5 mm laterally from A. The spots named C, D and E are aligned on the pons, equally interspaced by 0.5 mm and span from the median basal artery (C) to the lateral extremity of the ventral brainstem (E). In the rostral caudal direction, D is equidistant between superior and inferior cerebellar arteries. The F-stimulating spot is placed on the anterior inferior cerebellar artery between the median basal artery and the lateral ventral edge of the brainstem. H and I are aligned on the medulla, proximal (H) and distal (I) to the median basal artery. In the rostral caudal direction, they are equidistant from the inferior cerebellar artery and the first cervical VR. J is located on the first cervical segment of the spinal cord, laterally to the ventral spinal artery.

In a subgroup of preparations, the stimulation site was visually confirmed at the end of the experiment by electrolytically destroying the area of stimulation through strong electrical pulses (intensity = 16 mA, duration = 5 ms) delivered on the surface of pyramids (spot H) in the VLM.

Fictive locomotion (FL) patterns were recorded from the left (l) and right (r) L2 VRs (flexor motor commands) and from l and r L5 VRs (extensor motor commands). Alternating discharges between homolateral L2 and L5 VRs and between homosegmental VRs are considered the distinct feature of FL (Kiehn 2006). FL was electrically evoked by trains of rectangular single pulses applied to DRrL6-S1 (160 single pulses at 2 Hz, pulse duration = 0.1 ms, intensity = 15–37.5 µA or 1.5–3.5 Thr) or to the pyramid in the VLM (trains of single pulses at 1–2 Hz, pulse duration = 1–5 ms, intensity = 0.5–4.5 mA).

Serial Transection Experiments

In a subgroup of experiments, suprapontine structures were ablated from the whole CNS preparation by two serial horizontal transections. Firstly, precollicular decerebration was performed by surgically cutting the brain rostral to the fifth cranial nerves at the level of superior cerebellar arteries and caudal edge of inferior colliculi (Voituron et al. 2005). One hour later, a second transection was carried out at the level of the ninth cranial nerves to separate the pons and medulla. Before each cut, suction electrodes on cervical VRs were released to avoid any nerve damage and a new suction was adopted after cutting. In experiments with DR train stimulation, a further midthoracic transection (at the level of thoracic 4/5) was adopted to compare, in the same animal, FL in the intact CNS vs. the isolated spinal cord. Since in these experiments midthoracic transection did not affect the stability of lumbar VR signals, suctions were not released, thus allowing a direct comparison between the amplitude of signals before and after spinal transection.

Tissue Oxygen Assessment

The whole-CNS preparation was warmed to 25–27 °C and allowed to stabilize for 30 min prior to PO_2 measurements. Continuous sampling in our recording chamber was performed from 80 min until 4 hours from the induction of anesthesia, before any surgical procedures (total duration 160 min). PO_2 levels showed that the solution at the surface of the bath was slightly more oxygenated than the one at the bottom, with PO_2 levels of 559.42 ± 2.34 Torr at 300 µm under the surface of the oxygenated perfusing fluid, and 403.50 ± 6.89 Torr at 300 µm above the chamber floor (chamber depth = 4000 µm). Conversely, no differences were observed in PO_2 along the length of the recording chamber.

Measurement of PO_2 in both VLM and motor cortex was performed using a fiber-optic microsensor with a tip diameter of 50 µm (Optode, OxyMicro System, World Precision Instruments, FL, USA) implanted at a depth of 100 µm. The optode microsensor was mounted on a calibrated micromanipulator to enable fine control on the vertical plane. For VLM PO_2 measurements, the tip of the microsensor was horizontally aligned with the pair of XII cranial nerves and placed equidistant from the lateral emergence of the XII nerve, and the midline. For cortical oxygen assessment, the tip of the microsensor was placed horizontally, in the middle of the longitudinal fissure, 2 mm lateral from the midline. PO_2 measurements were taken every 1 s and were acquired directly by OxyMicro v7.0.0 software (OxyMicro System, World Precision Instruments, FL, USA). All PO_2 measurements were instantly corrected for temperature, which was on average 25.59 ± 0.28 °C. Overall tissue oxygenation was calculated for each preparation as the average of all 5 min bins that were continuously sampled during the entire experiment (160 min). To assess any decay in tissue oxygenation during the entire experiment (160 min), we compared, for each preparation, the PO_2 at the beginning (80 min; t_{80}) and at the end of the continuous oxygen assessment (240 min; t_{240}).

Slice Immunostaining and Cell Counting

At the end of electrophysiological experiments, CNS preparations were fixed with 4% paraformaldehyde at 4 °C for overnight incubation. Tissue was then cryopreserved in 30% sucrose in water and stored at 4 °C for immunostaining following our standard procedure. Briefly, CNS preparations were cut into 30-µm-thick axial sections using a sliding cryostat microtome and incubated with a blocking solution containing: 5% fetal calf serum, 5% bovine serum albumin, and 0.3% Triton X-100 in PBS, for one hour at room temperature. Then, slices were incubated overnight at 4 °C with the antibodies: NeuN (1:200) and β-III tubulin (1:2000) for neurons, and glial fibrillary acidic protein (GFAP; 1: 500) for astrocytes (Taccola et al. 2010; Cifra et al. 2012; Deumens et al. 2013). Primary antibodies were visualized using the corresponding secondary fluorescent antibody (Alexa Fluor 488 or 544 at 1:500 dilutions; Invitrogen).

To visualize cell nuclei, slices were incubated for 30 min in 1 µg/ml solution of 4′, 6-diamidino-2-phenylindole (DAPI) and mounted using the Vectastain medium (Vector Laboratories, Burlingame, CA). After incubation with the secondary antibody, slides were finally visualized with a TCS SP2 Leica confocal microscope (Leica Microsystems Srl, Italy), epifluorescence microscopy (Zeiss Axioskop2, Carl Zeiss MicroImaging, Thornwood, NY) or Nis-Eclipse microscope (NIKON, Amsterdam, Netherlands) with 10 × and 20 × magnifications. NeuN, β-III tubulin, and GFAP-positive cell density were quantified in a region of interest (RoI) of 730×730 µm^2 at 750 µm from the surface of the ventrolateral prefrontal cortex, using Image J software (http://imagej.nih.gov) on images at 20 × magnification. Note that the maximal thickness of the P0-2 brain was less than 4 mm.

When biomarker staining was diffuse, like with β-III tubulin and GFAP, signals were collected as mean fluorescence intensity, expressed in arbitrary units (AU) determined with densitometry analysis, using ImageJ software, in fields of 730×730 µm^2 area.

Data Analysis

To remove electrical interference, original traces were notched at 50 Hz through Clampfit 11.2 software (Molecular Devices Corporation, PA, USA). All spontaneous rhythmic motor discharges displaying large-amplitude depolarizations synchronous among bilateral VRs and appearing at regular intervals are ascribed to respiratory bursts. A burst is defined as a period of sustained membrane depolarization that originates with a rapid onset from the baseline and remains above a preset threshold (usually five times the standard deviation of baseline noise; Bracci et al. 1996). The time during which the membrane potential remains above the preset threshold is defined as burst duration (Bracci et al. 1996). Rhythmic discharges were also characterized based on their period, defined as the time between peaks of two consecutive cycles (Taccola and Nistri 2006; Dose et al. 2016). The ratio between standard deviation and mean value provides the coefficient of variation (CV), which is an index of consistency of responses (Taccola et al. 2020).

Mean electrically evoked reflex responses were obtained by averaging at least 15 traces not corrupted by any spontaneous activity.

Conduction velocity was calculated by dividing the time to peak of each response by the distance between stimulating and recording sites, as measured by a microcalibrated dial caliper (sensitivity = 20 µm).

Phase coupling between pairs of VRs was ascertained by the correlation coefficient function (CCF) using Clampfit 11.2 software. A positive CCF value ≥ 0.5 states that rhythmic signals from two VRs are synchronous, while CCF $\leq$ -0.5 accounts for alternating patterns (Taccola and Nistri 2005; Dose et al. 2016).

Statistical Analysis

Statistical analysis was performed with GraphPad InStat 3.10 (Inc., San Diego, California, USA).

All data in boxplots show sample median (horizontal segment), 75th and 25th percentiles (top and bottom edges of box) and 1.5 times the interquartile range (whiskers). The number of animals is indicated as n in the Results, and data are reported as mean ± SD values. Before assessing statistical differences among groups, a normality test was performed to select the use of either parametric or nonparametric tests.

Accordingly, parametric data were analyzed with paired or unpaired t test, one-way analysis of variance (ANOVA) and repeated measures ANOVA, whereas Mann–Whitney test, Kruskal–Wallis test, and Wilcoxon matched-pairs signed-rank test were used for nonparametric data.

Multiple comparisons ANOVA was followed by Tukey–Kramer multiple comparisons test, Fisher's LSD or Dunn's method. Differences were considered statistically significant when $P \leq 0.05$.

Results

The Entire CNS In Vitro Displays a Spontaneous and Stable Fictive Respiratory Rhythm

The expression of spontaneous respiratory motor patterns is a sign of the functionality of neuronal networks in the brainstem–spinal cord in vitro (Smith et al. 1990). Likewise, in a sample preparation of the entire CNS isolated from newborn rats, we recorded respiratory-related rhythmic discharges at a frequency of 0.04 Hz, which appeared synchronous (CCF = 0.84) among cervical and lumbar ventral roots (Fig. 2A). The average bursts are reported in Fig. 2B, showing a duration of 1.47 s for VRrC1 and 1.09 for VRrL5 and a peak amplitude equal to 0.25 mV and 0.06 mV, respectively. Interestingly, double bursts only seldom appeared, as visualized in the magnification of Fig. 2C where double- (red star) and single-peaked respiratory events follow in a row.

Pooled data from twelve experiments indicate that, in the first 30 min of continuous recordings, the spontaneous respiratory rhythm has a frequency of 0.06 ± 0.03 Hz, with single bursts that last on average 1.80 ± 0.52 s and peak amplitude of 0.24 ± 0.13 mV. In six of those preparations, fictive respiratory events seldom appeared double-peaked (on average, 8.17 ± 2.48 double-peaked burst out of 102.17 ± 63.02 total respiratory events) and eventually turned into single bursts in the following 30 min. However, the sporadic occurrence of double bursts did not affect mean rhythm frequency ($P = 0.448$; unpaired t test), burst duration ($P = 0.449$; unpaired t test), nor peak amplitude ($P = 0.240$; Mann–Whitney test).

To prove the stability of the fictive respiratory rhythm derived from the entire CNS preparation in vitro, long recordings were continuously performed for at least 4 h right after tissue isolation. Figure 2D traces the time course of the mean rhythm frequency in 5-min bins for five experiments. Respiratory events recorded in the first 20 min were similar to the ones recorded at the end of the time course as for frequency ($P = 0.536$; paired t test), duration ($P = 0.050$; paired t test), frequency CV ($P = 0.680$; paired *t* test) and amplitude ($P = 0.386$; paired t test; Fig. 2E, Table 1).

The stable fictive respiratory rhythm recorded for more than 4 hours demonstrates that the entire CNS in vitro is a sound preparation for studying the respiratory network in a more intact experimental setting.

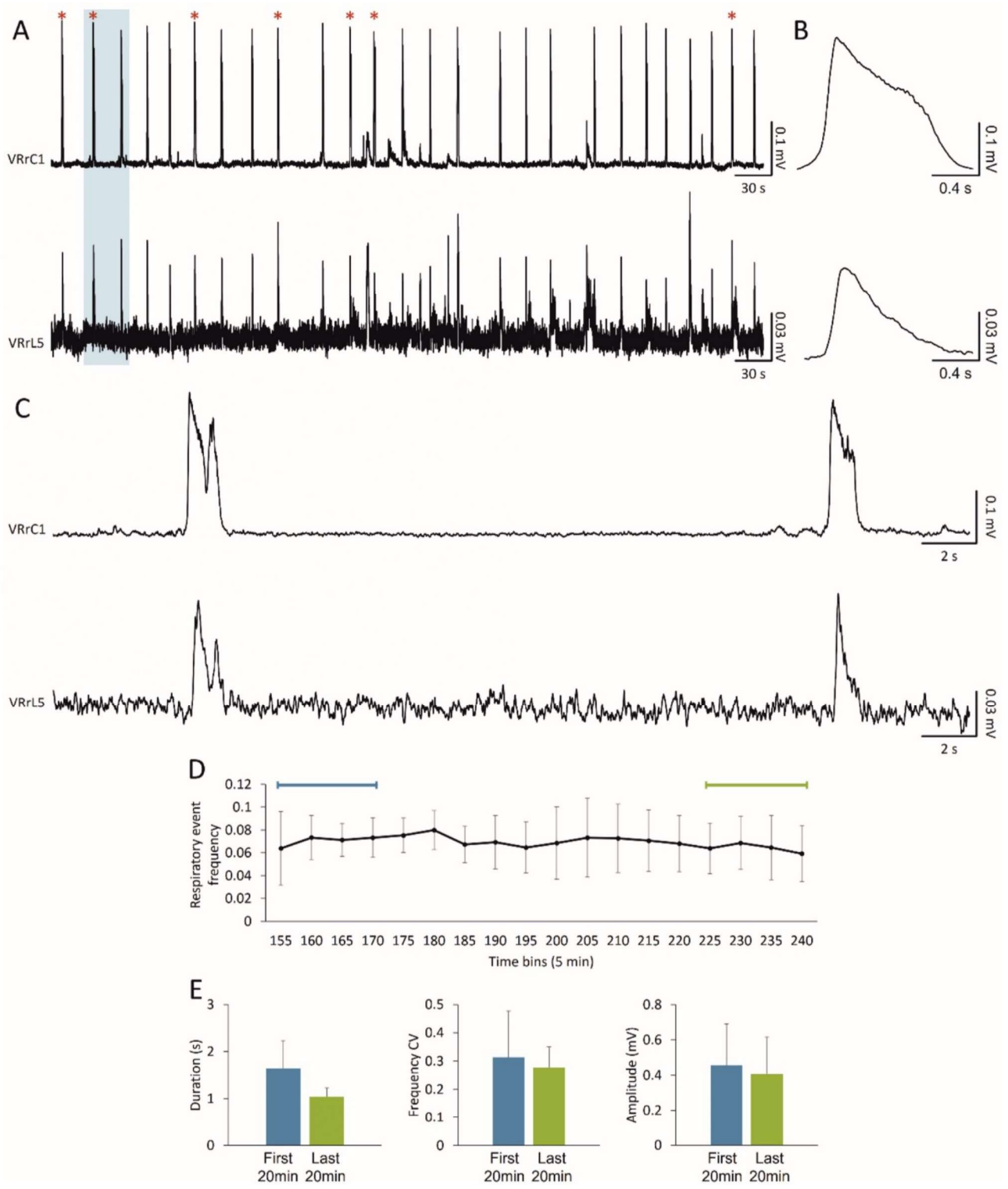

Fig. 2 In vitro preparation of the entire CNS expresses 4 hours of stable fictive respiration. **A** Spontaneous and synchronous respiratory bursts are recorded for up to 4 hours from both cervical and lumbar VRs. The occurrence of sporadic double bursts is tagged by red stars. **B** Average bursts summarize shape and duration of cervical and lumbar respiratory events. **C** Magnification of traces in the shaded rectangle in A. A double and a single peak burst follow one another on both cervical and lumbar VRs. **D** The average time course shows the frequency of fictive respiration for the entire length of the experiment for 5 min bins ($n = 5$). The time indicated lapses from the induction of anesthesia. **E** Respiratory events in the first and last 20 min of the time course in (**D**) remain unchanged as for duration, regularity of rhythm expressed as frequency CV, and amplitude

Table 1 Features of fictive respiratory events at the onset and the end of electrophysiological experiments

	First 20 min	Last 20 min
Frequency (Hz)	0.07 ± 0.03	0.07 ± 0.02
Duration (s)	1.65 ± 0.59	1.04 ± 0.19
Frequency CV	0.31 ± 0.16	0.28 ± 0.07
Amplitude (mV)	0.46 ± 0.24	0.41 ± 0.21

Punctiform Electrical Stimulation of the Ventral Surface of the Brainstem and Pons Elicits Distinct Motor Responses Along Lumbar Segments

To assess descending input conduction along spinal segments in the CNS preparation, motor-evoked potentials were induced by serial pulses of electrical stimulation on different sites of the ventral brainstem. On each preparation, electrical pulses were delivered to ten loci on each side of the brainstem, ranging from higher pontine structures to the upper cervical cord (locations are detailed in the Methods section).

The cartoon in Fig. 3A identifies the stimulating sites using different letters and a color code. The responses displayed below were serially evoked, in the same preparation, by electrically stimulating distinct sites and were recorded from the homolateral VRrL5. In a sample experiment, the stimulating electrode was moved in a rostral–caudal direction, generating larger and more delayed responses (Fig. 3A). Medial rostral pons (indicated by the letter "A" in Fig. 3A) was the highest site of stimulation that still generated appreciable evoked potentials from lumbar motor pools (L5), with a peak of 0.04 mV and a time to peak of 0.14 s. The largest (Fig. 3B) and earliest (Fig. 3C) motor-evoked response, with a peak of 1.84 mV and a time to peak of 0.08 s, was obtained by pulses supplied to the ventrolateral surface of the first cervical spinal segment (named as J). On the other hand, the most efficient brainstem stimulation corresponded to the supply of pulses to the pyramid (as indicated by the letter "H") with responses of 1.68 mV amplitude and 0.09 s time to peak. Contrariwise, in 17 preparations, spanning from 0- to 3-day-old newborns (5 preparations at P0; 4 at P1; 4 at P2 and 4 at P3) stimulation of lateral rostral pons and higher brain structures (dorsal cerebellum, ventral and dorsal mesencephalon, and cortex) always failed to elicit any reflexes from VRs (data not shown).

Average data describe responses evoked by serial multisite electrical stimulation in terms of amplitude (Fig. 3B) and time to peak (Fig. 3C) and report significantly larger responses from cervical spinal stimulation compared to rostral pulses (Fig. 3B; "A", "C", and "G"; $P < 0.001$; Kruskal–Wallis test, $n = 5–8$). Moreover, compared to all homolateral responses, the one originating from stimulation of the "J" site appears sooner (Fig. 3C; $P < 0.0001$; ANOVA test followed by Tukey–Kramer multiple comparisons test, $n = 5–8$).

The most rostral impulses that generated VRPs in three out of six experiments were delivered to the medial rostral pons (as indicated by the letter "A"), although responses were significantly lower compared to the ones elicited by pyramid stimulation ($P < 0.001$; Kruskal–Wallis test, $n = 5–8$).

To explore whether homolateral and contralateral stimulations evoked different spinal lumbar responses, simultaneous recordings were acquired from the right and left VRL5 when electrical pulses were serially applied to multiple sites of the brainstem–upper cervical cord. Figure 3D shows simultaneous recordings from bilateral VRL5 during electrical stimulation of the rostro-medial pons ("D") and VLM ("I"). On both sites, responses were higher and appeared earlier for homolateral ($peak_D = 1.20$ mV, time to $peak_D = 0.11$ s; $peak_I = 1.45$ mV, time to $peak_I = 0.11$ s) vs. contralateral stimulation ($peak_D = 0.77$ mV, time to $peak_D = 0.13$ s; $peak_I = 0.88$ mV, time to $peak_I = 0.11$ s). Most stimulating configurations generated homolateral (h) and contralateral (c) evoked responses of unchanged amplitude, excluding the pons ("C" and "D") and VLM ("I"; Fig. 3E; $n = 5–8$). As for latency of evoked responses expressed as time to peak, contralateral stimulation elicited delayed VRPs in all cases, except for the site indicated by the letter "C," which is very close to the brainstem midline (Fig. 3F; $n = 5–8$). Average values are reported in Table 2.

In summary, descending input recorded caudally from bilateral VRs of the lower lumbar cord shows the recruitment of specific functional pathways, having distinct latencies and motoneuronal recruitment mirroring the rostrocaudal supply of brainstem pulses.

Descending Input Elicited by Brainstem Stimulation Travels Along the Cord with Different Conduction Velocity

To explore the organization of descending spinal pathways recruited by brainstem stimulation, electrical pulses were delivered to the pyramid (H spot) and responses taken from homolateral VRs at several spinal levels were used to calculate conduction velocity. In Fig. 4A, evoked motor potentials were acquired from five spinal segments (from C1 to L5) in correspondence to the stimulation of the left medulla. Responses became lower and slower when recorded from more caudal spinal segments. While the upper cervical peak appeared sooner (C1; 0.02 s) and was more similar to lower cervical regions (C6; 0.02 s), the thoracic VR response was delayed (T9; 0.04 s) and even more delayed were responses

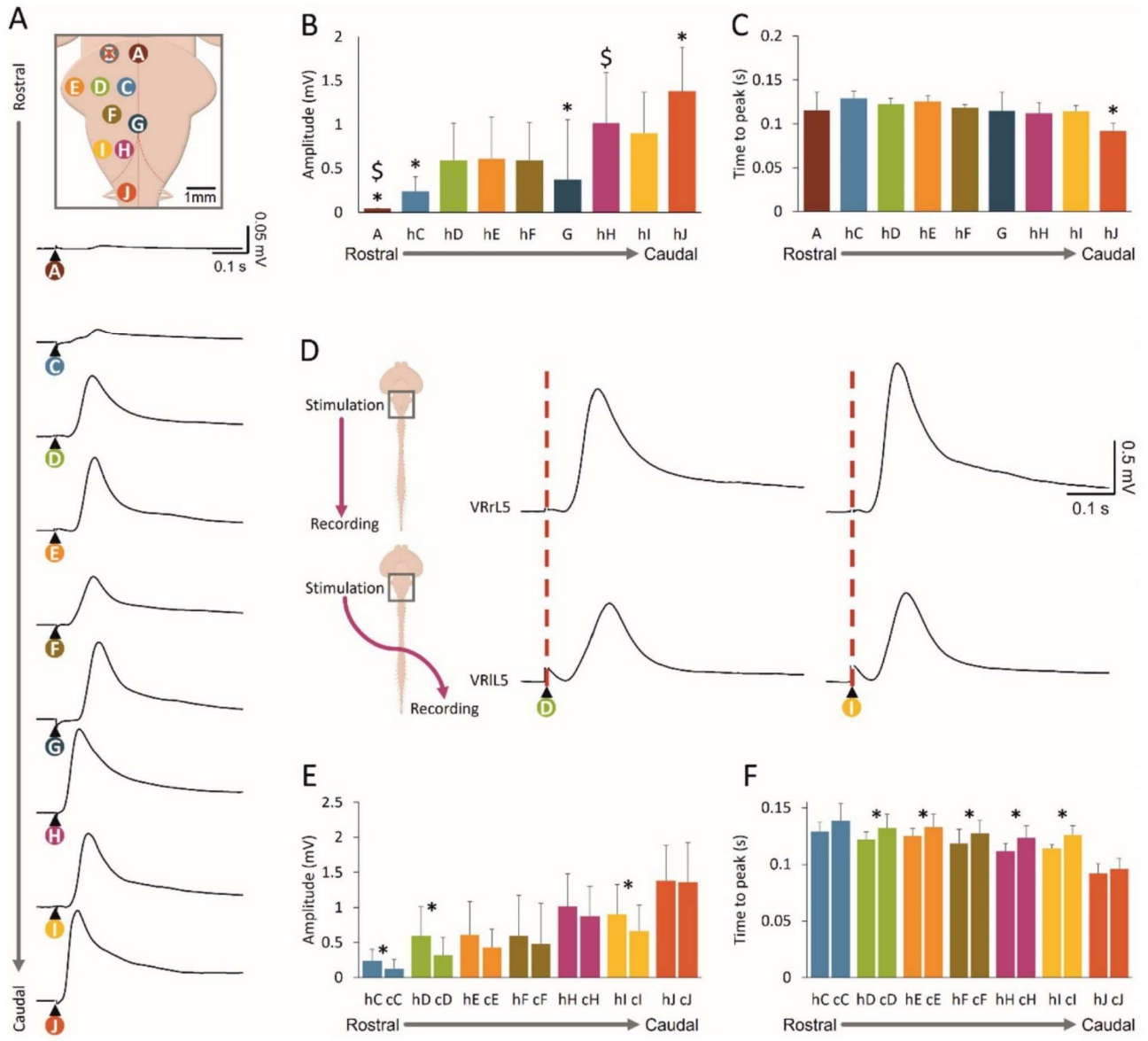

Fig. 3 Distinct motor responses from lumbar VRs are evoked by punctiform electrical stimulation of the ventral surface of the brainstem and pons. **A** Different sites of pons and medulla were serially stimulated by a custom-made punctiform electrode (intensity = 2 mA, duration = 1 ms) and mean motor potentials were recorded from VRrL5. Each site of stimulation is indicated with a different color and letter in the schematic cartoon, which is calibrated to the real sample dimensions. Please note that only one side of the cartoon is labeled. Serial stimulation of distinct sites evokes motor responses of different amplitude (**B**, $n = 5–8$; $^*P < 0.001$) and time to peak (**C**, $n = 5–8$; $^*P < 0.001$). **D** Motor responses are elicited from r-l VRL5 by serially stimulating "D" (left panel) or "I" (right panel) spots on the right medulla (same experiment as in A). For each pulse, homolateral (upper) and contralateral (bottom) responses are simultaneously acquired. Average traces come from 15 superimposed sweeps. **E** Histogram reports the peak amplitude of homolateral and contralateral responses by serially stimulating different sites. Homolateral responses evoked by stimulation of "C" ($n = 6$; $^*P = 0.006$), "D" ($n = 8$; $^*P = 0.010$), and "I" ($n = 7$; $^*P = 0.023$) are significantly higher than contralateral ones. (F) Histogram summarizes the time to peak of homolateral and contralateral responses when serially stimulating different sites. Homolateral responses to pulses applied to "D" ($n = 8$; $^*P = 0.043$), "E" ($n = 8$; $^*P = 0.031$), "F" ($n = 7$; $^*P = 0.020$), "H" ($n = 8$; $^*P < 0.001$), and "I" ($n = 7$; $^*P = 0.018$) are significantly faster in comparison with contralateral

derived from upper (L1; 0.05 s) and lower (L5; 0.09 s) lumbar segments.

Data collected from 5 experiments demonstrate that potentials recorded from thoracolumbar segments appear later than cervical responses (in Fig. 4B; $P < 0.001$; ANOVA). Pulse conduction velocity based on the actual distance between each pair of stimulating and recording sites revealed that the input descending to thoracic segments is

Table 2 Amplitude of homolateral and contralateral VR potentials elicited by punctiform electrical stimulation of different spots on the ventral surface of the brainstem

Location	A ($n=3$)	C ($n=6$)	D ($n=8$)	E ($n=8$)	F ($n=7$)	G ($n=6$)	H ($n=8$)	I ($n=7$)	J ($n=8$)
Homolateral peak amplitude (mV)	0.04 ± 0.00	0.24 ± 0.16	0.6 ± 0.48	0.61 ± 0.48	0.6 ± 0.43	0.37 ± 0.68	1.02 ± 0.58	0.9 ± 0.46	1.38 ± 0.5
Homolateral time to peak (m)	0.12 ± 0.02	0.13 ± 0.01	0.12 ± 0.01	0.13 ± 0.01	0.12 ± 0.00	0.12 ± 0.02	0.11 ± 0.01	0.11 ± 0.01	0.09 ± 0.01
Contralateral peak amplitude (mV)		0.13 ± 0.13	0.32 ± 0.25	0.43 ± 0.26	0.48 ± 0.37		0.88 ± 0.58	0.67 ± 0.42	1.36 ± 0.57
Contralateral time to peak (m)		0.14 ± 0.02	0.13 ± 0.01	0.13 ± 0.01	0.13 ± 0.01		0.12 ± 0.01	0.13 ± 0.01	0.1 ± 0.01
P value of homolateral and contralateral amplitude comparison		0.006 (paired t test)	0.010 (paired t test)	0.110 (Wilcoxon matched-pairs signed-ranks test)	0.097 (paired t test)		0.210 (paired t test)	0.023 (paired t test)	0.894 (paired t test)
P value of homolateral and contralateral time to peak comparison		0.143 (paired t test)	0.043 (paired t test)	0.031 (Wilcoxon matched-pairs signed-ranks test)	0.020 (paired t test)		< 0.001 (paired t test)	0.018 (paired t test)	0.123 (paired t test)

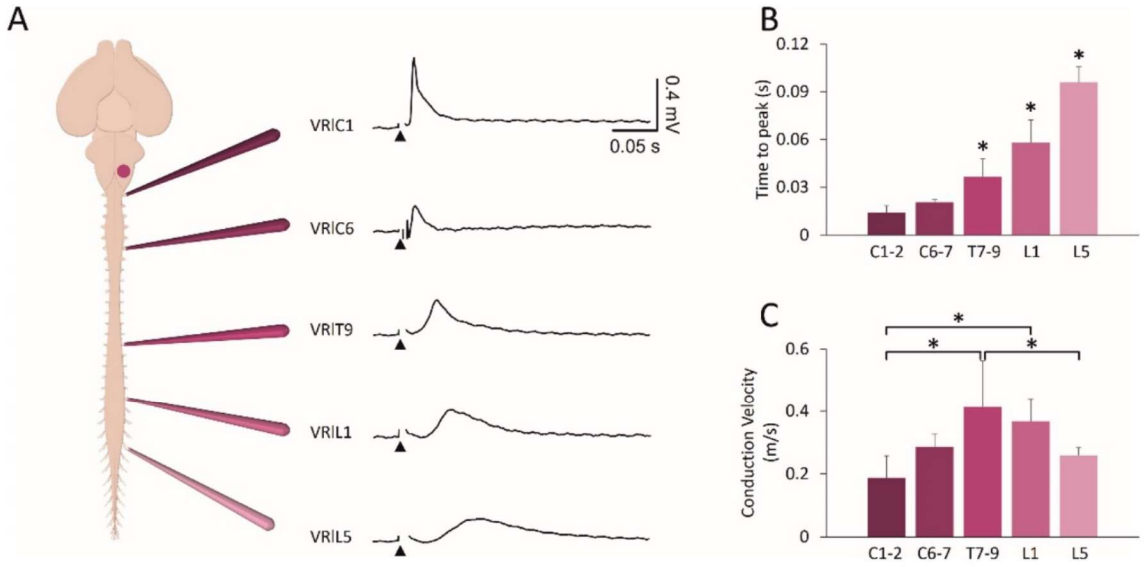

Fig. 4 Electrical stimulation of the brainstem reveals different conduction velocities along the cord. **A** Single electrical pulses (intensity = 2 mA, duration = 1 ms) applied to the left pyramids of the brainstem (spot H) evoke simultaneous responses from cervical (C1, C6), thoracic (T9), and lumbar (L1, L5) VR on the left side of the cord. Average traces arise from 15 superimposed sweeps. **B** Histogram of the time to peak of responses shows that the slowest response comes from the most caudal segments ($n=5$; $^*P<0.001$). **C** Histogram for conduction velocity of pulses follow a distinct trend ($^*P=0.001$)

Table 3 Time to peak and conduction velocity of spinal motor responses evoked by electrical stimulation of left ventrolateral medulla

	C1/C2	C6/C7	T7/8/9	L1	L5
Time to peak (s)	0.01 ± 0.00	0.02 ± 0.00	0.04 ± 0.012	0.06 ± 0.01	0.1 ± 0.01
Conduction velocity (m/s)	0.19 ± 0.07	0.29 ± 0.04	0.4 ± 0.15	0.37 ± 0.07	0.26 ± 0.03

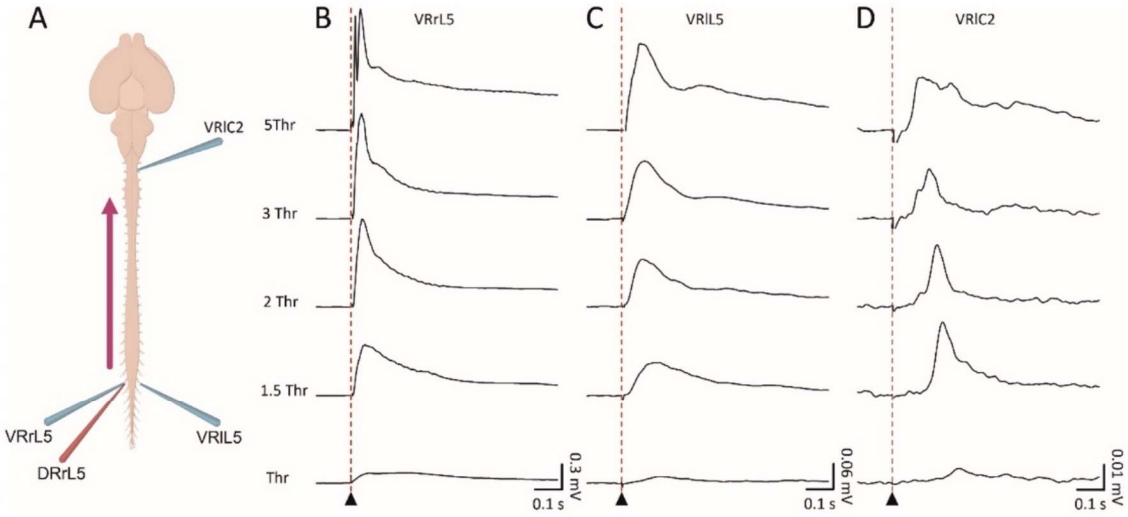

Fig. 5 Input/output caudal stimulation elicits evoked motor responses along the cord. Electrical pulses (intensity = 0.02–0.1 ms, duration = 0.1 ms) delivered to lumbar afferents of the L5 segment evoke responses from the homologous VRL5 (**B**), contralateral VRL5 (**C**) and contralateral higher cervical VRC2 (**D**). By increasing the strength of stimulation, responses appear sooner and higher. Average traces have been pooled from 15 superimposed sweeps

Table 4 Input–output experiments for electrical stimulation of DRrL5

Root		Thr	1.5 Thr	2 Thr	3 Thr	5 Thr
VRrL5	Amplitude (mV)	0.53 ± 0.5	0.87 ± 0.61	0.80 ± 0.47	0.84 ± 0.41	0.89 ± 0.42
	Time to peak (s)	0.05 ± 0.02	0.03 ± 0.02	0.03 ± 0.02	0.03 ± 0.02	0.03 ± 0.02
VRlL5	Amplitude (mV)	0.23 ± 0.29	0.45 ± 0.34	0.58 ± 0.48	0.67 ± 0.56	0.7 ± 0.59
	Time to peak (s)	0.08 ± 0.03	0.07 ± 0.02	0.07 ± 0.02	0.07 ± 0.02	0.07 ± 0.02
VRlC2	Amplitude (mV)	0.18 ± 0.15	0.16 ± 0.1	0.18 ± 0.12	0.20 ± 0.15	0.20 ± 0.13
	Time to peak (s)	0.12 ± 0.03	0.12 ± 0.02	0.12 ± 0.02	0.12 ± 0.02	0.12 ± 0.02

the fastest, and that the input to lumbar segments is faster than the cervical one (Fig. 4C; $P = 0.001$; ANOVA; Table 3).

The different conduction velocity of descending input elicited by brainstem stimulation suggests that brainstem stimulation enrolls a propriospinal network with distinct synaptic relays.

Electrical Stimulation of Caudal Dorsal Roots Evokes Ascending Input Along the Cord

After describing the conduction of descending input evoked by brainstem stimulation through caudal segments of the whole CNS in vitro, we sought to properly characterize the transit of ascending input. For this purpose, electrical pulses were delivered to caudal afferents while monitoring motor responses from rostral segments. In the sample experiment schematized by the cartoon in Fig. 5A, brief pulses (duration = 0.1 ms) were serially applied (0.03 Hz) to a lower lumbar (L5) DR, simultaneously recording responses from homologous and contralateral VRs and from a rostral cervical segment (C2). Input/output stimulation was supplied at augmenting intensities, expressed as multiples of the Thr calculated from the homologous lumbar VR (1 x, 1.5 x, 2 x, 3 x, 5 × Thr), evoking increasingly larger and faster potentials from all spinal VRs. At all strengths of stimulation, motor-evoked responses were higher from the homologous VR (Fig. 5B) than from the contralateral L5 (Fig. 5C, note the lower scale on the y-axis). Motor-evoked responses were

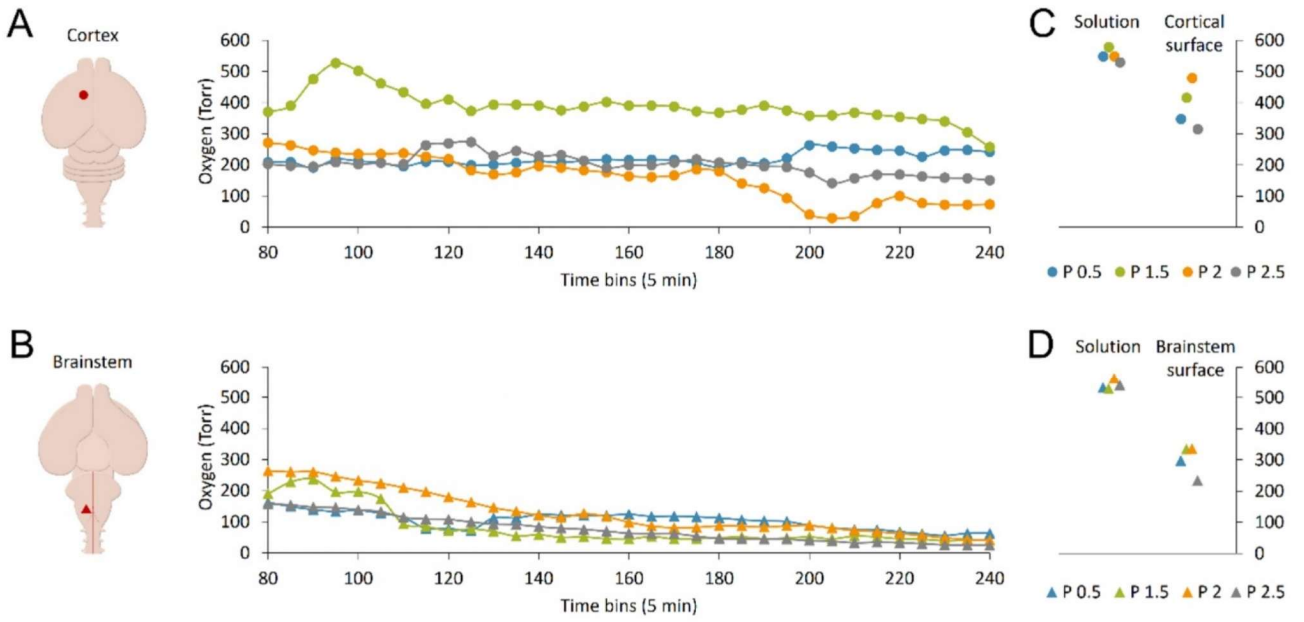

Fig. 6 Tissue oxygen levels in the cortex are higher than in the brainstem at all ages explored. In eight different preparations, PO_2 is continuously monitored at a 100 µm depth on the motor cortex (**A**) and brainstem (**B**). Left cartoons show the sites of the probe implant in the cortex (**A**) and brainstem (**B**). Time courses indicate the average PO_2 levels in 5 min bins for the entire duration of experiments, from 80 min to 4 h from anesthesia (circles in A for cortex, and triangles in B for brainstem). Each preparation is traced with different hues adopting the color code reported in (**C, D**). Right plots show the average PO_2 in the solution and on the surface of the cortex (**C**) and brainstem (**D**) for all preparations tested

also induced from upper cervical segments, albeit with lower and delayed potentials (Fig. 5D).

Input/output average values for each VR are reported in Table 4 for amplitude and time to peak ($n = 7$). Increases in stimulation strengths correspond to higher average peaks of lumbar DRVRPs, while cervical responses remain less affected. The average time to peak of all reflexes was slightly reduced at the first step of increasing stimulation (1 × Thr Vs 1.5 × Thr), while it remained unchanged for stronger pulses. Conduction of ascending input along the cord is maintained in the isolated CNS preparation, with rostral VRs far from the stimulating segment showing smaller responses with a later onset. However, no responses from the surface of dorsal motor cortices were acquired in correspondence to dorsal stimulation, even at higher strengths and durations of pulses (data not shown), reminiscent of the above-mentioned inability of the motor cortex to elicit spinal responses through electrical stimulation.

Pulse Oximetry Optical Assessments Show Preserved and Stable Oxygen Levels in the Cortex

Electrophysiological data exposed so far show a stable spontaneous respiratory activity from higher cervical VRs and an optimal pulse conduction along the brainstem–spinal cord axis. However, no motor responses were elicited by electrically stimulating the surface of the cortex or midbrain, as well as no surface potentials were recorded from the same sites following lumbosacral DR stimulation. To verify whether this lack of responses derives from hypoxic conditions of brain structures due to the time-consuming surgical procedures and the long maintenance in vitro, in a subset of eight preparations isolated from rats of 0.5, 1.5, 2, and 2.5 postnatal days, we continuously measured PO_2 through an Optode microsensor implanted 100 µm deep in either the motor cortex or the brainstem. Time courses show the dynamics of PO_2 during the entire experiment for each preparation, recorded either from the motor cortex (Fig. 6A, $n = 4$) or from the brainstem (Fig. 6B, $n = 4$). For all experiments, PO_2 was on average 545.83 ± 17.34 Torr ($n = 8$) in the bath solution, while it dropped to 388.98 ± 73.18 Torr for the cortex (Fig. 6C) and 300.03 ± 47.85 Torr for the brainstem (Fig. 6D) when measured on the tissue surface. Interestingly, 100 µm below the tissue surface, overall oxygenation of the cortex (240.55 ± 101.54 Torr, $n = 4$) was higher than the brainstem's (94.58 ± 23.70 Torr, $n = 4$; $P = 0.031$, t test).

In addition, for all ages explored, a common decaying trend in tissue oxygenation of the brainstem occurred over time ($t_{80} = 197.93 \pm 55.06$ Torr Vs $t_{240} = 42.53 \pm 15.97$ Torr; $P = 0.013$, paired t test, $n = 4$), while cortical PO_2 values remained stable throughout the entire experiment ($t_{80} = 264.75 \pm 88.17$ Vs $t_{240} = 180.66 \pm 85.45$; $P = 0.184$, paired t test, $n = 4$).

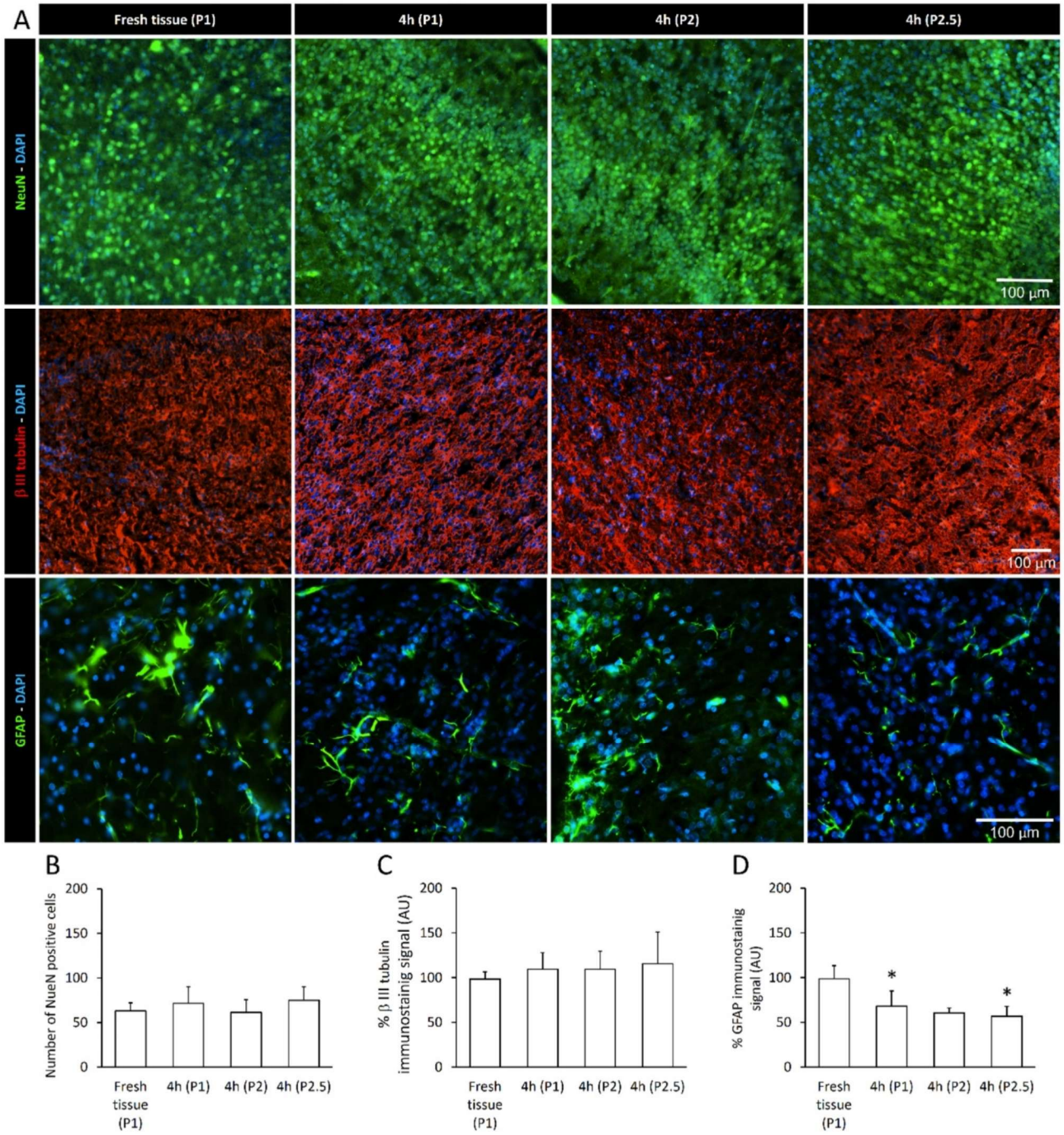

Fig. 7 Neuronal and glial staining of internal brain structures under the surface of the ventrolateral prefrontal cortex from the CNS in vitro. **A** Examples of NeuN (upper panels), β-III tubulin (middle panels) or GFAP staining (lower panels) at 750 µm from the surface of the ventrolateral prefrontal cortex. **B** Histogram shows the mean number of NeuN positive cells in RoIs of 730×730µm^2, showing no statistical difference among fresh tissue and the three preparations kept 4 h in vitro. **C–D** Histograms show mean β-III tubulin (**C**) and GFAP (**D**) in RoIs of 730×730µm^2, expressed as fluorescence intensity in arbitrary units (AU, percentage change from fresh tissue). No significant differences in β-III tubulin signal are apparent among fresh tissue and the 3 preparations kept 4 h in vitro. GFAP fluorescence intensity quantification for astrocytes indicates a decrease in immunoreactivity in two preparations kept 4 h in vitro (D; $*P = 0.0002$)

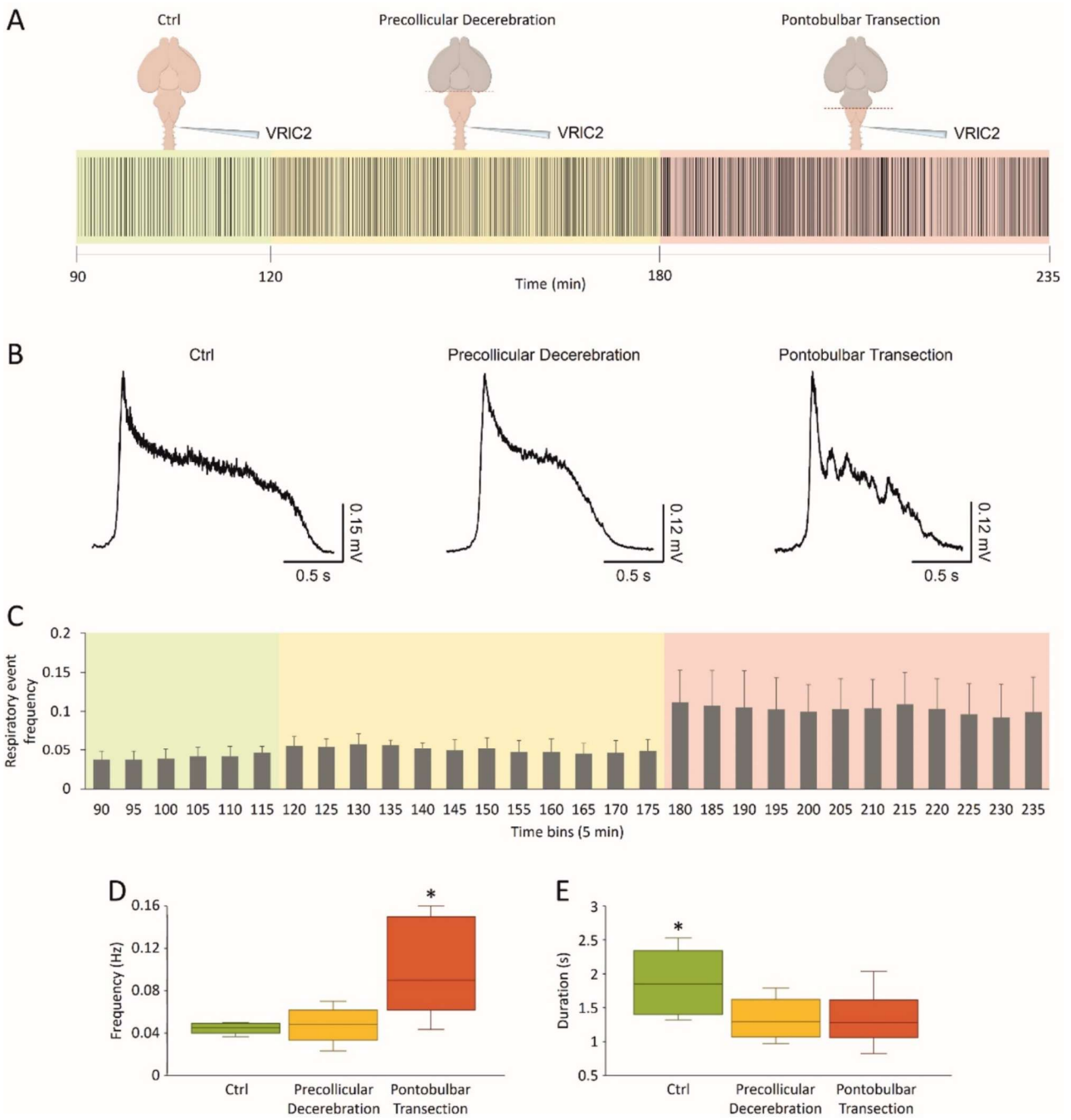

Fig. 8 Fictive respiration is modulated by suprapontine and pontomedullary structures. (A) Raster plot of continuous fictive respiration recorded from VRlC2 for an entire experiment. Time is calibrated at the onset of anesthesia. Fictive respiration in control (green pale background) remains stable after a precollicular decerebration (yellow pale background) and eventually becomes faster after the following pontobulbar transection (red pale background). **B** Average bursts from the same experiment in (**A**) are reported for the last five minutes of recordings in each experimental slot. Single events become shorter after precollicular decerebration, without any changes after the following pontobulbar transection. **C** An average time course from 8 experiments traces rhythm frequency in 5 min bins for the entire duration of experiments. The last five minutes of each experimental phase in C is used for statistical comparison of rhythm frequency (**D**, $*P = 0.002$) and burst duration (**E**, $*P = 0.016$)

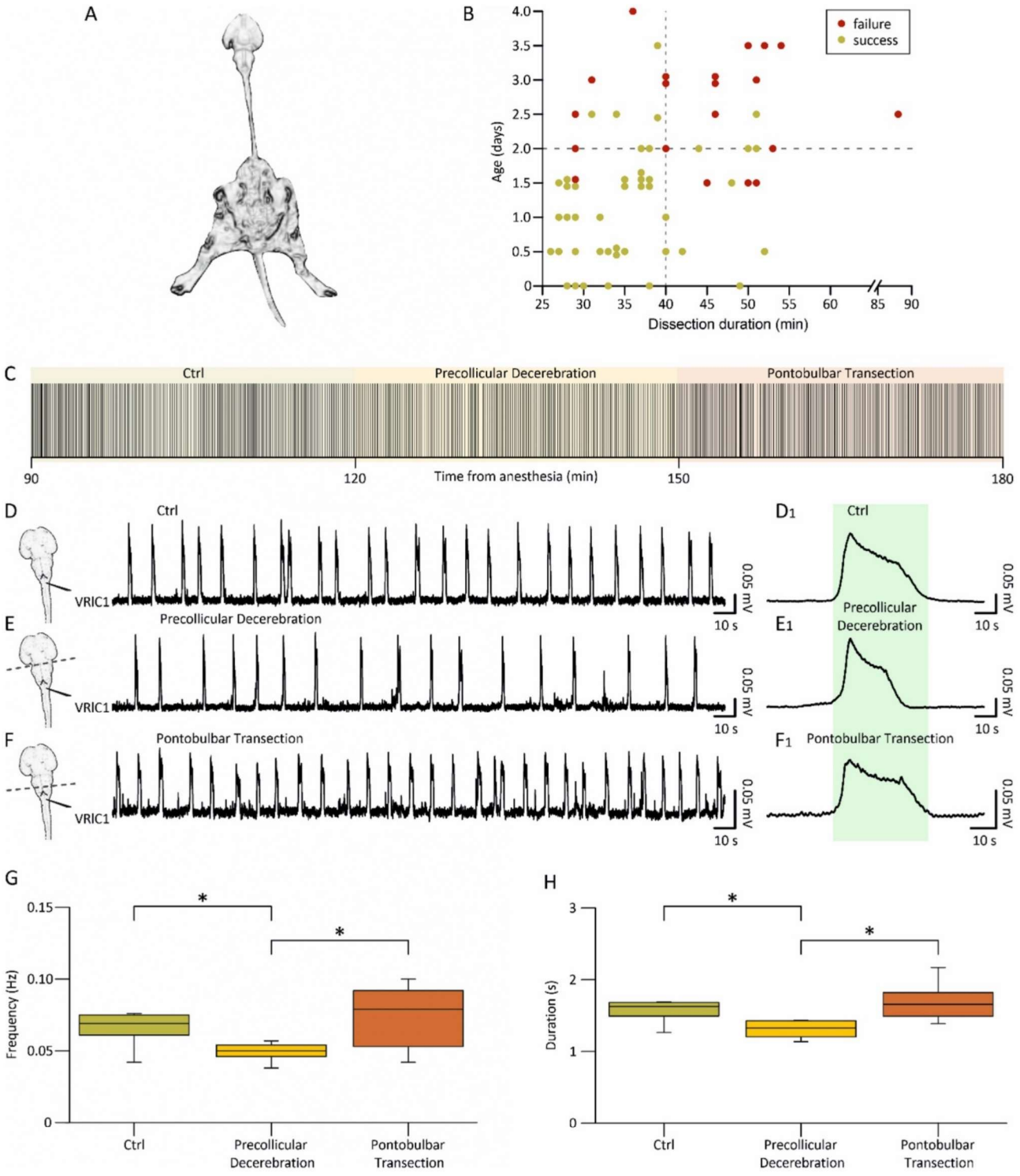

Histological Analysis of Neurons and Glial Cells Demonstrates Well-Structured Tissue Preservation In Vitro for Over 4 Hours

In Fig. 7, the topographical distribution of neuronal and non-neuronal cells was analyzed in brain structures at 750 µm from the surface of the ventrolateral prefrontal cortex, from one fresh tissue right after isolation of the entire CNS (P1) and from three different CNS preparations (P1–P2.5) maintained in the warmed recording chamber (25–27 °C) for the entire duration of experiments (4 h).

◂**Fig. 9** In vitro preparation of the entire CNS with hindlimbs attached expresses a stable fictive respiration that is affected by precollicular and pontomedullary serial transections. **A** Picture of the original in vitro preparation from a neonatal rat (P2), comprising the whole central nervous system with hindlimbs attached. Lower extremities and tail were left intact, along with ventral roots (VRs) and dorsal roots (DRs) below T13 segment. **B** Plot depicts each preparation as a single dot (66 preparations) describing age of the animal (Y-axis) and length of surgical dissection (X-axis). Dots are colored in green (success) or red (failure) based on the presence or absence of a stable respiratory rhythm after at least 4 h from the induction of anesthesia at the beginning of tissue isolation. Vertical dotted gray line at x = 40 min and horizontal dotted gray line at y = 2 days, define a bottom-left quadrant where the probability of having preparations with long-lasting breathing is highly consistent (44 successes out of 47 preparations). **C** Raster plot representing consecutive respiratory bursts continuously recorded from a cervical VR (lC1) in the intact CNS (Ctrl; 30 min; green shadow field) and after serial precollicular (30 min; yellow shadow field) and pontobulbar transections (30 min; red shadow field). Albeit the expected variability, rhythm frequency is reduced after decerebration, while it is increased by the subsequent pontomedullary transection. For the same experiments reported in (**C**), three trace segments from VRlC1 are taken at steady state in intact settings (**D**) and during the progressive reductions of the intact CNS preparation (**E**, **F**; see left cartoons). Burst frequency in the entire CNS (top trace) is slowed down by decerebration (middle trace) and then eventually speeded up after pontomedullary transection (bottom trace). (**D_1**, **E_1**, **F_1**) Average bursts calculated by superimposing single events are reported on the right, demonstrating that decerebration reduces burst duration, which eventually recovers after further tissue ablation. Differences in burst duration are highlighted by the green shaded field corresponding to the burst duration calculated in control. Effect of rostral structures ablation on the frequency of respiration is summarized by whisker plots from pooled data in G ($n = 9$), showing significant changes in the pace of rhythm from the intact CNS (green box, ctrl, $n = 9$) following precollicular decerebration (yellow box, precollicular transection, $n = 9$) and then pontomedullary transection (orange box, pontobulbar decerebration, $n = 6$; $^*P = 0.036$). **H** Whisker plots describing changes in burst duration from the intact CNS (green box, $n = 11$) following serial transections (yellow box, precollicular transection, $n = 11$; orange box, pontobulbar decerebration, $n = 8$; $^*P = 0.003$). Note that burst amplitude has not been evaluated since nerves were released from electrodes before each surgical ablation to avoid root damage

The average total number of neuronal cells, as labeled by NeuN in an RoI of 730×730 μm^2, is shown in Fig. 7A (green, first row) and quantified in B. The resulting mean density of NeuN positive cells, expressed as 10^{-4}/μm^2, was similar among fresh tissue (1.18 ± 0.04) and the three different CNS preparations (1.36 ± 0.12; 1.17 ± 0.07; 1.43 ± 0.05; $P > 0.05$, One-way ANOVA on ranks followed by all pairwise multiple comparisons with Dunn's method). Similarly, β-III tubulin immunoreactivity (red, Fig. 7A middle row, C) was similar among preparations.

To identify any stress of the tissue after 4 h in vitro, GFAP was targeted as a marker for the activation of astrocytes (Verkhratsky and Parpura 2016). The mean fluorescence intensity for GFAP immunoreactivity was analyzed in fresh tissue and three preparations. Our results did not show any increase in GFAP immunoreactivity, but in fact demonstrated a significant reduction in two out of three preparations kept 4 h in vitro (Fig. 7D, $P = 0.0002$, ANOVA followed by Kruskal–Wallis test versus fresh tissue; $n = 3$–11 slices).

These results demonstrated no cell death and absence of astrogliosis in the internal brain structures under the surface of the ventrolateral prefrontal cortex in the preparation of the entire CNS, despite the long maintenance in vitro. This model thus appears suitable for exploring the modulatory influences of brain centers on the brainstem and spinal networks.

Suprapontine Structures Modulate Neuronal Networks for Respiration

To better characterize the impact of higher rostral centers on the neuronal pathways involved in respiration, a spontaneous respiratory rhythm was derived initially from upper cervical segments in the whole CNS in vitro and then after precollicular decerebration followed by the ablation of pons (Fig. 8A). In a sample preparation, the dynamics of respiratory events were described throughout the entire experimental protocol (2.5 h; Fig. 8A, raster plot). The stable respiratory rhythm frequency (green field) was not affected by precollicular decerebration (yellow field), while it was speeded up after the following pontobulbar transection (red field). Average bursts were obtained by superimposing the events in the last 5 min of each phase of the experiment (Fig. 8B). Single respiratory bursts in the intact CNS (1.88 s; left) shortened after precollicular decerebration (1.24 s; middle) and remained short after pontobulbar transection (1.03 s; right).

The time course of the mean frequency from eight experiments is reported for 5 min bins in Fig. 8C. Frequency of the respiratory rhythm increased after pontobulbar transection (Fig. 8D; $P = 0.002$; repeated measures ANOVA followed by Tukey–Kramer multiple comparisons test), while burst duration was already reduced after precollicular decerebration (Fig. 8E; $P = 0.016$, repeated measures ANOVA followed by Tukey–Kramer multiple comparisons test).

Collectively, data indicate that suprapontine structures affect distinct features of the fictive respiratory rhythm, supporting the adoption of the whole CNS in vitro preparation to clarify the rostral modulation of brainstem networks.

The Isolated CNS with Legs Attached Expresses a Stable Spontaneous Fictive Respiration Modulated by Suprapontine Structures

Isolated preparations of brainstem and spinal cord with hindlimbs kept intact and connected to the spine have been used to explore both the functional coupling between

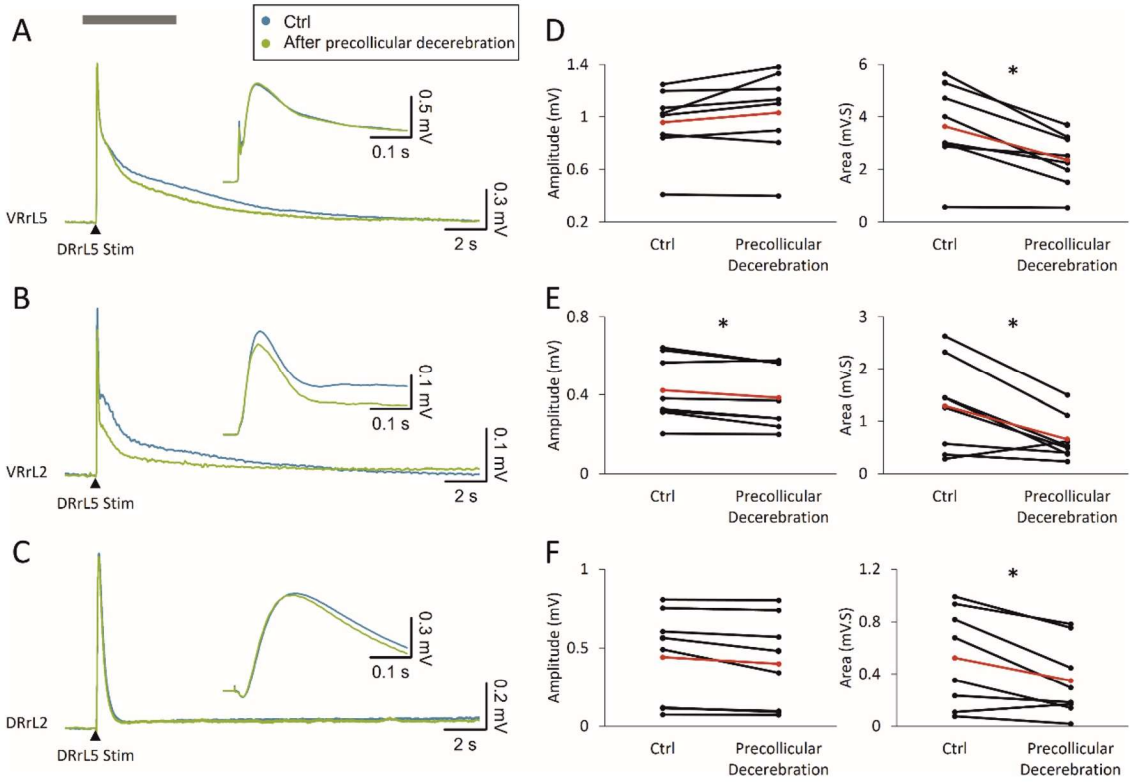

Fig. 10 Local lumbar networks involved in reflex responses are modulated by suprapontine structures. Superimposed average traces show that electrical pulses applied to a DRIL5 (intensity = 45 µA, pulse duration = 0.1 ms) induce both VR and DR potentials from VRrL5 (**A**), VRrL2 (**B**) and DRrL2 (**C**). After acquiring evoked responses in control (blue traces), the same stimulating protocol is repeated after precollicular decerebration (green traces). Inserts show the magnified onset of the response to better appreciate any changes in peak amplitude after decerebration. **D–F** For each recording site, pairs of responses before and after decerebration are quantified for amplitude and area. Red dots correspond to the mean value in each graph ($n = 8$; **D**, $^*P = 0.003$; **E**, amplitude $^*P = 0.016$, area $^*P = 0.039$; **F**, $^*P = 0.016$)

networks for respiration and locomotion (Giraudin et al. 2012), as well as the modulatory influence on spinal circuits played by the afferent feedback elicited by passive exercise (Dingu et al. 2018). However, to explore whether suprapontine structures contribute to integrating the afferent input elicited by passive leg movement, the definition of a more intact in vitro preparation became compelling. To this purpose, we isolated the whole CNS keeping the entire hindlimbs connected to the spine (Fig. 9A). This semi-intact preparation expresses a stable spontaneous respiratory rhythm for over 4 h when surgical procedures for tissue isolation are fast (≤40 min) and performed on younger animals (≤2 days old), as summarized in the scatter plot of Fig. 9B from 66 preparations. A sample respiratory rhythm from a 2-day-old neonatal preparation (raster plot in Fig. 9C) was progressively slowed down by precollicular decerebration (Fig. 9C, yellow field) and then speeded up by the following pontobulbar transection (Fig. 9C, red field). Original traces at steady state illustrate the regular bursting at 0.08 Hz in the intact preparation (Fig. 9D), which slowed down to 0.06 Hz after precollicular transection (Fig. 9E) and then accelerated to 0.10 Hz following ablation of the pons (Fig. 9F). In the intact preparation, the average single burst lasted 1.63 s (Fig. 9D1) and was reduced to 1.43 s after ablation of suprapontine structures (Fig. 9E1), while pontobulbar transection broadened burst duration to 1.84 s (Fig. 9F1). Pooled data from many experiments confirm the significant reduction in the bursting frequency after precollicular decerebration (from 0.07 ± 0.02 Hz to 0.05 ± 0.02 Hz; $P = 0.036$; one-way ANOVA followed by all pairwise multiple comparisons with Fisher's LSD method; $n = 9$) and its subsequent recovery after pontobulbar transection (0.07 ± 0.02 Hz; $P = 0.036$; one-way ANOVA followed by all pairwise multiple comparisons with Fisher's LSD method; $n = 6$). Similarly, burst duration was reduced by decerebration (from 1.72 ± 0.46 s to 1.22 ± 0.43 s; $P = 0.003$; one-way ANOVA on ranks followed by all pairwise multiple comparisons with Dunn's method; $n = 11$) and then broadened again after the following pontobulbar transection (1.68 ± 0.25; $P = 0.003$; one-way ANOVA on ranks followed by all pairwise multiple comparisons with Dunn's method; $n = 8$).

In summary, hindlimbs kept attached to the isolated CNS do not affect the expression of the spontaneous respiratory rhythm, nor its modulation provided by suprapontine structures. Thus, the whole CNS with legs attached represents an original setting to explore how respiration is tuned by afferent input reaching the brain from the periphery.

Suprapontine Structures Modulate Local Lumbar Circuitry

We thus explored whether the presence of suprapontine structures in the CNS preparation affects spinal motor networks in the lumbar cord. To characterize the state of excitability of spinal motor networks, we used dorsally evoked potentials derived from VRs in response to single electrical pulses supplied to dorsal afferents (Lev-Tov and Pinco 1992). Interestingly, afferent dorsal pulses also recruit a specific dorsal network along the cord (Taccola and Nistri 2005) that is involved in the presynaptic inhibition of input coming from the periphery (Rudomin 2009).

As shown in the sample mean traces reported in Fig. 10A and B, electrical stimulation (6–60 µA 2–3.3 Thr, 100 µs) of a DRlL5 in the isolated CNS elicits an early sharp peak from VRs coming essentially from an oligosynaptic pathway in the local microcircuitry, and a following long potential corresponding to the activation of a larger number of interneurons. A sharper potential is induced also from DRlL2 (Fig. 10C), following antidromic conduction of the primary afferent depolarization elicited by DRlL5 stimulation. Sample average traces in Fig. 10A–C were acquired before and after a precollicular transection, indicating that decerebration causes a faster decay of all responses and a 23% reduction in the peak of responses from VRrL2 (Fig. 10B).

Reflexes were acquired from both the intact CNS preparation (blue lines) and after precollicular decerebration on the same sample (green lines). As summarized in the plots of Fig. 10D–F, decerebration does not affect peak amplitude of rhythms acquired from VRrL5 ($P = 0.103$, paired, t test; $n = 8$) or DRrL2 ($P = 0.055$, paired, t test; $n = 8$), while peak amplitude of the VRrL2 rhythm is reduced ($P = 0.016$ paired, t test; $n = 8$).

Similarly, the area of all responses is depressed after precollicular transection ($Area_{VRrL2}$ $P = 0.039$, Wilcoxon matched-pairs signed-ranks test; $Area_{VRrL5}$ $P = 0.003$, paired t test; $Area_{DRrL2}$ $P = 0.016$ paired t test; $n = 8$).

These observations demonstrate that the lack of suprapontine structures deprives lumbar circuits of some modulatory influences, suggesting the adoption of the whole in vitro CNS preparation whenever interested in exploring supraspinal influences on spinal microcircuits.

Fictive Locomotor Patterns are Induced by Trains of Electrical Pulses Applied to Both Caudal Afferents and Ventrolateral Medulla

Fictive locomotion (FL; Kiehn 2006) consists in rhythmic electrical oscillations alternating at the segmental level between the two sides of the cord and, on the same side, among flexor and extensor motor pools. FL is a distinctive feature of the activation of the neuronal circuits for locomotion in the spinal cord preparation isolated from rostral thoracic segments to the cauda equina (Cazalets et al. 1992). To ascertain whether the recruitment of locomotor spinal networks in vitro is preserved even in the presence of suprapontine structures, we applied the canonical pattern of electrical stimulation (stereotyped trains of brief rectangular pulses at 2 Hz; Marchetti et al. 2001) to a caudal afferent of the entire isolated CNS. Sample traces in Fig. 11A were taken after about 1.5 hours from the beginning of the surgical procedures required for the isolation of the entire CNS, and show a cumulative depolarization evoked from four lumbar VRs when an 80 s train of rectangular pulses (duration = 0.1 ms) at 2 Hz (blue bar) was applied to DRrL6. At the top of the cumulative depolarization appeared an epoch of 34 rhythmic discharges in VRlL5, with a mean frequency of 0.45 Hz, that alternated between the flexor-related VRL1 and the extensor-related VRL5 on the right side of the cord, and between bilateral VRL5s. In the same preparation, after transecting the spinal cord at T3/T4 level (Fig. 11B, green bar), the same stimulating protocol elicited an episode of FL provided of 28 rhythmic oscillations with a mean frequency of 0.49 Hz in VRlL5. CCF analysis suggests a stronger phase coupling in the intact preparation ($CCF_{lL2\text{-}rL2} = -0.78$, $CCF_{lL2\text{-}lL5} = -0.85$) than after midthoracic transection ($CCF_{lL2\text{-}rL2} = -0.65$, $CCF_{lL2\text{-}lL5} = -0.66$).

In seven preparations, FL episodes were evoked by a train of 160 pulses at 2 Hz (intensity = 7.5–37.5 µA, 1.5–3.5 Thr; pulse duration = 0.1 ms) applied to lumbosacral afferents (DRrL6, DRrS1). Episodes of FL were equal before and after a midthoracic transection, as for mean number of locomotor-like oscillations (Fig. 11C; $P = 0.075$, paired t test), mean frequency of oscillations (Fig. 11D; frequency: $P = 0.974$, paired t test), mean variability of cycles (Fig. 11E; frequency CV: $P = 0.127$, paired t test), and left/right alternation (Fig. 11I; homosegmental CCF: $P = 0.797$, paired t test).

However, the total duration of FL episodes (67.50 ± 15.82 s vs. 57.61 ± 13.37 s; Fig. 11F; $P = 0.027$, paired t test), mean cumulative depolarization peak (Fig. 11G; $P = 0.023$, paired t test), and flexor/extensor alternation (Fig. 11H; $P = 0.038$, paired t test) were significantly reduced after disconnection from the brain. As opposed to transient epochs of FL patterns evoked in the

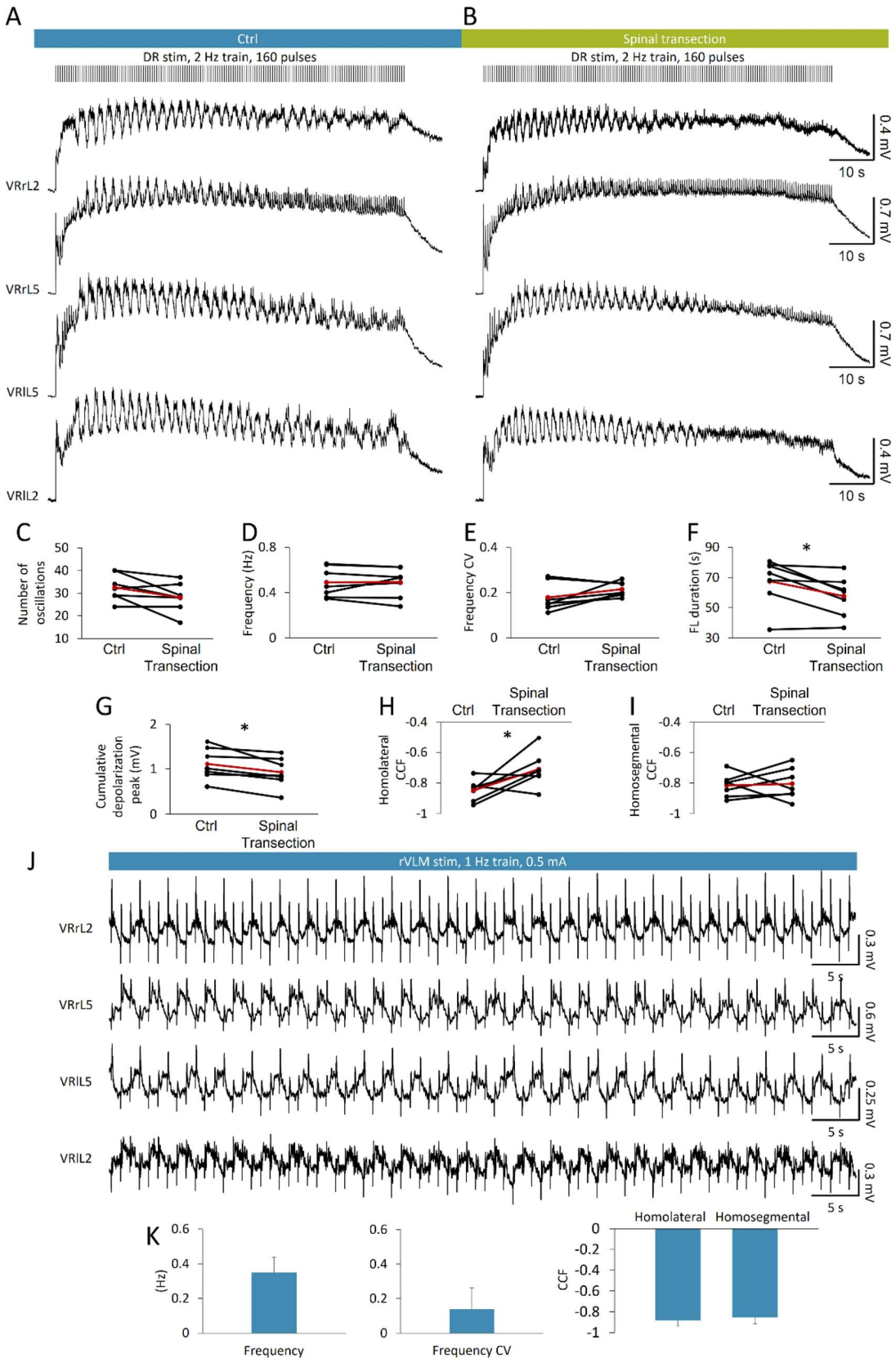
A
Ctrl
DR stim, 2 Hz train, 160 pulses
VRrL2
VRrL5
VRlL5
VRlL2
B
Spinal transection
DR stim, 2 Hz train, 160 pulses
0.4 mV
10 s
0.7 mV
10 s
0.7 mV
10 s
0.4 mV
10 s
C
Number of oscillations
Ctrl
Spinal Transection
D
Frequency (Hz)
Ctrl
Spinal Transection
E
Frequency CV
Ctrl
Spinal Transection
F
FL duration (s)
*
Ctrl
Spinal Transection
G
Cumulative depolarization peak (mV)
*
Ctrl
Spinal Transection
H
Homolateral CCF
Ctrl
Spinal Transection
*
I
Homosegmental CCF
Ctrl
Spinal Transection
J
rVLM stim, 1 Hz train, 0.5 mA
VRrL2
0.3 mV
5 s
VRrL5
0.6 mV
5 s
VRlL5
0.25 mV
5 s
VRlL2
0.3 mV
5 s
K
(Hz)
Frequency
Frequency CV
Homolateral
Homosegmental
CCF

◂**Fig. 11** Fictive locomotor patterns are elicited by repetitive electrical stimulation applied either to a lumbar DR or to the ventrolateral medulla. An epoch of FL is induced by a train of pulses (160 stimuli, 2 Hz, intensity = 22.5 µA, pulse duration = 0.1 ms) applied to DRrL6 both in control (**A**) and after a midthoracic transection (**B**). VR oscillations appear double alternated between homolateral L2 and L5 segments, and between homosegmental left and right motor pools. Pooled data from seven experiments indicate that, after a midthoracic transection, there are significant differences in fictive locomotion (FL) duration (**F**, $*P = 0.027$), cumulative depolarization peak amplitude (**G**, $*P = 0.023$) and homolateral CCF (cross-correlation function; **H**, $*P = 0.038$), with an unchanged number of oscillations (**C**, $*P = 0.075$), frequency (**D**, $*P = 0.974$), frequency CV (**E**, $*P = 0.127$) and homosegmental CCF (**I**, $*P = 0.797$). Red dots indicate the mean values in each graph. **J** Fictive locomotion is stably evoked by the continuous repetitive stimulation (1 Hz) of the right ventrolateral medulla (rVLM, "H" site; intensity = 0.5 mA, pulse duration = 1 ms). **K** Bars describe period, frequency CV homolateral and homosegmental CCFs of fictive locomotion oscillations as an average of four experiments

isolated spinal cord, which spontaneously decayed despite the continuous presence of stimulation (Dose et al. 2014), more stable locomotor-like oscillations were observed in the brainstem–spinal cord preparation in response to a train of electrical pulses applied to the VLM (Zaporozhets et al. 2004). To verify whether electrical stimulation of the VLM induces stable FL patterns in the entire CNS preparation, a train (intensity = 0.5 mA, duration = 1 ms, frequency = 1 Hz) of pulses was continuously applied to the VLM for a total duration of 12 min. In response to stimulation, stable discharges appeared at 0.33 Hz, alternating between homolateral extensor and flexor output (CCF = -0.96) and homosegmental left and right ventral roots (CCF = -0.91; Fig. 11J). The same experiment was repeated in four isolated preparations of the entire CNS, where FL patterns stably appeared for up to 12 min of continuous stimulations (intensity = 0.5–4.5 mA, duration = 1–5 ms, frequency = 1–2 Hz). Locomotor-like events were characterized by stable discharges (frequency CV = 0.14 ± 0.12, Fig. 11K) with a frequency of 0.35 ± 0.09 Hz (mean cycle period, Fig. 11K) and double alternating between pairs of VRs (homolateral CCF = -0.88 ± 0.06 and homosegmental CCF = -0.85 ± 0.06, Fig. 11K).

Collectively, FL patterns are evoked in the whole CNS in vitro by trains of electrical pulses applied either to lumbosacral afferents or to the VLM, proving this isolated preparation as a suitable model to study spinal circuits for locomotion in a more intact environment.

Discussion

In the present study, we introduce a more intact in vitro preparation of the entire CNS to explore the development of brain centers and their influence on both brainstem and spinal microcircuits, which express the rhythmic activities of breathing and locomotion, respectively.

The preparation maintains the conduction of descending and ascending input along the cord and shows a fictive respiratory rhythm that remains stable for over 4 hours. Both the well-preserved tissue oxygenation in the brainstem and cortical surfaces and optimal cell viability in the internal brain structures under the surface of the ventrolateral prefrontal cortex demonstrate the reliability of the in vitro brain for the entire duration of experiments.

Collectively, data indicate that suprapontine structures affect distinct features of fictive respiration, even when legs are kept attached to explore how afferent input from the periphery tune respiration. The lack of suprapontine structures also deprives lumbar circuits of some modulatory influences, since disconnection from higher centers generates poorer motor-evoked responses. Furthermore, in the whole CNS, electrically evoked FL patterns slightly increase the total duration and coordination of cycles.

Collectively, this more intact experimental setting allows for clarifying the rostral modulation of brainstem networks and for studying supraspinal influences on spinal microcircuits.

Influences of Suprapontine Structures on Brainstem Neuronal Networks for Respiration

Many studies about the suprapontine control of breathing indicate that multiple brain structures are involved in modulating respiration (Horn and Waldrop 1998; Fukushi et al. 2019).

In particular, the posterior hypothalamic area has been found crucial for modulating respiration in cats and rodents, hence suggesting that several neurogenic breathing disorders in humans can be ascribed to dysfunctions of the hypothalamus (Fukushi et al. 2019).

The posterior hypothalamus modulates respiratory changes during distinct emotional and arousal states and also receives input from the motor cortex (Fukushi et al. 2019). Many of the structures in the cortex and subcortex that are traditionally related to motor functions are also activated during ventilatory challenges. Cortical circuits not only receive afferent input from respiratory nuclei, but also strongly influence the respiratory control through descending projections. Indeed, phrenic and thoracic motoneurons receive descending input from the motor cortex (Rikard-Bell et al. 1985) and from the prefrontal cortex. Cortical input also reaches the midbrain through periaqueductal gray neurons, which modulate respiration when electrically stimulated (Beitz 1982). As a result, PET scans show premotor and motor cortices being active during both volitional breathing in human subjects (Colebatch et al. 1991) and during forced inspiration (Fink et al. 1996). In the latter

case, basal ganglia activation was also observed (Fink et al. 1996). Starting from the pioneer studies by Spencer (Spencer 1894), electrical stimulation has been used in most areas of the cortex, decreasing respiratory frequency. Moreover, results obtained by comparing changes in the respiratory frequency during hypoxia in decerebrated or decorticated awake cats indicate that descending influences from the cerebrum inhibit the activity of medullary respiratory centers, while inputs from the diencephalon facilitate it (Tenney and Ou 1977). Accordingly, in our experiments, precollicular decerebration speeded up fictive respiration and reduced the duration of each burst. The changes in the frequency of fictive respiration after diencephalic, mesencephalic, or pontobulbar transections demonstrate that, although neonatal rat's neuronal networks are still immature, the brain modulates the respiratory rhythm already at birth (Okada et al. 1993; Voituron et al. 2005). In the present work, we expanded previous observations using an entire CNS that also includes cortical structures. Furthermore, as opposed to the classical isolated brainstem plus spinal cord model (Suzue 1984), our CNS preparation maintains the cerebellum intact. Thus, it allows to explore any potential role of the cerebellum in selectively modulating respiratory functions, as cerebellar neurons in the rostral fastigial nucleus respond to both passive movement and respiratory challenges (Lutherer et al. 1989).

Influences of Suprapontine Structures on Spinal Reflex Pathways and Locomotor Circuits

In the current study, ablation of suprapontine structures affects the extent of electrically evoked responses from both VRs and DRs. DRVRPs are the result of the recruitment of a local spinal microcircuit mainly confined at the segmental level, from dorsal afferents to ventral motor pools, reverberating input along the cord through intersegmental propriospinal connections to elicit motor responses that are derived lower and more delayed the farther they move from the stimulation site (example in Fig. 5). The contribution of higher brain centers to the localized pathway that generates spinal reflexes is not completely unexpected, as Wolpaw and collaborators have demonstrated that volitional modulation of H reflexes requires the integrity of the sensorimotor cortex and cerebellum (Wolpaw 2007; Chen et al. 2016).

On the other hand, DRDRPs correspond to the antidromic conduction of the primary afferent depolarization elicited by electrical pulses supplied to a close DR. In in vitro preparations from neonatal rats, a diffused dorsal spinal system connects all dorsal horns, producing almost simultaneous responses from all DRs. While bilateral DRDRPs are synchronized through commissural pathways running below the central canal, the strong coupling among DR-evoked potentials on the same side might be due to heterosegmental ipsilateral connections among dorsal horn networks (Taccola and Nistri 2005). In intact animals, the presynaptic inhibition process generating DRDRPs has been described under the control of tonic pathways descending from distinct structures in the cerebellum and cerebral cortex (Hagbarth and Kerr 1954). However, isolation of the sole spinal cord in vitro to study primary afferent depolarization might have underestimated the role of the brain in spinally processing afferent input at birth.

Although corticospinal tracts are still immature in the first week of life (Clarac et al. 2004), present data demonstrate that somehow, even at the neonatal stage, brain input already influences spinal responses. How cortical input reaches spinal targets at this stage of development, though, is debatable. Considering the immaturity of corticospinal tracts in newborns, as defined in our study by the inability to record any motor-evoked potentials in response to electrical stimulation of the surface of the cortex, it is possible that subthreshold brain input passes through deep local connections relaying to the midbrain and then downstream. We speculate that this input likely reverberates to ventral motor pools through the propriospinal dorsal network involved in the presynaptic inhibition of afferent input. Rerouting through dorsal networks may be reminiscent of the dorsoventral gradient of maturation in the connections between cortex and spinal cord during postnatal development (Lakke 1997; Martin 2005).

In our study, ablation of suprapontine structures likely removed any descending modulatory tone on evoked motor responses and was accompanied by changes in antidromic dorsal root discharges. Interestingly, in the spinal cord isolated within the first few days after birth, electrical stimulation of pathways running in the ventral funiculus modulates synaptic transmission from primary afferents to lumbar motoneurons through the recruitment of spinal interneurons that mediate presynaptic inhibition (Vinay and Clarac 1999).

In the isolated CNS preparation, the contribution of the cerebellum should also be considered, as it may facilitate the descending system that tunes spinal dorsal horn activity by exploiting the extensive connections between the cerebellum and the cerebral cortex (Hagains et al. 2011).

As opposed to the DRVRPS and DRDRPS described above, brain disconnection only produces slight changes in the episodes of locomotor-like oscillations evoked by trains of pulses applied to a DR. The same observation occurred with FL patterns recorded in vivo, regardless of whether they were recorded from intact anesthetized or decorticated cats (Millhorn et al. 1987). Moreover, the fictive locomotor patterns elicited by sacrocaudal stimulation after spinal cord transection were very similar to the actual muscle recruitment occurring during real locomotion in intact cats (Frigon 2012). More strikingly, in an in vivo preparation of a decerebrate adult mouse, spinalization did not affect

the overall stable FL induced by L-DOPA plus 5HT, apart from marginal increases in rhythm frequency only (Meehan et al. 2012).

This evidence, as well as our results, is consistent with the fact that FL originates from neuronal networks located in the lumbosacral cord (Cazalets et al. 1995; Kjaerulff and Kiehn 1996; Cowley and Schmidt 1997; Kremer and Lev-Tov 1997). Yet, the small but significant changes we reported after brain disconnection, as for the total duration of FL episodes, mean cumulative depolarization peak, and flexor–extensor alternation, justify the adoption of our isolated CNS to investigate the subtle modulatory tone provided by descending input that reaches rhythmogenic spinal networks at birth.

Motor-Evoked Responses Evoked by Electrical Stimulation

In the current study, peripheral and brainstem stimulations were used to demonstrate the presence of functional ascending and descending pathways along the cord. Electrical pulses delivered to spinal DRs successfully induced motor-evoked potentials (MEPs), as well as broader pulses applied to different spots of the pons and medulla, as already shown in the isolated CNS of opossum (Nicholls et al. 1990). These results are consistent with the development of spinal tracts. Indeed, all ascending pathways reach their targets before the rat is born: thalamocortical at E15, spinocerebellar at E17, primary afferent fibers in the gracile nucleus in the medulla oblongata at E18-21, the first spinothalamic fibers at E18, and spinothalamic and medial lemniscal at E19. Similarly, around birth, also lumbar segments are reached by descending spinal pathways, as GABAergic, serotonergic, noradrenergic reticulospinal and vestibulospinal tracts, along with rubrospinal and parafascicularis prerubralis fibers (Kudo et al. 1993; Lakke 1997; Clarac et al. 2004). However, distinct descending tracts from the hypothalamus reach lumbar spinal segments only after birth, like the fibers from the nucleus paraventricularis and area lateralis at P1, or from the zona incerta at P2 (Lakke 1997). Even slower is the maturation of the corticospinal tract, which extends to cervical and thoracic segments at P3 and, only at P6, to lumbar segments (Clarac et al. 2004). Then, corticospinal axons increase consistently until P8-10, when structurally immature axons are gradually eliminated up to the end of the second week (Joosten et al. 1987; Schreyer and Jones 1988).

Accordingly, in our experiments, there were no chances of inducing any MEPs or to record sensory-evoked potentials (SEPs) at any of the ages explored (0–3 days old), even by lowering the stimulating electrode all the way to the surface of the midbrain. Indeed, peripheral electrical stimulation has been tested for inducing cortical surface potentials only starting from P3-5 rats (An et al. 2014). The lack of MEPs or SEPs in the first days of life may be a consequence of immature cortical dendritic and axonal morphogenesis, as well as of the lodgment of synapses in the neocortex reaching circuit refinement only at P10 (Lim et al. 2018). Moreover, the correct soma-dendritic polarity of cortical neurons is not appropriately defined until 5 postnatal days (Kasper et al. 1994).

As for functional maturation, neocortical pyramidal neurons already trigger action potentials at birth (McCormick and Prince 1987), although their biophysical membrane properties are still vestigial. Indeed, only from the beginning of the second week do they differentiate into adapting and non-adapting regular spiking cells (Franceschetti et al. 1998). Then, from the second week, their action potentials grow in amplitude and shorten in duration with higher firing frequency, until completely developed by the third week after birth (McCormick and Prince 1987).

Furthermore, spinal responses to brain stimuli might also be affected by the incomplete myelinization of descending pathways. Indeed, at one day of age, immunoreactivity to myelin was detected in the lower brain stem, whereas it was absent in the rest of the brain (Bjelke and Seiger 1989). Then, during the first and second postnatal weeks, myelination continues in caudal rostral progression, spreading from the spinal cord to the medulla oblongata, pons, mesencephalon, and finally telencephalon, eventually completing during the third week after birth (Bjelke and Seiger 1989; Doretto et al. 2011; Downes and Mullins 2014).

In line with the morphological and functional development of the cortex and corticospinal pathways, pups switch from crawling to walking only at P10. A mature motor behavior is then reached only at P15 (Clarac et al. 2004), although the cortex is still evolving with the further appearance of motor maps at day 35 and its continuous enlargement until adult size around day 60 (Young et al. 2012).

Histological and Oximetric Assessments of Brain Maintenance In Vitro

In our preparation of the entire CNS in vitro from neonatal rats, suprapontine structures already appeared to have functional links to brainstem and spinal circuits downstream, as they modulated fictive respiration and lumbar reflex activity. We speculate that, at birth, more inner brain centers, as hypothalamic areas or basal ganglia, that were inaccessible to our surface electrodes, might relay brain control over neuronal networks downstream.

Indeed, despite the absence of cortical potentials and cortically evoked spinal motor responses, histological analysis revealed the lack of astrogliosis and optimal neuron survival in the internal brain structures under the surface of the ventrolateral prefrontal cortex. Surprisingly, albeit neuronal preservation, we reported a reduced labeling of the brain-specific

astroglial protein GFAP after 4 h of maintenance in vitro, especially in older rats. This evidence is reminiscent of the reduction in GFAP without any hypothalamic cell loss that has been correlated to the initial stages of hypoglycemia (Holmes et al. 2016). These findings corroborate the use of the entire CNS preparation for up to 4 h with good tissue preservation. Furthermore, it may suggest that any use of this preparation that considers longer maintenance in vitro should be accompanied by additional cell viability assays also with a detailed study of astrocyte morphology.

Interestingly, oximetric assessments indicate optimal oxygenation of the cortex after 4 h in vitro, although we do not know whether these PO_2 levels correspond to full network functionality. However, the oxygenation we assessed in the cortex was almost twice the one we measured in the brainstem when a stable respiratory rhythm was recorded for the entire duration of the experiment. Notably, we found that PO_2 levels in the brainstem were similar to values already reported in the literature (Okada et al. 1993; Wilson et al. 2003; Zimmer et al. 2020). Furthermore, in our settings, PO_2 measurements on the surface of the recording chamber, close to the cortex, indicated values that were higher than those taken underneath, where the brainstem was positioned. In the current study, oxygenation within deep forebrain structures was not fully assessed. Therefore, one must adopt caution in extending the oximetric measures obtained from the superficial cortex also to inner brain areas, due to both the different metabolic requirements of distinct groups of neurons and their selective vulnerability to the lack of oxygen. Many factors contribute to the evolution of this pattern, including the development of the cerebral vasculature and the selective cellular oxidative metabolism (Ferriero 2001; McQuillen et al. 2003). However, since cortical neurons are more sensitive to hypoxia in comparison with basal ganglia and thalamus (Northington et al. 2001), we can infer that, in our preparation, inner brain structures received enough oxygen to maintain their functionality for the entire length of experiments.

The absence of cell death and astrogliosis in the brain, as well as the preserved levels of tissue oxygen throughout the experiments, support the use of the entire CNS preparation from neonatal rats to explore the development of supraspontine structures and their role in modulating brainstem and spinal circuits.

Perspectives

The entire isolated CNS allows to study the maturation of corticospinal tracts and the developmental changes in functional coupling among cortical, brainstem, and spinal networks. Moreover, the same approach can be replicated on transgenic mice, exploiting optogenetic and epigenetic techniques for the selective activation of distinct neuronal pools regulating intrinsic rhythmic functions. We repute that the proposed experimental tool can launch new studies on the quite unexplored field of corticomotor plasticity using in vitro preparations.

Acknowledgements GT is grateful to Mrs. Elisa Ius for her excellent assistance in preparing the manuscript.

Author Contributions GT contributed to the study conception and design. AM, RA, GM, and GT performed experiments. Material preparation, data collection, and analysis were performed by all authors. The first draft of the manuscript was written and illustrated by AM and GT, and all the authors commented on previous versions of the manuscript and approved the final manuscript.

Funding Open access funding provided by Scuola Internazionale Superiore di Studi Avanzati - SISSA within the CRUI-CARE Agreement. The project was supported by SISSA intramural funds, through 5xmille IRPEF 2019 and 2020; BAZ and GM were supported by Universidad Austral, CONICET, Ministry of Science, Technology and Productive Innovation of Argentina through the Fund for Scientific and Technological Research (FONCYT, PICT-2020-SERIEA-00928) and IBRO Collaborative Research Grant.

Data Availability The datasets generated during and/or analyzed during the current study are available from the corresponding author upon reasonable request.

Declarations

Conflict of Interest The authors have no relevant financial or non-financial interest to disclose.

Ethical Approval The study was performed in line with the principles of the Italian Animal Welfare Act 24/3/2014 n. 26 implementing the European Union directive on animal experimentation (2010/63/ EU). The study complied with the ARRIVE guidelines.

Consent to Participate All the authors give their formal consent to participate in the present manuscript.

Consent for Publication All the authors give their formal consent for the publication of the present manuscript.

References

An S, Kilb W, Luhmann HJ (2014) Sensory-Evoked and Spontaneous Gamma and Spindle Bursts in Neonatal Rat Motor Cortex. J Neurosci 34:10870–10883

Beitz AJ (1982) The organization of afferent projections to the midbrain periaqueductal gray of the rat. Neuroscience 7:133–159

Bjelke B, Seiger Å (1989) Morphological distribution of MBP-like immunoreactivity in the brain during development. Int J Dev Neurosci 7:145–164

Blivis D, Mentis GZ, O'Donovan MJ, Lev-Tov A (2007) Differential effects of opioids on sacrocaudal afferent pathways and central pattern generators in the neonatal rat spinal cord. J Neurophysiol 97:2875–2886

Bracci E, Ballerini L, Nistri A (1996) Spontaneous rhythmic bursts induced by pharmacological block of inhibition in lumbar motoneurons of the neonatal rat spinal cord. J Neurophysiol 75:640–647

Cazalets JR, Sqalli-Houssaini Y, Clarac F (1992) Activation of the central pattern generators for locomotion by serotonin and excitatory amino acids in neonatal rat. J Physiol 455:187–204

Cazalets JR, Borde M, Clarac F (1995) Localization and organization of the central pattern generator for hindlimb locomotion in newborn rat. J Neurosci 15:4943–4951

Chen XY, Wang Y, Chen Y, Chen L, Wolpaw JR (2016) The inferior olive is essential for long-term maintenance of a simple motor skill. J Neurophysiol 116:1946–1955

Cifra A, Mazzone GL, Nani F, Nistri A, Mladinic M (2012) Postnatal developmental profile of neurons and glia in motor nuclei of the brainstem and spinal cord, and its comparison with organotypic slice cultures. Dev Neurobiol 72:1140–1160

Clarac F, Brocard F, Vinay L (2004) The maturation of locomotor networks Progress in Brain Research. Elsevier, Amsterdam, pp 57–66

Colebatch JG, Adams L, Murphy K, Martin AJ, Lammertsma AA, Tochon-Danguy HJ, Clark JC et al (1991) Regional cerebral blood flow during volitional breathing in man. J Physiol 443:91–103

Cowley KC, Schmidt BJ (1997) Regional distribution of the locomotor pattern-generating network in the neonatal rat spinal cord. J Neurophysiol 77:247–259

Danneman PJ, Mandrell TD (1997) Evaluation of five agents/methods for anesthesia of neonatal rats. Lab Anim Sci 47:386–395

Deumens R, Mazzone GL, Taccola G (2013) Early spread of hyperexcitability to caudal dorsal horn networks after a chemically-induced lesion of the rat spinal cord in vitro. Neuroscience 229:155–163

Dingu N, Deumens R, Taccola G (2018) Afferent input induced by rhythmic limb movement modulates spinal neuronal circuits in an innovative robotic in vitro preparation. Neuroscience 394:44–59

Doretto S, Malerba M, Ramos M, Ikrar T, Kinoshita C, De Mei C, Tirotta E et al (2011) Oligodendrocytes as regulators of neuronal networks during early postnatal development. PLoS ONE 6:e19849

Dose F, Taccola G (2016) Two distinct stimulus frequencies delivered simultaneously at low intensity generate robust locomotor patterns. Neuromodul Technol at the Neural Interface 19:563–575

Dose F, Zanon P, Coslovich T, Taccola G (2014) Nanomolar oxytocin synergizes with weak electrical afferent stimulation to activate the locomotor CPG of the rat spinal cord in vitro. PLoS ONE 9:e92967

Dose F, Deumens R, Forget P, Taccola G (2016) Staggered multi-site low-frequency electrostimulation effectively induces locomotor patterns in the isolated rat spinal cord. Spinal Cord 54:93–101

Downes N, Mullins P (2014) The development of myelin in the brain of the juvenile rat. Toxicol Pathol 42:913–922

Dreshaj IA, Haxhiu MA, Martin RJ, Young JK (2003) The basomedial hypothalamus modulates the ventilatory response to hypoxia in neonatal rats. Pediatr Res 53:945–949

Etlin A, Blivis D, Ben-Zwi M, Lev-Tov A (2010) Long and short multifunicular projections of sacral neurons are activated by sensory input to produce locomotor activity in the absence of supraspinal control. J Neurosci 30:10324–10336

Eugenín J, Nicholls JG (2000) Control of respiration in the isolated central nervous system of the neonatal opossum Monodelphis domestica. Brain Res Bull 53:605–613

Ferriero DM (2001) Oxidant mechanisms in neonatal hypoxia-ischemia. Dev Neurosci 23:198–202

Fink GR, Corfield DR, Murphy K, Kobayashi I, Dettmers C, Adams L, Frackowiak RS, Guz A (1996) Human cerebral activity with increasing inspiratory force: a study using positron emission tomography. J Appl Physiol 81:1295–1305

Franceschetti S, Sancini G, Panzica F, Radici C, Avanzini G (1998) Postnatal differentiation of firing properties and morphological characteristics in layer V pyramidal neurons of the sensorimotor cortex. Neuroscience 83:1013–1024

Frigon A (2012) Central pattern generators of the mammalian spinal cord. Neuroscientist 18:56–69

Fukushi I, Yokota S, Okada Y (2019) The role of the hypothalamus in modulation of respiration. Respir Physiol Neurobiol 265:172–179

Giraudin A, Le Bon-Jego M, Cabirol M-J, Simmers J, Morin D (2012) Spinal and pontine relay pathways mediating respiratory rhythm entrainment by limb proprioceptive inputs in the neonatal rat. J Neurosci 32:11841–11853

Hagains CE, Senapati AK, Huntington PJ, He J-W, Peng YB (2011) Inhibition of spinal cord dorsal horn neuronal activity by electrical stimulation of the cerebellar cortex. J Neurophysiol 106:2515–2522

Hagbarth K-E, Kerr DIB (1954) Central influences on spinal afferent conduction. J Neurophysiol 17:295–307

Holmes AP, Wong SQ, Pulix M, Johnson K, Horton NS, Thomas P, de Magalhães JP, Plagge A (2016) Reductions in hypothalamic Gfap expression, glial cells and α-tanycytes in lean and hypermetabolic Gnasxl-deficient mice. Mol Brain 9:39

Horn EM, Waldrop TG (1998) Suprapontine control of respiration. Respir Physiol 114:201–211

Joosten EAJ, Gribnau AAM, Dederen PJWC (1987) An anterograde tracer study of the developing corticospinal tract in the rat: three components. Dev Brain Res 36:121–130

Kasper EM, Larkman AU, Lübke J, Blakemore C (1994) Pyramidal neurons in layer 5 of the rat visual cortex. II. Development of electrophysiological properties: physiological development of layer 5 pyramidal neurons. Journal of Comparative Neurology 339:475–494

Kiehn O (2006) Locomotor circuits in the mammalian spinal cord. Annu Rev Neurosci 29:279–306

Kiehn O, Butt SJB (2003) Physiological, anatomical and genetic identification of CPG neurons in the developing mammalian spinal cord. Prog Neurobiol 70:347–361

Kiehn O, Kjaerulff O (1996) Spatiotemporal characteristics of 5-HT and dopamine-induced rhythmic hindlimb activity in the in vitro neonatal rat. J Neurophysiol 75:1472–1482

Kjaerulff O, Kiehn O (1996) Distribution of networks generating and coordinating locomotor activity in the neonatal rat spinal cord in vitro: a lesion study. J Neurosci 16:5777–5794

Kremer E, Lev-Tov A (1997) Localization of the spinal network associated with generation of hindlimb locomotion in the neonatal rat and organization of its transverse coupling system. J Neurophysiol 77:1155–1170

Kudo N, Furukawa F, Okado N (1993) Development of descending fibers to the rat embryonic spinal cord. Neurosci Res 16:131–141
Lakke EAJF (1997) The projections to the spinal cord of the rat during development: a timetable of descent. Springer, Berlin Heidelberg, Berlin, Heidelberg
Lev-Tov A, Pinco M (1992) In vitro studies of prolonged synaptic depression in the neonatal rat spinal cord. J Physiol 447:149–169
Lim L, Mi D, Llorca A, Marín O (2018) Development and functional diversification of cortical interneurons. Neuron 100:294–313
Lutherer LO, Williams JL, Everse SJ (1989) Neurons of the rostral fastigial nucleus are responsive to cardiovascular and respiratory challenges. J Auton Nerv Syst 27:101–111
Mandadi S, Whelan PJ (2009) A new method to study sensory modulation of locomotor networks by activation of thermosensitive cutaneous afferents using a hindlimb attached spinal cord preparation. J Neurosci Methods 182:255–259
Marchetti C, Beato M, Nistri A (2001) Alternating rhythmic activity induced by dorsal root stimulation in the neonatal rat spinal cord in vitro. J Physiol 530:105–112
Martin JH (2005) The Corticospinal System: From Development to Motor Control. Neuroscientist 11:161–173
McCormick DA, Prince DA (1987) Post-natal development of electrophysiological properties of rat cerebral cortical pyramidal neurones. J Physiol 393:743–762
McQuillen PS, Sheldon RA, Shatz CJ, Ferriero DM (2003) Selective vulnerability of subplate neurons after early neonatal hypoxia-ischemia. J Neurosci 23:3308–3315
Meehan CF, Grondahl L, Nielsen JB, Hultborn H (2012) Fictive locomotion in the adult decerebrate and spinal mouse *in vivo*: Fictive locomotion in the decerebrate mouse. J Physiol 590:289–300
Millhorn DE, Eldridge FL, Waldrop TG, Kiley JP (1987) Diencephalic regulation of respiration and arterial pressure during actual and fictive locomotion in cat. Circ Res 61:I53-59
Nicholls JG, Stewart RR, Erulkar SD, Saunders NR (1990) Reflexes, fictive respiration and cell division in the brain and spinal cord of the newborn opossum, Monodelphis domestica, isolated and maintained in vitro. J Exp Biol 152:1–15
Northington FJ, Ferriero DM, Graham EM, Traystman RJ, Martin LJ (2001) Early neurodegeneration after hypoxia-ischemia in neonatal rat is necrosis while delayed neuronal death is apoptosis. Neurobiol Dis 8:207–219
Okada Y, Mückenhoff K, Holtermann G, Acker H, Scheid P (1993) Depth profiles of pH and PO2 in the isolated brain stem-spinal cord of the neonatal rat. Respir Physiol 93:315–326
Phifer CB, Terry LM (1986) Use of hypothermia for general anesthesia in preweanling rodents. Physiol Behav 38:887–890
Rikard-Bell GC, Bystrzycka EK, Nail BS (1985) Cells of origin of corticospinal projections to phrenic and thoracic respiratory motoneurones in the cat as shown by retrograde transport of HRP. Brain Res Bull 14:39–47
Rudomin P (2009) In search of lost presynaptic inhibition. Exp Brain Res 196:139–151
Schreyer DJ, Jones EG (1988) Axon elimination in the developing corticospinal tract of the rat. Dev Brain Res 38:103–119
Smith JC, Greer JJ, Liu GS, Feldman JL (1990) Neural mechanisms generating respiratory pattern in mammalian brain stem-spinal cord in vitro. I. Spatiotemporal patterns of motor and medullary neuron activity. J Neurophysiol 64:1149–1169
Spencer WG (1894) The effect produced upon respiration by faradic excitation of the cerebrum in the monkey, dog, cat, and rabbit. Philosoph Transactions Royal Soc London (b) 185:609–657
Suzue T (1984) Respiratory rhythm generation in the in vitro brain stem-spinal cord preparation of the neonatal rat. J Physiol 354:173–183
Taccola G (2011) The locomotor central pattern generator of the rat spinal cord in vitro is optimally activated by noisy dorsal root waveforms. J Neurophysiol 106:872–884
Taccola G, Nistri A (2005) Characteristics of the electrical oscillations evoked by 4-aminopyridine on dorsal root fibers and their relation to fictive locomotor patterns in the rat spinal cord in vitro. Neuroscience 132:1187–1197
Taccola G, Nistri A (2006) Fictive locomotor patterns generated by tetraethylammonium application to the neonatal rat spinal cord in vitro. Neuroscience 137:659–670
Taccola G, Mladinic M, Nistri A (2010) Dynamics of early locomotor network dysfunction following a focal lesion in an *in vitro* model of spinal injury. Eur J Neurosci 31:60–78
Taccola G, Gad P, Culaclii S, Ichiyama RM, Liu W, Edgerton VR (2020) Using EMG to deliver lumbar dynamic electrical stimulation to facilitate cortico-spinal excitability. Brain Stimul 13:20–34
Takakusaki K, Saitoh K, Harada H, Kashiwayanagi M (2004) Role of basal ganglia–brainstem pathways in the control of motor behaviors. Neurosci Res 50:137–151
Tazerart S, Vinay L, Brocard F (2008) The persistent sodium current generates pacemaker activities in the central pattern generator for locomotion and regulates the locomotor rhythm. J Neurosci 28:8577–8589
Tenney SM, Ou LC (1977) Ventilatory response of decorticate and decerebrate cats to hypoxia and CO2. Respir Physiol 29:81–92
Van Hartesveldt C, Lindquist D (1978) Behavioral effects of unilateral basal gangliar lesions in neonatal rats. Dev Psychobiol 11:151–160
Verkhratsky A, Parpura V (2016) Astrogliopathology in neurological, neurodevelopmental and psychiatric disorders. Neurobiol Dis 85:254–261
Vinay L, Clarac F (1999) Antidromic discharges of dorsal root afferents and inhibition of the lumbar monosynaptic reflex in the neonatal rat. Neuroscience 90:165–176
Voituron N, Frugière A, Gros F, MacRon JM, Bodineau L (2005) Diencephalic and mesencephalic influences on ponto-medullary respiratory control in normoxic and hypoxic conditions: an in vitro study on central nervous system preparations from newborn rat. Neuroscience 132:843–854
Wilson RJA, Chersa T, Whelan PJ (2003) Tissue PO2 and the effects of hypoxia on the generation of locomotor-like activity in the in vitro spinal cord of the neonatal mouse. Neuroscience 117:183–196
Wolpaw JR (2007) Spinal cord plasticity in acquisition and maintenance of motor skills. Acta Physiol 189:155–169
Young NA, Vuong J, Teskey GC (2012) Development of motor maps in rats and their modulation by experience. J Neurophysiol 108:1309–1317
Zaporozhets E, Cowley KC, Schmidt BJ (2004) A reliable technique for the induction of locomotor-like activity in the in vitro neonatal rat spinal cord using brainstem electrical stimulation. J Neurosci Methods 139:33–41
Zimmer MB, Fong AY, Milsom WK (2020) Effect of temperature, age and the pons on respiratory rhythm in the rat brainstem-spinal cord. Respir Physiol Neurobiol 273:103333

A focal traumatic injury to the spinal cord causes an immediate and massive spreading depolarization sustained by chloride ions, with transient network dysfunction and remote cortical glia changes.

Atiyeh Mohammadshirazi[a,b], Graciela L. Mazzone[c], Benjamín A. Zylberberg[c], Luca Mio[a], Giulio Pistorio[a], Carmen Falcone[a], Giuliano Taccola[a,b*]

[a]Neuroscience Department, International School for Advanced Studies (SISSA), Via Bonomea 265, Trieste, Italy.

[b]Applied Neurophysiology and Neuropharmacology Lab, Istituto di Medicina Fisica e Riabilitazione (IMFR), Via Gervasutta 48, Udine, UD, Italy.

[c]Instituto de Investigaciones en Medicina Traslacional CONICET - Universidad Austral, Av. Pte. Perón 1500, Pilar, Buenos Aires, Argentina.

*_Corresponding author_: Prof. Giuliano Taccola, via Bonomea 265, Trieste, (TS) Italy; taccola@sissa.it

Keywords: Spinal shock, Motor evoked potentials, Fictive locomotion, Isolated Central Nervous System, Tissue oxygenation, Neonatal SCI.

Acknowledgments: GT is grateful to Mrs. Elisa Ius for her excellent assistance in preparing the manuscript and to John Fischetti for technical support in fabricating the impactor. The study was supported by intramural SISSA grants through the 5xMILLE2020 framework.
CF is grateful for Early Career Fellowship awarded to CF from the Human Technopole (Milan, Italy).

Abbreviations: ANOVA, analysis of variance; C, cervical; CCF, cross-correlation function; Ca^{2+}, calcium ions; Cl^-, chloride ions; CNS, central nervous system; Ctrl, control; CV, coefficient of variation; DAPI, 4', 6-diamidino-2-phenylindole; DR, dorsal root; DRG, dorsal root ganglia; K^+, potassium ions; l, left; L, lumbar;

P, postnatal; PO_2, partial pressure of oxygen; r, right; RMS, root mean square; SCI, spinal cord injury; SD, spreading depression; Th, threshold; T, thoracic; VR, ventral root.

Author Contributions. GT contributed to the study conception and design. AM, GM, LM, GP and GT performed experiments. Material preparation, data collection and analysis were performed by all authors. The first draft of the manuscript was written and illustrated by GT and AM. GM and CF commented on previous versions of the manuscript. All authors approved the final manuscript.

Competing Interests. The authors have no relevant financial or non-financial interest to disclose. The impactor adopted in the study is currently being patented by SISSA and is available upon request.

Data Availability. The datasets generated during and/or analyzed during the current study are available from the corresponding author on reasonable request.

Ethics approval. The study was performed in line with the principles of the Italian Animal Welfare Act 24/3/2014 n. 26 implementing the European Union directive on animal experimentation (2010/63/ EU). The study complied with the ARRIVE guidelines.

Consent to participate. All authors give their formal consent to participate to the present manuscript.

Consent for publication. All authors give their formal consent for the publication of the present manuscript.

Abstract

In clinics, physical injuries to the spinal cord cause a temporary motor areflexia below lesion, known as spinal shock. This topic is still underexplored due to the lack of preclinical SCI models that do not use

anesthesia, which would affect spinal excitability. Our innovative design considered a custom-made micro impactor that provides localized and calibrated strikes to the ventral surface of the thoracic spinal cord of the entire CNS isolated from neonatal rats. Before and after injury, multiple ventral root (VR) recordings continuously traced respiratory rhythm, baseline spontaneous activities, and electrically-induced reflex responses. As early as 200 ms after impact, an immediate transient depolarization spread from the injury site to the whole spinal cord with distinct segmental velocities. Stronger strikes induced higher potentials causing, at the site of injury, a transient drop in tissue oxygen levels and a massive cell death with complete disconnection of longitudinal tracts. Below the impact site, expiratory rhythm and spontaneous lumbar activity were suppressed. On lumbar VRs, reflex responses transiently halted but later recovered to control values, while electrically-induced fictive locomotion remained perturbed. Moreover, low-ion modified Krebs solutions differently influenced impact-induced depolarizations, the magnitude of which amplified in low-Cl^-. Moreover, remote changes in cortical glia occurred soon after spinal damage. Overall, our novel in vitro platform traces the immediate functional consequences of impacts to the spinal cord during development. This basic study provides insights on the SCI pathophysiology, unveiling an immediate chloride dysregulation and transient remote glial changes in the cortex.

Introduction

A spinal cord injury (SCI) demonstrates that the mature central nervous system (CNS) cannot regenerate nor repair itself after traumatic insults. Because of this vulnerability, an SCI often causes a permanent loss of sensory and motor control over the body parts innervated by spinal neurons located below the level of injury. Eventually, an SCI results in a long-life debilitating condition characterized by motor paralysis and a variegated spectrum of functional deficits and complications. To date, there is no cure against paralysis and current rehabilitation still focuses mainly on strengthening the able part of the body to compensate for the loss of volitional motor control over the rest. Support in daily tasks mainly occur through classical mobility aids, such as a wheelchair and crutches, but also using newly introduced technologies, such as exoskeletons (Gad et al., 2017) and advanced brain machine interfaces (Lorach et al., 2023), which however allow only minor functional benefits.

Nevertheless, some scattered and unpredictable spontaneous neurologic recoveries have been reported (Kirshblum et al., 2021) and, in less severe injuries, a substantial spontaneous regain of functions plateaued at 16 weeks after injury (Geisler et al., 2001). Spontaneous recoveries still challenge our

understanding of the pathophysiological mechanisms of an SCI and of the residual potential of the cord to repair spinal circuits.

In particular, pediatric spinal injuries, which account for 1-10% of all SCIs (Carreon et al., 2004), show higher rates of spontaneous functional recovery compared to adults (Eleraky et al., 2000; Wang et al., 2004). Likewise, the study of traumatic injuries in the developing mammalian spinal tissue, also in comparison with adults (Clarke et al., 2009), is compelling to clarify the peculiar pathophysiological mechanisms of neonatal SCIs, in the hope to identify the reasons for the enhanced recoveries in children and possibly expand them to all people with SCI.

Established models of SCI use adult mammals (Kjell and Olson, 2016) under anesthesia. However, when administered near the time of injury, anesthetics affect the damage progression as, based upon the different drug adopted, they can exert a neuroprotective effect (Salzman et al., 1993; Davis and Grau, 2023) or, on the contrary, exacerbate the hypoxic neuronal injury caused by transitory hypotension (Robba et al., 2017). In addition, up to date, only few reports described standardized and calibrated SCI models using immature spinal tissues (Taccola et al., 2010; Mladinic et al., 2013).

Another missing tile for the overall understanding of an SCI is the identification of the immediate events that take place during a physical impact to the spinal cord. In particular, it is still unknown how the primary mechanical insult to the spinal tissue contributes to trigger the subsequent cascade of pathological events known as secondary damage, which eventually determines the extent of tissue damage and hinders the chances of achieving a functional recovery (Carlson et al., 1998).

Indeed, after injury, a temporary loss or depression of all, or most, spinal reflex activity takes place below the lesion. This phenomenon is called spinal shock, and the underlying mechanisms are not fully clarified (Ditunno et al., 2004). A spinal shock clinically persists for days or weeks, depending on which reflex is clinically being tested for reappearance. However, when duration is defined based on the initial recovery of any one reflex, then the spinal shock lasts no longer than 20 - 60 min (Ditunno et al., 2004).

The lack of reflex activity has been mainly attributed both to the sudden disappearance of the predominantly facilitatory tonic influence exerted by descending supraspinal tracts, and to an increased presynaptic inhibition. In addition, depression of synaptic activities also depends on the hyperpolarization of spinal neurons due to an excessive accumulation of potassium (Atkinson and Atkinson, 1996).

In pediatric SCIs, reflexes recover sooner, likely because descending supraspinal tracts in children are not fully developed, thereby normal descending inhibition to spinal inhibitory pathways is less affected by an SCI compared to adults, mitigating the depression of spinal networks during shock (Guttmann, 1976).

Experimentally, the main features of a spinal shock parallel those of an early depolarization of the entire spinal cord following a trauma, also known as injury potential, which spreads rostrally and caudally from the site of impact. This early depolarization is sustained by a transient extracellular ionic disbalance (Goodman et al., 1985; Wang et al., 2015) and is similar to a cortical spreading depression (SD), which exhibits a marked, enduring reduction in the intrinsic electrical activity of neurons, eventually spreading from the original source out in all directions and involving increasingly distant parts of the cerebral cortex (Leao, 1944, 1947). A cortical SD is triggered, among other causes (Gerasimova et al., 2021), by traumatic brain injuries (Hermann et al., 1999).

In both amphibians and rodents, a compressive injury to the cord is followed both by SD-like waves characterized by a velocity of propagation of around 10-15 mm/min, and by a rapid and reversible increase in extracellular concentrations of K^+ ions (Streit et al., 1995; Gorji et al., 2004). Interestingly, electrically evoked potentials were transiently abolished during spinal SD waves, eventually returning to baseline values only after about twenty minutes. This phenomenon suggests that spinal SD might determine areflexia after spinal shock (Gorji et al., 2004). The same study also described how the SD evoked by an injury to the brain cortex reduced excitability of spinal neurons located in upper spinal segments, indicating that SD-like waves induced by an injury maintain a form of conduction among cortical and spinal structures (Gorji et al., 2004).

However, the appearance of any neuronal changes in the brain after SCI is controversial, with conclusions spanning from the absence of cellular loss (Crawley et al., 2004) to extensive retrograde neurodegeneration (Feringa and Vahlsing, 1985; Hains et al., 2003). A detailed study after spinal cord contusion in mice described SCIs as complex events affecting the entire CNS and generating cognitive changes and depressive-like behaviors, associated with reactive microglia and neuronal loss in the hippocampus and cerebral cortex (Wu et al., 2014). However, the authors failed to detect a significant neuronal death in brain districts even after two weeks after SCI, suggesting only chronic inflammatory changes. However, it is still unknown whether immediate pathological signals are transiently triggered in the brain right after an impact to the spinal cord. The presence of a pathological sign could actually provide a novel marker to more realistically characterize the severity of a lesion and envisage potential recoveries.

Obstacles to the comprehension of a spinal shock and the related transient changes in the brain reside in some technical challenges that arise from the preclinical models currently available. Indeed, fully anesthetized animals do not allow to record the electrical activity of spinal neurons in the same instants when the physical impact occurs, due to both motion and electrical artifacts generated by standard experimental impactors, which interfere with the low amplitude of currents involved. As a consequence,

the earliest injury potential has been recorded only after four minutes from the impact (Goodman et al., 1985). This temporal limitation sums up to the effects of anesthetics that depress neuronal excitability and are used in preclinical models at the time of the physical trauma. A solution to avoid any technical artifacts, as well as any consequences of anesthetics, is the adoption of the neonatal preparation of the entire central nervous system in vitro (CNS; (Mohammadshirazi et al., 2023; Apicella and Taccola, 2023)), which does not require the administration of any drugs. In addition, the rodent spinal cord can be optimally damaged through a low-noise calibrated micro impactor recently designed in the laboratory. Using this setting, we aim at quantifying the immediate events triggered by a physical insult to the cord and their spread from the site of injury both caudally toward spinal segments, and rostrally up to brain structures. In addition, we will assess any spontaneous functional recoveries occurring in the neonatal spinal circuitry.

Methods

In vitro preparation of the isolated entire CNS

All procedures were approved by the International School for Advanced Studies (SISSA) ethics committee and are in accordance with the guidelines of the National Institutes of Health (NIH) and the Italian Animal Welfare Act 24/3/2014 n. 26, implementing the European Union directive on animal experimentation (2010/63/EU). Every effort was made to minimize the number of animals used and to ensure their well-being. A total of 92 postnatal (P) Wistar rats (P0-P3) of random sexes were included in this study.

Experiments were performed on in vitro preparations of the entire isolated central nervous system (CNS; (Mohammadshirazi et al., 2023)). Newborn rats were subjected to cryoanesthesia (Danneman and Mandrell, 1997). After disappearance of the paw pinch reflex, surgical procedures considered the quick removal of: forehead at orbital line, ribs cage, internal stomach and forelimbs. The preparation was then transferred to a petri dish filled with oxygenated Krebs solution that contained (in mM): 113 NaCl, 4.5 KCl, 1 $MgCl_2 7H_2O$, 2 $CaCl_2$, 1 NaH_2PO_4, 25 $NaHCO_3$, and 30 glucose, gassed with 95% O_2 - 5% CO_2 (PO_2 533.65 ± 44.05 Torr), pH 7.4, 299.62 ± 3.2 mOsm/kg. Under microscopic guidance, craniotomy and ventral laminectomy were performed keeping the dorsal vertebra and dorsal root ganglia (DRG) intact. Afterwards, the entire CNS preparation was maintained in oxygenated Krebs solution at room temperature for 15 minutes and then mounted in the recording chamber (total volume = 4.7 ml, flow rate = 7 mL/min, controlled temperature = 25-27° C, TC-324C Warner Instruments, USA). For stable electrophysiological recordings, the preparation was fixed ventral side up with insect pins passing through dorsal vertebrae. For selective root recordings, VRs and DRs were detached from DRGs.

186

187 *Extracellular Recordings*

188 DC-coupled recordings were obtained from both VRs and DRs using monopolar suction electrodes realized
189 by pulling tight-fitting glass pipettes (1.5 mm outer diameter, 0.225 mm wall thickness; Hilgenberg,
190 Germany). Electrodes were connected to a differential amplifier (DP-304, Warner Instruments, Hamden,
191 CT, USA; high-pass filter = 0.1 Hz, low-pass filter = 10 kHz, gain X 1000). Analog signals were filtered
192 through a noise eliminator (D400, Digitimer Ltd, UK), then digitized (Digidata 1440, Molecular Devices
193 Corporation, Downingtown, PA, USA; digital Bessel low-pass filter at 10 Hz; sampling rate = 5 kHz) and
194 visualized real-time with the software Clampex 10.7 (Molecular Devices Corporation, Downingtown, PA,
195 USA).

196

197 *Electrical Stimulation*

198 Trains of rectangular electrical pulses (pulse duration = 0.1 ms, frequency = 0.1 Hz) were supplied to
199 sacrocaudal afferents through a programmable stimulator (STG4002, Multichannel System, Reutlingen,
200 Germany) using bipolar glass suction electrodes connected two close silver wires (500-300 µm). Stimulus
201 intensity (40-160 µA) was attributed as times to threshold (Th), where Th is the lowest intensity required
202 to elicit a small deflection of VRrL5 baseline. To generate epochs of fictive locomotor patterns (Kiehn,
203 2006), 160 rectangular pulses (duration = 0.1 ms, intensity = 37.5-150 µA, 1-5 × Th) were supplied at 2 Hz
204 to sacrocaudal afferents for a total length of 80 s. Recordings were acquired in the same preparation from
205 r and l VRL2 (for bilateral flexor commands) and VRrL5 (for extensor output).

206

207 *Spinal cord injury*

208 A calibrated physical impact to the thoracic (T) cord was provided using a custom-made micro-impactor
209 device specifically designed and shielded to allow simultaneous electrophysiological recordings from the
210 neonatal CNS in vitro. The device is currently being patented by SISSA and is available upon request
211 (https://www.valorisation.sissa.it/device-mechanically-stimulating-biological-material-and-its-
212 procedure). The impactor tip (diameter = 2 mm) was precisely positioned on the ventral surface of the
213 spinal cord (T10) using a manipulator. The micro-impactor was controlled through a dedicated software
214 that allows to precisely set impact parameters (displacement, speed, acceleration, deceleration, and
215 pause time). In our experiments, the maximum severity of compression without completely transecting
216 the neonatal spinal cord (diameter around 3-4 mm) was obtained with the impactor tip descending into
217 the cord by 2656 µm from the spinal surface, at an average speed of 4 mm/s, maintaining an acceleration

and deceleration of 6.1 ± 0.05 mm/s². After the impact, the tip of the impactor was promptly returned to its original position at the same speed, acceleration, and deceleration. For minor severities of injury, varying displacements and velocities of the impactor rod were considered (625 µm at 2 mm/s, 1250 µm at 2.8 mm/s, and 1875 µm at 3.4 mm/s), while keeping acceleration and deceleration constant.

Modified Krebs solutions

Three modified Krebs solutions were prepared. The low chloride solution (in mM) was composed of: 56.5 NaCl, 56.5 sodium isethionate, 4.5 KCl, 1 $MgCl_2 7H_2O$, 2 $CaCl_2$, 1 NaH_2PO_4, 25 $NaHCO_3$, and 30 glucose (297.62 ± 3.8 mOsm/kg). The low calcium solution (in mM) contained: 113 NaCl, 4.5 KCl, 1 $MgCl_2 7H_2O$, 1 $CaCl_2$, 1 NaH_2PO_4, 25 $NaHCO_3$, and 30 glucose. The low potassium solution (in mM) was prepared with: 113 NaCl, 2.25 KCl, 1 $MgCl_2 7H_2O$, 2 $CaCl_2$, 1 NaH_2PO_4, 25 $NaHCO_3$, and 30 glucose. The three modified Krebs solutions were gassed with 95% O_2 - 5% CO_2 and their osmolarity was adjusted by adding sucrose to mimic the osmolarity of control Krebs solution. To assess the different impact of modified Krebs solutions on spinal reflexes, analysis was performed on five responses randomly chosen in control, and five in the last two minutes of low-ion perfusions (from the 88th to 90th minute for low Cl^-, and from the 28th to 30th minute for low Ca^{2+} and low K^+).

Tissue Oxygen Assessment

PO_2 measurements in the spinal cord were conducted using a fiber-optic microsensor with a 50 µm tip diameter (Optode, OxyMicro System, World Precision Instruments, FL, USA). The microsensor was implanted at 100µm deep into the cord in the anterior funiculus between L1 and L2 segments. Measurements were taken at the sampling rate of one per second and were directly acquired using OxyMicro v7.0.0 software (OxyMicro System, World Precision Instruments, FL, USA). Temperature during all PO_2 measurements was maintained within the range of 25-27 °C.

To ascertain whether high K^+ perfusions affect measurements of the microsensor probe, test experiments considered positioning the tip of the microsensor in the recording chamber void of any preparation. PO_2 values remained unchanged in standard Krebs solution (610.29 ± 7.63) and during 10 mM K^+ applications (613 ± 8.53) indicating that tissue oxygen assessments did not change during perfusion with potassium ions (Sl. Fig. 4 B).

Slice Immunostaining and Cell Counting

After electrophysiological experiments, spinal cords were fixed overnight in 4% paraformaldehyde at 4°C and then tissue was cryopreserved with 30% sucrose in phosphate buffered saline (PBS), following our standard procedures (Taccola et al., 2008, 2010). Spinal cords were cut in 20-µm (coronal or longitudinal) slices using a sliding cryostat microtome. To detect neurons and motoneurons, slices were incubated overnight at 4 °C with blocking solution for 1 h and then with mouse monoclonal anti-NeuN or SMI 32 antibody (1:200; Merck Millipore, Milan, Italy; ABN78 and 1: 200; Covance, Berkeley, CA, catalog # SMI-32P, respectively) in 5% fetal calf serum (FCS), 5% bovine serum albumin (BSA), and 0.3% Triton X-100 in PBS. After three washes in PBS, floating sections were incubated for 2 h at room temperature with the goat anti-mouse Alexa 488-labeled secondary antibody (1:500, Invitrogen). To visualize cell nuclei, slices were incubated in 1 µg/ml solution of 4', 6-diamidino-2-phenylindole (DAPI). Sections were washed three times in PBS for 5 min and mounted using Vectashield® medium (Vector Laboratories, Burlingame, CA) and coverslips. NeuN and SMI 32 positive cells were assessed in a complete set of z-stack images, typically at a depth of 4-µm, using confocal series acquired by Nis-Eclipse microscope (20x magnification, NIKON, Amsterdam, Netherlands) at 20× magnification. The number of SMI 32 positive cells was determined by VolocityTM software (https://www.volocity4d.com, Improvision, Coventry, UK) while Image J software (NIH, https://imagej.nih.gov/ij/index.html) was adopted for NeuN positive cells.

Cortical glia immunohistochemistry and image acquisition

Brain specimens from 16 pups which fixed at 25 minutes, 1.5 hours, 2.5 hours post-injury were sectioned into 20 µm-thick coronal sections using a cryostat. Sections were processed for free-floating immunohistochemistry following a previously published protocol (Ciani et al., 2023). In detail, slices were pre-treated with 0.1% Sudan Black (in 70% Ethanol) for 30 min for autofluorescence reduction, quickly washed with 70% ethanol, and incubated with 10% serum blocking solution for 1 h at room temperature. Then, sections were incubated with the primary antibody, anti-S100b (rabbit, Abcam #ab52642, RRID: AB_882426), diluted in 2% blocking solution and stored overnight at 4° C degrees. Subsequently, sections were washed with 1X- PBS three times, and incubated with the secondary antibody, AlexaFluor#488 conjugated polyclonal anti-rabbit antibody (1:400, Invitrogen, #A-21206 RRID: AB_141633), diluted in 2% serum blocking solution. Finally, DAPI was used (1:500, #10236276001, Hoffmann-La Roche, Basel, Switzerland) to stain nuclei.

Pictures were taken using Nikon A1/R confocal, with a 60X oil objective. To include all cells among the whole tissue thickness, images were taken as z-stacks of at least 20 steps of 1 µm, to include an optical section thickness of at least 20 µm.

Data Analysis

Data analysis was performed using Clampfit 10.7 software (Molecular Devices Corporation, PA, USA). Spontaneous rhythmic motor discharges recorded from cervical VRs, with a period of 24.27 ± 16.13 s, were attributed to respiratory bursts that were also derived synchronous among bilateral lumbar VRs (Mohammadshirazi et al., 2023; Apicella and Taccola, 2023). The coefficient of variation (CV), an indicator of response consistency, was determined by the ratio between standard deviation and mean value (Taccola et al., 2020). To calculate conduction velocity, the latency of each response was divided by the distance between the center of the impacted area and the recording sites, as precisely measured using a microcalibrated dial caliper (sensitivity = 20 µm). The correlation coefficient function (CCF) was used to measure phase coupling between pairs of VRs using Clampfit 10.7 software. A CCF value of ≥ 0.5 indicates synchronous rhythmic signals from two VRs, while a CCF value of ≤ -0.5 indicates alternating signals (Taccola and Nistri, 2005; Dose et al., 2016).

Immunofluorescent images from cerebral cortex were analyzed to quantify the number of both S100b+ astrocytes and total DAPI+ cells, per each region of interest (ROI) using the Volocity software (Quorum Technologies Inc., CA).

Statistical Analysis

Statistical analysis was performed with GraphPad InStat 3.10 (Inc., San Diego, California, USA). In the Results section, the number of animals is denoted as "n", and data is presented as mean ± standard deviation (SD) values. Before conducting comparisons among groups, a normality test was performed to select the appropriate parametric or non-parametric tests. Parametric data were analyzed with paired student t-test, one-way analysis of variance (ANOVA) or repeated measure analysis, while non-parametric data were analyzed using Kruskal-Wallis, Mann-Whitney, Friedman, or Wilcoxon matched-pairs signed-ranks tests. Multiple comparisons ANOVA was followed by Tukey-Kramer or Dunnett multiple comparisons tests. Differences were considered statistically significant when P value ≤ 0.05.

Results

A physical impact to the cord elicits an immediate depolarizing potential.

To investigate the immediate events following a contusive spinal cord injury, a custom-made impactor was employed to induce a physical impact at thoracic spinal cord level of an in vitro preparation of entire CNS (Mohammadshirazi et al., 2023). The careful design of the impactor included a proper shielding to

minimize any electrical interference during operation, to allow simultaneous electrophysiological recordings during the impact.

In an exemplar experiment, a brief and intense impact (time = 650 ms, displacement = 2656 µm) on the ventral cord (T10) led to a massive depolarization, simultaneously recorded rostral and caudal to the compression site from cervical and lumbar VRs, respectively (Fig. 1 A). Injury-induced potentials started 194.4 ms after the impact on VRrL5, and 225.2 ms on VRrC2. On VRrL5, a depolarization peak of 6.86 mV is reached after 2.66 s, followed by a depolarizing plateau lasting 3.52 s (Fig. 1 B) and spontaneously recovering to baseline in less than 15 minutes. VRrC2 generated a smaller depolarization peak (1.47 mV). The profile of the average injury-induced potential from VRrL5 reveals a peak of 8.21 ± 1.32 mV and a latency of 178.41 ± 15.17 ms after the impact, recovering to 81.11 ± 12.56 % six min later (Fig. 1 G).

To confirm that the observed sudden increment in DC levels is indeed a genuine potential rather than an artifact, we performed supplementary four experiments, Firstly, where the device solely acted in the bath close to the preparation, without touching the cord. (Sl. Fig. 1 A, B). Furthermore, when multiple impacts of equal severity (displacement = 2656 µm) were serially applied to the same site (T10) for five times, with a lag of less than 10 seconds between any two consecutive impacts, peaks of injury-induced potentials remained stable, hence excluding any summation of artifacts (Sl. Fig. 1 C). In another trial, the impact was delivered at the top of a large depolarization (16.46 mV) produced by perfusing 50 mM KCl. No injury-evoked depolarization was noticed when the preparation was already maximally depolarized by the high K^+ concentrations (Sl. Fig. 1 D). Finally, no baseline deflections were recorded from VRrL5 when the impact was inflicted to the T10 segment of a spinal tissue inactivated by both high temperature (100° C) and long-lasting (1 h) oxygen deprivation (Sl. Fig. 4 C), proving the biological origin of depolarization after injury. Collectively, these tests revealed the absence of any baseline drift produced either by the engine itself or by the sudden movement of the tip in the recording bath.

To monitor the respiratory rhythm originated by neuronal networks located in the brainstem (Del Negro et al., 2018), spontaneous rhythmic bursts were recorded from cervical VRs of the isolated CNS (Mohammadshirazi et al., 2023; Apicella and Taccola, 2023). The respiratory rhythm can also be recorded from lumbar VRs, which drive the recruitment of chest muscles to assist the expiratory phase (Giraudin et al., 2008). Noteworthy, respiratory bursting recorded from upper cervical VRs, 30 mins after injury, was not affected by the thoracic impact to the cord (Fig. 1 C, D). In seven preparations, respiration frequency from VRC2 was 84.28 ± 20.29 % of pre-impact control (P = 0.709, paired t-test). To assess any early and transient alteration of the respiratory rhythm during the impact, 20 respiratory bursts from cervical VRs were analyzed right before and soon after the injury. In 4 out of 7 preparations, the first respiratory event

after the impact was delayed, showing an early perturbation of the neuronal networks in the brainstem generating the respiratory rhythm (Sl. Fig. 2). Albeit not consistent among all preparations, this effect was observed in the majority of experiments, regardless of the magnitude of injury potentials from cervical VRs and the age of animals (Sl. Fig. 2).

Contrariwise, impact at T10 largely suppressed on both VRrL5 and VRrC2 those sporadic episodes that appeared synchronous among all neonatal motor pools as a result of the spontaneous motor activity reverberating through a diffuse propriospinal network within the neonatal spinal cord ((Cazalets, 2005); Fig. 1 C, D). This observation was repeated in 20 out of 24 preparations.

To quantify the peak of injury-induced depolarization, high potassium (10 mM) was applied for 10 min before the impact to the same exemplar preparation (Fig. 1 A). KCl generated depolarizations that were smaller in VRrL5 (40.34%) and greater in VRrC2 (177.9%) compared to the ones induced by the following impact (Fig. 1 A).

A second exposure to 10 mM KCl after injury produced on both VRs the same depolarizations as the pre-impact application, demonstrating that the total number of functional motoneurons was unaffected by the impact in segments rostral and caudal to the lesion site (Fig. 1 A). Pooled data from five preparations showed that the peak of average injury-induced depolarizations from VRrL5 was significantly higher than the depolarizations elicited by 10 mM KCl ($P < 0.001$, Repeated measures analysis, $n = 5$; Fig. 1 E). Conversely, in the same group of preparations, the average injury-induced depolarization from VRrC2 was lower than the one elicited at lumbar levels ($P < 0.001$), and significantly lower than the depolarization determined by a second application of 10 mM KCl (Fig. 1 F; $P = 0.046$, Repeated measures analysis, $n = 5$). Notably, at both L5 and C2 levels, potentials elicited by rising KCl concentrations were comparable before and after the impact (Fig. 1 E, F). This confirms that an injury targeted to the low thoracic cord (T10) does not reduce the overall activation of motoneurons located in motor pools far from the injury site, which remain equally functional once directly activated by KCl. Furthermore, distinct lumbar segments of sham and injured spinal cords were treated with a selective marker for motoneurons in the ventral horns (SMI-32 antibody). Histological processing visualized a similar SMI-32 staining in the ventral cord of the sham and injured preparations, for both L1-L3 and L3-L5 segments (Fig. 1 H). Mean data from 49 slices from a total of eight animals (four sham intact and four injured spinal cords) confirmed no significant difference in the number of SMI-32 positive cells ($P = 0.709$, ANOVA), hence excluding the acute death of any lumbar motoneurons after the low thoracic injury and related spread depolarization.

375 Collectively, a physical insult to the mid-thoracic spinal cord triggers a transient and massive
376 depolarization spreading along the entire spinal cord, suppressing the spontaneous motor activity that is
377 derived synchronous among all neonatal VRs, yet without any cellular loss of lumbar motor pools.

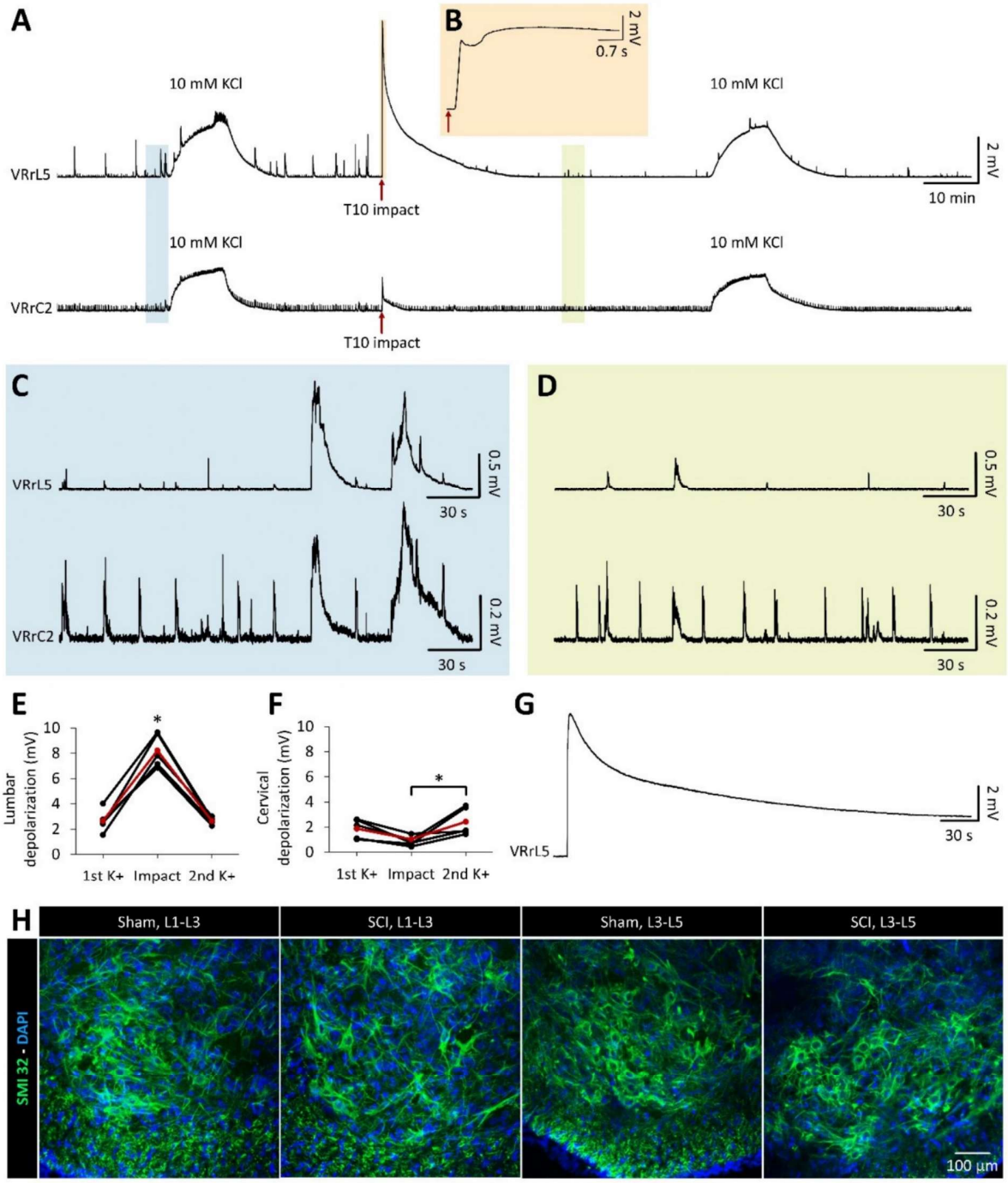

378
379 **Figure 1. A transient depolarization immediately follows a physical injury to the spinal cord.**
380 **A.** Long continuous recordings from VRrL5 and VRrC2, while the cord is being impacted at T10 (red
381 arrows). Before and after the impact, 10mM KCl were perfused for ten minutes to compare maximum

recruitment of motor pools. **B.** Magnification highlights the depolarization at VRrL5 in the first five seconds after impact (red arrows). **C, D.** Faster time scales of VR traces in A, corresponding to the shaded blue and green fields that are recorded before and after the impact, respectively. After the impact, spontaneous rhythmic respiratory events on VRrC2 persist unchanged, while the lumbar respiratory activity disappears. Spontaneous sporadic bursting from VRs is largely reduced by the trauma. **E.** From pooled data from five experiments, amplitude of impact-induced depolarization recorded from VRrL5 significantly exceeds the depolarization-induced by 10 mM KCl before and after the impact (*, $P < 0.001$). Mean values are indicated by the red dots and line. **F.** In cervical motor pools, depolarization after injury is notably smaller than after a second application of potassium (*, $P = 0.046$). Mean values are indicated by the red dots and line. **G.** Superimposed depolarizations from VRrL5 in five experiments. **H**. SMI 32 labelling of samples collected 90 min after the impact display a comparable number of motoneurons in L1 to L3, and in L3 to L5 segments of both, sham and SCI experiments.

Calibrated impacts of increasing strength elicit higher peaks of depolarization.

To assess the effects of varying degrees of severity of a spinal impact, increasing vertical displacements of the impactor rod were set. In each preparation, four different levels of compression (625 µm, 1250 µm, 1875 µm, and 2656 µm) were serially applied to the spinal cord at T10. A mild impact (625 µm) resulted in a moderate depolarization that was simultaneously recorded from VRrL2, VRrL5, and VRrL6, and which quickly recovered without perturbing the spontaneous baseline activity (Fig. 2 A). By increasing the strength of injury from 1250 to 1875 µm, progressively higher peaks of potentials were produced. At 1875 µm, the maximum level of depolarization was reached and could not be further increased even by the following most intense compression (2656 µm), likely due to the repetitive damage to the cord at the site of the impact (Fig. 2 A). Taking the VRrL5 recording of a sample experiment, the mildest trauma generated a depolarization of 1.4 mV, rising to 1.46 mV for 1250 µm, 3.52 mV for 1875 µm and eventually 2.41 mV during the strongest impact (2656 µm, Fig. 2 A). The impact at 2656 µm was used throughout the rest of the study to generate the most severe compression without completely transecting the neonatal spinal cord. Across all lumbar VRs, the extent of the depolarization elicited by 10 mM KCl was the same before and after the protocol of serial compressions, confirming that an injury at T10 does not affect the recruitment of motor pools below the lesion (Fig. 2 A). However, the spontaneous rhythmic motor activity arising synchronous from all VRs was largely reduced by the second impact (1250 µm) and up (Fig. 2 A).

Pooled data from five experiments (Fig. 2 B) confirms that the amplitude of the injury-induced depolarization augments with stronger impacts, with significant higher peaks for VRrL5 (1875 Vs. 625 µm; $P = 0.019$, Kruskal-Wallis test), and for VRrL2 (1250 Vs 625 µm; $P = 0.024$, ANOVA). Moreover, for each injury intensity, depolarizations appeared by-and-by smaller, the farther the recording site was from the site of compression. This common trend is more evident for impacts at 1250 µm, where the peak of injury-induced depolarization was significantly higher for VRrL2 compared to VRrL6 (Fig. 2 B, $P = 0.009$; Kruskal-

418 Wallis test, n = 5 for VRrL2 and VRrL5; n = 4 for VRrL6). Likewise, injury-induced depolarizations also
419 appeared sooner in segments closer to the impact site, rather than from more caudal ones. Indeed, for all
420 impact strengths, induced depolarization occurred first at L2, then at L5, and finally at L6 spinal segments,
421 reaching a statistical significance for potentials elicited by the mildest impact (625 µm) at T10, between
422 VRrL2 and VRrL6 (Fig. 2 C, P = 0.001, Kruskal-Wallis test, n = 5 for VRrL2 and VRrL5; n = 4 for VRrL6).
423 Noteworthy, latency of depolarization recorded from each root was unchanged among the four intensities
424 of injury showing that impact severity does not affect the velocity of depolarization spreading along the
425 spinal cord.
426 The customized in vitro impactor allowed to consistently trace the features of injury-induced potentials
427 for increasing severities of compression, showing that stronger impacts generate higher potentials
428 without affecting their velocity of propagation from the impact site.
429

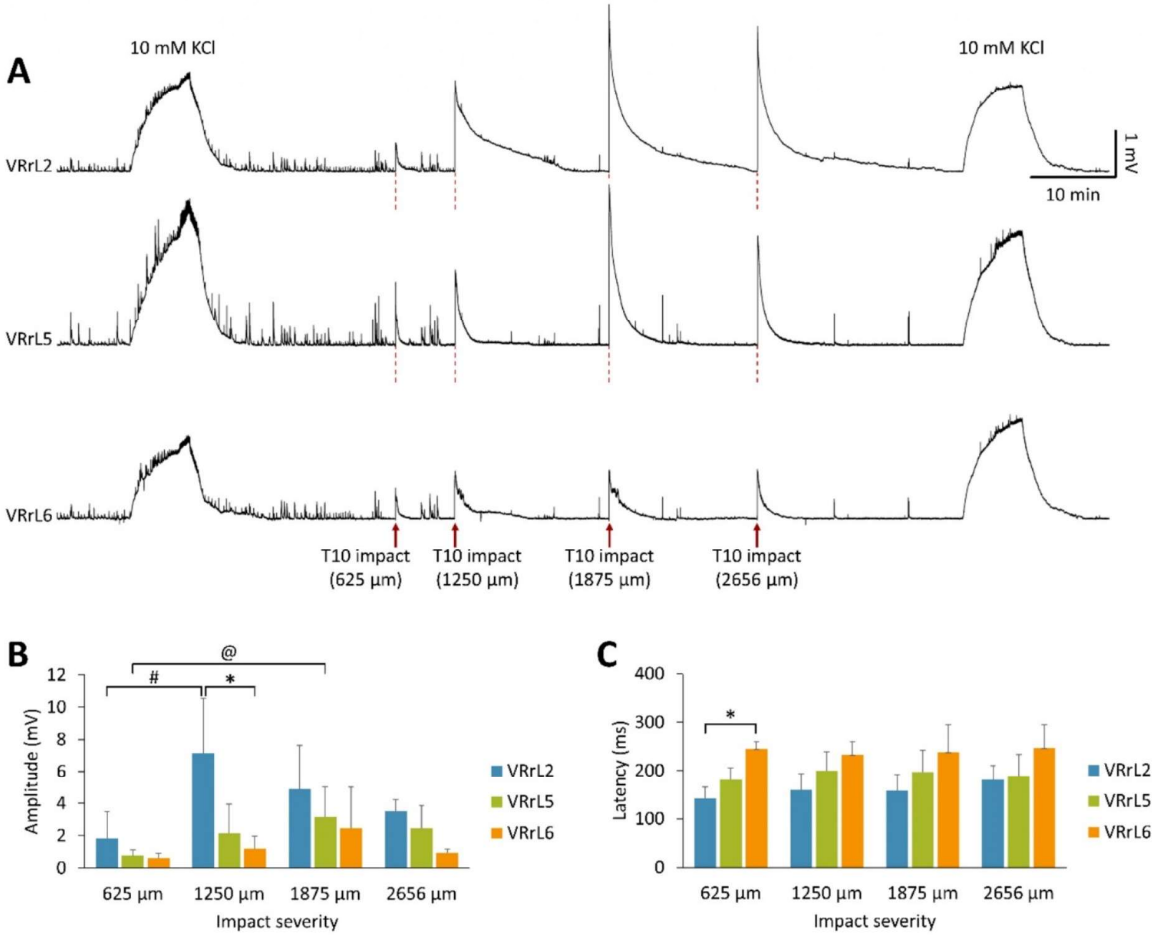

430
431 **Figure 2. Calibrated impacts of increasing severity elicit higher injury potentials and dramatically reduce**
432 **spontaneous network activity.**

A. Simultaneous recordings from VRrL2, VRrL5, VRrL6, during four serial impacts of increasing severity (from 625 to 2656 µm of tip displacement) at T10. Spontaneous baseline activity progressively reduces with stronger impacts, until its almost complete suppression after repetitive injuries. At the beginning and at the end of the experiment, 10 mM potassium were administered to confirm the unaffected recruitment of motor pools. **B.** Bars summarize the amplitude of injury-induced depolarizations arranged by different severities of impact. Larger injury potentials appear from VRs closer to the injury site (*P = 0.009 for VRrL2 vs. VRrL6 at 1250 µm) and after impacts of increasing strengths (@P = 0.019 for 625 µm vs. 1875 µm from VRrL5; #P = 0.024 for 625 µm vs. 1250 µm from VRrL2). **C.** Histogram reports the latency of injury-induced depolarizations for different severities of impact. The injury potential spreads from the lesion site to lumbar segments following a rostrocaudal propagation (*P = 0.001, for VRrL2 vs. VRrL6).

Injury potentials propagate rostrally and caudally from the site of impact in ventro-dorsal directions.

To better investigate the propagation of injury-induced depolarization along the entire spinal cord, we collected data from numerous VRs, out of a dataset of 44 preparations injured at the ventral aspect of T10 with the strongest impact (2656 µm tip displacement, Fig. 3 A). Injury potentials of different amplitude were recorded from distinct spinal segments, with the highest peaks from VRL1 and L2 being significantly larger than those derived at the extremities (Fig. 3 B, see Table 1 for statistical details). Injury potentials progressively slowed down the farther they were recorded from the impact site, with the lowest latency recorded at VRL1 (Fig. 3 C, see Table 2 for statistical details). Resulting velocity of the rostro-caudal conduction of injury-induced depolarizations from the site of impact to VRL1 (4.44 mm far from impact) was 0.03 ± 0.01 m/s, equal to the caudo-rostral conduction from the site of impact to VRT5 (4.83 mm far from impact, P = 0.451, Mann-Whitney test, n = 3 for T5 and n = 18 for L1).

To gain insights on the dorsal-ventral propagation of injury-induced depolarization, we simultaneously derived from both VRrL1 and DRrL1 while impacting the ventral side of the cord at T10. Data pooled from many experiments (Fig. 3 D) indicates that the impact leads to injury potentials that propagate also to the dorsal part of the cord, although they appear smaller (P = 0.041, paired t-test, n = 5) and spread more slowly (P = 0.015, paired t-test, n = 4) than ventrally elicited potentials.

Present data indicates that a physical impact to the spinal cord elicits a strong wave of depolarization that departs from the site of injury and invests the entire spinal cord with the same velocity, affecting also dorsal segments. This observation provides the rationale for ascertaining the functionality of spinal networks above and below the site of injury.

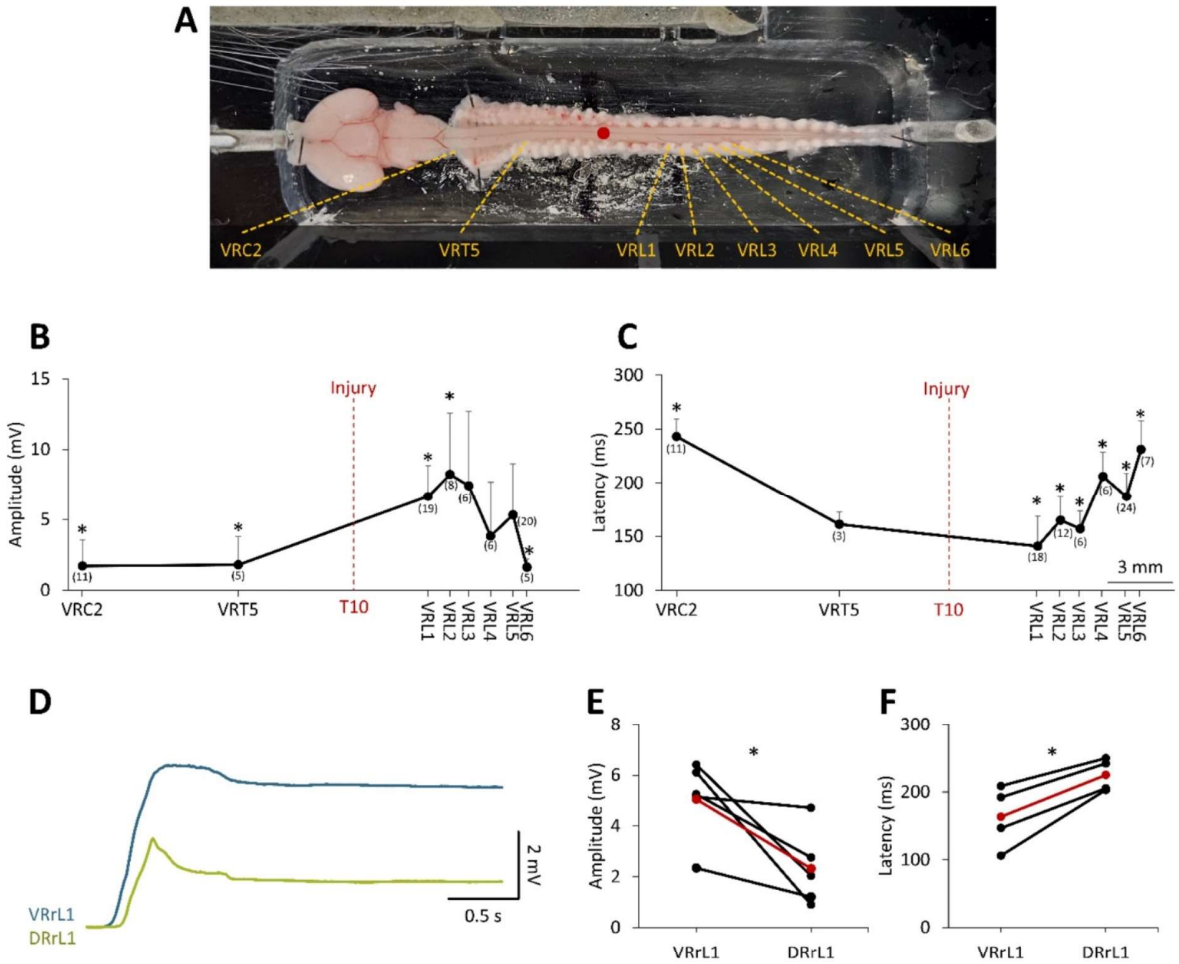

464
465 **Figure 3. Impact-induced depolarization spreads from the injury site to the whole spinal cord.**
466 **A.** A ventral view of the CNS preparation with dorsal vertebrae attached. VRs recordings are taken from
467 the VRs indicated by dotted yellow lines, while the injury site at the T10 segment is highlighted by a red
468 dot. **B.** Mean amplitudes of injury potentials from several VRs. Red dotted line indicates the level of injury
469 (T10). Number of experiments for each VR is indicated in brackets. Statistically significant amplitudes are
470 indicated by *, as described in Table 1. **C.** Mean latencies of injury potentials from several VRs. Red dotted
471 line indicates the level of injury (T10). Number of experiments for each VR is indicated in brackets.
472 Statistically significant amplitudes are indicated by *, as described in Table 2. **D.** Superimposed mean
473 traces from simultaneous recordings of injury potentials from both, DR (green trace) and VR (blue trace),
474 at L1 (n = 4). **E, F.** Injury potentials from DRrL1 are significantly smaller (E; *P = 0.041) and slower (F; *P =
475 0.015) than recorded from VRrL1. Red dots and line show average values.
476
477

Amplitude								
Vs	**VRC2**	**VRT5**	**VRL1**	**VRL2**	**VRL3**	**VRL4**	**VRL5**	**VRL6**
VRC2		P>0.05	P<0.01	P<0.01	P>0.05	P>0.05	P>0.05	P>0.05
VRT5	ns		P>0.05	P<0.05	P>0.05	P>0.05	P>0.05	P>0.05

VRL1	*	ns		P>0.05	P>0.05	P>0.05	P>0.05	P<0.05
VRL2	*	*	ns		P>0.05	P>0.05	P>0.05	P<0.05
VRL3	ns	ns	ns	ns		P>0.05	P>0.05	P>0.05
VRL4	ns	ns	ns	ns	ns		P>0.05	P>0.05
VRL5	ns	ns	ns	ns	ns	ns		P>0.05
VRL6	ns	ns	*	*	ns	ns	ns	
Average	1.72	1.79	6.64	8.23	7.42	3.83	5.33	1.6
SD	1.84	1.99	2.20	4.37	5.28	3.85	3.67	0.59

Table 1. Amplitude values of impact-induced depolarizations from different VRs. P values correspond to Kruskal-Wallis test.

Latency								
Vs	**VRC2**	**VRT5**	**VRL1**	**VRL2**	**VRL3**	**VRL4**	**VRL5**	**VRL6**
VRC2		P>0.05	P<0.001	P<0.001	P<0.001	P>0.05	P<0.05	P>0.05
VRT5	ns		P>0.05	P>0.05	P>0.05	P>0.05	P>0.05	P>0.05
VRL1	*	ns		P>0.05	P>0.05	P<0.01	P<0.01	P<0.001
VRL2	*	ns	ns		P>0.05	P>0.05	P>0.05	P<0.05
VRL3	*	ns	ns	ns		P>0.05	P>0.05	P<0.05
VRL4	ns	ns	*	ns	ns		P>0.05	P>0.05
VRL5	*	ns	*	ns	ns	ns		P>0.05
VRL6	ns	ns	*	*	*	ns	ns	
Average	243.13	161.2	140.81	165.03	157.1	205.97	187.19	231.31
SD	16.36	11.79	28	22.14	16.7	22.84	21.68	26.62

Table 2. Latency values of impact-induced depolarizations from different VRs. P values correspond to Kruskal-Wallis test.

An impact generates potentials that equally propagate to both sides of the cord, and disconnects the lumbar cord from descending respiratory input.

To confirm the symmetrical propagation of injury-induced depolarizations along both sides of the cord, simultaneous VR recordings were obtained from both left and right VRs at L1, in response to a physical impact at T10. In a sample experiment, continuous recordings were acquired from VRlL1, VRrL1, and

VRrC2 (Fig. 4 A). After the impact, VR injury-induced potentials peaked at 10.15 mV and 11.38 mV for left and right VRs, respectively. Average data from four experiments indicated an equal extent of impact-induced depolarizations on both sides of the L1 spinal segment (Fig. 4 B, $P > 0.999$, Wilcoxon matched-pairs signed-ranks test).

Furthermore, in the same sample experiment, spontaneous rhythmic bursts (0.02 ± 0.01 Hz) originating from respiratory networks in the brainstem (Mohammadshirazi et al., 2023; Apicella and Taccola, 2023) were simultaneously recorded in control from cervical and lumbar VRs (Fig. 4 C, left). In injured preparations, fictive respiration disappeared from all lumbar VRs, while after 20 mins from the impact, spontaneous rhythmic bursts from VRC2 persisted with a frequency similar to control (0.02 ± 0.01 Hz, Fig. 4 C, right). This observation was repeated in seven preparations, confirming both the injury-induced suppression of lumbar respiratory events, and the endurance of fictive respiration from cervical VRs with unchanged frequency from pre-injury controls (0.05 ± 0.03 Hz from 20 min pre-injury, 0.05 ± 0.02 Hz from 20 min post-injury, $P = 0.709$, paired t-test).

In summary, the equal magnitude of bilateral injury potentials propagating to lumbar VRs confirms the midline location of the impact. Moreover, the disappearance of respiratory bursts below the site of injury indicates that lumbar motor pools are completely disconnected from supraspinal respiratory centers.

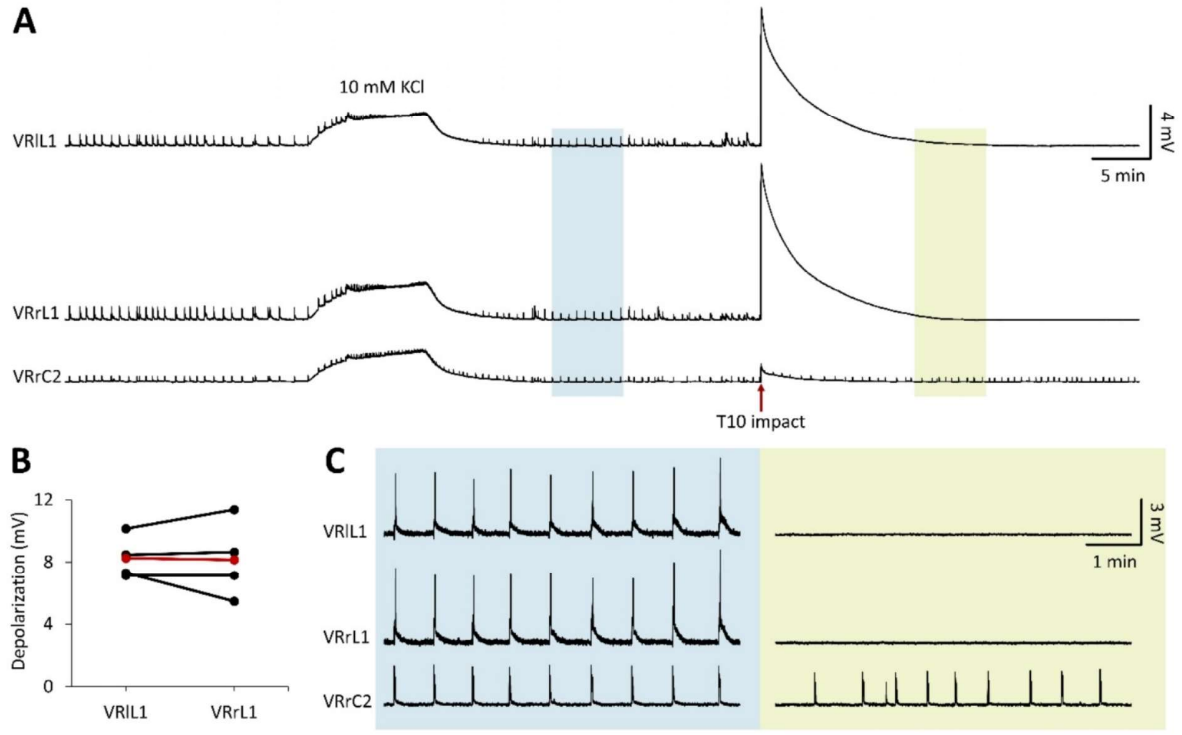

Figure 4. Impact evokes equal bilateral injury potentials and disconnects lumbar motor pools from descending respiratory input.

A. Continuous and simultaneous recordings from VRrL1, VRlL1, and VRrC2 showing the exposure to a high potassium solution (10 mM, 10 min) and to the following impact at T10. **B.** The plot visualizes the equal amplitude of injury-induced depolarizations recorded from left and right L1 VRs (n = 4). Red dots and red line correspond to average values. **C.** Magnifications correspond to the pale regions of continuous traces in A, and highlight rhythmic respiratory bursts in control (blue panel) and 21.8 min after the impact (green panel). Fictive respiration originating from brainstem structures is maintained at VRrC2 but disappeared from lumbar VRs due to the interruption of descending input beyond the site of impact.

Impact causes extensive neuronal loss at the contusion site and completely disconnects ascending afferent input.

Disappearance of respiratory episodes from the lumbar cord indicates that descending respiratory input from the brainstem are blocked at the level of impact. To investigate whether also the conduction of ascending input is interrupted by the impact, we recorded ascending input from VRs, as evoked by continuous electric stimulations (intensity = 100 µA, pulse duration = 0.1 ms, frequency = 0.1 Hz) of sacrocaudal afferents (Etlin et al., 2010). Simultaneous recordings were taken above and below the level of impact. In a sample experiment, single reflex responses in control were 1.26 and 0.13 mV as recorded from VRrL5 and VRrC2, respectively (blue traces in Fig. 5 A). At the peak of injury-induced depolarization, both responses vanished (Fig. 5 A). After 38 s from the impact, reflex responses from VRrL5 reappeared and eventually stabilized after 8 min, albeit reduced in amplitude to 41 % of pre-impact control. Cervical responses were completely abolished (green traces in Fig. 5 A). The disappearance of cervical reflexes after the impact was replicated in nine out of nine preparations.

To exclude that the reduced lumbar reflex amplitude arose from an interference produced by the impactor movement, rather than from a real depolarization caused by the injured tissue, in a subset of experiments, lumbar responses were allowed to recover after being transiently abolished by a first impact at T10. Then, the spinal cord was completely transected at L1 level (Sl. Fig. 3 A, B) and a second impact at T10 was performed, which did not evoke any injury potentials from the disconnected caudal cord nor varied the amplitude of reflex responses (Sl. Fig. 3 B). Noteworthy, the second impact still elicited an injury potential from the rostral cord (Sl. Fig. 3 B).

To visualize the anatomical damage caused by the impact, histological assessments were performed on sagittal sections of the entire spinal cord. The ventral spinal cord at the site of impact (dotted yellow rectangle) showed negligible neuronal labeling for NeuN due to an extensive cell loss (Fig. 5 B).

In another example, magnifications of horizontal slices from serial close spinal segments confirmed a lower number of NeuN positive cells at the injury site from 5 injured spinal cords (Fig. 5 C). Pooled data

from five experiments demonstrated the significant reduction of NeuN-positive cells at the injury site (T10) compared to rostral (T9) and caudal (T11) segments ($P < 0.001$, ANOVA; see Fig. 5 D).

This histological evidence describes a massive neuronal damage at the site of injury and corroborates the functional deficits reported above, namely the complete interruption of longitudinal spinal input at the level of impact.

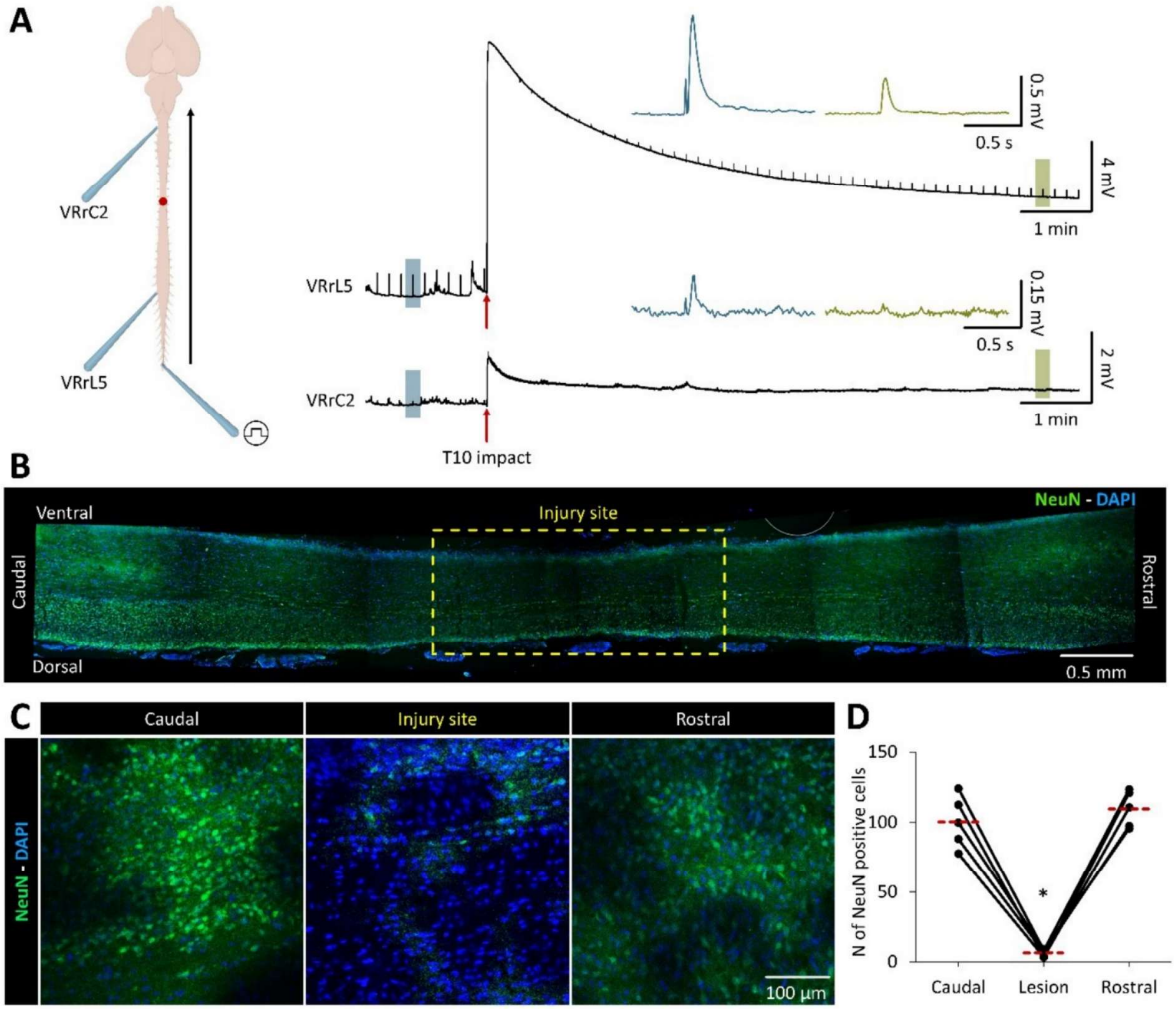

Figure 5. Contusion suppresses ascending conduction of afferent input and causes massive neuronal death at the site of ventral impact.

A. The cartoon depicts the CNS preparation with the impact site on the ventral aspect of T10 (red dot). Extracellular electrodes are positioned at C2 and L5 rVRs, and repetitive electrical pulses (0.1 Hz, 100 µA, duration = 100 µs) are supplied to cauda equine to elicit ascending input (arrow). Right traces show simultaneous recordings from VRrL5 and VRrC2 with reflex responses appearing in control and magnified in the blue insert. After the depolarization induced by the impact (red arrow), evoked motor responses are abolished on both VRs. During repolarization, responses progressively reappear on lumbar VR, while lumbar reflexes become visible again after 38 s from the impact and recover towards the original size by the time (8 min, top green insert). Contrariwise, reflexes from VRrC2 do not recover (bottom green insert).

B. Reconstruction of sagittal slices of a spinal cord (caudal left, rostral right, ventral up, dorsal down) as processed with DAPI and NeuN staining. A massive cellular loss is visible on the ventral aspect of the impact site. The base of the dotted yellow rectangle is calibrated to the width of the impactor tip. C. Magnifications of horizontal slices stained with DAPI and NeuN, and collected from serial spinal segments at caudal level (T11, left), injury site (T10, middle) and rostral spinal cord (T9, right The lack of NeuN (green) staining at the site of impact indicates extensive neuronal loss. D. The plot quantifies the statistical reduction of NeuN-positive cells at the injury site compared to both rostral and caudal segments (*P < 0.001). Red dotted lines correspond to the average number of NeuN positive cells.

Cord oxygenation drops after a spinal impact.

After an SCI, systemic hypotension and pericyte constriction of spinal capillaries decrease spinal oxygen delivery, reducing oxygen concentration on spinal tissues (Partida et al., 2016; Li et al., 2017). To quantify PO_2 in spinal cord tissue during contusion, an oximeter sensor was positioned 100 µm deep into the cord on the anterior funiculus between L1 and L2 VRs, while continuous electrophysiological signals were derived from VRrL1. Impact at T10 (red arrow) induced a large depolarization (5.23 mV, Fig. 6 A), which recovered to baseline after 12 min. In a sample experiment, tissue oxygen was continuously monitored, showing PO_2 values oscillating between 20.44 and 50.91 Torr in control (Fig. 6 B). Immediately after the impact (red arrow), PO_2 dropped to 8.12 Torr, but recovered pre-impact values after 10 min, perfectly matching the profile of DC level changes (Fig. 6 A, B). The time course of average PO_2 from nine preparations indicated that tissue oxygen content in control (31.19 ± 7.36 Torr) dropped to 11.68 ± 4.03 Torr after the impact, and then slowly recovered to the 78.74 % of control after 30 min (Fig. 6 C).

Oxygen consumption for in vitro preparations parallels the level of cellular activity (Wilson et al., 2003). To provide a reference for spinal oxygen consumption during a large depolarization, the CNS was perfused for ten minutes with a modified Krebs solution containing 10 mM KCl. High K^+ (10 mM) induced a mean depolarization of 1.83 ± 0.54 mV from VRL1, while average PO_2 measured from the L1 spinal segment dropped to 9.54 ± 2.14 Torr (Sl. Fig. 4 A).

The link between the increased neural activity induced by a large depolarization and the PO_2 consumption was confirmed using a CNS preparation that underwent a functional inactivation through heat-shock (100°C) and then a continuous perfusion with oxygenated Krebs. Here, no depolarization was recorded from VRrL5 after exposure to high K^+ (10 mM), while the oximeter probe inserted at L1 spinal level derived a mean PO_2 of 528 ± 8.74 Torr equal to pre-K^+ control values. In the same preparation, the spinal impact did not elicit any depolarizations from VRrL5, with PO_2 measurements that remained unchanged before and during the impact (505.76 ± 2.57 in control and 508.75 ± 3.16 Torr during impact, Sl. Fig. 4 C).

Collectively, the impact-induced drop in PO_2 parallels the kinetics of impact-induced depolarization. Furthermore, a spinal impact largely reduced spinal tissue oxygen to levels comparable to a strong network activation using 10 mM K^+.

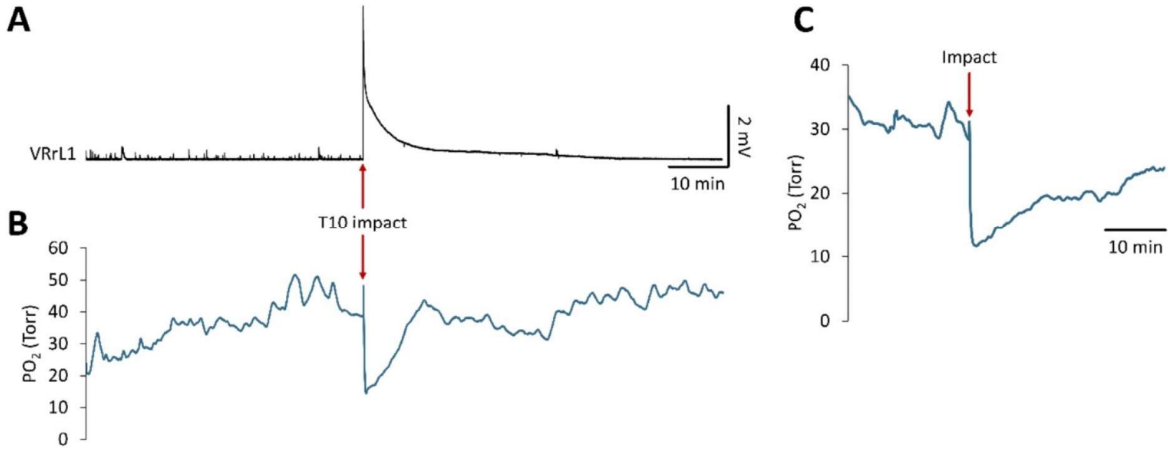

Figure 6. Impact drops oxygen tension of the spinal cord with a pattern that resembles the profile of injury-induced depolarization.
A. Continuous trace from VRrL1 with a large depolarization at the site of impact at T10 (red arrow). **B.** Simultaneous PO_2 measurements performed from the anterior funiculus between L1/L2 VRs in the same experiment as in A. PO_2 drops right after the impact, eventually recovering to baseline, mirroring the depolarization profile in A. **C.** Average spinal PO_2 profile before and after the impact (red arrow, n = 9).

Impact transiently suppresses lumbar motor reflexes.

A compression of the spinal cord is followed by a spinal shock, characterized by the suppression of motor evoked responses lasting beyond the moment of the first insult (Ditunno et al., 2004). To confirm the presence of a shock phase in our in vitro SCI model, stimuli were continuously supplied to sacrocaudal afferents (frequency = 0.1 Hz; intensity = 100 µA, 5 × Th; pulse duration = 0.1 ms) while motor reflexes were derived from VRrL5 in control and after the impact (Fig. 7 A). Firstly, the concentration of potassium was raised to 10 mM, eliciting a depolarization of 4.05 mV at steady state. At the peak of the K^+-induced depolarization, reflexes were suppressed, but recovered to baseline during the subsequent washout in normal Krebs (Fig. 7 A). After the washout, motor evoked responses appeared transiently suppressed at the peak of the impact-induced depolarization (9.69 mV) but, as the baseline repolarized, also pre-impact values fully recovered after 31.06 min from the impact (Fig. 7 A). A second exposure to high K^+ concentrations (10 mM) evoked a depolarization of 4.55 mV, which abolished motor reflexes until a normal Krebs solution was perfused and led to a full recovery of reflexes (Fig. 7 A). The profile representing

changes in the amplitude of reflex responses throughout the experiment displays a complete suppression of motor reflexes in correspondence to a spinal cord depolarization of about 4 mV, regardless of whether it was elicited by perfusing the whole preparation with high potassium ions or by applying a localized impact at T10 (red arrow, Fig. 7 B). Similar evidence was obtained from five preparations, where trains of pulses (frequency = 0.1 Hz, intensity = 1.6-6.15 Th, pulse duration = 0.1ms) applied to sacrocaudal afferents evoked spinal reflexes from VRrL5 (peak amplitude = 0.77 ± 0.2 mV). After 27.91 ± 6.06 s from the impact at T10, electrically evoked responses reappeared, and recovered to 90% of pre-impact values after 18.25 ± 12.2 minutes. In the same five preparations, the time of reappearance of the first reflex after impact was not correlated to the amplitude of the injury potential (correlation coefficient = -443, P = 0.455). Through multiple simultaneous recordings, comparable transient suppressions of DRVRPs were reported across VRs at spinal segments L1, L2, L4, L5, L6 on both sides.

In summary, in the current study, the calibrated and localized impact to the cord has always been followed by a transient suppression of evoked reflexes from spinal motor pools.

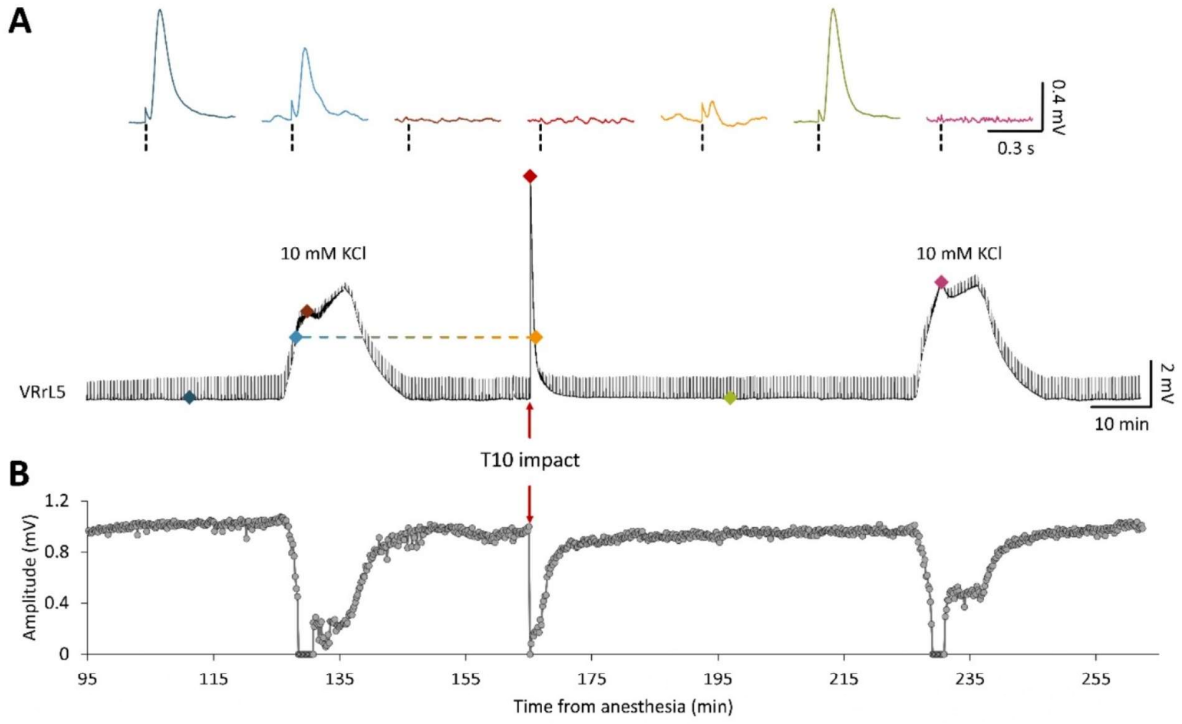

Figure 7. Motor reflexes vanish at the peak of both, chemically- and impact-induced depolarizations. **A.** A 178 min long recording from VRrL5 during the continuous delivery of electrical pulses to sacrocaudal afferents (0.1 Hz) to evoke motor responses. Motor reflexes are traced in control, during high K^+ (10 mM) perfusion, wash out, impact to T10 (red arrow) and a second K^+ application. Top inserts magnify single reflexes (dotted vertical lines correspond to artifacts of stimulation) for distinct instants of the experiment as indicated by the colored dots below. At the top of each depolarization, motor reflexes are suppressed

(brown, red and purple top traces). **B.** Time course of reflex amplitude for the trace in A demonstrates that reflexes vanish (amplitude = 0 mV) at the peak of depolarizations, regardless of whether they are elicited by the perfusion of the entire CNS with high K^+ or by a localized impact to the cord.

A thoracic impact alters electrically-induced fictive locomotor patterns.

Results collected so far indicate that, after an impact, the entire spinal cord experiences a transient large depolarization, with neuronal death only at the injury site. To explore whether the depolarization induced by the impact affects the functionality of lumbar spinal networks for locomotion, stereotyped trains of rectangular pulses (frequency = 2 Hz, intensity = 1-5 × Th, pulse duration = 0.1 ms) were applied to sacrocaudal afferents for 80 seconds. In response to stimulation, episodes of locomotor-like oscillations alternating between flexor and extensor commands, and between left and right motor pools were recorded from both VRL2 and from one VRL5, in control and at different time points after the impact (15, 60 and 120 min post-SCI). In a sample experiment, fictive locomotor patterns recorded in control from VRrL2 were characterized by a cumulative depolarization of 0.7 mV with 28 superimposed alternating cycles ($CCF_{homolateral}$ = -0.70, $CCF_{homosegmental}$ = -0.87), defined by a peak amplitude of 0.33 ± 0.08 μV and a period of 2.89 ± 0.74 s (Fig. 8 A and magnification at steady state in Fig. 8 B). In the same preparation, the impact reduced cumulative depolarization (0.5 mV, 15 min post-SCI), generating smaller (0.16 ± 0.06 μV, 15 min post-SCI) and slightly less regular locomotor-like oscillations (period CV = 0.28, 15 min post-SCI Vs. period CV in control = 0.26), regardless of their unchanged number (28, 15 min post-SCI). Although some features of fictive locomotion eventually recovered to control values, cumulative depolarization, cycle amplitude and periodicity were still reduced even after two hours from the impact (Fig. 8 A and magnified at steady state in Fig. 8 B).

Pooled data from seven experiments confirms that the impact unaltered several characteristics of fictive locomotion (Sl. Fig. 5) but did reduce cumulative depolarization (Fig. 9 A; n = 6, P = 0.002, repeated measures analysis) and amplitude of cycles from VRrL2 (Fig. 9 B; n = 6, P < 0.001, repeated measures analysis). In addition, duration of fictive locomotion episodes from VRrL2 after 60 minutes from the impact (Fig. 9 C; n = 7, P = 0.031, repeated measures analysis), and period of cycles of VRrL2 after 15 and 60 minutes from the impact, were significantly lower than in control (Fig. 9 D; n = 7, P = 0.008, repeated measures analysis). Similarly, 15- and 60-min post-impact, episodes from VRrL5 were faster than in the control group (Fig. 9 E; n = 6, P = 0.002, Friedman test), as well as more irregular at 15 minutes post-impact (Fig. 9 F; n = 7, P = 0.006, repeated measures analysis). Notably, after injury, oscillations from both extensor and flexor commands (Fig. 9 G; homolateral CCF, n = 7, P = 0.013, repeated measures analysis),

672 as well as from the left and right sides of the cord (Fig. 9 H; homosegmental CCF, n = 7, P = 0.001, repeated
673 measures analysis) exhibited poorer alternating coupling than controls.
674 In summary, a calibrated impact to the thoracic cord affects the functionality of lumbar locomotor circuits,
675 generating less coordinated locomotor-like oscillations, with shorter and faster cycles of locomotor-like
676 patterns especially from flexor motor pools.
677

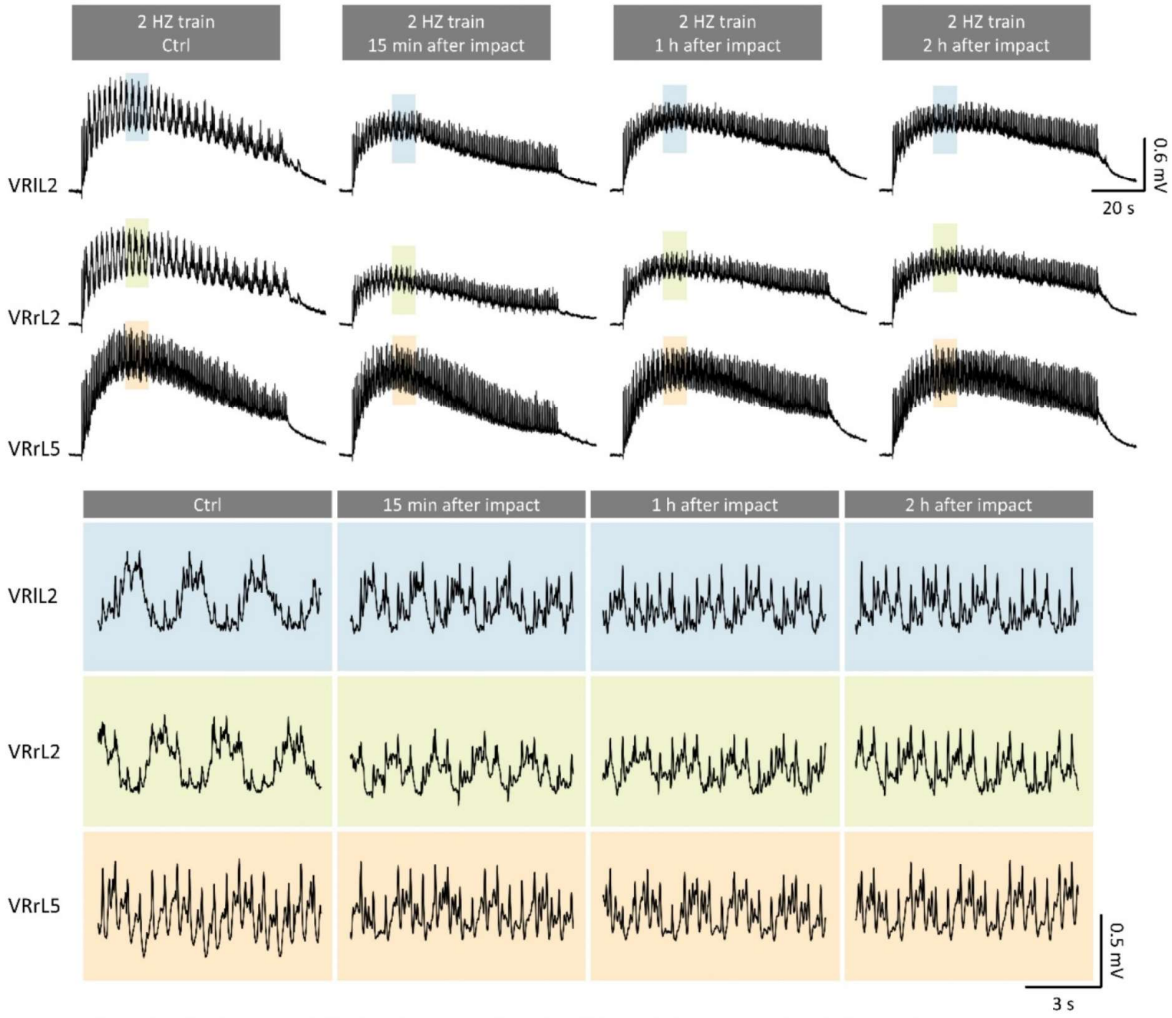

678
679 **Figure 8. Electrically-induced fictive locomotion is affected by a localized thoracic compression.**
680 **A.** Serial 2 Hz trains of stereotyped rectangular pulses (intensity = 125 µA, duration = 0.1 ms) are applied
681 to sacrocaudal afferents to evoke epochs of locomotor-like oscillations from VRIL2, VRrL2, and VRrL5.
682 Fictive locomotion patterns were recorded in control, and then 15 minutes, one hour, and two hours after
683 injury. **B.** Magnifications of simultaneous traces (blue for VRIL2, green for VRrL2, and orange for VRrL5)
684 correspond to oscillations captured at steady state in A (shaded rectangles). Note the out-of-phase cycles
685 recorded from the three VRs, with reduced amplitude and periodicity after the impact.
686

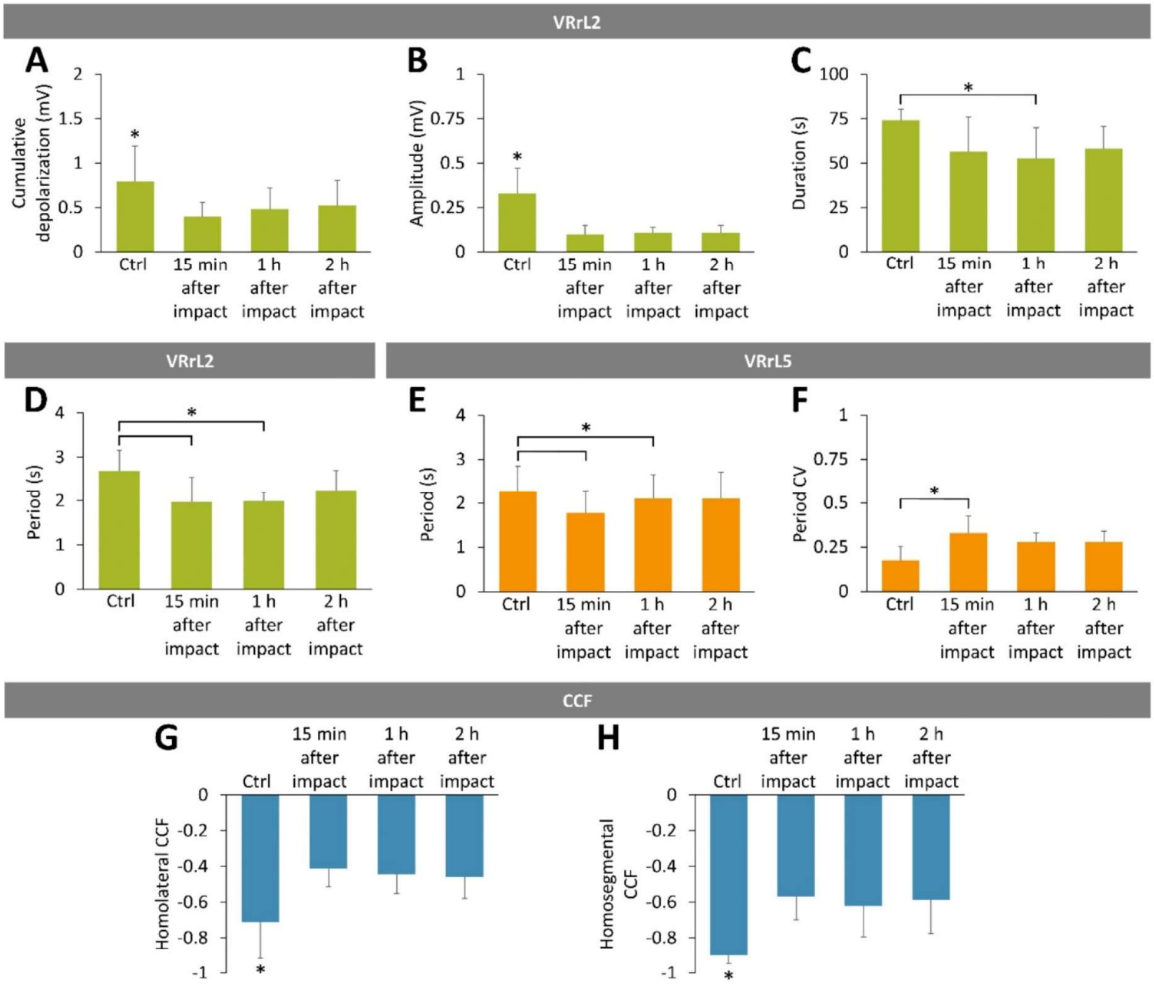

Figure 9. Impact perturbs the features of electrically-induced fictive locomotion.
A-D. Green bars describe average values for the main descriptors of fictive locomotor patterns reported from VRrL2 in control and at 15 minutes, 1 hour, and 2 hours following the injury. **A.** Cumulative depolarization significantly decreases after impact (*P = 0.002). **B.** Impact largely reduces the amplitude of oscillations (*P < 0.001). **C.** Episodes of fictive locomotion are shorter one-hour after the impact (*P = 0.031). **D.** Period of oscillations is significantly smaller 15 minutes and one-hour post-impact (*P = 0.008). **E-F.** Orange bars describe average values for the main descriptors of fictive locomotor patterns reported from VRrL5 in control and at 15 minutes, 1 hour, and 2 hours following the injury. **E**. Periods of FL oscillations 15 minutes and one hour after injury are significantly shorter than in the control group (*P = 0.002). **F.** Period CV is higher than in control only at 15-minute post-injury (*P = 0.006). **G.** Phase coupling between extensor and flexor commands (homolateral CCF, *P = 0.013) is poorer after the impact. **H.** Phase coupling between the left and right output (homosegmental CCF, *P = 0.001) reduces post injury.

Impact-induced depolarization is sustained by chloride ions.

To investigate whether ionic disbalances sustain the depolarization that follows the impact, separate experiments considered injuring the cord during perfusion with either of the three modified Krebs solutions containing low concentrations of chloride (Cl^-), calcium (Ca^{2+}), and potassium (K^+) ions,

705 respectively. Continuous recordings were performed from preparations initially perfused with normal
706 oxygenated Krebs solution, and then with one of the low-ion Krebs solutions for 30-90 min before the
707 impact and for 15 min afterwards. As soon as a single low-ion solution was applied, the DC level of the
708 baseline recorded from VRrL5 hyperpolarized and, after 18 min, reached a steady-state mean level of -
709 10.42 ± 2.23 mV for low Cl^- (n = 5), -0.49 ± 0.39 mV (n = 7) for low Ca^{2+} and -1.11 ± 0.75 mV for low K^+ (n =
710 7; Sl. Fig. 6 A).
711 Whether low-ion solutions affected spinal synaptic transmission was verified by continuously monitoring
712 the reflex responses elicited from VRrL5 in response to trains of weak electric pulses (frequency = 0.1 Hz,
713 intensity = 50-160 μA, 2-8 × Th) applied to sacrocaudal afferents. Three pairs of superimposed sample
714 traces from three preparations show that reflex amplitudes were differently affected by the transition
715 from a normal Krebs solution (blue traces) to each low-ion perfusion (green traces). In particular,
716 compared to the normal Krebs solution, the peak of responses remained unchanged when perfusing low
717 Cl^- (Fig. 10 A, left), while it reduced to 30.69 % during perfusion with low Ca^{2+} solution (Fig. 10 A, middle)
718 and augmented to 117.88 % after the transition to low K^+ (Fig. 10 A, right). Pooled data from many
719 experiments confirms that the peak of mean reflexes was unchanged by low Cl^- (n = 6, P = 0.923, paired t-
720 test), while it significantly reduced after low Ca^{2+} (n = 7, P = 0.001, paired t-test) and it increased with low
721 K^+ (n = 7, P = 0.017, paired t-test; Fig. 10 B). Conversely, latency of responses was only affected by the
722 transition to the low Cl^- solution (P = 0.001, paired t-test; Fig. 10 C, left) without any changes appearing
723 with low Ca^{2+} (P = 0.069, paired t-test, Fig. 10 C, middle) or low K^+ (P = 0.297, paired t-test; Fig. 10 C, right).
724 Impacts occurring during perfusion with low-ion solutions generated different peaks and profiles of injury-
725 induced potentials. Comparison between three mean traces recorded for up to 3.5 min after the impact
726 (red arrows) demonstrates that low Cl^- concentrations (n = 6, Fig. 10 D, left) generate higher peaks of
727 injury potentials compared to the other two modified Krebs solutions. Furthermore, despite a lower peak
728 of depolarization, low Ca^{2+} broadened the average injury potentials with the appearance of a delayed
729 component in the repolarizing phase (n = 7; Fig. 10 D, middle). Low K^+ perfusion showed a peak similar to
730 low Ca^{2+} depolarizations, but with a sharper repolarizing phase (n = 7; Fig. 10 D, right).
731 Comparison among the mean amplitude of injury potentials generated by the impact during perfusion in
732 normal Krebs (5.46 ± 3.54 mV; n = 23) and in the presence of the three low-ion solutions indicated a
733 significantly higher depolarization for impacts occurring in low Cl^- (10.56 ± 3.57 mV, P = 0.048, Kruskal-
734 Wallis test, n = 6, Fig. 10 E). Nevertheless, after impact in low Cl^-, reflex responses were suppressed with
735 a time course reminiscent of post-injury reflexes in normal Krebs solution, with a first reappearance of

responses after 20.64 ± 6.15 s from the impact and the recovery to 90% of pre-impact values after 11.08 ± 4.61 mins.

Impacts in the presence of the modified Krebs solutions revealed the distinct role of Cl^- ions in sustaining the extent of injury potentials, albeit the duration of spinal shock and the suppression of reflex responses were comparable among the different media.

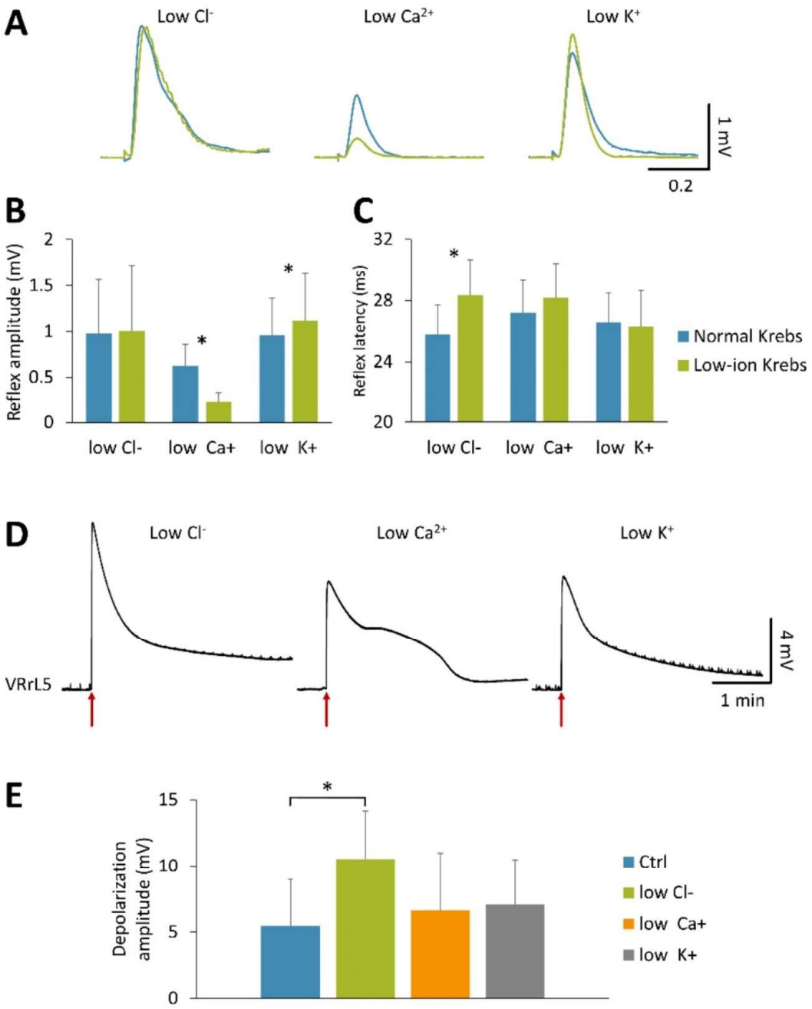

Figure 10. Low-ion solutions differently influence synaptic transmission and impact-induced depolarization.

A. Superimposed pairs of electrically-induced reflex responses representing transition from normal Krebs solution (blue traces) to modified Krebs solutions (green traces) with low Cl^- (left), low $Ca2^+$ (middle), and low K^+ (right) concentrations. **B.** Mean amplitude of reflex responses in normal Krebs (blue bars) or low-ion solutions (green bars) point out a significantly smaller peak during application of low Ca^{2+} ($P < 0.001$), and a higher amplitude after transition to low K^+ ($P = 0.017$) solutions. **C.** Mean values of latency of reflex responses in normal Krebs (blue bars) and low-ion solutions (green bars) report significantly slower responses when the low Cl^- solution is perfused ($P = 0.001$). **D.** Four-minute traces from VRrL5 related to

752 the average profiles of injury potentials during perfusion with low-ion solutions (left, low Cl^-, n = 6; middle,
753 low Ca^{2+}, n = 7; right, low K^+, n = 7). **E.** Average peak amplitude of impact-induced depolarizations during
754 perfusion in control Krebs and low-ion solutions. Low Cl^- solution augments the amplitude of
755 depolarization (*P < 0.05).
756

757 ***An impact to the spinal cord alters cortical glial.***

758 To evaluate the impact of spinal injury on brain structures, the cerebral cortex was examined at two time
759 points: the acute phase (25 minutes post-injury) and late phase (two hours post-injury). Given that the
760 experiments were conducted during the peak of astrogenesis in rats, the density of astrocytes in the
761 cerebral cortex was assessed as an indicator of the potential effects of the spinal insult. Astrocytes were
762 identified through immunostaining of cortical samples for the S100b marker, followed by counterstaining
763 with DAPI. The density of astrocytes was calculated by dividing the number of S100b-positive cells by the
764 total cell count. In the dorsomedial cortex (at the level of the primary motor area, M1, Fig. 11 A), average
765 astrocyte density was significantly reduced 25 minutes post-injury (25.85 % of sham) with a partial
766 recovery two-hours post-injury (55.78 % of sham; Fig. 11 B, D; P = 0.033, Kruskal-Wallis test, n = 3, 3, 6).
767 Contrarywise, in the ventrolateral cortex (including both primary and secondary somatosensory areas, S1
768 and S2, Fig. 11 A), astrocyte mean density was 54.35 % of sham, 25 min post-injury, and then significantly
769 decreased two-hours post-injury (50.90 % of sham; Fig. 11 C, E; P = 0.037, Kruskal-Wallis test, n = 3, 4, 7).
770 In summary, density of cortical astrocytes transiently changed, first at the level of the primary motor area
771 and subsequently in both somatosensory areas, mirroring the spreading of depolarization from the injury
772 site in the spinal cord.

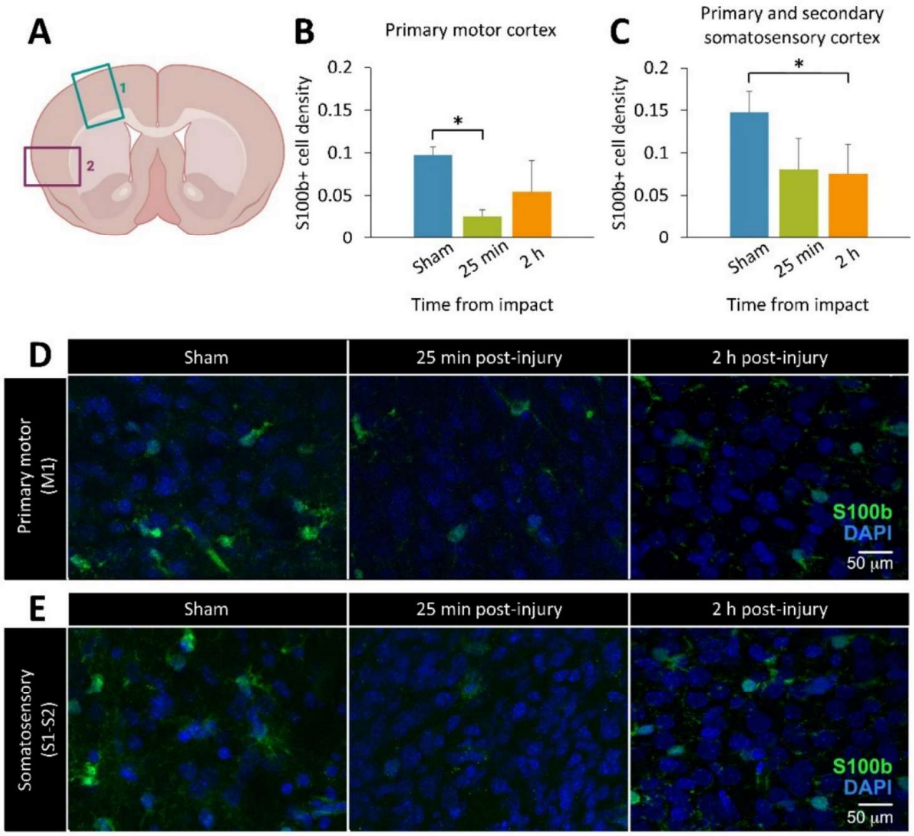

Figure 11. Remote changes in cortical glia occur after spinal damage.
A. Illustration showing a coronal section of the cerebral cortex used for analysis. Square 1 indicates the dorsomedial cortex, including the primary motor area; Square 2 indicates dorsolateral and ventrolateral cortices, including both primary and secondary somatosensory cortices. **B.** Average S100b+ cell density in the primary motor cortex, 25 minutes and 2 hours post-injury, compared to sham. **C.** Average S100b+ cell density in the primary and secondary somatosensory cortices, 25 minutes and 2 hours post-injury, compared to sham. **D.** Representative confocal images from the primary motor cortex in sham, 25 minutes and 2 hours post-injury. S100b (in green) was used to label astrocytes, DAPI (in blue) was used to counterstain total cell nuclei. Images were taken at 60X oil objective magnification. **E.** Confocal images from the somatosensory cortex at the same time points as in D.

Discussion

The current study is centered around tracing the immediate consequences of a traumatic injury to the spinal cord. For the purpose, we designed a novel experimental platform composed of a classical electrophysiological set up for multiple and simultaneous nerve recordings and stimulation, combined with an oximetric implantable probe, and associated with the invention and use of an ad hoc low-noise mini-impactor. This experimental infrastructure has been tailored to best exploit the innovative version of the whole CNS isolated from neonatal rats we recently introduced (Mohammadshirazi et al., 2023). To provide a more physiological and stable site for a traumatic impact, we adopted a more conservative

surgery that maintained dorsal vertebral laminae and DRGs mostly intact. The impactor was carefully shielded to simultaneously allow VR recordings, and was created as to allow consistent and calibrated focal impacts through a fully programmable software interface. Each impact triggered a transient and massive depolarization spreading from the injury site to the whole spinal cord, symmetrically propagating across the left and right sides of the cord, and also to the dorsal cord, although with smaller and slower potentials than the ventrally elicited ones. Several fundamental features of the pathophysiology of a severe acute SCI were reproduced in our experiments, such as: 1) an extensive neuronal loss at the site of injury, with a transient drop in tissue oxygen content; 2) a complete interruption of longitudinal input at the level of impact with a disconnection of the sublesional lumbar cord from both, descending motor commands and ascending afferent input; and 3) a momentary suppression of evoked spinal reflexes. Additionally, our setting highlighted the disappearance of the spontaneous motor activity that is characteristically recorded from the spinal VRs of preparations isolated from newborn rats, showing a drop in the excitability of sensorimotor networks, resembling the flaccid muscle tone displayed in clinics during a spinal shock.

As opposed to the massive neuronal loss at the site of injury, sublesional lumbar motor pools did not undergo any histological changes, while the functionality of locomotor networks was slightly affected, even after two hours from the impact, showing less coordinated locomotor-like cycles, especially from flexor motor pools. Interestingly, after SCI, tail flexor motoneurons underwent distinct morphological alterations, such as a reduction in soma size and an overall decrease in dendritic branching, which concur to the development of spasticity in chronically injured animals (Kitzman, 2005). These morphological changes parallel the selective expression of GABA receptor subunits for flexor, but no extensor, motoneurons in chronic paraplegic rats that with a spinal transection during the first postnatal week (Khristy et al., 2009). Similarly, in paraplegic patients, the appearance of spasms is associated with the exaggerated appearance of flexor reflexes (Hiersemenzel et al., 2000).

In our experiments, the large depolarization triggered by the trauma was further broadened by the low extracellular concentrations of calcium ions, which facilitate the extrusion of calcium from injured spinal cells. This observation confirms the well-known massive calcium release during acute SCIs (Young and Koreh, 1986). Surprisingly, we discovered a crucial role for the rapid outflow of chloride ions in sustaining injury potentials immediately after trauma, as we noticed a maximal depolarization upon increasing the driving force for chloride ions. To the best of our knowledge, this is the first time that chloride ions have been linked to the initial response triggered by a physical trauma to the spinal cord. This evidence could

be pivotal in deciphering the origin of the dysregulation of intracellular chloride concentrations that sustain spasticity in persons with chronic SCI.

A novel in vitro model to trace the immediate consequences of a physical injury to the spinal cord.

Starting from the pioneering device introduced by Allen (Allen, 1911), several variations of the original weight drop impactor have been proposed (Wrathall et al., 1985; Kwo et al., 1989) and adopted worldwide, with a standardization for adult rodents (Young and Bracken, 1992; Basso et al., 1996). These resources had a tremendous impact on current knowledge about SCI, but several features of the technique inherently move the outcomes of these experimental injuries far from a clinical scenario. First of all, ethics requires animals to be fully anesthetized, inevitably affecting the composition of spinal tissue (Salzman et al., 1993; Robba et al., 2017; Davis and Grau, 2023). Secondly, breathing chest movements and heartbeat contribute to uniquely vary inter-animal conditions at the time of injury, hence limiting the consistency of the outcome produced by any two identical injury paradigms. Furthermore, the technique only allows a dorsal injury, avoiding the challenging surgical procedures required to transiently move the trunk internal organs to have access to the ventral cord. Hence, it is impractical to replicate a ventral SCI, which is a widely spread condition in clinical epidemiology (Ahuja et al., 2017). Last but not least, currently available impactors generate mechanical interference, coming from the engine or the piston that drive the rod's vertical displacement, jeopardizing any simultaneous electrophysiological recordings close to lesion site. Our system overcomes all mentioned weaknesses, albeit limited to basic research investigations using in vitro tissue isolated from newborn rodents. Our approach is not intended to replace preclinical tests for the translation of novel treatments in clinics, but to offer an optimal complementary step to challenge innovative basic ideas to target the immediate consequences of a physical injury to the nervous tissue. Our platform is unique in tracing the events at the base of a spinal shock, a topic that has been quite forsaken among the vast SCI research. The constraint of using immature tissue, because of its optimal in vitro survival, hinders highly detailed studies on the physiopathology of adult SCIs, but opens up to the investigation of the still underexplored field of pediatric injuries (Carreon et al., 2004).

In addition, some in vitro models have been defined to explore the mechanical stimulation of the CNS, studying axonal mechanobiology and neuronal membrane deformations, using stretch forces (Aomura et al., 2016) or shear strains (LaPlaca et al., 2005; Bottlang et al., 2007) on cell cultures, and on organotypical or acute CNS slices. While these techniques trace the molecular dynamics at single cell level after mechanical forces have been applied, they cannot pair the informative content of simultaneous electrophysiological recordings. On the other hand, our calibrated microimpactor applies even sudden

and orthogonal compressive forces to the nervous tissue of an isolated preparation of the entire CNS, that maintains the multifaced composition of the distinct neural structures. Notably, the low noise design of the device and the stability of the preparation at the impact site allows continuous and stable DC recordings even at the time of impact, with no artifact that prevents signal acquisition after the impact. To the best of our knowledge, no other electrophysiological setups are currently available to record spinal potentials, apart from one attempt that provided recordings after more than four minutes from the impact and after electrodes had been replaced and repositioned, hence limiting the reliability of internal pre-injury controls (Goodman et al., 1985).

Neuronal source of injury potentials acquired in the current study.

The main concern of any well-educated electrophysiologists is the certainty of the genuine biological origin of any acquired signals, to exclude any confounding baseline drifts due to environmental interferences or electromechanical artifacts from the equipment of electrophysiological set-ups. That said, albeit the presence of injury potentials triggered by a physical impact to the cord has already been reported (Goodman et al., 1985; Wang et al., 2015), we wanted to verify the nature of the large depolarization we recorded about 200 ms after the impactor's functioning. Noteworthy, the device was carefully designed, fabricated, and tested to minimize any sources of electromagnetic emissions, which are stereotyped and instantaneous at the moment of activation.

We collected several convincing proofs about the spinal origin of the potentials we acquired after impact delivery. Namely, we observed that: 1) potentials occur with a latency of hundreds of milliseconds from both engine activation and actual physical strike to the cord; 2) while artifacts are synchronous across all recording sites, the potentials we derived from VRs own different latencies and slower potentials the farther we moved from the impact site; 3) similarly, derived potentials propagate ventro-dorsally, appearing on DRs only after homologous VRs; 4) motor reflexes are suppressed at the top of each potential, and they gradually recover during baseline repolarization, similarly to the reappearance of motor reflexes washing out from high K^+ concentrations; 5) the injury potential pairs with a reduction in tissue oxygen; 6) amplitude and profile of potentials are modulated in the presence of modified ion solutions.

Additionally, we designed several experimental protocols to confirm that the large deflection of DC level following the impact corresponds to a real neuronal potential, and it is not the mere result of either the engine interference, mechanical movements produced, or the quick displacement of the tip in the bath. Thus, tests aimed at proving that: I) when the device was activated in the bath close to the preparation,

but without touching the cord, no baseline drifts were produced; II) when serial impacts of equal severity were applied to the same site, the peaks of potentials remained stable, hence excluding any summation of artifacts; III) no potentials were recorded when the device acted on a preparation that was already maximally depolarized by high K^+ concentrations; IV) no DC deflections were recorded when the impact was inflicted to a heat-inactivated anoxic spinal cord; V) the injury-related potential was lost when a second impact was inflicted after complete disconnection of the lesion site from the recording VRs. This convincing evidence proves that potentials recorded in correspondence to the activation of the impactor are not artifacts driven by the device engine, nor by the movement of the tip in the recording chamber filled with Krebs medium. Interestingly, the novel platform we introduced allows to elicit and quantify true injury potentials, making it a reliable and consistent tool to study spinal mechanobiology in vitro.

Chloride surge after a traumatic injury to the cord: a potential link to clinical spasticity.

The insurgence of spasticity-like behaviors in SCI rodents has been convincingly attributed to a dysregulation of intracellular chloride concentrations (Boulenguez et al., 2010; Mazzone et al., 2021), with a reduced expression of the membrane carrier KCC2, which co-transports potassium and chloride outside the cell (Boulenguez et al., 2010). However, how an SCI affects chloride exchange in spinal neurons is still to be clarified. The current study suggests that a large chloride conductance sustains the early depolarization that follows a physical injury to the spinal cord. Indeed, the peak of potential was higher for impacts occurring in a low-chloride modified medium, which increases the driving force of inward chloride currents (Takahashi, 1990). We hypothesize that the immediate overflow of chloride ions triggered by a physical injury to spinal tissue sustains a surge of extracellular chloride concentrations, possibly reversing the equilibrium potential of chloride ions. Starting from this early excitatory phase, the net movement of chloride ions across the membrane of spinal neurons possibly still remains perturbed throughout the chronic phase, leading the development of spasticity. Moreover, our results show both, a stable suppression of spontaneous motor activity from VRs and a transient phase of areflexia, right after the impact, followed by a gradual recovery of reflex responses during the following repolarizing phase. However, since motor reflexes consistently reappeared after a fixed amount of time from the impact, regardless of the extent of injury-induced depolarization and of the low concentration of extracellular chloride ions, it can be assumed that reflex depression was not a mere consequence of the overflow of chloride ions triggered by the impact. Thus, network excitation due to the immediate depolarization might be contrasted in the early phases by a following large depression of network excitability that is not directly linked to the extent of the first depolarization. This network inhibition would deserve further

pharmacological investigations. Later on, network hyperexcitability prevails and thus spasticity appears. However, time constraints related to our acute in vitro model hindered the possibility to test the occurrence of any chronic spastic-like activity after injury. We are also aware that the neonatal spinal cord used in the current study still presents an immature and opposite reversed chloride gradient (Gao and Ziskind-Conhaim, 1995). This latter feature, although far from adult physiology, makes the neonatal spinal tissue much closer to the extracellular environment after SCI, where the chloride equilibrium is reverted towards that of immature tissues (Lu et al., 2008). We speculate that, albeit spasticity clinically appears only later on, after the recovery from the spinal shock, the molecular elements at the base of spasticity, such as the dysregulation of intracellular chloride concentrations, already start hundreds of milliseconds after the physical injury to the cord. This hypothesis supports the rationale for introducing immediate pharmacological (Liabeuf et al., 2017; Marcantoni et al., 2020) or electrical (Mekhael et al., 2019; Malloy and Côté, 2024) interventions to neuromodulate the shift in chloride concentrations as an early treatment to alleviate the appearance of spasticity in chronic SCIs.

Transient changes affecting the entire CNS

In the majority of our experiments, we observed that respiratory activity driven by the respiratory central pattern generator (CPG) in the brainstem was temporarily disrupted by spinal cord injury (SCI), presenting a transient pause that suggests an acute supraspinal alteration in network activity. While local effects of SCI have been thoroughly explored across various models, the broader impact on suprapontine structures, particularly within the cerebral cortex, remains less understood. Previous research has demonstrated that SCI can lead to both immediate and long-term reorganization of the cerebral cortex. For instance, an immediate functional reorganization of the primary somatosensory cortex was observed in anesthetized rats following a complete thoracic spinal cord transection (Aguilar et al., 2010). Additionally, SCI has been linked to inflammation in the brain, notably within the primary motor cortex, marked by the activation of microglia (Wu et al., 2014; Hu et al., 2022). Astrocytes can also be relevant to the effects elicited by SCI, as they play a crucial role in shaping neural circuits, including the regulation of synaptic development and function, as well as in neuroinflammatory contexts where they may exhibit both neuroprotective and neurotoxic actions. However, to the best of our knowledge, the immediate effects of SCI on cortical astroglia have not been investigated. Our research aimed to assess the immediate impact of SCI on cortical astrocytes in the primary motor cortex and the primary and secondary somatosensory areas. We observed a significant decrease in astrocyte density in the primary motor cortex during the acute phase, 25 minutes post-impact, with no significant changes detected in the late phase (two hours post-injury). Conversely, a

significant decrease in astrocyte density was noted in the primary and secondary somatosensory areas during the late phase, but not earlier. This shift from an early effect in one area to a later effect in another mirrors the changes observed in the spinal cord. Given that our experiments were conducted during the peak period of astrocyte generation in the rodent cortex (P0-P3), the observed changes in astrocyte density may reflect variations in the rate of astrocyte generation. We propose that the decrease in astrocyte density is likely attributable to a slowdown in cortical astrogenesis in response to the spinal injury, rather than a selective loss of astrocytes. This suggests a broader impact of SCI on cortical function and structure beyond the immediate site of injury.

Our findings suggest a complex relationship between SCI and cortical astrocyte responses, with significant changes in astrocyte density occurring in distinct temporal and spatial patterns across different cortical regions. These observations highlight the potential for SCI to influence cortical function and development far beyond the immediate site of injury. The decrease in astrocyte density may signify a disruption in the normal trajectory of cortical astrogenesis in response to SCI during development, potentially impacting cortical plasticity and recovery. Future studies will be necessary to elucidate the molecular mechanisms underlying these changes in astrocytes following SCI, also of different severity, in both early postnatal models and in adult models. Investigations into the specific signaling pathways involved in astrocyte responses could provide valuable insights for targeted interventions to assess astrocyte activity after SCI and hopefully to better diagnose functional recoveries. Additionally, exploring the interactions between astrocytes, other glial cells, and neurons in the context of SCI could further our understanding on the precise roles played by astrocytes in the cortical response to SCI.

References

Aguilar, J., D. Humanes-Valera, E. Alonso-Calvino, J.G. Yague, K.A. Moxon, et al. 2010. Spinal Cord Injury Immediately Changes the State of the Brain. Journal of Neuroscience 30(22): 7528–7537. doi: 10.1523/JNEUROSCI.0379-10.2010.

Ahuja, C.S., J.R. Wilson, S. Nori, M.R.N. Kotter, C. Druschel, et al. 2017. Traumatic spinal cord injury. Nat Rev Dis Primers 3(1): 17018. doi: 10.1038/nrdp.2017.18.

Allen, A.R. 1911. Surgery of experimental lesion of spinal cord equivalent to crush injury of fracture dislocation of spinal column: A preliminary report. JAMA LVII(11): 878. doi: 10.1001/jama.1911.04260090100008.

Aomura, S., H. Nakadate, Y. Kaneko, A. Nishimura, and R. Willinger. 2016. Stretch-induced functional disorder of axonal transport in the cultured rat cortex neuron. Integr Mol Med 3(3): 654–660. doi: 10.15761/IMM.1000218.

Apicella, R., and G. Taccola. 2023. Passive limb training modulates respiratory rhythmic bursts. Sci Rep 13(1): 7226. doi: 10.1038/s41598-023-34422-2.

Atkinson, P.P., and J.L.D. Atkinson. 1996. Spinal Shock. Mayo Clinic Proceedings 71(4): 384–389. doi: 10.4065/71.4.384.

Basso, D.M., M.S. Beattie, J.C. Bresnahan, D.K. Anderson, A.I. Faden, et al. 1996. MASCIS evaluation of open field locomotor scores: effects of experience and teamwork on reliability. Journal of Neurotrauma 13(7): 343–359. doi: 10.1089/neu.1996.13.343.

Bottlang, M., M.B. Sommers, T.A. Lusardi, J.J. Miesch, R.P. Simon, et al. 2007. Modeling neural injury in organotypic cultures by application of inertia-driven shear strain. Journal of Neurotrauma 24(6): 1068–1077. doi: 10.1089/neu.2006.3772.

Boulenguez, P., S. Liabeuf, R. Bos, H. Bras, C. Jean-Xavier, et al. 2010. Down-regulation of the potassium-chloride cotransporter KCC2 contributes to spasticity after spinal cord injury. Nat Med 16(3): 302–307. doi: 10.1038/nm.2107.

Carlson, S.L., M.E. Parrish, J.E. Springer, K. Doty, and L. Dossett. 1998. Acute inflammatory response in spinal cord following impact injury. Experimental Neurology 151(1): 77–88. doi: 10.1006/exnr.1998.6785.

Carreon, L.Y., S.D. Glassman, and M.J. Campbell. 2004. Pediatric spine fractures: a review of 137 hospital admissions. Journal of Spinal Disorders & Techniques 17(6): 477–482. doi: 10.1097/01.bsd.0000132290.50455.99.

Cazalets, J.-R. 2005. Metachronal propagation of motoneurone burst activation in isolated spinal cord of newborn rat: Metachronal propagation of motor bursts. The Journal of Physiology 568(2): 583–597. doi: 10.1113/jphysiol.2005.086850.

Ciani, C., G. Pistorio, M. Mearelli, and C. Falcone. 2023. Immunofluorescence protocol for localizing protein targets in brain tissue from diverse model and non-model mammals. STAR Protocols 4(3): 102482. doi: 10.1016/j.xpro.2023.102482.

Clarke, E.C., S. Cheng, and L.E. Bilston. 2009. The mechanical properties of neonatal rat spinal cord in vitro, and comparisons with adult. Journal of Biomechanics 42(10): 1397–1402. doi: 10.1016/j.jbiomech.2009.04.008.

Crawley, A.P., M.T. Jurkiewicz, A. Yim, S. Heyn, M.C. Verrier, et al. 2004. Absence of localized grey matter volume changes in the motor cortex following spinal cord injury. Brain Research 1028(1): 19–25. doi: 10.1016/j.brainres.2004.08.060.

Danneman, P.J., and T.D. Mandrell. 1997. Evaluation of five agents/methods for anesthesia of neonatal rats. Lab Anim Sci 47(4): 386–395.

Davis, J.A., and J.W. Grau. 2023. Protecting the injured central nervous system: Do anesthesia or hypothermia ameliorate secondary injury? Experimental Neurology 363: 114349. doi: 10.1016/j.expneurol.2023.114349.

1022 Del Negro, C.A., G.D. Funk, and J.L. Feldman. 2018. Breathing matters. Nat Rev Neurosci 19(6): 351–367.
1023 doi: 10.1038/s41583-018-0003-6.

1024 Ditunno, J.F., J.W. Little, A. Tessler, and A.S. Burns. 2004. Spinal shock revisited: a four-phase model.
1025 Spinal Cord 42(7): 383–395. doi: 10.1038/sj.sc.3101603.

1026 Dose, F., R. Deumens, P. Forget, and G. Taccola. 2016. Staggered multi-site low-frequency
1027 electrostimulation effectively induces locomotor patterns in the isolated rat spinal cord. Spinal
1028 Cord 54(2): 93–101. doi: 10.1038/sc.2015.106.

1029 Eleraky, M.A., N. Theodore, M. Adams, H.L. Rekate, and V.K.H. Sonntag. 2000. Pediatric cervical spine
1030 injuries: report of 102 cases and review of the literature. Journal of Neurosurgery: Spine 92(1):
1031 12–17. doi: 10.3171/spi.2000.92.1.0012.

1032 Etlin, A., D. Blivis, M. Ben-Zwi, and A. Lev-Tov. 2010. Long and short multifunicular projections of sacral
1033 neurons are activated by sensory input to produce locomotor activity in the absence of
1034 supraspinal control. Journal of Neuroscience 30(31): 10324–10336. doi:
1035 10.1523/JNEUROSCI.1208-10.2010.

1036 Feringa, E.R., and H.L. Vahlsing. 1985. Labeled corticospinal neurons one year after spinal cord
1037 transection. Neuroscience Letters 58(3): 283–286. doi: 10.1016/0304-3940(85)90067-9.

1038 Gad, P., Y. Gerasimenko, S. Zdunowski, A. Turner, D. Sayenko, et al. 2017. Weight bearing over-ground
1039 stepping in an exoskeleton with non-invasive spinal cord neuromodulation after motor complete
1040 paraplegia. Front. Neurosci. 11: 333. doi: 10.3389/fnins.2017.00333.

1041 Gao, B.X., and L. Ziskind-Conhaim. 1995. Development of glycine- and GABA-gated currents in rat spinal
1042 motoneurons. Journal of Neurophysiology 74(1): 113–121. doi: 10.1152/jn.1995.74.1.113.

1043 Geisler, F.H., W.P. Coleman, G. Grieco, and D. Poonian. 2001. Measurements and recovery patterns in a
1044 multicenter study of acute spinal cord injury. Spine 26(Supplement): S68–S86. doi:
1045 10.1097/00007632-200112151-00014.

1046 Gerasimova, E., G. Burkhanova, K. Chernova, A. Zakharov, D. Enikeev, et al. 2021.
1047 Hyperhomocysteinemia increases susceptibility to cortical spreading depression associated with
1048 photophobia, mechanical allodynia, and anxiety in rats. Behavioural Brain Research 409:
1049 113324. doi: 10.1016/j.bbr.2021.113324.

1050 Giraudin, A., M.-J. Cabirol-Pol, J. Simmers, and D. Morin. 2008. Intercostal and abdominal respiratory
1051 motoneurons in the neonatal rat spinal cord: spatiotemporal organization and responses to limb
1052 afferent stimulation. Journal of Neurophysiology 99(5): 2626–2640. doi: 10.1152/jn.01298.2007.

1053 Goodman, R.M., K. Wachs, S. Keller, and P. Black. 1985. Spontaneous spinal cord “injury potential” in the
1054 rat. Neurosurgery 17(5): 757–759. doi: 10.1227/00006123-198511000-00005.

1055 Gorji, A., P.K. Zahn, E.M. Pogatzki, and E.-J. Speckmann. 2004. Spinal and cortical spreading depression
1056 enhance spinal cord activity. Neurobiology of Disease 15(1): 70–79. doi:
1057 10.1016/j.nbd.2003.09.014.

1058 Guttmann, L. 1976. Spinal shock. Handbook of clinical neurology. North-Holland Publishing Co:
1059 Amsterdam.

1060 Hains, B.C., J.P. Klein, C.Y. Saab, M.J. Craner, J.A. Black, et al. 2003. Upregulation of Sodium Channel Na_v
1061 1.3 and Functional Involvement in Neuronal Hyperexcitability Associated with Central
1062 Neuropathic Pain after Spinal Cord Injury. J. Neurosci. 23(26): 8881–8892. doi:
1063 10.1523/JNEUROSCI.23-26-08881.2003.

1064 Hermann, D.M., G. Mies, and K.-A. Hossmann. 1999. Biochemical changes and gene expression following
1065 traumatic brain injury: Role of spreading depression. Restor Neurol Neurosci 14(2–3): 103–108.

1066 Hiersemenzel, L.-P., A. Curt, and V. Dietz. 2000. From spinal shock to spasticity: Neuronal adaptations to
1067 a spinal cord injury. Neurology 54(8): 1574–1582. doi: 10.1212/WNL.54.8.1574.

1068 Hu, X., Y. Zhang, L. Wang, J. Ding, M. Li, et al. 2022. Microglial activation in the motor cortex mediated
1069 NLRP3-related neuroinflammation and neuronal damage following spinal cord injury. Front. Cell.
1070 Neurosci. 16: 956079. doi: 10.3389/fncel.2022.956079.

1071 Khristy, W., N.J. Ali, A.B. Bravo, R. De Leon, R.R. Roy, et al. 2009. Changes in GABAA receptor subunit
1072 gamma 2 in extensor and flexor motoneurons and astrocytes after spinal cord transection and
1073 motor training. Brain Research 1273: 9–17. doi: 10.1016/j.brainres.2009.03.060.

1074 Kiehn, O. 2006. Locomotor circuits in the mammalian spinal cord. Annu Rev Neurosci 29: 279–306. doi:
1075 10.1146/annurev.neuro.29.051605.112910.

1076 Kirshblum, S., B. Snider, F. Eren, and J. Guest. 2021. Characterizing natural recovery after traumatic
1077 spinal cord injury. Journal of Neurotrauma 38(9): 1267–1284. doi: 10.1089/neu.2020.7473.

1078 Kitzman, P. 2005. Alteration in axial motoneuronal morphology in the spinal cord injured spastic rat.
1079 Experimental Neurology 192(1): 100–108. doi: 10.1016/j.expneurol.2004.10.021.

1080 Kjell, J., and L. Olson. 2016. Rat models of spinal cord injury: from pathology to potential therapies.
1081 Disease Models & Mechanisms 9(10): 1125–1137. doi: 10.1242/dmm.025833.

1082 Kwo, S., W. Young, and V. Decrescito. 1989. Spinal cord sodium, potassium, calcium, and water
1083 concentration changes in rats after graded contusion injury. Journal of Neurotrauma 6(1): 13–
1084 24. doi: 10.1089/neu.1989.6.13.

1085 LaPlaca, M.C., D.K. Cullen, J.J. McLoughlin, and R.S. Cargill. 2005. High rate shear strain of three-
1086 dimensional neural cell cultures: a new in vitro traumatic brain injury model. Journal of
1087 Biomechanics 38(5): 1093–1105. doi: 10.1016/j.jbiomech.2004.05.032.

1088 Leao, A.A.P. 1944. Spreading depression of activity in the cerebral cortex. Journal of Neurophysiology
1089 7(6): 359–390. doi: 10.1152/jn.1944.7.6.359.

1090 Leao, A.A.P. 1947. Further observations on the spreading depression of activity in the cerebral cortex.
1091 Journal of Neurophysiology 10(6): 409–414. doi: 10.1152/jn.1947.10.6.409.

1092 Li, Y., A.M. Lucas-Osma, S. Black, M.V. Bandet, M.J. Stephens, et al. 2017. Pericytes impair capillary blood
1093 flow and motor function after chronic spinal cord injury. Nat Med 23(6): 733–741. doi:
1094 10.1038/nm.4331.

1095 Liabeuf, S., L. Stuhl-Gourmand, F. Gackière, R. Mancuso, I. Sanchez Brualla, et al. 2017. Prochlorperazine
1096 increases KCC2 function and reduces spasticity after spinal cord injury. Journal of Neurotrauma
1097 34(24): 3397–3406. doi: 10.1089/neu.2017.5152.

1098 Lorach, H., A. Galvez, V. Spagnolo, F. Martel, S. Karakas, et al. 2023. Walking naturally after spinal cord
1099 injury using a brain–spine interface. Nature 618(7963): 126–133. doi: 10.1038/s41586-023-
1100 06094-5.

1101 Lu, Y., J. Zheng, L. Xiong, M. Zimmermann, and J. Yang. 2008. Spinal cord injury-induced attenuation of
1102 GABAergic inhibition in spinal dorsal horn circuits is associated with down-regulation of the
1103 chloride transporter KCC2 in rat. The Journal of Physiology 586(23): 5701–5715. doi:
1104 10.1113/jphysiol.2008.152348.

1105 Malloy, D.C., and M.-P. Côté. 2024. Multi-session transcutaneous spinal cord stimulation prevents
1106 chloride homeostasis imbalance and the development of hyperreflexia after spinal cord injury in
1107 rat. Experimental Neurology 376: 114754. doi: 10.1016/j.expneurol.2024.114754.

1108 Marcantoni, M., A. Fuchs, P. Löw, D. Bartsch, O. Kiehn, et al. 2020. Early delivery and prolonged
1109 treatment with nimodipine prevents the development of spasticity after spinal cord injury in
1110 mice. Sci. Transl. Med. 12(539): eaay0167. doi: 10.1126/scitranslmed.aay0167.

1111 Mazzone, G.L., A. Mohammadshirazi, J.B. Aquino, A. Nistri, and G. Taccola. 2021. GABAergic mechanisms
1112 can redress the tilted balance between excitation and inhibition in damaged spinal networks.
1113 Mol Neurobiol 58(8): 3769–3786. doi: 10.1007/s12035-021-02370-5.

1114 Mekhael, W., S. Begum, S. Samaddar, M. Hassan, P. Toruno, et al. 2019. Repeated anodal trans-spinal
1115 direct current stimulation results in long-term reduction of spasticity in mice with spinal cord
1116 injury. The Journal of Physiology 597(8): 2201–2223. doi: 10.1113/JP276952.

1117 Mladinic, M., A. Nistri, and G. Taccola. 2013. Acute spinal cord injury in vitro: insight into basic
1118 mechanisms. In: Aldskogius, H., editor, Animal Models of Spinal Cord Repair. Humana Press,
1119 Totowa, NJ. p. 39–62

1120 Mohammadshirazi, A., R. Apicella, B.A. Zylberberg, G.L. Mazzone, and G. Taccola. 2023. Suprapontine
1121 structures modulate brainstem and spinal networks. Cell Mol Neurobiol. doi: 10.1007/s10571-
1122 023-01321-z.

1123 Partida, E., E. Mironets, S. Hou, and V. Tom. 2016. Cardiovascular dysfunction following spinal cord
1124 injury. Neural Regen Res 11(2): 189. doi: 10.4103/1673-5374.177707.

1125 Robba, C., E. Qeva, B. Borsellino, S. Aloisio, G. Tosti, et al. 2017. Effects of propofol or sevoflurane
1126 anesthesia induction on hemodynamics in patients undergoing fiberoptic intubation for cervical
1127 spine surgery: A randomized, controlled, clinical trial. J Anaesthesiol Clin Pharmacol 33(2): 215.
1128 doi: 10.4103/0970-9185.209733.

1129 Salzman, S.K., W.A. Lee, S. Sabato, A.A. Mendez, C.A. Agresta, et al. 1993. Halothane anesthesia is
1130 neuroprotective in experimental spinal cord injury: early hemodynamic mechanisms of action.
1131 Res Commun Chem Pathol Pharmacol 80(1): 59–81.

1132 Streit, D.S., C.R. Ferreira Filho, and H. Martins-Ferreira. 1995. Spreading depression in isolated spinal
1133 cord. Journal of Neurophysiology 74(2): 888–890. doi: 10.1152/jn.1995.74.2.888.

1134 Taccola, G., P. Gad, S. Culaclii, R.M. Ichiyama, W. Liu, et al. 2020. Using EMG to deliver lumbar dynamic
1135 electrical stimulation to facilitate cortico-spinal excitability. Brain Stimulation 13(1): 20–34. doi:
1136 10.1016/j.brs.2019.09.013.

1137 Taccola, G., G. Margaryan, M. Mladinic, and A. Nistri. 2008. Kainate and metabolic perturbation
1138 mimicking spinal injury differentially contribute to early damage of locomotor networks in the in
1139 vitro neonatal rat spinal cord. Neuroscience 155(2): 538–555. doi:
1140 10.1016/j.neuroscience.2008.06.008.

1141 Taccola, G., M. Mladinic, and A. Nistri. 2010. Dynamics of early locomotor network dysfunction following
1142 a focal lesion in an *in vitro* model of spinal injury. European Journal of Neuroscience 31(1): 60–
1143 78. doi: 10.1111/j.1460-9568.2009.07040.x.

1144 Taccola, G., and A. Nistri. 2005. Characteristics of the electrical oscillations evoked by 4-aminopyridine
1145 on dorsal root fibers and their relation to fictive locomotor patterns in the rat spinal cord in
1146 vitro. Neuroscience 132(4): 1187–1197. doi: 10.1016/j.neuroscience.2005.02.012.

1147 Takahashi, T. 1990. Inward rectification in neonatal rat spinal motoneurones. The Journal of Physiology
1148 423(1): 47–62. doi: 10.1113/jphysiol.1990.sp018010.

1149 Wang, M.Y., D.J. Hoh, S.P. Leary, P. Griffith, and J.G. McComb. 2004. High Rates of Neurological
1150 Improvement Following Severe Traumatic Pediatric Spinal Cord Injury: Spine 29(13): 1493–1497.
1151 doi: 10.1097/01.BRS.0000129026.03194.0F.

1152 Wang, A.-H., G.-H. Zhang, C. Zhang, X.-L. Huo, and T. Song. 2015. Injury potentials of spinal cord in ex
1153 vivo compression injury model. IEEE, Milan. p. 4659–4662

1154 Wilson, R.J.A., T. Chersa, and P.J. Whelan. 2003. Tissue PO2 and the effects of hypoxia on the generation
1155 of locomotor-like activity in the in vitro spinal cord of the neonatal mouse. Neuroscience 117(1):
1156 183–196. doi: 10.1016/S0306-4522(02)00831-X.

1157 Wrathall, J.R., R.K. Pettegrew, and F. Harvey. 1985. Spinal cord contusion in the rat: Production of
1158 graded, reproducible, injury groups☆. Experimental Neurology 88(1): 108–122. doi:
1159 10.1016/0014-4886(85)90117-7.

1160 Wu, J., Z. Zhao, B. Sabirzhanov, B.A. Stoica, A. Kumar, et al. 2014. Spinal cord injury causes brain
1161 inflammation associated with cognitive and affective changes: role of cell cycle pathways.
1162 Journal of Neuroscience 34(33): 10989–11006. doi: 10.1523/JNEUROSCI.5110-13.2014.

1163 Young, W., and M.B. Bracken. 1992. The second national acute spinal cord injury study. J Neurotrauma 9
1164 Suppl 1: S397-405.

1165 Young, W., and I. Koreh. 1986. Potassium and calcium changes in injured spinal cords. Brain Research
1166 365(1): 42–53. doi: 10.1016/0006-8993(86)90720-1.

1167

1168

1169 **Supplementary Information**

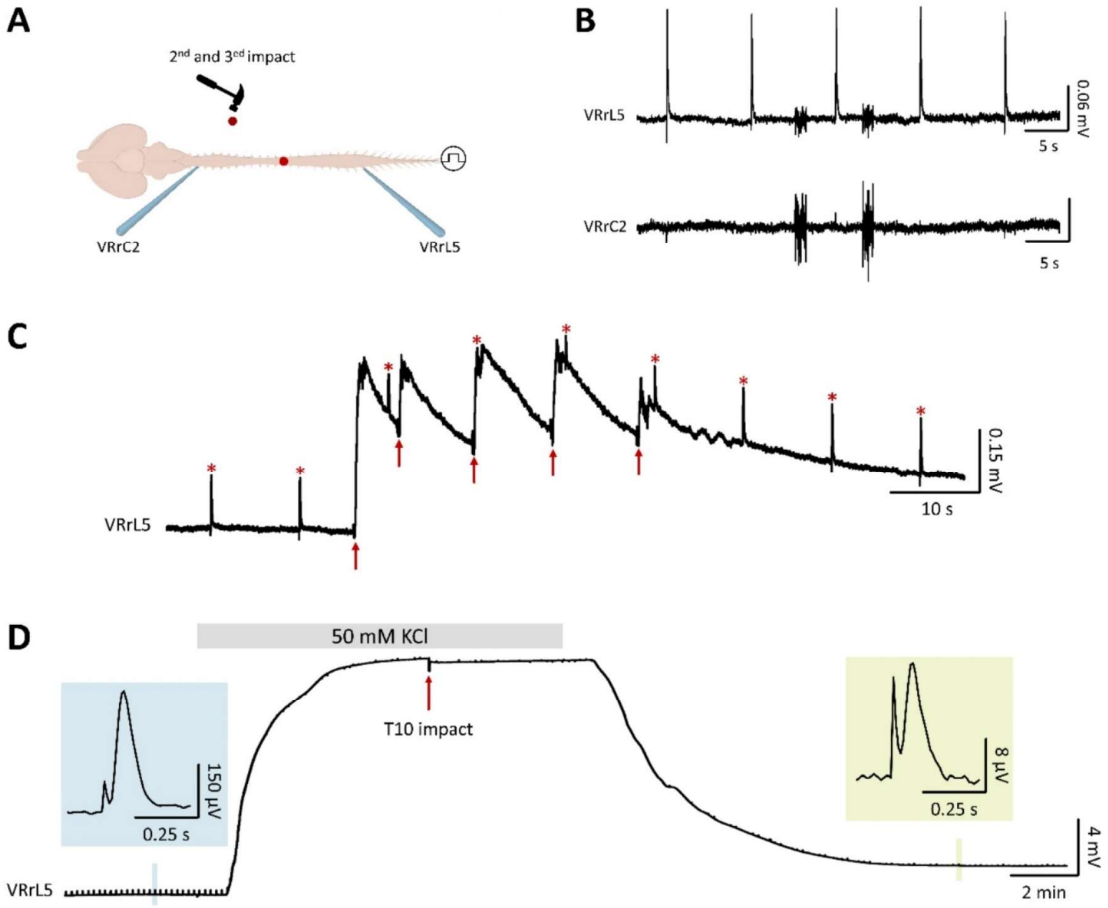

1170

1171 **Supplementary figure 1.**

1172 **A.** The cartoon describes an experiment in which, after an initial impact at T10, the tip of the impactor
1173 was lowered twice in the recording chamber far from the preparation. Simultaneous VR recordings were
1174 taken during the continuous delivery of electric pulses to sacrocaudal afferents. **B.** Two impacts delivered
1175 in the bath, away from the preparation, did not depolarize traces from VRrL5 and VRrC2, but generated
1176 brief noisier baselines. **C.** A VRrL5 recording during continuous electrical stimulation (red stars) applied to
1177 sacrocaudal afferents (0.1 Hz). Five serial impacts were applied at T10 (red arrows) showing consistent
1178 depolarization peaks. **D.** An impact (red arrows) delivered at the peak of a large depolarization elicited by
1179 50 mM KCl did not generate any injury-potential depolarizations. After 15 min from the impact in 50 mM
1180 KCl, an electrically induced reflex (pale green) reappeared, albeit 95% lower than the peak of a pre-injury
1181 control response (pale blue).

1182

1183

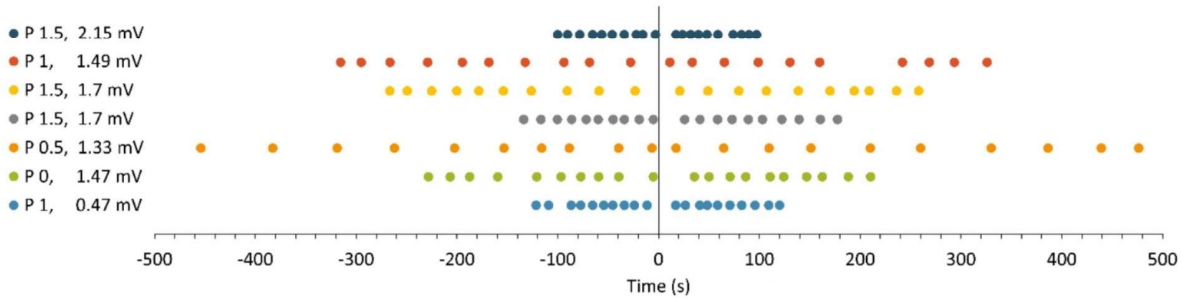

Supplementary figure 2.

Data pooled from 7 experiments display 20 respiratory events (colored dots) from VRrC2 around the impact (time = 0 s). After the impact, the first respiratory bursts were transiently paused in 4 experiments (blue, green, grey, dark blue). Age of preparations and injury potentials recorded from VRrC2 are both listed on the left side for each experiment.

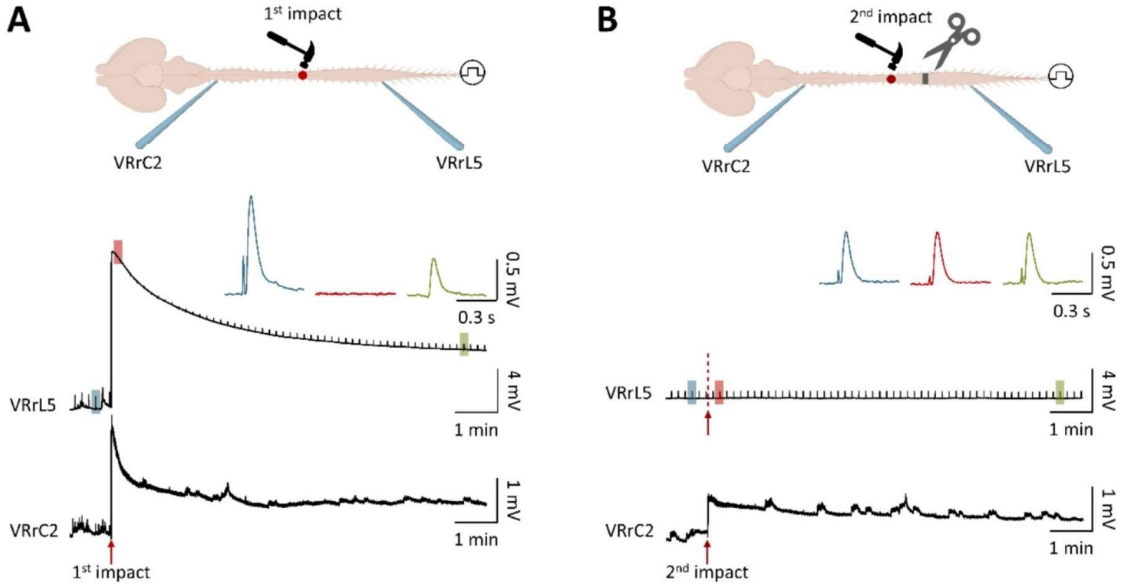

Supplementary figure 3.

A. In the cartoon, glass electrodes derive signals from VRrL5 and VRrC2 from a CNS preparation that was injured at thoracic level (red dot and hammer). Below, simultaneous traces during continuous delivery of electrical pulses to sacrocaudal afferents (0.1 Hz, intensity = 160 μA) around the impact (red arrow) show synchronous injury potentials from VRrL5 and VRrC2 with suppressed reflexes that were reversible for VRrL5 but not for VRrC2. Examples of magnified single reflex responses from VRrL5 are reported as top inserts: in control (blue trace), immediately after the impact (red trace) and after 8.2 min recovery (green trace). Normal reflexes are abolished immediately after the impact, but reappear later on. **B.** In the same preparation, a second impact to the same site, but after a complete transection at L1 spinal level (top cartoon) elicits an injury potential only from VRrC2, while reflexes from VRrL5 were unchanged by the impact to the disconnected rostral cord. Examples of magnified single reflex responses from VRrL5 show the same peak amplitude in control (blue trace), immediately after (red trace) and 8.2 min after (green trace) the impact to the disconnected rostral cord.

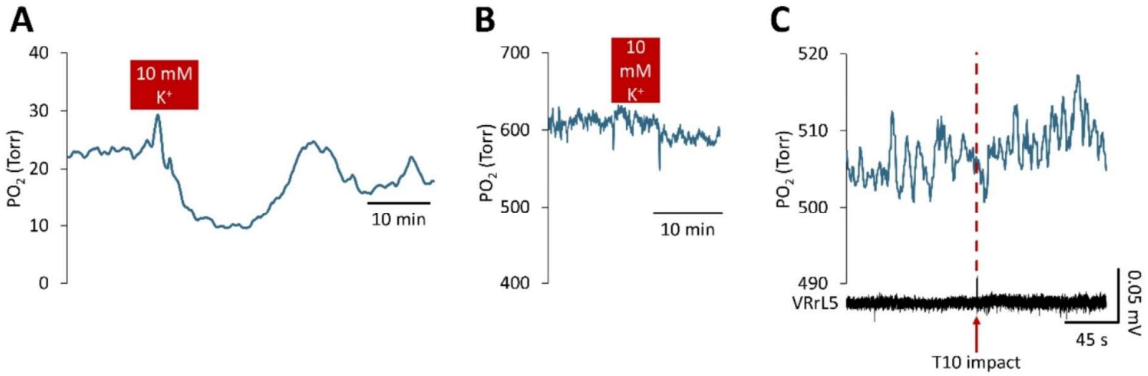

Supplementary figure 4.

A. Time course of average spinal partial pressure of oxygen (PO_2) derived at L1 spinal level (n = 8). 10 min of high K^+ (10 mM, red rectangle) transiently drops the content of tissue oxygen that later recovered. **B.** PO_2 assessment in a chamber without any preparation shows perfusion of high K^+ (10 mM, red rectangle) does not affect the microsensor probe. **C.** Simultaneous tissue oxygen values from L1 spinal level (top) and extracellular recordings from VRL5 (bottom) are taken around the impact at T10 (red dotted line) in a CNS preparation exposed to 100° C. Unchanged tissue oxygen levels and absence of injury potentials after the impact proves that the CNS preparation is not vital after heat shock.

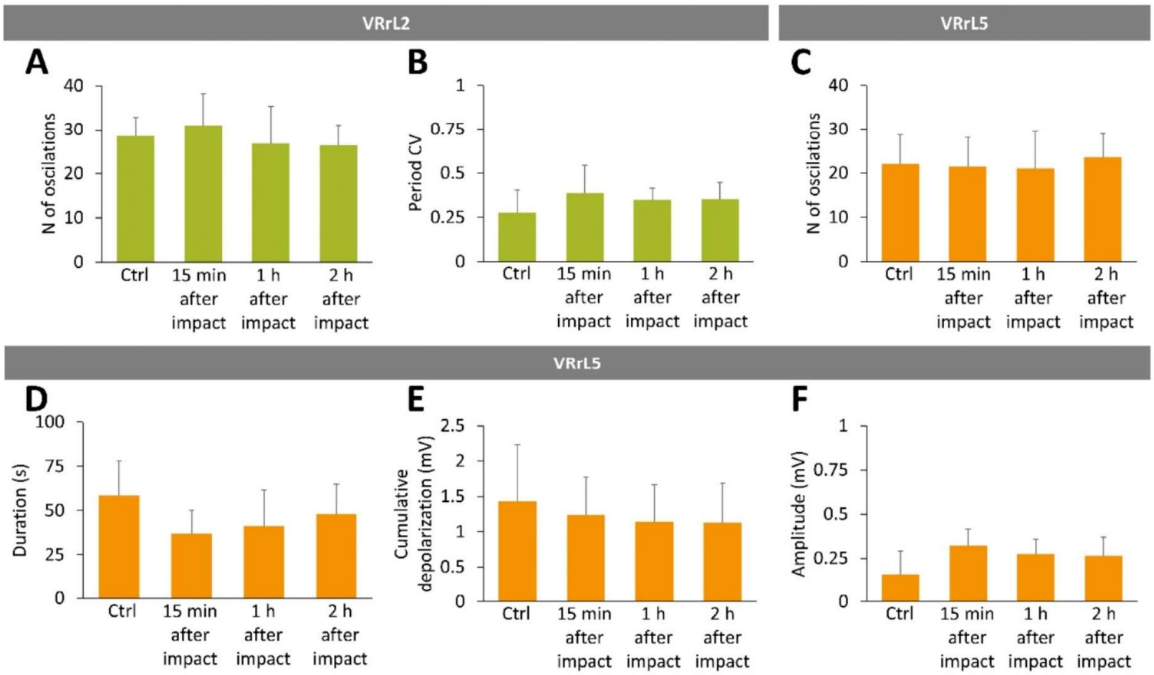

Supplementary figure 5.

A-B. Green bars describe average values for the main descriptors of fictive locomotor patterns recorded from VRrL2 in control and at 15 minutes, 1 hour, and 2 hours following injury. **A.** No changes occur in the number of oscillations. **B.** Coefficient of variation (CV) of period did not change after the impact. **C-F.**

Orange bars describe average values for the main descriptors of fictive locomotor patterns recorded from VRrL5 in control and at 15 minutes, 1 hour, and 2 hours following the injury. **C.** Number of oscillations did not vary after the impact. **D.** Duration of oscillations was unchanged post-injury. **E.** No changes occur in the values of cumulative depolarization. **F.** Amplitude of oscillations remained unvaried.

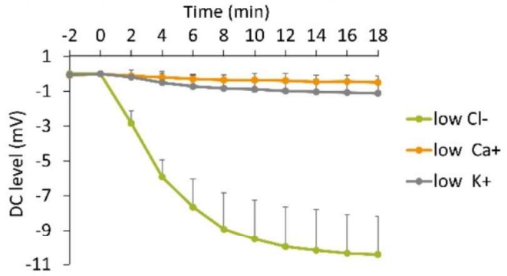

Supplementary figure 6.
The time course of the DC-level of the VRrL5 baseline during perfusion with modified Krebs solutions for low Cl^- (green), low Ca^{2+} (orange) and low K^+ (grey).

An electrophysiological study about the pharmacological manipulation of the immediate consequences of a spinal trauma reveals a crucial role for TRPV4 antagonism.

Atiyeh Mohammadshirazi[a,b], Giuliano Taccola[a,b*]

[a]Neuroscience Department, International School for Advanced Studies (SISSA), Via Bonomea 265, Trieste, Italy.

[b]Applied Neurophysiology and Neuropharmacology Lab, Istituto di Medicina Fisica e Riabilitazione (IMFR), Via Gervasutta 48, Udine, UD, Italy.

Corresponding author: Dr. Giuliano Taccola, via Bonomea 265, Trieste, (TS) Italy; taccola@sissa.it.

Authors institutional email addresses and ORCID ID numbers:

Atiyeh Mohammadshirazi:	atiyeh.mohammadshirazi@sissa.it	0000-0002-3734-4427
Giuliano Taccola:	taccola@sissa.it	0000-0003-2675-1438

Acknowledgments: GT is grateful to Mrs. Elisa Ius for her excellent assistance in preparing the manuscript and to John Fischetti for technical support in fabricating the impactor. The study was supported by intramural SISSA grants through the 5xMILLE2020 framework.

Abbreviations CNS, central nervous system; Ctrl, control; DAPI, 4', 6-diamidino-2-phenylindole; DR, dorsal root; DRG, dorsal root ganglia; L, lumbar; P, postnatal; r, right; RMS, root mean square; SCI, spinal cord injury; Th, threshold; T, thoracic; VR, ventral root.

Ethics approval: The study was performed in line with the principles of the Italian Animal Welfare Act 24/3/2014 n. 26 implementing the European Union directive on animal experimentation (2010/63/ EU).

The study complied with the ARRIVE guidelines. The animal protocol was approved by the Italian Ministry of Health with the *notifica* n. 22DAB.N.52M dated Oct 30th, 2019, and approved by SISSA ACUC (OPBA) committee (verbale n.17/3019).

Abstract

A physical trauma to the spinal cord produces an immediate massive depolarizing injury potential accompanied both by a transient episode of spinal hypoxia, and an extensive cell loss at the level of injury, which interrupts conduction of longitudinal input along white matter tracts. Afterwards, the transient hypotonia and areflexia characterize the following spinal shock phase. The relationship between the extent of injury potentials and spinal cord injury (SCI) progression, as well as the potential pharmacological modulation of the immediate consequences of a trauma, have not yet been explored. To limit the peak of injury potentials and speed up recovery of reflex motor responses, we serially applied selective neurochemicals in the exact moment of an experimental physical trauma delivered through a calibrated device impacting the mid-thoracic cord of an entire CNS preparation of neonatal rats. Continuous lumbar root recordings monitored baseline DC-levels and reflex responses elicited by trains of electric pulses applied to sacrocaudal afferents. In uninjured preparations, each agent showed distinct effects on baseline polarization, modulation of synaptic responses, and appearance of bursting activity. Interestingly, neurochemicals acting on glutamatergic-, adenosinergic-, glycinergic- or GABAergic receptors, did not affect the monitored outcome when each parameter was normalized against pre-injury values. Conversely, the selective TRPV4 antagonist, RN1734, unlike the TRPA1 antagonist, AP18, reduced peak of injury potentials and speeded up full recovery of reflex responses within 1 min from trauma. Similarly, blockage of gap junctions quickly, yet partially, restored motor reflexes, while antagonism of $GABA_A$ receptors restored full reflexes, though slightly later. The current study indicates that both mechanosensitive TRPV4 receptors and GABAergic transmission reduce the immediate pathological consequences of a trauma when applied at the moment of impact, envisaging a clinical translation for preventing accidental spinal lesions during the most delicate spinal surgeries.

Keywords: mechanoreceptors, spinal shock, motor evoked potentials, isolated central nervous system, neonatal SCI.

Introduction

We have recently described the immediate (150-200 ms) functional changes occurring when combining a physical trauma applied to the spinal cord of the entire CNS isolated from neonatal rats, with the use of an ad hoc designed micro impactor (Mohammadshirazi et al., 2023, 2024). Each impact consistently triggered an early depolarization that paralleled the injury potential reported in preclinical studies, with an amplitude that was proportional to the strike intensity and modulated by varying extracellular ion concentrations. At injury level, extensive cellular loss and disconnection of input along the spinal cord parallel a severe clinical spinal cord injury (SCI). Moreover, hypotonia and areflexia that characterize clinical spinal shocks were mimicked in vitro by the suppression of spontaneous motor activity from all VRs and by the transient failure of afferent pulses, which reflect the impairment of spinal synaptic transmission.

In the present study, we explored the possibility to limit the extent of depolarization after injury, promptly restore reflexes and protect neuronal networks, through the pharmacological manipulation of membrane receptors mediating fast ionic currents in the spinal cord. Besides the multiple neurotransmitter systems investigated so far to reactivate sensory motor networks after injury (Musienko et al., 2011), neurochemicals acting on ionotropic receptors implicated in the pathophysiology of acute SCIs, might represent an optimal target to limit the sudden depolarization following an impact to the spinal cord. In particular, since low extracellular concentrations of chloride ions reduce the peak of injury potentials (Mohammadshirazi et al., 2024), chloride-mediated fast inhibitory neurotransmission can be exploited by acting on both, glycine and $GABA_A$ receptors. Furthermore, a massive surge of glutamate has been reported as an early consequence of a SCI (Liu et al., 1991; McAdoo et al., 1999, 2000; Xu, 2004), suggesting to reduce the early functional changes induced by the trauma by blocking ionotropic glutamate receptors already during the impact, using APV and CNQX, which mostly suppress spinal synaptic transmission (Mayer and Westbrook, 1987; Bracci et al., 1996a). However, apart from ionotropic receptors, the wave of ions sustaining tissue depolarization could also spread along the cord through gap junctions. Gap junctions have been linked to axonal dysfunctions after SCI, as their blockage through carbenoxolone limited the loss of impulse conduction (Goncharenko et al., 2014).

Micro dialysis sampling at injury level also highlighted the acute release of adenosine (McAdoo et al., 2000), suggesting to limit the first consequences of a trauma by applying either adenosine, or the broad antagonist of adenosine receptors, caffeine, or more selectively, the A1 receptor blocker, DPCPX, which has been reported to modulate sensorimotor networks in the spinal cord (McAdoo et al., 2000; Taccola et al., 2020).

Due to stretch forces produced on the membrane of spinal neurons at the injury epicenter, mechanoreceptors might also be involved in the trauma. Mechanosensitive neurons express a broad class of mechanically gated ion channels, which are activated by sheer forces applied to close-by membranes and are coupled to cations currents (Garcia-Elias et al., 2014). However, although described in the spinal cord of lampreys (Grillner et al., 1982) and lizards (Alibardi, 2019), only few evidence exists about the presence of functional mechanoreceptors in the ventral spinal cord of mammals.

Among the four superfamilies of mechanoreceptors (Valle et al., 2012), the TRP family includes the transient receptor potential, vanilloid 4 (TRPV4). TRPV4 is a calcium-permeable non-selective cation channel expressed by astrocytes and neurons, and is widespread in the central nervous system (CNS), including the spinal cord, although at lower levels (Kumar et al., 2020). Once activated, TRPV4 depolarizes cell membrane, but also modulates ligand-gated chloride channels, such as $GABA_A$ receptors and strychnine-sensitive GlyR (Qi et al., 2018). TRPV4 channels are activated by a wide range of stimuli, as they are osmoreceptors sensing mechanical stimulation due to cell swelling, but also thermosensors for warm temperatures above 27° C (Kumar and Han, 2022). Impacts to the spinal cord increase the expression of TRPV4 during the early inflammatory phase of an SCI, proportionately to the severity of trauma (Kumar et al., 2020; Kumar and Han, 2022). Genetic suppression of TRPV4 or intraperitoneal administration of the selective pharmacological TRPV4 antagonist 1 h after SCI, enhanced neuroprotection against SCI-induced endothelial damage with preserved blood-spinal cord barrier integrity, attenuated neuroinflammation, and reduced glial scarring at the epicenter of injury, with some motor recovery in hindlimbs (Kumar et al., 2020).

Our hypothesis is that mechanoreceptors are immediately activated by an impact and, even before the opening of the ionotropic receptors considered herein, they could be responsible for the extracellular ion imbalance that sustains both injury potentials and transient reflex suppression during spinal shock. To this aim, in the present study, spinal impacts of equal severity were singularly performed on different preparations. Each preparation was then perfused with a single neuroactive drug before the impact and for the following recovery phase. Amplitude and latency of injury potentials and time-courses of recovery of spinal reflexes were compared to untreated injured cords. Surprisingly, glutamatergic-, adenosinergic-, glycinergic- or GABAergic receptors, were not implicated in sustaining the peak of injury potentials that follow a physical trauma to the spinal cord. However, the selective TRPV4 antagonist, RN1734, but not so the TRPA1 antagonist, AP18, limited the insurgence of the immediate consequences of the impact when applied at the moment of compression. Moreover, blockage of gap junctions speeded up the partial recovery of reflex responses, while the antagonism of $GABA_A$ receptors fully restored reflexes, though

slightly later. This evidence shows the crucial roles played by mechanosensitive TRPV4 receptors, as well as by GABAergic transmission, in the pathophysiology of an acute spinal trauma, suggesting potential implications for a clinical translation aimed at limiting accidental damages to the cord during the most delicate spinal surgeries.

Methods

To explore the pharmachological modulation of the immediate consequences of a traumatic injury to spinal cord, we adopted the in vitro preparation of the entire CNS isolated from neonatal rats (Mohammadshirazi et al., 2023; Apicella and Taccola, 2023) with intact dorsal laminae (Mohammadshirazi et al., 2024). Continuous nerve recordings were performed from VRrL5, while sacrocaudal afferents were electrically stimulated at low frequency throughout the experiment (Fig. 1A). A calibrated severe impact was provided to the ventral side of the tenth segment of the thoracic spinal cord (T10).

In vitro preparation of the isolated entire CNS

All procedures were approved by the International School for Advanced Studies (SISSA) ethics committee and are in accordance with the guidelines of the National Institutes of Health (NIH) and the Italian Animal Welfare Act 24/3/2014 n. 26, implementing the European Union directive on animal experimentation (2010/63/EU). Every measure was taken to minimize the number of animals used and to ensure their welfare.

In vitro preparations of the entire isolated central nervous system (CNS; Mohammadshirazi et al., 2023; Apicella and Taccola, 2023) coming from 94 postnatal (P0 - P2.5) Wistar rats were utilized in this study. Following cryoanesthesia (Phifer and Terry, 1986; Danneman and Mandrell, 1997; Goldberg, 2015) and the disappearance of the paw pinch reflex, quick surgical procedures were performed including removal of: forehead at orbital line, rib cage, internal organs, and forelimbs. Dissection continued under the microscope in a petri dish filled with an oxygenated Krebs solution that contained (in mM): 113 NaCl, 4.5 KCl, 1 $MgCl_2 7H_2O$, 2 $CaCl_2$, 1 NaH_2PO_4, 25 $NaHCO_3$, and 30 glucose, gassed with 95% O_2 - 5% CO_2, pH 7.4, 299.62 ± 3.2 mOsm/kg. Craniotomy and ventral laminectomy were then performed, keeping dorsal vertebra and dorsal root ganglia (DRG) intact (Mohammadshirazi et al., 2024), and the preparation was maintained in the oxygenated Krebs solution at room temperature for 15 minutes and thus transferred to the recording chamber with perfusing oxygenated Krebs solution (7 mL/min) and controlled temperature

of 25-27° C (TC-324C Warner Instruments, USA). For electrophysiological recordings, the preparation was fixed ventral side up and selected VRs were detached from DRGs.

Extracellular recordings

Monopolar suction electrodes were created by pulling tight-fitting glass pipettes (1.5 mm outer diameter, 0.225 mm wall thickness; Hilgenberg, Germany) and used to obtain DC-coupled recordings from VRrL5. Electrodes were connected to a differential amplifier (DP-304, Warner Instruments, Hamden, CT, USA) and signals were acquired with X 1000 gain, 0.1 Hz high-pass and 10 kHz low-pass filter. After noise elimination of analog signals (D400, Digitimer Ltd, UK), traces were digitized with a sampling rate of 5 kHz and low-pass filtrated at 10 Hz (Digidata 1440, Molecular Devices Corporation, Downingtown, PA, USA; digital Bessel) and visualized real-time (software Clampex 10.7, Molecular Devices Corporation, Downingtown, PA, USA).

Electrical Stimulation

A programmable stimulator (STG4002, Multichannel System, Reutlingen, Germany) and bipolar glass suction electrodes connected to two paired silver wires (500-300 µm) were utilized to produce electrical stimulations. Trains of rectangular electrical pulses of 40-160 µA intensity, 0.1 ms pulse duration, and 0.1 Hz frequency were supplied to the *cauda equina* (Etlin et al., 2010). Stimulus intensity was imputed as times to threshold (Th), which is defined as the lowest intensity required to elicit a slight deflection of VRrL5 baseline.

Spinal cord injury

A custom-made and shielded micro-impactor device was used to provide a traumatic damage to the spinal cord of the entire CNS in vitro (Mohammadshirazi et al., 2024).

A calibrated impact was applied to the ventral surface of thoracic 10 (T10) while electrophysiological recordings were simultaneously performed. A dedicated software controlled the vertical movement of the impactor tip (diameter = 2 mm). To provide a severe damage to the spinal cord, the impactor tip descended quickly (time = 650 ms) into the cord by 2656 µm from the spinal surface (speed = 4 mm/s, acceleration and deceleration = 6.1 ± 0.05 mm/s) and promptly returned to the original position with the same acceleration and deceleration speed.

Pharmacology

Based on their solubility product constant (Ksp), powders of pharmacological agents were dissolved in proper solvent to make concentrated stocks that were then serially diluted in oxygenated Krebs solution to reach the final concentration. All pharmacological agents were perfused into the recording chamber while the impact was being performed on the spinal cord. Concentration and time of application are mentioned in Table 1. All chemicals were provided by Sigma-Aldrich (Merk Life Science S.r.l., Italy).

Table 1. Pharmacological agents applied in the study, final concentration, type of solvent, and time of perfusion.

Agents	Concentration (µM)	Solvent	Time of application before impact (min)	Time of application after impact (min)
DL-2-amino-5- phosphonopentanoic acid (APV)	100	Water	20	5
6-Cyano-7-nitroquinoxaline-2,3-dione disodium salt hydrate (CNQX)	20	DMSO	20	5
carbenoxolone disodium (CBX)	100	Water	50	5
adenosine (ADO)	1000	Krebs	5	15
caffeine	300	Water	15	5
8-cyclopentyl-1,3-dipropylxanthine (DPCPX)	5	Sodium hydroxide	5	5
AP-18	20, 50, 66	DMSO	15	5
RN-1734	10, 20, 50, 100	DMSO	15	5
glycine (Gly)	500	Krebs	20	5
1(S),9(R)-(−)-bicuculline methiodide (bic)	20	Water	20	10
strychnine (str)	1	Water	20	10

Data and statistical analysis

Data analysis was pursued using Clampfit 10.7 software (Molecular Devices Corporation, PA, USA), and statistical analysis was performed with GraphPad InStat 3.10 (Inc., San Diego, California, USA). The number of animals is indicated as "n", and data is denoted as mean ± standard deviation (SD). The latency is defined as the time spanning from either, the electrical stimulation or the mechanical artifact, to the onset

of increased DC level. Time to peak refers to the temporal delay from the artifact of stimulation to the peak of the subsequent evoked response. Power spectrum analysis was done to generate a frequency domain representation, revealing the power levels of different frequency components in the signal. Bursting activity was quantified in terms of power spectrum magnitude, expressed as Root Mean Square (RMS; Deumens et al., 2013) and measured with Clampex 10.7 (Molecular Devices Corporation, Downingtown, PA, USA). This statistical tool quantifies any increase in frequency and/or amplitude of rhythmic activity, defined as a complex rhythm composed of multiple harmonics. Prior to any other statistical tests, a normality test was performed. Parametric paired student t-test or non-parametric Wilcoxon matched-pairs test, or Kruskal-Wallis test following Dunn's multiple comparisons to control data were utilized. Differences with a P value ≤ 0.05 are considered significant.

Results

A traumatic injury to the spinal cord generates a large, transient injury potential.

In an exemplar experiment, the impact caused a depolarization that started after only 186.44 ms, peaked at 7.14 mV after 5.42 s from the impact (Fig. 1B, C), and recovered within approximately 25 minutes. In 12 preparations, the same traumatic injury generated a sudden potential with a latency of 188.62 ± 8.70 ms that reached a maximal mean amplitude of 5.50 ± 2.84 mV, and recovered to baseline in 11.99 ± 8.93 min.

A reference of the extent of depolarization that corresponds to a massive recruitment of motor pools in control was calculated for each animal. A ten-minute perfusion with a high K^+ physiological solution (10 mM) depolarized VRs by 2.57 ± 1.09 mV (n = 12). In the same experiments, the mean amplitude of the depolarization induced by injury in physiological solution was more than double (226.79 ± 121.63 %, n = 12) than the one elicited by high potassium.

In a sample experiment, a train of electrical pulses (0.1 ms pulse duration, 0.1 Hz frequency, 160 µA intensity) was continuously applied to sacrocaudal afferents (Fig. 1B) and induced, in control, a motor reflex response of 0.49 mV amplitude, which diminished at the peak of the potassium-induced depolarization (29.92 % of control) with a full recovery (101.12 % of control) in 2.70 min after injury. Contrarywise, motor reflex responses totally disappeared at the peak of the injury-induced potential, with a substantial recovery (80.79 % of control; Fig. 1B) after 36.33 min from injury. Notewhorty, recovery of evoked responses after both, chemically and mechanically induced depolarizations, confirms that neither a perfusion with 10 mM KCl nor a severe impact at T10 reduced functionality of lumbar motor pools (Fig 1B). In 6 experiments, trains of stimuli (60 - 160 µA intensity) evoked mean motor reflex responses of 0.82 ± 0.25 mV amplitude in control, which were largely reduced at the peak of the potassium-induced depolarization (0.21 ± 0.19 mV) with a full recovery (96.86 ± 2.86 %) after 7.76 ± 3.68 min of washing. Moreover, mean reflexes were completely suppressed at the peak of the injury-induced potential, with a substantial recovery to baseline values after 18.49 ± 10.21 min from injury (n = 6).

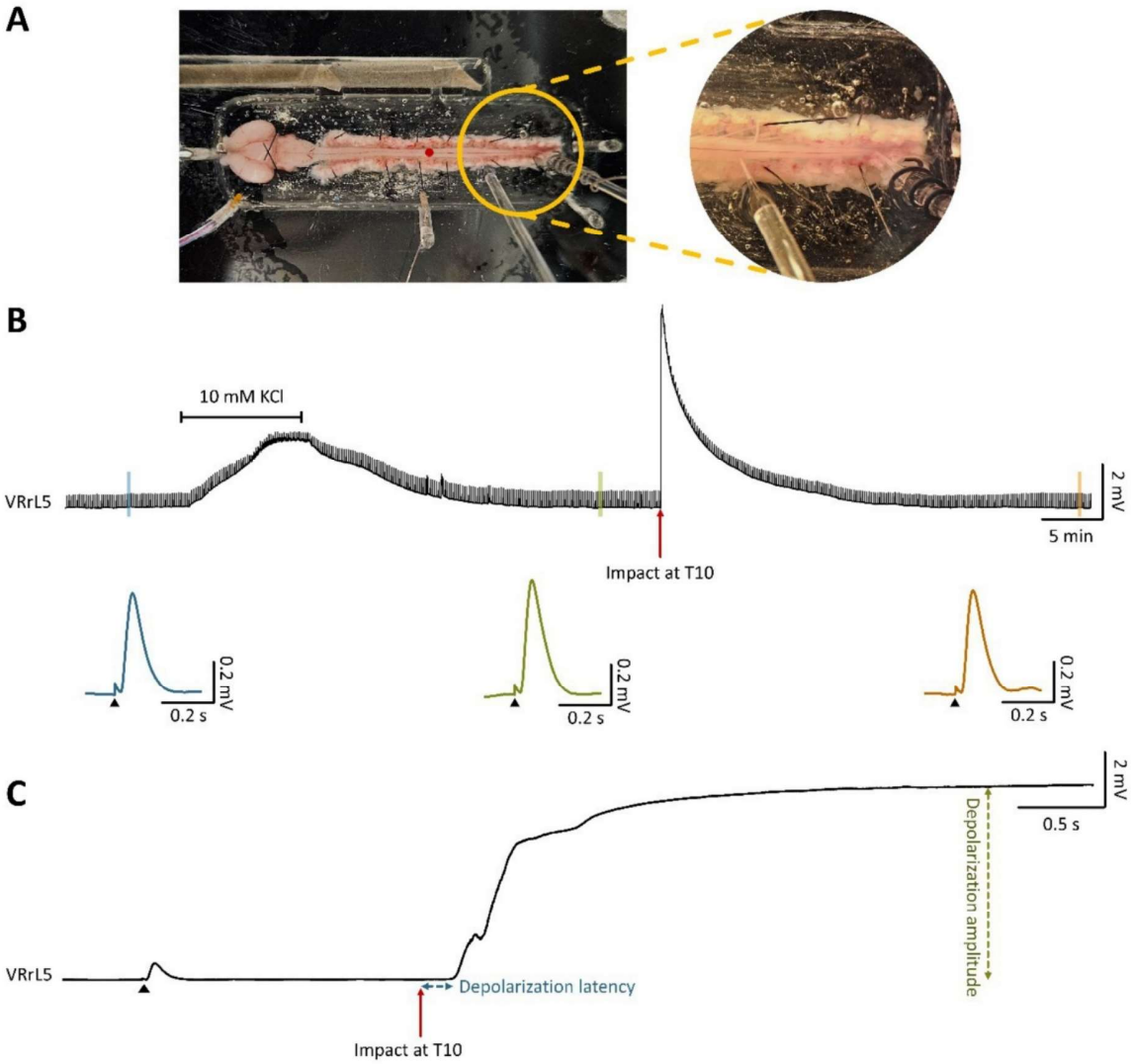

Figure 1. Transient depolarization induced by a physical injury to the spinal cord in an in vitro CNS preparation.

A. A picture of the electrophysiological setup for in vitro preparations of the entire CNS with intact dorsal aspects of vertebrae. Throughout the experiment, continuous recordings were derived from VRrL5, as electrical stimulation was applied to sacrocaudal afferents every 10 seconds. Physical impact was performed at T10 (red dot). **B.** A long continuous recording from VRrL5, while the cord was impacted at T10 (red arrow). Ten minutes perfusion with 10 mM KCl represent an internal control to quantify the high recruitment of motor pools. Below, three examples of electrically induced reflex responses are magnified before (blue) and after (green) KCl application, and once recovered from impact-induced depolarization (orange). **C.** A magnified 6-second trace extracted from B, highlights the instants around the impact and defines latency (blue dotted arrow) and amplitude (green dotted arrow) of impact-induced depolarization.

Effects of traumatic injury over baseline activity and electrically evoked responses

To modulate the extent of depolarization and the suppression of reflex responses after injury, in separate experiments, selected neurochemicals were perfused (Table 1) and their effects on baseline activity was explored before injury. Antagonism of inotropic glutamate receptors, using APV (100 µM) + CNQX (20 µM), slightly polarized DC level, reaching a peak of 0.29 ± 0.10 mV (n = 5) after 7.45 ± 2.20 min perfusion and remaining stable thereafter. With APV + CNQX, reflex responses gradually decreased, reaching 20 % of their original value in amplitude within 5.39 ± 1.25 minutes, and completely disappeared after 8.31 ± 1.77 minutes (n = 5). Adenosine (1 mM) polarized baseline by 0.34 ± 0.12 mV after 4.21 ± 0.59 minutes (n = 6), but also reduced and delayed reflex responses (Table 2, amplitude: P = 0.003, time to peak: P = 0.041, paired t-test). Caffeine (300 µM), a non-specific adenosine receptor antagonist, did not affect DC levels, but increased the latency of reflex responses (Table 2, P = 0.039, paired t-test). Following glycine (500 µM) application, a small depolarization of 1.70 ± 0.66 mV (n = 6) occurred within 2.31 ± 0.42 minutes. Within 6.06 ± 2.46 minutes, a spontaneous repolarization occurred, settling the baseline at 0.88 ± 0.33 mV above the original DC level, while amplitude of reflex responses decreased significantly (Table 2, P < 0.001, paired t-test). Application of the $GABA_A$ receptor antagonist, bicuculline (20 µM), depolarized baseline by 2.60 ± 0.75 mV within 4.02 ± 0.49 min (n = 4), which repolarized to baseline (0.16 ± 0.17 mV) after 7.16 ± 1.83 min of continuous application of bicuculline, accompanied by rhythmic bursting (Bracci et al., 1997). Spectral analysis was performed on 5-minute segments of traces recorded in bicuculline at steady-state. Resulting mean RMS value was 8.68 times greater than the RMS calculated from baseline spontaneous activity in control, mirroring the appearance of a rhythmic activity (from 0.10 ± 0.05 in control, to 0.83 ± 0.38 during bicuculline; P < 0.001, paired t-test, n = 11). Also, application of the glycinergic receptor antagonist, strychnine (str, 1 µM), induced bursting activity (Bracci et al., 1996b) with a mean RMS value 2.58 times higher than the one calculated for baseline spontaneous activity in control before str application (from 0.13 ± 0.09 to 0.34 ± 0.2; P = 0.031, paired t-test, n = 5). Finally, when bicuculline (20 µM) and strychnine (1 µM) were co-applied, baseline depolarized on average by 2.97 ± 0.99 mV within 4.11 ± 0.84 minutes from application of drugs and then spontaneously ripolarized to original baseline values within 6.22 ± 0.91 minutes of continuous application of bic + str (n = 12). Appearance of disinhibited bursting (Bracci et al., 1997) corresponds to an 8.46 fold increase in mean RMS compared to pre-drug applications (from 0.12 ± 0.15 mV in control to 1.03 ± 0.27 mV in str + bic; P < 0.001, paired t-test, n = 7). Application of the gap junction blocker, carbenoxolone (CBX, 100 µM), the selective antagonist for adenosine A1 receptors, DPCPX (5 µM), the TRPA1 channel blocker, AP-18 (20, 50, 66 µM), or the TRPV4 channel antagonist, RN1734 (10, 20, 50, 100 µM), did not significantly alter DC levels nor reflex responses.

Detailed changes in reflex amplitude, as well as time to peak values and associated statistical analyses, are provided in Table 2.

Table 2. Amplitude and time to peak of reflex responses, with statistical comparisons before and after the application of each pharmacological agent.

Agents	n	Reflex parameter	Before application	After affection of the drug	Test	P value
CBX	5	Amplitude (mv)	0.33 ± 19	0.28 ± 0.16	paired t-test	0.180
	7	Time to peak (ms)	75.82 ± 6.63	78.07 ± 4.50	paired t-test	0.281
ADO	6	Amplitude (mv)	1.11 ± 0.46	0.55 ± 0.26	paired t-test	0.003
	6	Time to peak (ms)	75.67 ± 5.41	71.62 ± 3.58	paired t-test	0.041
caffeine	5	Amplitude (mv)	0.85 ± 0.47	0.80 ± 0.51	Wilcoxon matched-pairs test	0.313
	5	Time to peak (ms)	77.06 ± 5.13	80.05 ± 5.10	paired t-test	0.039
DPCPX	5	Amplitude (mv)	0.40 ± 0.13	0.78 ± 0.68	Wilcoxon matched-pairs test	0.813
	5	Time to peak (ms)	78.36 ± 4.81	78.17 ± 5.80	paired t-test	0.800
RN1734	4	Amplitude (mv)	0.42 ± 0.23	0.34 ± 0.21	Wilcoxon matched-pairs test	0.25
	4	Time to peak (ms)	79.83 ± 4.05	86.68 ± 6.12	Wilcoxon matched-pairs test	0.125
Gly	6	Amplitude (mv)	0.62 ± 0.22	0.38 ± 0.18	paired t-test	0.0003
	6	Time to peak (ms)	80.93 ± 3.93	79.3 ± 2.32	paired t-test	0.119
str	5	Amplitude (mv)	0.60 ± 0.17	0.90 ± 0.35	Wilcoxon matched-pairs test	0.125
	5	Time to peak (ms)	76.12 ± 6.66	82.57 ± 7.78	paired t-test	0.101

Pharmacological manipulation of the peak of injury potentials.

All pharmachological agents used have been applied in the recording bath in the exact moment when physical injury was produced to the thoracic segment (T10) of the spinal cord. Concentrations, as well as timing of application, were defined as time values before and after the impact (Table 1). DC level of baseline was continuously recorded from VRrL5. The peak of injury-induced depolarization was normalized to that previously elicited by the application of a high potassium medium (10 mM) in the same experiments (Fig. 2A). Among all drugs tested, only RN1734 at concentrations greater than 50 µM significantly reduced, on average, the normalized amplitude of injury potentials by 35.25 % compared to control untreated preparations (P = 0.034, Kruskal-Wallis Test followed by Dunn's Multiple Comparisons Test; Fig. 2B). However, no significant differences were observed in the onset of injury potentials in response to the application of any of the drugs tested (P = 0.522, Kruskal-Wallis Test followed by Dunn's Multiple Comparisons Test). In summary, impact-induced depolarization was smaller when RN1734 was perfused to the preparation during impact.

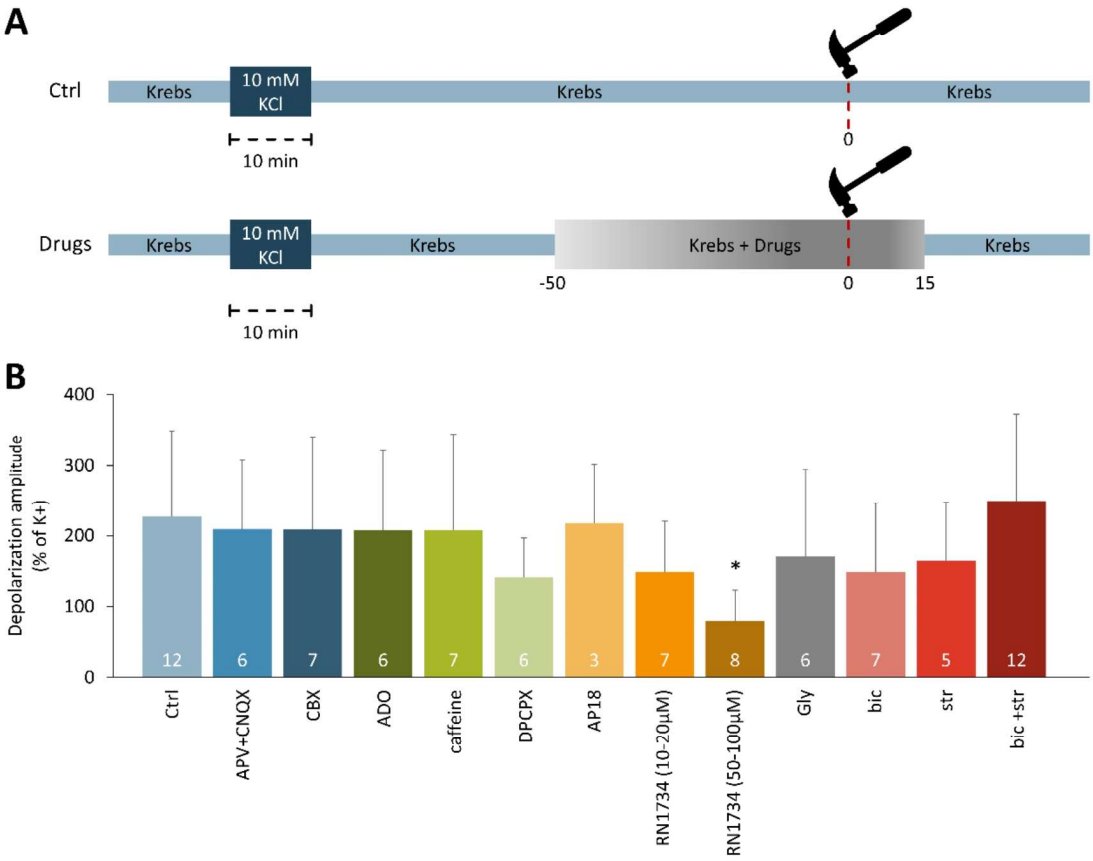

Figure 2. Amplitude of injury-potentials is reduced by TRPV4 antagonism
A. Bar chart schematizes the experimental protocols used for impacts on untreated preparations (ctrl, above) and during perfusion with neurochemicals (drugs, below). **B.** Histogram displays the normalized amplitude of injury-induced depolarization recorded from VRrL5 during the impact in the presence of different pharmacological agents. Values are normalized as percentages of potassium-induced depolarizations in the same preparation (* P = 0.034). Total number of experiments in each group is indicated within each bar.

Pharmacological manipulation of motor reflex responses.

Dynamics of the recovery of motor reflex responses following injury varied with each drug tested (Fig. 3A). Amplitude of responses was normalized to pre-impact values for each preparation. Two time-points were considered. In untreated injured preparations, a slow spontaneous recovery in the peak of motor-evoked responses occurred after injury, reaching 28.97 ± 17.17 % of pre-impact after one minute and 45.64 ± 28.05 % after two minutes. Conversely, in preparations treated with CBX, responses partially recovered to 66.39 ± 19.32 % of pre-impact control values immediately after the impact (1 min). At the same time point, RN1734 completely restored pre-impact motor evoked responses (90.70 ± 28.48 %). Both, CBX and RN1734 significantly improved the amplitude of normalized responses one minute after impact, when

compared to the peak of normalized motor reflexes in untreated spinal cords (P = 0.004, Kruskal-Wallis Test followed by Dunn's Multiple Comparisons Test; Fig. 3B). With a longer delay from the trauma (2 min), also bic brought to a full recovery of normalized reflex amplitude values (72.33 ± 16.86 % of pre-impact), (P = 0.040, Kruskal-Wallis Test followed by Dunn's Multiple Comparisons Test; Fig. 3C). Moreover, no significant difference was observed in the rate of reflex recovery following application of any of the other drugs tested at either time ponts. Collectively, after a physical trauma to the spinal cord, CBX speeded up the early partial recovery of motor evoked responses, while both, RN1734 and bic, stably restored full responses even if with a temporal profile that makes RN1734 more effective than bic.

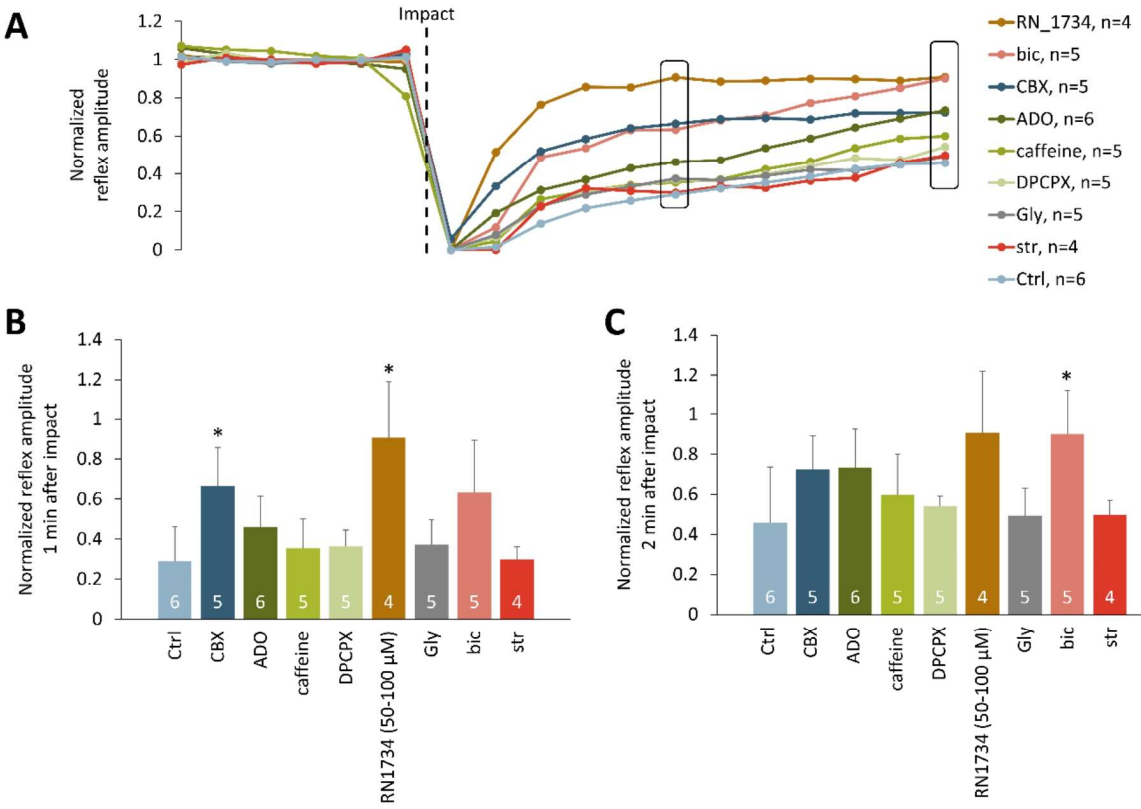

Figure 3. Motor reflex responses after a physical impact to cord recover with different rates depending on drug exposures.

A. A 3-minute time course representing motor reflex amplitude recorded from VRrL5 after exposure to different drugs. Values are normalized to the average responses before the impact (indicated by the dotted line). **B.** Bar chart illustrates normalized reflex responses one minute after the impact (corresponding to the left square in A, * P = 0.004). **C.** Normalized reflex responses two minutes after the impact (corresponding to the right square in A, * P = 0.040). The total number of experiments in each group is indicated within each bar.

References

Alibardi, L. 2019. Cerebrospinal fluid-contacting neurons in the regenerating spinal cord of lizards and amphibians are likely mechanoreceptors. Journal of Morphology 280(9): 1292–1308. doi: 10.1002/jmor.21031.

Apicella, R., and G. Taccola. 2023. Passive limb training modulates respiratory rhythmic bursts. Sci Rep 13(1): 7226. doi: 10.1038/s41598-023-34422-2.

Bracci, E., L. Ballerini, and A. Nistri. 1996a. Spontaneous rhythmic bursts induced by pharmacological block of inhibition in lumbar motoneurons of the neonatal rat spinal cord. Journal of Neurophysiology 75(2): 640–647. doi: 10.1152/jn.1996.75.2.640.

Bracci, E., L. Ballerini, and A. Nistri. 1996b. Localization of Rhythmogenic Networks Responsible for Spontaneous Bursts Induced by Strychnine and Bicuculline in the Rat Isolated Spinal Cord. J. Neurosci. 16(21): 7063–7076. doi: 10.1523/JNEUROSCI.16-21-07063.1996.

Bracci, E., M. Beato, and A. Nistri. 1997. Afferent Inputs Modulate the Activity of a Rhythmic Burst Generator in the Rat Disinhibited Spinal Cord In Vitro. Journal of Neurophysiology 77(6): 3157–3167. doi: 10.1152/jn.1997.77.6.3157.

Danneman, P.J., and T.D. Mandrell. 1997. Evaluation of five agents/methods for anesthesia of neonatal rats. Lab Anim Sci 47(4): 386–395.

Deumens, R., G.L. Mazzone, and G. Taccola. 2013. Early spread of hyperexcitability to caudal dorsal horn networks after a chemically-induced lesion of the rat spinal cord in vitro. Neuroscience 229: 155–163. doi: 10.1016/j.neuroscience.2012.10.036.

Etlin, A., D. Blivis, M. Ben-Zwi, and A. Lev-Tov. 2010. Long and short multifunicular projections of sacral neurons are activated by sensory input to produce locomotor activity in the absence of supraspinal control. Journal of Neuroscience 30(31): 10324–10336. doi: 10.1523/JNEUROSCI.1208-10.2010.

Garcia-Elias, A., S. Mrkonjić, C. Jung, C. Pardo-Pastor, R. Vicente, et al. 2014. The TRPV4 Channel. In: Nilius, B. and Flockerzi, V., editors, Mammalian Transient Receptor Potential (TRP) Cation Channels. Springer Berlin Heidelberg, Berlin, Heidelberg. p. 293–319

Goldberg, M.E. 2015. Response to Protocol Review Scenario: Protocol is acceptable. Lab Anim 44(6): 204–205. doi: 10.1038/laban.784.

Goncharenko, K., E. Eftekharpour, A.A. Velumian, P.L. Carlen, and M.G. Fehlings. 2014. Changes in gap junction expression and function following ischemic injury of spinal cord white matter. Journal of Neurophysiology 112(9): 2067–2075. doi: 10.1152/jn.00037.2013.

Grillner, S., A. McClellan, and K. Sigvardt. 1982. Mechanosensitive neurons in the spinal cord of the lamprey. Brain Research 235(1): 169–173. doi: 10.1016/0006-8993(82)90208-6.

Kumar, H., and I. Han. 2022. The neuroscience of transient receptor potential vanilloid type 4 (TRPV4) and spinal cord injury. Cellular, Molecular, Physiological, and Behavioral Aspects of Spinal Cord Injury. Elsevier. p. 229–238

Kumar, H., C.S. Lim, H. Choi, H.P. Joshi, K.-T. Kim, et al. 2020. Elevated TRPV4 Levels Contribute to Endothelial Damage and Scarring in Experimental Spinal Cord Injury. J. Neurosci. 40(9): 1943–1955. doi: 10.1523/JNEUROSCI.2035-19.2020.

Liu, D., W. Thangnipon, and D.J. McAdoo. 1991. Excitatory amino acids rise to toxic levels upon impact injury to the rat spinal cord. Brain Research 547(2): 344–348. doi: 10.1016/0006-8993(91)90984-4.

Mayer, M.L., and G.L. Westbrook. 1987. The physiology of excitatory amino acids in the vertebrate central nervous system. Progress in Neurobiology 28(3): 197–276. doi: 10.1016/0301-0082(87)90011-6.

McAdoo, D.J., G. Robak, G.-Y. Xu, and M.G. Hughes. 2000. Adenosine release upon spinal cord injury. Brain Research 854(1–2): 152–157. doi: 10.1016/S0006-8993(99)02333-1.

McAdoo, D.J., G.-Y. Xu, G. Robak, and M.G. Hughes. 1999. Changes in Amino Acid Concentrations over Time and Space around an Impact Injury and Their Diffusion Through the Rat Spinal Cord. Experimental Neurology 159(2): 538–544. doi: 10.1006/exnr.1999.7166.

Mohammadshirazi, A., R. Apicella, B.A. Zylberberg, G.L. Mazzone, and G. Taccola. 2023. Suprapontine structures modulate brainstem and spinal networks. Cell Mol Neurobiol. doi: 10.1007/s10571-023-01321-z.

Mohammadshirazi, A., G.L. Mazzone, B.A. Zylberberg, L. Mio, G. Pistorio, et al. 2024. A focal traumatic injury to the spinal cord causes an immediate and massive spreading depolarization sustained by chloride ions, with transient network dysfunction and remote cortical glia changes. doi: 10.1101/2024.07.15.603535.

Musienko, P., R. Van Den Brand, O. Marzendorfer, R.R. Roy, Y. Gerasimenko, et al. 2011. Controlling Specific Locomotor Behaviors through Multidimensional Monoaminergic Modulation of Spinal Circuitries. Journal of Neuroscience 31(25): 9264–9278. doi: 10.1523/JNEUROSCI.5796-10.2011.

Phifer, C.B., and L.M. Terry. 1986. Use of hypothermia for general anesthesia in preweanling rodents. Physiology & Behavior 38(6): 887–890. doi: 10.1016/0031-9384(86)90058-2.

Qi, M., C. Wu, Z. Wang, L. Zhou, C. Men, et al. 2018. Transient Receptor Potential Vanilloid 4 Activation-Induced Increase in Glycine-Activated Current in Mouse Hippocampal Pyramidal Neurons. Cell Physiol Biochem 45(3): 1084–1096. doi: 10.1159/000487350.

Taccola, G., B.H. Salazar, R. Apicella, M.K. Hogan, P.J. Horner, et al. 2020. Selective Antagonism of A1 Adenosinergic Receptors Strengthens the Neuromodulation of the Sensorimotor Network During Epidural Spinal Stimulation. Front. Syst. Neurosci. 14: 44. doi: 10.3389/fnsys.2020.00044.

Valle, M.E.D., T. Cobo, J.L. Cobo, and J.A. Vega. 2012. Mechanosensory neurons, cutaneous mechanoreceptors, and putative mechanoproteins. Microscopy Res & Technique 75(8): 1033–1043. doi: 10.1002/jemt.22028.

Xu, G. 2004. Concentrations of glutamate released following spinal cord injury kill oligodendrocytes in the spinal cord. Experimental Neurology 187(2): 329–336. doi: 10.1016/j.expneurol.2004.01.029.

DISCUSSION

1. A novel in vitro preparation of the entire CNS

Modulatory influences of supra-pontine structures on brainstem and spinal networks

The intricate tapestry of neural circuits emerges from the complex interplay and integration of countless neurons. Understanding the function of these circuits necessitates a holistic approach that considers the coordinated activity of diverse CNS regions. To unravel the complexities of neural processing, investigating how different CNS structures modulate one another is paramount. By examining these interconnections, researchers can elucidate the mechanisms underlying physiological CNS function, as well as pathological conditions. This integrative perspective is essential for developing effective therapeutic strategies targeting specific neural circuits (Behrens and Sporns, 2012).

Physiologists have long utilized partial preparations of the nervous system to investigate neural circuits and understand the physiology of the nervous system (Clarac et al., 2004b). The preparation of spinal cord or brainstem-spinal cord of various neonates such as lamprey (Cohen and Wallén, 1980; Grillner et al., 1991), amphibians (Wheatley et al., 1992), chicks (O'Donovan et al., 1992), rodents (Otsuka and Konishi, 1974; Suzue, 1984; Smith and Feldman, 1987) have been extensively used to investigate the spinal intrinsic motor activities and respiratory rhythm generation. Neonatal partial CNS in vitro preparations with attached peripheral organs provide valuable insights into complex physiological interactions that are difficult to study in isolated tissues or in vivo models (Kerkut and Bagust, 1995). By preserving sections of the CNS alongside peripheral organs, these preparations allow for the investigation of neural circuits in a more integrated context with sensory feedback. They are particularly advantageous for studying motor and autonomic functions, as they enable real-time monitoring of physiological responses, such as respiration and motor output, in response to experimental manipulations. For example, the spinal cord-rib preparation allows for the monitoring of inspiratory and expiratory activities during central chemoreceptor activation, as well as the evaluation of internal intercostal muscle activity (Smith et al., 1990; Iizuka, 1999). The heart-brainstem preparation allows for detailed studies of cardiovascular and respiratory neurons, phrenic nerve activity, the integrity of central coupling between the respiratory rhythm generator and cardiac vagal motor neurons, and analysis of medullary cardio-respiratory neurons (Paton, 1996). Additionally, in vitro preparations from adult turtles, with the shell attached, allow researchers to study the neural generation of the scratch reflex (Keifer and Stein, 1983). Finally, spinal cord-legs preparations offer insights into the role of passive limb movements in spinal network activity. Studies on these preparations have shown that continuous passive limb training can modulate hindlimb rhythmic activity, providing a model for exploring spinal network plasticity and motor output (Dingu et al., 2018). Moreover, spinal cord-brainstem preparations have been deemed sufficient for studying motor

outputs originating from or controlled by lower brain centers, such as those involved in respiration or locomotor activities in neonates (Clarac et al., 2004b). While these experimental models of partial CNS have provided valuable insights, a preparation that allows to trace the modulation of brain on spinal neurons is compelling to better understand the integrative physiology of neural circuits for motor output. Indeed, even at this early stage of development, descending input from higher brain centers can significantly influence the properties of rhythmic motor outputs (Mohammadshirazi et al., 2023).

The first attempt to introduce a more complete CNS preparation in vitro was with the neonatal opossum, which is developmentally equivalent to embryonic day 14 in rats and lacks a cerebellum (Nicholls et al., 1990; Eugenín and Nicholls, 2000). The subsequent development of an entire CNS preparation from neonatal rats (Mohammadshirazi et al., 2023) adopted a mammalian model more widely used for SCI studies, with a more developed experimental preparation than opossum although limited to the first three post-natal days of survival in vitro.

Our data demonstrated that precollicular decerebration and pontobulbar transection alter the frequency and duration of spontaneous respiratory bursts. This evidence indicates that, even at the early postnatal stages, a descending modulatory input from higher brain centers modulates features of the respiratory rhythm such as duration, shape and rhythm (Mohammadshirazi et al., 2023). This observation is consistent with experiments in adult in vivo animals, showing that various regions, including the caudal hypothalamus, midbrain, and cortex, play crucial roles in controlling respiration (Horn and Waldrop, 1998).

Although descending tracts like the corticospinal tract are not fully developed in early neonatal rats (Lakke, 1997; Clarac et al., 2004a), the local microcircuits of the spinal cord are modulated by suprapontine structures (Mohammadshirazi et al., 2023). Our investigation reveal that the ablation of suprapontine structures alters motor reflex responses from VRs and retrograde responses of DRs, suggesting that supraspinal centers exert remarkable control over spinal reflex circuitry, likely through descending pathways that modulate spinal neuron excitability (Mohammadshirazi et al., 2023). Previous research has identified the motor cortex, brainstem reticular formation, and cerebellum as key supraspinal regions involved in modulating spinal reflexes (Gernandt and Gilman, 1961; Chen and Wolpaw, 1995). Additionally, our data show that a midthoracic transection perturbs the activity of central pattern generators (CPGs), reducing the total duration and coordination of fictive locomotor cycles (Mohammadshirazi et al., 2023). This aligns with the current view about the CPG activity as initiated and fine-tuned by inputs from descending locomotor commands originating from neurons in the brainstem and midbrain (Kiehn, 2006).

It must be considered that neonatal CNS preparations developmental stage introduces some limitations. In neonates, neural circuits are still undergoing maturation, with descending pathways

often underdeveloped (Lakke, 1997; Clarac et al., 2004a) and the organization of cortical neurons not yet fully established (Marín, 2013; Lim et al., 2018). These factors may influence the extent to which findings translate to adult systems. Additionally, neonatal neurons exhibit distinct membrane equilibrium properties that can affect their excitability and neurotransmission, particularly in response to inhibitory signals (Mazzone et al., 2021). Another key consideration is the heightened regenerative capacity observed in neonatal tissues, which is typically much lower in mature CNS tissue (Wang et al., 2004; Stewart et al., 2022). This can lead to differences in injury recovery dynamics and the effectiveness of therapeutic interventions. Despite these limitations, neonatal preparations remain an invaluable model for investigating foundational processes in CNS development and trauma, offering a controlled platform to explore early-stage injury mechanisms and potential repair strategies. Moreover, adopting neonatal preparations is the most insightful tool to investigate the pathophysiology of pediatric injuries that mainly had been inferred from adult preclinical models.

Future perspectives

The in vitro preparation of the entire CNS from neonatal rats offers a versatile platform with extensive research applications. This approach provides an opportunity to investigate diverse issues such as neural development, motor circuits, and trauma. In developmental research, the preparation allows for detailed studies of the maturation of neural circuits and the establishment of functional connectivity in rodents. It can be explored how genetic factors and environmental influences shape neural development, shedding light on plasticity and mechanisms underlying neurodevelopmental disorders.

This model enables us to investigate how descending inputs from supraspinal centers modulate rhythmic spinal cord activity and reflex motor outputs, enhancing our understanding in the intricate mechanisms involved in movement control. The preparation where the limbs remain attached, also provide the possibility to investigate the integration between limb movement and higher functions such as respiration (Apicella and Taccola, 2023).

Additionally, this in vitro preparation has been replicated in mice, further extending its applications also including transgenic animals. By integrating optogenetic and chemogenetic techniques, the precise manipulation and study of specific neuronal populations and circuits can be investigated in genetic disease models as well.

The preparation is particularly valuable for studying spinal cord or traumatic brain injury (TBI). By inducing calibrated and consistent lesions, researchers can monitor real-time electrophysiological, biochemical, and molecular changes throughout the CNS. This facilitates detailed exploration of injury-induced depolarization, neurochemical alterations, and short-term potential recovery processes, as

well as the evaluation of any therapeutic interventions aimed at reducing cell damage and promoting repair.

Overall, the in vitro preparation of the entire CNS from neonatal rats offers a comprehensive tool for studying development, the functional organization and integration among neural circuits, trauma, with the added flexibility of extending these studies to genetically modified experimental models.

2. Investigating the immediate consequences of an SCI

Immediate depolarization following a physical damage to the cord

The immediate phase following a traumatic SCI, defined as the first 2 hours post-injury, is characterized by necrotic cell death, ischemia, hemorrhage, edema, mechanical disruption of cell membranes, and a surge in extracellular glutamate to excitotoxic levels (Siddiqui et al., 2015). The majority of destruction following an SCI is attributed to secondary injury mechanisms that develop over 1-2 hours to 2 days after the injury (Norenberg et al., 2004). However, understanding the dynamics of the immediate damage and identifying the initial factors that start the deadly cascade of the secondary injury require further investigation.

In this study, we utilized electrophysiological recordings at the actual moment of spinal cord damage to investigate the earliest consequences of a traumatic SCI (Mohammadshirazi et al., 2024). By utilizing the isolated preparation of the CNS that excludes the influence of blood circulation and peripheral nervous system, we were able to narrow our investigation to the direct effects of the injury on the CNS itself, providing a clearer understanding of the immediate neurogenic responses to trauma.

We validated our in vitro SCI model through several key assessments. Histological analysis confirmed neuronal loss at the lesion site, while no morphological or functional changes were observed in motor pools below the injury. The disconnection of ascending tracts was assessed by the absence of cervical ventral root responses to electrically evoked stimulation of the sacrocaudal afferents following the injury. Additionally, the disappearance of rhythmic expiratory bursts from lumbar ventral roots confirmed the disruption of descending tracts (Mohammadshirazi et al., 2024).

In the present research, we observed a rapid depolarization within approximately 200 ms following the onset of the impact, with recovery occurring over the next 15 minutes (Mohammadshirazi et al., 2024). The occurrence of injury potentials triggered by physical impact to the spinal cord has been previously documented, even though not continuously recorded (Goodman et al., 1985; Wang et al., 2015). Several factors suggest the observed depolarization in our study is a genuine physiological response rather than an artifact: 1) the absence of depolarization when the device operated without contacting the preparation; 2) consistent peak of depolarizations with consecutive impacts at short intervals; 3) the lack of injury potential at the peak of high-potassium-induced depolarization; 4) the inability of the depolarization to propagate through a severed preparation; and 5) absence any DC

deflections when the impact was inflicted to a heat-inactivated anoxic spinal cord (Mohammadshirazi et al., 2024).

The observed depolarization was accompanied by a drop in tissue oxygen levels, both of which recovered over the same timeframe. While changes in spinal cord oxygen levels can be considered indirect evidence of neuronal activity, similar profiles of oxygen levels and injury potential suggest a causal relationship between injury and an increased oxygen consumption by cells. Additionally, the drop in oxygen levels during perfusion with high concentration of potassium further supports the connection between tissue oxygen content and neuronal activity.

Moreover, as the severity of the injury increased, the magnitude of the depolarization intensified as well. The varying latencies of injury-induced depolarization recorded from different roots indicated that this depolarization spread from the ventral injury site to rostral, caudal, and dorsal regions. Additionally, following the injury electrically induced responses transiently disappeared and spontaneous activities largely reduced.

Reflex responses evoked through sacrocaudal afferents and recorded from lumbar ventral roots disappeared at the peak of depolarization, gradually recovering in a manner reminiscent of spinal shock, where reflexes temporarily vanish below the injury site (Mohammadshirazi et al., 2024). This finding aligns with previous reports that compound action potentials are reduced and subsequently recover following ex vivo spinal cord compression (Wang et al., 2015, 2016). Interestingly, the reappearance of the first reflex response after the impact was not correlated to the amplitude of the injury potential. This evidence suggests that these two events rely on two different mechanisms.

The immediate depolarization following SCI initially triggers network overexcitation, and this is likely followed by a depression of network excitability due to inactivation of voltage dependent sodium channels. Our data demonstrate that the injury altered various aspects of electrically induced fictive locomotor activity, particularly affecting the alternation between left and right, flexor and extensor (Mohammadshirazi et al., 2024). This changes underscore the importance of balanced network activity in excitation and inhibition, which is crucial for the expression of locomotor patterns necessary for rhythmic activation of limb extensor and flexor muscles (Mazzone et al., 2021). Excitatory neurotransmission, primarily mediated by glutamate, plays an essential role in locomotion, as its pharmacological blockade halts locomotor activity (Cazalets et al., 1992). Additionally, the inhibition mediated by GABA and glycine is essential for maintaining the motor pattern alternating between bilateral motor pools, and between flexor- and extensor-related commands (Cazalets et al., 1994). When this inhibitory transmission is blocked, the CPG's alternation is suppressed, leading to the emergence of slow, synchronous rhythmic motor discharges (Mazzone et al., 2021). This matter

suggests that the neurotransmission imbalance, which likely begins immediately following spinal cord injury, contributes to the compromised function of fictive locomotion.

Role of chloride ion in SCI pathophysiology

An SCI leads to a substantial increase in the extracellular concentration of various neurotransmitters, including GABA. Experimental studies have demonstrated a marked elevation in GABA levels following an initial glutamate surge at the lesion site 40 min after SCI in vivo, which rapidly recovers to pre-injury levels (Panter et al., 1990; McAdoo et al., 2000; Mazzone et al., 2021). It has been suggested that the elevation of GABA plays a crucial role in restoring locomotor network activity after injury by counterbalancing the excessive excitation induced by glutamate, thereby preventing excitotoxic damage (Mazzone et al., 2021).

In mature neurons, activated $GABA_A$ receptors allow chloride (and HCO^{3-}) ions to enter the postsynaptic neuron. This influx of chloride ions can hyperpolarize the neuron, making it less likely to fire. However, in early postnatal life, the chloride concentration gradient is reversed, leading to chloride ions exiting the neuron. This net movement of chloride ions sustains an inward current that depolarizes the neuron, increasing its excitability. This depolarizing effect of GABA, despite being excitatory, ultimately acts as an inhibitor in neonatal spinal neurons due to its shunting effect and the inactivation of voltage-gated sodium channels, which limits the impact of incoming excitatory signals (Gao and Ziskind-Conhaim, 1995; Mazzone et al., 2021). A good example of inhibitory depolarizing nature of GABA is physiologically shown in adult DRGs in which spinal afferents are involved in the presynaptic inhibition regulating pain-related and sensory-motor input (Willis, 1999; Rudomin, 2009).

The Sodium Potassium Chloride Cotransporter 1 (NKCC1) and Potassium Chloride Cotransporter 2 (KCC2) are essential chloride-cation cotransporters that regulate chloride homeostasis and neuronal excitability (Mazzone et al., 2021). The balance between KCC2 and NKCC1 expression shifts dramatically during development. In neonates, NKCC1 predominates, while KCC2 becomes more prominent in adults (Blaesse et al., 2009). The higher expression of NKCC1 in neonates contributes to a more positive chloride equilibrium potential. This causes chloride ions to flow out of neurons, leading to depolarization and increased neuronal excitability. In contrast, in adults, the increased expression of KCC2 lowers intracellular chloride levels, reaching the mature chloride homeostasis and reducing the overall neuronal excitability (Mazzone et al., 2021).

Following an SCI, a disruption in the balance between NKCC1 and KCC2 expressions have been observed. This disruption is characterized by the downregulation of KCC2 and the upregulation of NKCC1, resulting in a shift in the chloride equilibrium potential towards a more depolarized state. This shift increases neuronal excitability and may contribute to the development of neuropathic pain and muscle spasticity and hyperreflexia (Cramer et al., 2008; Boulenguez et al., 2010; Hasbargen et al.,

2010). Many studies have demonstrated that pharmacological manipulation or alteration of gene expression to decrease NKCC1 and increase KCC2 levels can restore chloride homeostasis and ameliorate hypersensitivity, spasticity, and promote functional recovery following SCI (Mazzone et al., 2021).

Our findings indicate that a low-chloride modified Krebs solution enhances the peak amplitude of injury potentials (Mohammadshirazi et al., 2024), likely by changing the driving force for chloride currents. This suggests that the initial depolarization following spinal cord injury is sustained, at least in the immature tissue, by significant chloride conductance. We hypothesize that the immediate overflow of chloride ions triggered by a physical injury to spinal tissue sustains a surge of extracellular chloride concentrations, possibly changing the equilibrium potential of chloride ions. This early excitatory phase may set the stage for ongoing disturbances in chloride channels conductance across neuronal membranes throughout the chronic phase. However, the neonatal spinal cord exhibits an immature chloride gradient (Gao and Ziskind-Conhaim, 1995), which offers a model closer to the post-SCI environment, where the chloride equilibrium shifts toward an immature state. Although spasticity typically emerges in the chronic phase, it is possible that the molecular mechanisms underlying spasticity, such as dysregulated intracellular chloride concentrations, begin with the initiation of the injury potential making the rationale for any acute antispastic interventions targeting chloride channels.

Remote transient changes in cortical astrocytes

Although the effects of SCI and its pathophysiology close to the injury site have been extensively studied, the broader implications for distant brain structures remain less explored. By adopting an innovative experimental platform, we were not only able to investigate the immediate electrophysiological events in the spinal cord at the moment of injury, but also examine the early pathophysiological changes occurring in regions remote from the injury site. We observed a transient lower density of astrocytes expressing calcium-binding protein S100b (Donato, 1999; Gonzalez et al., 2020) in the primary motor cortex within 25 minutes after the injury, and in the primary and secondary somatosensory cortex two hours post-injury (Mohammadshirazi et al., 2024). Considering that the experiments were performed during the peak of astrogenesis in rats, astrocyte density in the cerebral cortex was evaluated to indicate the potential effects of spinal injury. The observed decrease in astrocyte density is likely due to a slowdown in cortical astrogenesis in response to the spinal damage rather than the selective loss of astrocytes. Moreover, the glial expression of S100 might influence calcium-dependent processes such as neurotransmitter release, glutamate uptake, and modulation of synaptic activity (Donato, 2001). S100 proteins can be released into the extracellular space during inflammation, and they can act as damage-associated molecular patterns and trigger inflammatory

responses, contributing to conditions such as neurodegenerative diseases and multiple sclerosis (Gonzalez et al., 2020). Contrariwise, S100b has been shown to have neuroprotective effects under certain conditions, promoting neuronal survival and reducing oxidative stress (Gerlach et al., 2006; Gonzalez et al., 2020). Studies have confirmed that injured neuronal and glial cultures release S100b, highlighting its protective role (Ellis et al., 2007). Our findings suggest a reduction in glia that express S100b following SCI. Albeit the reduction in S100b should be considered detrimental for neuroprotection, paradoxically it may play a beneficial role in the immediate inflammatory response.

Future perspectives

The findings presented in this study open several avenues for future research aimed at further unraveling the complex pathophysiological mechanisms triggered by SCI. A critical area for investigation is the immediate cascade of events following SCI. The rapid depolarization observed within milliseconds of injury likely initiates a series of biochemical and cellular processes that shape long-term outcomes. By focusing on this critical time window and dissecting the initial event, we can gain deeper insights into the mechanisms that influence the progression of SCI. Moreover, understanding the immediate changes following a physical trauma may suggest translational studies aimed at limiting accidental damages to the cord during the most delicate spinal surgeries.

Understanding the protective roles of GABA and chloride during this period, and how their imbalance contributes to chronic conditions such as spasticity and neuropathic pain, could lead to novel therapeutic interventions focused on restoring chloride homeostasis in the injured spinal cord. Early interventions aimed at modulating chloride transporters like NKCC1 and KCC2, while leveraging the protective role of GABAergic signaling, could offer a unique opportunity to mitigate the long-term consequences of SCI and support rehabilitation efforts.

The observed astrocytic responses in cortical regions distant from the injury site present an intriguing area for further research. The transient reduction of cells expressing S100b in these areas suggests a potential systemic response following SCI, which may play a significant neuroprotective role. Understanding the dynamics of S100b expression and its impact on neuronal survival and synaptic function could yield valuable insights into the brain's adaptive response to spinal trauma. These responses may contribute to longer-term pathologies, highlighting the importance of studying distant neurophysiological effects alongside local injury mechanisms.

Future work could also focus on identifying early cortical biomarkers to predict the severity of SCI and tailor therapeutic interventions. Additionally, a deeper understanding of individual variability in response to SCI may pave the way for personalized treatment approaches, optimizing care for each spinal cord injured person. By addressing the earliest events post-injury, we stand a better chance of reducing long-term damage and enhancing the effectiveness of rehabilitation strategies.

3. Pharmacological manipulation of injury potential

Role of TRPV4 following an SCI

To mitigate the transient hypoxia and the neuronal damage at the site of the injury, neurochemicals that selectively target ion channels involved in the acute phase of SCI were tested to reduce the initial depolarization caused by SCI. To limit the transient suppression of the motor reflexes during the spinal shock the same neurochemicals were applied up to two minutes after the trauma, and the peak of electrically induced VR potentials were monitored (Mohammadshirazi and Taccola, 2024). Interestingly, among all treatments only RN1734 significantly reduced the peak amplitude of immediate injury potentials following SCI (Mohammadshirazi and Taccola, 2024).

Transient receptor potential vanilloid 4 (TRPV4), also referred to as osmo-sensitive transient receptor potential channel (OTRPC4), vanilloid receptor-related osmotically activated channel (VR-OAC), vanilloid receptor-like (VRL-2), and TRP-12 (Garcia-Elias et al., 2014), is a member of the TRP ion channel family (Wissenbach et al., 2000). This non-selective cation channel is permeable to calcium, potassium, magnesium, and sodium (Kumar et al., 2018) and is activated by various stimuli, including mechanical stress, osmotic changes, heat, acidic pH, citrate, and oxidative stress (Garcia-Elias et al., 2014; Liu et al., 2020). TRPV4, which is expressed by astrocytes and neurons, contributes to depolarizing the cell membrane upon stretch activation and modulates ligand-gated ion channels such as $GABA_A$ and glycine receptors (Hong et al., 2016; Qi et al., 2018).

Following SCI, TRPV4 expression significantly increases in a few hours after the trauma, with levels correlating with the severity of the injury (Kumar et al., 2020). Inhibition or genetic suppression of TRPV4 within one hour post-SCI has been shown to enhance neuroprotection by preventing endothelial damage and preserving the blood-spinal cord barrier. This approach also attenuates neuroinflammation and reduces glial scarring at the injury site, with partial motor recovery observed in the hindlimbs (Kumar et al., 2020). The elevation of TRPV4 expression in the acute phase of SCI has been linked to the inflammatory response (Kumar et al., 2020; Kumar and Han, 2022). In our experimental setting the lack of blood circulation prevents inflammatory response. However, TRPV4 channels were still activated following the injury. This suggests that TRPV4 activation in SCI is not solely dependent on the inflammatory response but may occur as a result of mechanical stretch of membranes as well. Along with other ionotropic receptors, TRPV4 may contribute to the extracellular ion imbalance that drives both injury potentials and the transient suppression of reflexes during spinal shock.

Moreover, our data indicates that after a physical trauma to the spinal cord, carbenoxolone accelerates the partial recovery of motor evoked responses. However, both RN1734 and bicuculline fully restore the responses, with RN1734 acting faster than bicuculline (Mohammadshirazi and Taccola, 2024).

Physical trauma activates TRPV4 channels, causing an influx of cations into the cells. Blocking these channels significantly reduces the injury potential to 39 % compared to untreated injured cords. Following the injury-induced depolarization, reflex responses disappear due to overexcitation. As the baseline repolarizes, reflex responses reappear and progressively increase until they return to their original amplitude in about 30 minutes. Our data showed no correlation between the injury-induced depolarization amplitude and the timing of the first reflex response reappearance in control groups. However, when TRPV4 channels are blocked, the injury potential is smaller and the baseline recovers sooner than in control experiments. In this case, the reflex responses also recover faster. It can be hypothesized that the pharmacological blockage of TRPV4 channels prevents the activation of a subsequent cascade of events that sustain further reflex inhibition. Indeed, the flow of cations caused by activation of TRPV4, activates the gap junctions, prolonging the depolarizing state of motor pools. Therefore, blocking gap junctions with carbenoxolone leads to a partial recovery of reflex responses around the first minute following the physical trauma. Afterwards, the injury-induced depolarization sustained by the activation of TRPV4 also would recruit GABAergic neurons. Thus, blocking GABAergic receptors by bicuculline restored reflexes in two minutes after the injury, a faster recovery than in untreated injured spinal cord. In conclusion, the injury-induced depolarization is sustained by the activation of TRPV4 channels that results in the activation of the gap junctions and GABAergic transmission.

Future perspectives

The findings presented in this study offer important insights into the early molecular events following SCI, with particular emphasis on the essential role of TRPV4 in initiation of injury-induced depolarization. Our data indicate that a selective inhibition using RN1734 leads to a marked reduction in the peak of injury potentials. This underscores TRPV4 as a promising target in limiting accidental damages during spinal surgeries for controlling network excitability and reducing subsequent neural damage.

Moreover, the downstream signaling pathways triggered by TRPV4, along with its interactions with gap junctions and GABAergic transmission during spinal shock, represent compelling areas for therapeutic intervention. Further research is needed to refine the timing of agents like RN1734, carbenoxolone, and bicuculline and as well as delayed applications of these agents to optimize their potential therapeutic impact and promote faster reflex recovery. A deeper understanding of these early-phase molecular processes will be crucial for advancing neuroprotective strategies and creating new therapeutic opportunities to mitigate secondary injury and enhance functional recovery for individuals with SCI.

CONCLUSION

This PhD project aimed to investigate the immediate consequences of traumatic SCI and explore strategies to limit them. To achieve this, a recently developed in vitro preparation of the entire CNS from neonatal rats was employed, which offered a real-time setting for studying SCI. A custom-made calibrated impactor was used to deliver precise traumatic damage to the spinal cord. Following the characterization of the injury-induced depolarization, various pharmacological interventions were tested to mitigate this initial damage. This research identified the mechanism behind the first event following traumatic spinal cord injury, presenting a novel therapeutic target for the SCI field. These findings offer promising potential for further validation in preclinical studies and eventual clinical translation. Overall, this work advances the understanding of SCI pathophysiology and lays the groundwork for future therapeutic developments.

REFERENCES

Aguilar, J., D. Humanes-Valera, E. Alonso-Calvino, J.G. Yague, K.A. Moxon, et al. 2010. Spinal cord injury immediately changes the state of the brain. Journal of Neuroscience 30(22): 7528–7537. doi: 10.1523/JNEUROSCI.0379-10.2010.

Ahuja, C.S., J.R. Wilson, S. Nori, M.R.N. Kotter, C. Druschel, et al. 2017. Traumatic spinal cord injury. Nat Rev Dis Primers 3(1): 17018. doi: 10.1038/nrdp.2017.18.

Alizadeh, A., S.M. Dyck, and S. Karimi-Abdolrezaee. 2019. Traumatic Spinal Cord Injury: An Overview of Pathophysiology, Models and Acute Injury Mechanisms. Front. Neurol. 10: 282. doi: 10.3389/fneur.2019.00282.

Allen, A.R. 1911. Surgery of experimental lesion of spinal cord equivalent to crush injury of fracture dislocation of spinal column: A preliminary report. JAMA LVII(11): 878. doi: 10.1001/jama.1911.04260090100008.

Apicella, R., and G. Taccola. 2023. Passive limb training modulates respiratory rhythmic bursts. Sci Rep 13(1): 7226. doi: 10.1038/s41598-023-34422-2.

Ashby, P., M. Verrier, and E. Lightfoot. 1974. Segmental reflex pathways in spinal shock and spinal spasticity in man. Journal of Neurology, Neurosurgery & Psychiatry 37(12): 1352–1360. doi: 10.1136/jnnp.37.12.1352.

Atkinson, P.P., and J.L.D. Atkinson. 1996. Spinal Shock. Mayo Clinic Proceedings 71(4): 384–389. doi: 10.4065/71.4.384.

Bajrektarevic, D., and A. Nistri. 2016. Delayed application of the anesthetic propofol contrasts the neurotoxic effects of kainate on rat organotypic spinal slice cultures. NeuroToxicology 54: 1–10. doi: 10.1016/j.neuro.2016.03.001.

Barnes, C.D., R.J. Joynt, and B.A. Schottelius. 1962. Motoneuron resting potentials in spinal shock. American Journal of Physiology-Legacy Content 203(6): 1113–1116. doi: 10.1152/ajplegacy.1962.203.6.1113.

Basso, D.M., M.S. Beattie, and J.C. Bresnahan. 1996. Graded Histological and Locomotor Outcomes after Spinal Cord Contusion Using the NYU Weight-Drop Device versus Transection. Experimental Neurology 139(2): 244–256. doi: 10.1006/exnr.1996.0098.

Behrens, T.E., and O. Sporns. 2012. Human connectomics. Current Opinion in Neurobiology 22(1): 144–153. doi: 10.1016/j.conb.2011.08.005.

Benabid, A.L., T. Costecalde, A. Eliseyev, G. Charvet, A. Verney, et al. 2019. An exoskeleton controlled by an epidural wireless brain–machine interface in a tetraplegic patient: a proof-of-concept demonstration. The Lancet Neurology 18(12): 1112–1122. doi: 10.1016/S1474-4422(19)30321-7.

Bennett, J., J.M. Das, and P.D. Emmady. 2024. Spinal Cord Injuries. StatPearls. StatPearls Publishing, Treasure Island (FL)

Blaesse, P., M.S. Airaksinen, C. Rivera, and K. Kaila. 2009. Cation-Chloride Cotransporters and Neuronal Function. Neuron 61(6): 820–838. doi: 10.1016/j.neuron.2009.03.003.

Boulenguez, P., S. Liabeuf, R. Bos, H. Bras, C. Jean-Xavier, et al. 2010. Down-regulation of the potassium-chloride cotransporter KCC2 contributes to spasticity after spinal cord injury. Nat Med 16(3): 302–307. doi: 10.1038/nm.2107.

Bradbury, E.J., and E.R. Burnside. 2019. Moving beyond the glial scar for spinal cord repair. Nat Commun 10(1): 3879. doi: 10.1038/s41467-019-11707-7.

Bradbury, E.J., L.D.F. Moon, R.J. Popat, V.R. King, G.S. Bennett, et al. 2002. Chondroitinase ABC promotes functional recovery after spinal cord injury. Nature 416(6881): 636–640. doi: 10.1038/416636a.

Bregman, B.S., and M.E. Goldberger. 1982. Anatomical Plasticity and Sparing of Function After Spinal Cord Damage in Neonatal Cats. Science 217(4559): 553–555. doi: 10.1126/science.7089581.

Burns, A.S., and J.F. Ditunno. 2001. Establishing prognosis and maximizing functional outcomes after spinal cord injury: a review of current and future directions in rehabilitation management. Spine 26(Supplement): S137–S145. doi: 10.1097/00007632-200112151-00023.

Calancie, B., J.G. Broton, K. John Klose, M. Traad, J. Difini, et al. 1993. Evidence that alterations in presynaptic inhibition contribute to segmental hypo- and hyperexcitability after spinal cord injury in man. Electroencephalography and Clinical Neurophysiology/Evoked Potentials Section 89(3): 177–186. doi: 10.1016/0168-5597(93)90131-8.

Cao, F., X. Yang, W. Liu, W. Hu, G. Li, et al. 2008. Elevation of neuron-specific enolase and S-100β protein level in experimental acute spinal cord injury. Journal of Clinical Neuroscience 15(5): 541–544. doi: 10.1016/j.jocn.2007.05.014.

Carlson, S.L., M.E. Parrish, J.E. Springer, K. Doty, and L. Dossett. 1998. Acute inflammatory response in spinal cord following impact injury. Experimental Neurology 151(1): 77–88. doi: 10.1006/exnr.1998.6785.

Carreon, L.Y., S.D. Glassman, and M.J. Campbell. 2004. Pediatric spine fractures: a review of 137 hospital admissions. Journal of Spinal Disorders & Techniques 17(6): 477–482. doi: 10.1097/01.bsd.0000132290.50455.99.

Cazalets, J.R., Y. Sqalli-Houssaini, and F. Clarac. 1992. Activation of the central pattern generators for locomotion by serotonin and excitatory amino acids in neonatal rat. The Journal of Physiology 455(1): 187–204. doi: 10.1113/jphysiol.1992.sp019296.

Cazalets, J.R., Y. Sqalli-Houssaini, and F. Clarac. 1994. GABAergic inactivation of the central pattern generators for locomotion in isolated neonatal rat spinal cord. The Journal of Physiology 474(1): 173–181. doi: 10.1113/jphysiol.1994.sp020011.

Chen, X.Y., and J.R. Wolpaw. 1995. Operant conditioning of H-reflex in freely moving rats. Journal of Neurophysiology 73(1): 411–415. doi: 10.1152/jn.1995.73.1.411.

Cheriyan, T., D.J. Ryan, J.H. Weinreb, J. Cheriyan, J.C. Paul, et al. 2014. Spinal cord injury models: a review. Spinal Cord 52(8): 588–595. doi: 10.1038/sc.2014.91.

Choi, E., S. Gattas, N. Brown, J. Hong, J. Limbo, et al. 2021. Epidural electrical stimulation for spinal cord injury. Neural Regen Res 16(12): 2367. doi: 10.4103/1673-5374.313017.

Clarac, F., F. Brocard, and L. Vinay. 2004a. The maturation of locomotor networks. Progress in Brain Research. Elsevier. p. 57–66

Clarac, F., E. Pearlstein, J.F. Pflieger, and L. Vinay. 2004b. The in vitro neonatal rat spinal cord preparation: a new insight into mammalian locomotor mechanisms. Journal of Comparative Physiology A: Sensory, Neural, and Behavioral Physiology 190(5): 343–357. doi: 10.1007/s00359-004-0499-2.

Cohen, A.H., and P. Wallén. 1980. The neuronal correlate of locomotion in fish: "Fictive Swimming" Induced in an in Vitro Preparation of the Lamprey Spinal Cord. Exp Brain Res 41(1). doi: 10.1007/BF00236674.

Cramer, S.W., C. Baggott, J. Cain, J. Tilghman, B. Allcock, et al. 2008. The Role of Cation-Dependent Chloride Transporters in Neuropathic Pain Following Spinal Cord Injury. Mol Pain 4: 1744-8069-4–36. doi: 10.1186/1744-8069-4-36.

Crawley, A.P., M.T. Jurkiewicz, A. Yim, S. Heyn, M.C. Verrier, et al. 2004. Absence of localized grey matter volume changes in the motor cortex following spinal cord injury. Brain Research 1028(1): 19–25. doi: 10.1016/j.brainres.2004.08.060.

Dickman, C.A., H.L. Rekate, V.K.H. Sonntag, and J.M. Zabramski. 1989. Pediatric Spinal Trauma: Vertebral Column and Spinal Cord Injuries in Children. Pediatr Neurosurg 15(5): 237–256. doi: 10.1159/000120476.

Dingu, N., R. Deumens, and G. Taccola. 2018. Afferent Input Induced by Rhythmic Limb Movement Modulates Spinal Neuronal Circuits in an Innovative Robotic In Vitro Preparation. Neuroscience 394: 44–59. doi: 10.1016/j.neuroscience.2018.10.016.

Ditunno, J.F., J.W. Little, A. Tessler, and A.S. Burns. 2004. Spinal shock revisited: a four-phase model. Spinal Cord 42(7): 383–395. doi: 10.1038/sj.sc.3101603.

Donato, R. 1999. Functional roles of S100 proteins, calcium-binding proteins of the EF-hand type. Biochimica et Biophysica Acta (BBA) - Molecular Cell Research 1450(3): 191–231. doi: 10.1016/S0167-4889(99)00058-0.

Donato, R. 2001. S100: a multigenic family of calcium-modulated proteins of the EF-hand type with intracellular and extracellular functional roles. The International Journal of Biochemistry & Cell Biology 33(7): 637–668. doi: 10.1016/S1357-2725(01)00046-2.

Dreier, J.P. 2011. The role of spreading depression, spreading depolarization and spreading ischemia in neurological disease. Nat Med 17(4): 439–447. doi: 10.1038/nm.2333.

Eidelberg, E., J. Sullivan, and A. Brigham. 1975. Immediate consequences of spinal cord injury: possible role of potassium in axonal conduction block. Surg Neurol 3(6): 317–321.

Eleraky, M.A., N. Theodore, M. Adams, H.L. Rekate, and V.K.H. Sonntag. 2000. Pediatric cervical spine injuries: report of 102 cases and review of the literature. Journal of Neurosurgery: Spine 92(1): 12–17. doi: 10.3171/spi.2000.92.1.0012.

Ellis, E.F., K.A. Willoughby, S.A. Sparks, and T. Chen. 2007. S100B protein is released from rat neonatal neurons, astrocytes, and microglia by *in vitro* trauma and anti-S100 increases trauma-induced delayed neuronal injury and negates the protective effect of exogenous S100B on

neurons. Journal of Neurochemistry 101(6): 1463–1470. doi: 10.1111/j.1471-4159.2007.04515.x.

Endo, T., C. Spenger, T. Tominaga, S. Brene, and L. Olson. 2007. Cortical sensory map rearrangement after spinal cord injury: fMRI responses linked to Nogo signalling. Brain 130(11): 2951–2961. doi: 10.1093/brain/awm237.

Eugenín, J., and J.G. Nicholls. 2000. Control of respiration in the isolated central nervous system of the neonatal opossum, Monodelphis domestica. Brain Research Bulletin 53(5): 605–613. doi: 10.1016/S0361-9230(00)00394-4.

Fawcett, J.W., A. Curt, J.D. Steeves, W.P. Coleman, M.H. Tuszynski, et al. 2007. Guidelines for the conduct of clinical trials for spinal cord injury as developed by the ICCP panel: spontaneous recovery after spinal cord injury and statistical power needed for therapeutic clinical trials. Spinal Cord 45(3): 190–205. doi: 10.1038/sj.sc.3102007.

Fehlings, M.G., and R. Nashmi. 1995. Assessment of axonal dysfunction in an in vitro model of acute compressive injury to adult rat spinal cord axons. Brain Research 677(2): 291–299. doi: 10.1016/0006-8993(95)00141-C.

Fehlings, M.G., and R.G. Perrin. 2005. The role and timing of early decompression for cervical spinal cord injury: Update with a review of recent clinical evidence. Injury 36(2): S13–S26. doi: 10.1016/j.injury.2005.06.011.

Feringa, E.R., and H.L. Vahlsing. 1985. Labeled corticospinal neurons one year after spinal cord transection. Neuroscience Letters 58(3): 283–286. doi: 10.1016/0304-3940(85)90067-9.

Fouad, K., C. Ng, and D.M. Basso. 2020. Behavioral testing in animal models of spinal cord injury. Experimental Neurology 333: 113410. doi: 10.1016/j.expneurol.2020.113410.

Fry, E.J. 2001. Central Nervous System Regeneration: Mission Impossible? Clin Exp Pharma Physio 28(4): 253–258. doi: 10.1046/j.1440-1681.2001.03417.x.

Gao, B.X., and L. Ziskind-Conhaim. 1995. Development of glycine- and GABA-gated currents in rat spinal motoneurons. Journal of Neurophysiology 74(1): 113–121. doi: 10.1152/jn.1995.74.1.113.

Garcia-Elias, A., S. Mrkonjić, C. Jung, C. Pardo-Pastor, R. Vicente, et al. 2014. The TRPV4 Channel. In: Nilius, B. and Flockerzi, V., editors, Mammalian Transient Receptor Potential (TRP) Cation Channels. Springer Berlin Heidelberg, Berlin, Heidelberg. p. 293–319

Geisler, F.H., W.P. Coleman, G. Grieco, and D. Poonian. 2001. Measurements and recovery patterns in a multicenter study of acute spinal cord injury. Spine 26(Supplement): S68–S86. doi: 10.1097/00007632-200112151-00014.

Gerlach, R., G. Demel, H.-G. König, U. Gross, J.H.M. Prehn, et al. 2006. Active secretion of S100B from astrocytes during metabolic stress. Neuroscience 141(4): 1697–1701. doi: 10.1016/j.neuroscience.2006.05.008.

Gernandt, B.E., and S. Gilman. 1961. Differential supraspinal control of spinal centers. Experimental Neurology 3(3): 307–324. doi: 10.1016/0014-4886(61)90018-8.

Ghosh, A., F. Haiss, E. Sydekum, R. Schneider, M. Gullo, et al. 2010. Rewiring of hindlimb corticospinal neurons after spinal cord injury. Nat Neurosci 13(1): 97–104. doi: 10.1038/nn.2448.

Giuliano Taccola and John Fischetti. 2023. Device for mechanically stimulating biological material and uses thereof. https://www.patentauction.com/patent.php?nb=18775.

Gonzalez, L.L., K. Garrie, and M.D. Turner. 2020. Role of S100 proteins in health and disease. Biochimica et Biophysica Acta (BBA) - Molecular Cell Research 1867(6): 118677. doi: 10.1016/j.bbamcr.2020.118677.

Goodman, R.M., K. Wachs, S. Keller, and P. Black. 1985. Spontaneous spinal cord "injury potential" in the rat. Neurosurgery 17(5): 757–759. doi: 10.1227/00006123-198511000-00005.

Gorji, A., P.K. Zahn, E.M. Pogatzki, and E.-J. Speckmann. 2004. Spinal and cortical spreading depression enhance spinal cord activity. Neurobiology of Disease 15(1): 70–79. doi: 10.1016/j.nbd.2003.09.014.

Grafstein, B. 1956. Mechanism of spreading cortical depression. Journal of Neurophysiology 19(2): 154–171. doi: 10.1152/jn.1956.19.2.154.

Grillner, S., P. Wallen, L. Brodin, and A. Lansner. 1991. Neuronal Network Generating Locomotor Behavior in Lamprey: Circuitry, Transmitters, Membrane Properties, and Simulation. Annu. Rev. Neurosci. 14(1): 169–199. doi: 10.1146/annurev.ne.14.030191.001125.

Guttmann, L. 1970. Spinal shock and reflex behaviour in man. Spinal Cord 8(2): 100–110. doi: 10.1038/sc.1970.19.

Hagan, M.J., J. Feler, F. Sun, O.P. Leary, A. Bajaj, et al. 2022. Spinal cord injury in adult and pediatric populations. Interdisciplinary Neurosurgery 29: 101594. doi: 10.1016/j.inat.2022.101594.

Hains, B.C., J.P. Klein, C.Y. Saab, M.J. Craner, J.A. Black, et al. 2003. Upregulation of Sodium Channel $Na_v1.3$ and Functional Involvement in Neuronal Hyperexcitability Associated with Central Neuropathic Pain after Spinal Cord Injury. J. Neurosci. 23(26): 8881–8892. doi: 10.1523/JNEUROSCI.23-26-08881.2003.

Hall, M. 1841. On the Diseases and Derangements of the Nervous System. Baillière.

Harreveld, A.V. 1959. Compounds in brain extracts causing spreading depression of cerebral cortical activity and contraction of crustacean muscle. Journal of Neurochemistry 3(4): 300–315. doi: 10.1111/j.1471-4159.1959.tb12636.x.

Hasbargen, T., M.M. Ahmed, G. Miranpuri, L. Li, K.T. Kahle, et al. 2010. Role of NKCC1 and KCC2 in the development of chronic neuropathic pain following spinal cord injury. Annals of the New York Academy of Sciences 1198(1): 168–172. doi: 10.1111/j.1749-6632.2010.05462.x.

Hermann, D.M., G. Mies, and K.-A. Hossmann. 1999. Biochemical changes and gene expression following traumatic brain injury: Role of spreading depression. Restor Neurol Neurosci 14(2–3): 103–108.

Herzer, K.R., Y. Chen, A.W. Heinemann, and M. González-Fernández. 2016. Association Between Time to Rehabilitation and Outcomes After Traumatic Spinal Cord Injury. Archives of Physical Medicine and Rehabilitation 97(10): 1620-1627.e4. doi: 10.1016/j.apmr.2016.05.009.

Hilton, B.J., E. Anenberg, T.C. Harrison, J.D. Boyd, T.H. Murphy, et al. 2016. Re-Establishment of Cortical Motor Output Maps and Spontaneous Functional Recovery via Spared Dorsolaterally Projecting Corticospinal Neurons after Dorsal Column Spinal Cord Injury in Adult Mice. J. Neurosci. 36(14): 4080–4092. doi: 10.1523/JNEUROSCI.3386-15.2016.

Hong, Z., Y. Tian, M. Qi, Y. Li, Y. Du, et al. 2016. Transient Receptor Potential Vanilloid 4 Inhibits γ-Aminobutyric Acid-Activated Current in Hippocampal Pyramidal Neurons. Front. Mol. Neurosci. 9. doi: 10.3389/fnmol.2016.00077.

Horn, E.M., and T.G. Waldrop. 1998. Suprapontine control of respiration. Respiration Physiology 114(3): 201–211. doi: 10.1016/S0034-5687(98)00087-5.

Huebner, E.A., and S.M. Strittmatter. 2009. Axon Regeneration in the Peripheral and Central Nervous Systems. In: Koenig, E., editor, Cell Biology of the Axon. Springer Berlin Heidelberg, Berlin, Heidelberg. p. 305–360

Ichiyama, R.M., J. Broman, R.R. Roy, H. Zhong, V.R. Edgerton, et al. 2011. Locomotor Training Maintains Normal Inhibitory Influence on Both Alpha- and Gamma-Motoneurons after Neonatal Spinal Cord Transection. J. Neurosci. 31(1): 26–33. doi: 10.1523/JNEUROSCI.6433-09.2011.

Iizuka, M. 1999. Intercostal expiratory activity in an *in vitro* brainstem-spinal cord-rib preparation from the neonatal rat. The Journal of Physiology 520(1): 293–302. doi: 10.1111/j.1469-7793.1999.00293.x.

Inanici, F., S. Samejima, P. Gad, V.R. Edgerton, C.P. Hofstetter, et al. 2018. Transcutaneous Electrical Spinal Stimulation Promotes Long-Term Recovery of Upper Extremity Function in Chronic Tetraplegia. IEEE Trans. Neural Syst. Rehabil. Eng. 26(6): 1272–1278. doi: 10.1109/TNSRE.2018.2834339.

Ishikawa, T., H. Suzuki, K. Ishikawa, S. Yasuda, T. Matsui, et al. 2014. Spinal cord ischemia/injury. Curr Pharm Des 20(36): 5738–5743. doi: 10.2174/1381612820666140204113252.

Jacobs, K.M., and J.P. Donoghue. 1991. Reshaping the Cortical Motor Map by Unmasking Latent Intracortical Connections. Science 251(4996): 944–947. doi: 10.1126/science.2000496.

Kaur, J., J. Flores Gutiérrez, and A. Nistri. 2016. Neuroprotective effect of propofol against excitotoxic injury to locomotor networks of the rat spinal cord *in vitro* (P. Bolam, editor). Eur J of Neuroscience 44(7): 2418–2430. doi: 10.1111/ejn.13353.

Keifer, J., and P.S.G. Stein. 1983. In vitro motor program for the rostral scratch reflex generated by the turtle spinal cord. Brain Research 266(1): 148–151. doi: 10.1016/0006-8993(83)91318-5.

Kerkut, G.A., and J. Bagust. 1995. The isolated mammalian spinal cord. Progress in Neurobiology 46(1): 1–48. doi: 10.1016/0301-0082(94)00055-M.

Kiehn, O. 2006. Locomotor circuits in the mammalian spinal cord. Annu Rev Neurosci 29: 279–306. doi: 10.1146/annurev.neuro.29.051605.112910.

Kirshblum, S., S. Millis, W. McKinley, and D. Tulsky. 2004. Late neurologic recovery after traumatic spinal cord injury. Archives of Physical Medicine and Rehabilitation 85(11): 1811–1817. doi: 10.1016/j.apmr.2004.03.015.

Kirshblum, S., B. Snider, F. Eren, and J. Guest. 2021. Characterizing natural recovery after traumatic spinal cord injury. Journal of Neurotrauma 38(9): 1267–1284. doi: 10.1089/neu.2020.7473.

Kjell, J., and L. Olson. 2016. Rat models of spinal cord injury: from pathology to potential therapies. Disease Models & Mechanisms 9(10): 1125–1137. doi: 10.1242/dmm.025833.

Ko, H.-Y. 2018. Revisit Spinal Shock: Pattern of Reflex Evolution during Spinal Shock. Korean J Neurotrauma 14(2): 47. doi: 10.13004/kjnt.2018.14.2.47.

Ko, H.-Y., J. Ditunno, V. Graziani, and J. Little. 1999. The pattern of reflex recovery during spinal shock. Spinal Cord 37(6): 402–409. doi: 10.1038/sj.sc.3100840.

Kole, A.J., R.P. Annis, and M. Deshmukh. 2013. Mature neurons: equipped for survival. Cell Death Dis 4(6): e689–e689. doi: 10.1038/cddis.2013.220.

Kouhzaei, S., I. Rad, K. Khodayari, and H. Mobasheri. 2013. The Neuroprotective Ability of Polyethylene Glycol is Affected by Temperature in Ex Vivo Spinal Cord Injury Model. J Membrane Biol 246(8): 613–619. doi: 10.1007/s00232-013-9574-3.

Kraig, R.P., and C. Nicholson. 1978. Extracellular ionic variations during spreading depression. Neuroscience 3(11): 1045–1059. doi: 10.1016/0306-4522(78)90122-7.

Krassioukov, A.V., A. Ackery, G. Schwartz, Y. Adamchik, Y. Liu, et al. 2002. An in vitro model of neurotrauma in organotypic spinal cord cultures from adult mice. Brain Research Protocols 10(2): 60–68. doi: 10.1016/S1385-299X(02)00180-0.

Kumar, H., and I. Han. 2022. The neuroscience of transient receptor potential vanilloid type 4 (TRPV4) and spinal cord injury. Cellular, Molecular, Physiological, and Behavioral Aspects of Spinal Cord Injury. Elsevier. p. 229–238

Kumar, H., S.-H. Lee, K.-T. Kim, X. Zeng, and I. Han. 2018. TRPV4: a Sensor for Homeostasis and Pathological Events in the CNS. Mol Neurobiol 55(11): 8695–8708. doi: 10.1007/s12035-018-0998-8.

Kumar, H., C.S. Lim, H. Choi, H.P. Joshi, K.-T. Kim, et al. 2020. Elevated TRPV4 Levels Contribute to Endothelial Damage and Scarring in Experimental Spinal Cord Injury. J. Neurosci. 40(9): 1943–1955. doi: 10.1523/JNEUROSCI.2035-19.2020.

Kunkel-Bagden, E., H.-N. Dai, and B.S. Bregman. 1992. Recovery of function after spinal cord hemisection in newborn and adult rats: Differential effects on reflex and locomotor function. Experimental Neurology 116(1): 40–51. doi: 10.1016/0014-4886(92)90174-O.

Kwo, S., W. Young, and V. Decrescito. 1989. Spinal cord sodium, potassium, calcium, and water concentration changes in rats after graded contusion injury. Journal of Neurotrauma 6(1): 13–24. doi: 10.1089/neu.1989.6.13.

Lakke, E.A.J.F. 1997. The projections to the spinal cord of the rat during development: a timetable of descent. Springer Berlin Heidelberg, Berlin, Heidelberg.

Lauritzen, M. 1994. Pathophysiology of the migraine aura: The spreading depression theory. Brain 117(1): 199–210. doi: 10.1093/brain/117.1.199.

Lauritzen, M., J.P. Dreier, M. Fabricius, J.A. Hartings, R. Graf, et al. 2011. Clinical relevance of cortical spreading depression in neurological disorders: migraine, malignant stroke, subarachnoid and intracranial hemorrhage, and traumatic brain injury. J Cereb Blood Flow Metab 31(1): 17–35. doi: 10.1038/jcbfm.2010.191.

Leao, A.A.P. 1944. Spreading depression of activity in the cerebral cortex. Journal of Neurophysiology 7(6): 359–390. doi: 10.1152/jn.1944.7.6.359.

Leao, A.A.P. 1947. Further observations on the spreading depression of activity in the cerebral cortex. Journal of Neurophysiology 10(6): 409–414. doi: 10.1152/jn.1947.10.6.409.

Lim, L., D. Mi, A. Llorca, and O. Marín. 2018. Development and Functional Diversification of Cortical Interneurons. Neuron 100(2): 294–313. doi: 10.1016/j.neuron.2018.10.009.

Lindquist, B.E. 2023. Spreading depolarizations pose critical energy challenges in acute brain injury. Journal of Neurochemistry: jnc.15966. doi: 10.1111/jnc.15966.

Liu, N., J. Wu, Y. Chen, and J. Zhao. 2020. Channels that Cooperate with TRPV4 in the Brain. J Mol Neurosci 70(11): 1812–1820. doi: 10.1007/s12031-020-01574-z.

Lorach, H., A. Galvez, V. Spagnolo, F. Martel, S. Karakas, et al. 2023. Walking naturally after spinal cord injury using a brain–spine interface. Nature 618(7963): 126–133. doi: 10.1038/s41586-023-06094-5.

Lynskey, J.V. 2008. Activity-dependent plasticity in spinal cord injury. JRRD 45(2): 229–240. doi: 10.1682/JRRD.2007.03.0047.

Ma, M., D.M. Basso, P. Walters, B.T. Stokes, and L.B. Jakeman. 2001. Behavioral and Histological Outcomes Following Graded Spinal Cord Contusion Injury in the C57Bl/6 Mouse. Experimental Neurology 169(2): 239–254. doi: 10.1006/exnr.2001.7679.

Marín, O. 2013. Cellular and molecular mechanisms controlling the migration of neocortical interneurons. Eur J Neurosci 38(1): 2019–2029. doi: 10.1111/ejn.12225.

Mazzone, G.L., A. Mohammadshirazi, J.B. Aquino, A. Nistri, and G. Taccola. 2021. GABAergic mechanisms can redress the tilted balance between excitation and inhibition in damaged spinal networks. Mol Neurobiol 58(8): 3769–3786. doi: 10.1007/s12035-021-02370-5.

Mazzone, G.L., and A. Nistri. 2014. S100β as an early biomarker of excitotoxic damage in spinal cord organotypic cultures. Journal of Neurochemistry 130(4): 598–604. doi: 10.1111/jnc.12748.

McAdoo, D.J., G. Robak, G.-Y. Xu, and M.G. Hughes. 2000. Adenosine release upon spinal cord injury. Brain Research 854(1–2): 152–157. doi: 10.1016/S0006-8993(99)02333-1.

Mccouch, G.P., C.-N. Liu, and W.W. Chambers. 1966. Descending tracts and spinal shock in the monkey (Macaca mulatta). Brain 89(2): 359–376. doi: 10.1093/brain/89.2.359.

Mekki, M., A.D. Delgado, A. Fry, D. Putrino, and V. Huang. 2018. Robotic Rehabilitation and Spinal Cord Injury: a Narrative Review. Neurotherapeutics 15(3): 604–617. doi: 10.1007/s13311-018-0642-3.

Mladinic, M., A. Nistri, and G. Taccola. 2013. Acute spinal cord injury in vitro: insight into basic mechanisms. In: Aldskogius, H., editor, Animal Models of Spinal Cord Repair. Humana Press, Totowa, NJ. p. 39–62

Mohammadshirazi, A., R. Apicella, B.A. Zylberberg, G.L. Mazzone, and G. Taccola. 2023. Suprapontine structures modulate brainstem and spinal networks. Cell Mol Neurobiol. doi: 10.1007/s10571-023-01321-z.

Mohammadshirazi, A., G.L. Mazzone, B.A. Zylberberg, L. Mio, G. Pistorio, et al. 2024. A focal traumatic injury to the spinal cord causes an immediate and massive spreading depolarization sustained by chloride ions, with transient network dysfunction and remote cortical glia changes. doi: 10.1101/2024.07.15.603535.

Mohammadshirazi, A., and G. Taccola. 2024. An electrophysiological study about the pharmacological manipulation of the immediate consequences of a spinal trauma reveals a crucial role for TRPV4 antagonism. doi: 10.1101/2024.10.03.616499.

Moxon, K.A., A. Oliviero, J. Aguilar, and G. Foffani. 2014. Cortical reorganization after spinal cord injury: Always for good? Neuroscience 283: 78–94. doi: 10.1016/j.neuroscience.2014.06.056.

Nacimiento, W., and J. Noth. 1999. What, If Anything, Is Spinal Shock? Arch Neurol 56(8): 1033. doi: 10.1001/archneur.56.8.1033.

Nardone, R., Y. Höller, F. Brigo, M. Seidl, M. Christova, et al. 2013. Functional brain reorganization after spinal cord injury: Systematic review of animal and human studies. Brain Research 1504: 58–73. doi: 10.1016/j.brainres.2012.12.034.

Nasser, M.W., M. Elbaz, D.K. Ahirwar, and R.K. Ganju. 2015. Conditioning solid tumor microenvironment through inflammatory chemokines and S100 family proteins. Cancer Letters 365(1): 11–22. doi: 10.1016/j.canlet.2015.05.002.

Nepomuceno, P., W.H. Souza, M. Pakosh, K.E. Musselman, and B.C. Craven. 2024. Exoskeleton-based exercises for overground gait and balance rehabilitation in spinal cord injury: a systematic review of dose and dosage parameters. J NeuroEngineering Rehabil 21(1): 73. doi: 10.1186/s12984-024-01365-2.

Nicholls, J.G., R.R. Stewart, S.D. Erulkar, and N.R. Saunders. 1990. Reflexes, fictive respiration and cell division in the brain and spinal cord of the newborn opossum, Monodelphis domestica, isolated and maintained in vitro. Journal of Experimental Biology 152(1): 1–15. doi: 10.1242/jeb.152.1.1.

Norenberg, M.D., J. Smith, and A. Marcillo. 2004. The Pathology of Human Spinal Cord Injury: Defining the Problems. Journal of Neurotrauma 21(4): 429–440. doi: 10.1089/089771504323004575.

Nout, Y.S., M.S. Beattie, and J.C. Bresnahan. 2012. Severity of Locomotor and Cardiovascular Derangements after Experimental High-Thoracic Spinal Cord Injury Is Anesthesia Dependent in Rats. Journal of Neurotrauma 29(5): 990–999. doi: 10.1089/neu.2011.1845.

O'Donovan, M., E. Sernagor, G. Sholomenko, S. Ho, M. Antal, et al. 1992. Development of spinal motor networks in the chick embryo. J. Exp. Zool. 261(3): 261–273. doi: 10.1002/jez.1402610306.

Otsuka, M., and S. Konishi. 1974. Electrophysiology of mammalian spinal cord in vitro. Nature 252(5485): 733–734. doi: 10.1038/252733a0.

Pandamooz, S., M.S. Salehi, M.I. Zibaii, A. Safari, M. Nabiuni, et al. 2019. Modeling traumatic injury in organotypic spinal cord slice culture obtained from adult rat. Tissue and Cell 56: 90–97. doi: 10.1016/j.tice.2019.01.002.

Panter, S.S., S.W. Yum, and A.I. Faden. 1990. Alteration in extracellular amino acids after traumatic spinal cord injury. Annals of Neurology 27(1): 96–99. doi: 10.1002/ana.410270115.

Park, H.-P., Y. Jeon, J. Hwang, H. Kang, S.-W. Lim, et al. 2005. Isoflurane preconditioning protects motor neurons from spinal cord ischemia: Its dose–response effects and activation of mitochondrial adenosine triphosphate-dependent potassium channel. Neuroscience Letters 387(2): 90–94. doi: 10.1016/j.neulet.2005.06.072.

Patar, A., P. Dockery, L. Howard, and S.S. McMahon. 2019. Cell viability in three *ex vivo* rat models of spinal cord injury. Journal of Anatomy 234(2): 244–251. doi: 10.1111/joa.12909.

Paton, J.F.R. 1996. A working heart-brainstem preparation of the mouse. Journal of Neuroscience Methods 65(1): 63–68. doi: 10.1016/0165-0270(95)00147-6.

Petruska, J.C., R.M. Ichiyama, D.L. Jindrich, E.D. Crown, K.E. Tansey, et al. 2007. Changes in Motoneuron Properties and Synaptic Inputs Related to Step Training after Spinal Cord Transection in Rats. J. Neurosci. 27(16): 4460–4471. doi: 10.1523/JNEUROSCI.2302-06.2007.

Qi, M., C. Wu, Z. Wang, L. Zhou, C. Men, et al. 2018. Transient Receptor Potential Vanilloid 4 Activation-Induced Increase in Glycine-Activated Current in Mouse Hippocampal Pyramidal Neurons. Cell Physiol Biochem 45(3): 1084–1096. doi: 10.1159/000487350.

Rahman, Md.A., N.S. Tharu, S.M. Gustin, Y.-P. Zheng, and M. Alam. 2022. Trans-Spinal Electrical Stimulation Therapy for Functional Rehabilitation after Spinal Cord Injury: Review. JCM 11(6): 1550. doi: 10.3390/jcm11061550.

Raineteau, O., and M.E. Schwab. 2001. Plasticity of motor systems after incomplete spinal cord injury. Nat Rev Neurosci 2(4): 263–273. doi: 10.1038/35067570.

Ramirez, S., A. Mukherjee, S. Sepulveda, A. Becerra-Calixto, N. Bravo-Vasquez, et al. 2021. Modeling Traumatic Brain Injury in Human Cerebral Organoids. Cells 10(10): 2683. doi: 10.3390/cells10102683.

Rasmussen, R., and E.M. Carlsen. 2016. Spontaneous Functional Recovery from Incomplete Spinal Cord Injury. J. Neurosci. 36(33): 8535–8537. doi: 10.1523/JNEUROSCI.1684-16.2016.

Rudomin, P. 2009. In search of lost presynaptic inhibition. Exp Brain Res 196(1): 139–151. doi: 10.1007/s00221-009-1758-9.

Rupp, R., F. Biering-Sørensen, S.P. Burns, D.E. Graves, J. Guest, et al. 2021. International Standards for Neurological Classification of Spinal Cord Injury. Topics in Spinal Cord Injury Rehabilitation 27(2): 1–22. doi: 10.46292/sci2702-1.

Sang, H., L. Cao, P. Qiu, L. Xiong, R. Wang, et al. 2006. Isoflurane Produces Delayed Preconditioning against Spinal Cord Ischemic Injury via Release of Free Radicals in Rabbits. Anesthesiology 105(5): 953–960. doi: 10.1097/00000542-200611000-00016.

Schwab, J.M., K. Brechtel, C.-A. Mueller, V. Failli, H.-P. Kaps, et al. 2006. Experimental strategies to promote spinal cord regeneration—an integrative perspective. Progress in Neurobiology 78(2): 91–116. doi: 10.1016/j.pneurobio.2005.12.004.

Shabbir, A., E. Bianchetti, and A. Nistri. 2015. The volatile anesthetic methoxyflurane protects motoneurons against excitotoxicity in an in vitro model of rat spinal cord injury. Neuroscience 285: 269–280. doi: 10.1016/j.neuroscience.2014.11.023.

Sharif-Alhoseini, M., M. Khormali, M. Rezaei, M. Safdarian, A. Hajighadery, et al. 2017. Animal models of spinal cord injury: a systematic review. Spinal Cord 55(8): 714–721. doi: 10.1038/sc.2016.187.

Sherrington, C. 1897. Croonian lecture.— The mammalian spinal cord as an organ of reflex action. Proc. R. Soc. Lond. 61(369–377): 220–221. doi: 10.1098/rspl.1897.0025.

Shi, R., and A.R. Blight. 1996. Compression injury of mammalian spinal cord in vitro and the dynamics of action potential conduction failure. Journal of Neurophysiology 76(3): 1572–1580. doi: 10.1152/jn.1996.76.3.1572.

Siddiqui, A.M., M. Khazaei, and M.G. Fehlings. 2015. Translating mechanisms of neuroprotection, regeneration, and repair to treatment of spinal cord injury. Progress in Brain Research. Elsevier. p. 15–54

Silva, N.A., N. Sousa, R.L. Reis, and A.J. Salgado. 2014. From basics to clinical: A comprehensive review on spinal cord injury. Progress in Neurobiology 114: 25–57. doi: 10.1016/j.pneurobio.2013.11.002.

Simpson, R.K., C.S. Robertson, and J.C. Goodman. 1996. The Role of Glycine in Spinal Shock. The Journal of Spinal Cord Medicine 19(4): 215–224. doi: 10.1080/10790268.1996.11719437.

Smith, J.C., and J.L. Feldman. 1987. In vitro brainstem-spinal cord preparations for study of motor systems for mammalian respiration and locomotion. Journal of Neuroscience Methods 21(2–4): 321–333. doi: 10.1016/0165-0270(87)90126-9.

Smith, J.C., J.J. Greer, G.S. Liu, and J.L. Feldman. 1990. Neural mechanisms generating respiratory pattern in mammalian brain stem-spinal cord in vitro. I. Spatiotemporal patterns of motor and medullary neuron activity. Journal of Neurophysiology 64(4): 1149–1169. doi: 10.1152/jn.1990.64.4.1149.

Smith, P.M., and N.D. Jeffery. 2005. Spinal Shock-Comparative Aspects and Clinical Relevance. Journal of Veterinary Internal Medicine 19(6): 788–793. doi: 10.1111/j.1939-1676.2005.tb02766.x.

Somjen, G.G. 2001. Mechanisms of spreading depression and hypoxic spreading depression-like depolarization. Physiological Reviews 81(3): 1065–1096. doi: 10.1152/physrev.2001.81.3.1065.

Stewart, A.N., L.A.T. Jones, and J.C. Gensel. 2022. Improving translatability of spinal cord injury research by including age as a demographic variable. Front. Cell. Neurosci. 16: 1017153. doi: 10.3389/fncel.2022.1017153.

Streit, D.S., C.R. Ferreira Filho, and H. Martins-Ferreira. 1995. Spreading depression in isolated spinal cord. Journal of Neurophysiology 74(2): 888–890. doi: 10.1152/jn.1995.74.2.888.

Suzue, T. 1984. Respiratory rhythm generation in the in vitro brain stem-spinal cord preparation of the neonatal rat. The Journal of Physiology 354(1): 173–183. doi: 10.1113/jphysiol.1984.sp015370.

Taccola, G., P. Gad, S. Culaclii, R.M. Ichiyama, W. Liu, et al. 2020. Using EMG to deliver lumbar dynamic electrical stimulation to facilitate cortico-spinal excitability. Brain Stimulation 13(1): 20–34. doi: 10.1016/j.brs.2019.09.013.

Taccola, G., G. Margaryan, M. Mladinic, and A. Nistri. 2008. Kainate and metabolic perturbation mimicking spinal injury differentially contribute to early damage of locomotor networks in the in vitro neonatal rat spinal cord. Neuroscience 155(2): 538–555. doi: 10.1016/j.neuroscience.2008.06.008.

Taccola, G., M. Mladinic, and A. Nistri. 2010. Dynamics of early locomotor network dysfunction following a focal lesion in an in vitro model of spinal injury. European Journal of Neuroscience 31(1): 60–78. doi: 10.1111/j.1460-9568.2009.07040.x.

Takeda, H., V.J. Caiozzo, and V.O. Gardner. 1993. A Functional In Vitro Model for Studying the Cellular and Molecular Basis of Spinal Cord Injury: Spine 18(9): 1125–1133. doi: 10.1097/00007632-199307000-00003.

Varadarajan, S.G., J.L. Hunyara, N.R. Hamilton, A.L. Kolodkin, and A.D. Huberman. 2022. Central nervous system regeneration. Cell 185(1): 77–94. doi: 10.1016/j.cell.2021.10.029.

Wakabayashi, Y., H. Komori, T. Kawa-Uchi, K. Mochida, M. Takahashi, et al. 2001. Functional Recovery and Regeneration of Descending Tracts in Rats After Spinal Cord Transection in Infancy: Spine 26(11): 1215–1222. doi: 10.1097/00007632-200106010-00009.

Wang, M.Y., D.J. Hoh, S.P. Leary, P. Griffith, and J.G. McComb. 2004. High Rates of Neurological Improvement Following Severe Traumatic Pediatric Spinal Cord Injury: Spine 29(13): 1493–1497. doi: 10.1097/01.BRS.0000129026.03194.0F.

Wang, A., X. Huo, G. Zhang, X. Wang, C. Zhang, et al. 2016. Effect of DSPE-PEG on compound action potential, injury potential and ion concentration following compression in ex vivo spinal cord. Neuroscience Letters 620: 50–56. doi: 10.1016/j.neulet.2016.03.045.

Wang, A.-H., G.-H. Zhang, C. Zhang, X.-L. Huo, and T. Song. 2015. Injury potentials of spinal cord in ex vivo compression injury model. IEEE, Milan. p. 4659–4662

Weightman, A.P., M.R. Pickard, Y. Yang, and D.M. Chari. 2014. An in vitro spinal cord injury model to screen neuroregenerative materials. Biomaterials 35(12): 3756–3765. doi: 10.1016/j.biomaterials.2014.01.022.

Wendt, S., E. Wogram, L. Korvers, and H. Kettenmann. 2016. Experimental cortical spreading depression induces NMDA receptor dependent potassium currents in microglia. J. Neurosci. 36(23): 6165–6174. doi: 10.1523/JNEUROSCI.4498-15.2016.

Wheatley, M., M. Edamura, and R.B. Stein. 1992. A comparison of intact and in-vitro locomotion in an adult amphibian. Exp Brain Res 88(3). doi: 10.1007/BF00228189.

WHO. 2024. Spinal cord injury. World Health Organization (WHO). [https://www.who.int/news-room/fact-sheets/detail/spinal-cord-injury#:~:text=Globally%2C%20over%2015%20million%20people,violence%2C%20and%20ar

e%20thus%20preventable.](https://www.who.int/news-room/fact-sheets/detail/spinal-cord-injury#:~:text=Globally%2C%20over%2015%20million%20people,violence%2C%20and%20are%20thus%20preventable.).

Willis. 1999. Dorsal root potentials and dorsal root reflexes: a double-edged sword. Experimental Brain Research 124(4): 395–421. doi: 10.1007/s002210050637.

Windmüller, O., U. Lindauer, M. Foddis, K.M. Einhäupl, U. Dirnagl, et al. 2005. Ion changes in spreading ischaemia induce rat middle cerebral artery constriction in the absence of NO. Brain 128(9): 2042–2051. doi: 10.1093/brain/awh545.

Wissenbach, U., M. Bödding, M. Freichel, and V. Flockerzi. 2000. Trp12, a novel Trp related protein from kidney. FEBS Letters 485(2–3): 127–134. doi: 10.1016/S0014-5793(00)02212-2.

Woodward, S.K.A., J.M. Treherne, G.W. Knott, J. Fernandez, Z.M. Varga, et al. 1993. Development of Connections by Axons Growing Through Injured Spinal Cord of Neonatal Opossum in Culture. Journal of Experimental Biology 176(1): 77–88. doi: 10.1242/jeb.176.1.77.

Wrathall, J.R., R.K. Pettegrew, and F. Harvey. 1985. Spinal cord contusion in the rat: Production of graded, reproducible, injury groups☆. Experimental Neurology 88(1): 108–122. doi: 10.1016/0014-4886(85)90117-7.

Wu, J., Z. Zhao, B. Sabirzhanov, B.A. Stoica, A. Kumar, et al. 2014. Spinal cord injury causes brain inflammation associated with cognitive and affective changes: role of cell cycle pathways. Journal of Neuroscience 34(33): 10989–11006. doi: 10.1523/JNEUROSCI.5110-13.2014.

Yagüe, J.G., D. Humanes-Valera, J. Aguilar, and G. Foffani. 2014. Functional reorganization of the forepaw cortical representation immediately after thoracic spinal cord hemisection in rats. Experimental Neurology 257: 19–24. doi: 10.1016/j.expneurol.2014.03.015.

Yang, T., Y. Dai, G. Chen, and S. Cui. 2020a. Dissecting the Dual Role of the Glial Scar and Scar-Forming Astrocytes in Spinal Cord Injury. Front. Cell. Neurosci. 14: 78. doi: 10.3389/fncel.2020.00078.

Yang, B., F. Zhang, F. Cheng, L. Ying, C. Wang, et al. 2020b. Strategies and prospects of effective neural circuits reconstruction after spinal cord injury. Cell Death Dis 11(6): 439. doi: 10.1038/s41419-020-2620-z.

Yu, Q.J., Q.S. Zhou, H.B. Huang, Y.L. Wang, S.F. Tian, et al. 2008. Protective Effect of Ketamine on Ischemic Spinal Cord Injury in Rabbits. Annals of Vascular Surgery 22(3): 432–439. doi: 10.1016/j.avsg.2008.03.003.

Ziu, E., L.J. Weisbrod, and F.B. Mesfin. 2024. Spinal Shock. StatPearls. StatPearls Publishing, Treasure Island (FL)